

Combining tissue engineering and gene delivery to enhance peripheral nerve regeneration

Francesca Busuttì

Thesis submitted in fulfilment of the requirements for the degree of Doctor of
Philosophy

University College London

Department of Pharmacology
UCL School of Pharmacy
29-39 Brunswick Square
London, WC1N 1AX

January 2019

I, Francesca Busuttil confirm that the work presented in this thesis is my own. Where information has been derived from other sources, I confirm that this has been indicated in the thesis.

Abstract

There has been an increased interest in the development of nerve repair devices to improve peripheral nerve regeneration following injury. The aim of this study was to investigate whether nerve repair devices containing genetically modified cells overexpressing VEGF-A₁₆₅ would augment regeneration. An *in vitro* proof-of-concept study was carried out to deliver marker genes (luciferase and eGFP) to a rat Schwann cell line (SCL4.1/F7) using a lentiviral vector. The transduced cells were used to produce engineered neural tissue and bioluminescence imaging was used to assess cell viability in the constructs. It was initially thought the presence of the luciferase gene in the expression cassette would allow real-time and sustained imaging of the cells in the engineered neural tissue. However, while bioluminescence imaging provided an indication of cell viability *in vitro*, it proved to be ineffective for *in vivo* and *ex vivo* imaging. Having established that SCL4.1/F7 cells were amenable to lentiviral transduction, a lentiviral vector delivering the VEGF-A₁₆₅ gene was designed and produced. The VEGF-A₁₆₅ produced by the transduced SCL4.1/F7 cells increased endothelial cell viability, migration and tube formation *in vitro*. It also increased SCL4.1/F7 cell proliferation and migration. SCL4.1/F7 cells overexpressing VEGF-A₁₆₅ were found to increase endothelial cell network formation and neurite length in 3D co-culture models. Foetal human neural stem cells and rat adipose derived stem cells were also successfully transduced with the lentiviral vector delivering VEGF-A₁₆₅. Based on the *in vitro* results, it was postulated that EngNT made from SCL4.1/F7 cells overexpressing VEGF-A₁₆₅ implanted into a rat model of sciatic nerve injury would enhance regeneration. Unexpectedly, a pilot study revealed that this did not result in improved functional recovery or increased axon and blood vessel counts compared to controls. The results from this study highlight that attention needs to be paid to the dose and duration of expression of VEGF-A₁₆₅ to optimise both its angiogenic and neurotrophic effects.

The research work disclosed in this publication is partially funded by the Endeavour Scholarship Scheme (Malta). Scholarships are part-financed by the European Union - European Social Fund (ESF) - Operational Programme II – Cohesion Policy 2014-2020 “Investing in human capital to create more opportunities and promote the well-being of society”.

Impact statement

Peripheral nerve injuries affect ~5% of trauma patients (Li *et al.*, 2014) and may have a serious impact on patient quality of life, resulting from loss of motor, sensory or autonomic function. Despite refinement in surgical techniques, insufficient functional recovery after peripheral nerve injury remains a significant clinical challenge, with only 40-70% of adults regaining some functional activity following injury (Rochkind *et al.*, 2014a). Further, the current clinical gold standard, the nerve autograft, is associated with several other disadvantages, including the sacrifice of a functioning nerve and possible neuroma formation at the donor site (Grinsell *et al.*, 2014).

The limited efficacy of current treatment has propelled the development of tissue engineered constructs as an alternative to the nerve autograft (Gu *et al.*, 2014). However, while biomaterial conduits have already been approved for clinical use, none of them offer complete functional recovery (Belanger *et al.*, 2016). Supplementing the biomaterial conduits with therapeutic cells is thought to enhance peripheral nerve engineering strategies, as cells provide structural and trophic support. However, tissue engineering is currently limited by the inability to adequately vascularise tissues following implantation (Lovett *et al.*, 2009). Therefore, additional strategies for enhancing vascularisation are essential to ensure the survival of tissue engineered constructs *in vivo* as insufficient vascularisation can lead to improper cell integration or cell death (Rouwkema *et al.*, 2008).

Angiogenic factors are currently being investigated as a means of inducing vascularisation in tissue engineered constructs (Novosel *et al.*, 2011). In order to overcome problems with the delivery of such factors, the current study investigates the use of genetically modified cells which overexpress vascular endothelial growth factor (VEGF). Once incorporated into tissue engineered constructs used for peripheral nerve repair, these cells can provide a local and sustained release of VEGF. It is thought that the combination of tissue engineering and gene delivery may provide the optimal environment for axonal regeneration, and following further investigation and refinement, may be applicable to translational research to promote peripheral nerve regeneration.

Acknowledgements

I would like to thank Dr Ahad Rahim for the opportunity to work in his lab during my PhD and for his guidance throughout.

My thanks also extend to Dr James Phillips for his support and advice over the past three years. I would also like to thank the members of James' lab for helping me on numerous occasions, especially Adam and Mel. Special thanks to Mel for being there for me in and out of the lab and to Maha for being a friendly face throughout the past year.

Thanks also go to Dr Dave Gathercole for assistance with the confocal microscope, Caitlin Broadbent for helping me with flow cytometry and Dr Michael Hughes for teaching me how to produce lentiviral vectors.

I would also like to thank my funding bodies, the Endeavour Scholarship Scheme and the UCL Graduate Research Scholarship, for providing me with the funding which made this PhD possible.

Lastly, I would like to thank my parents for their unwavering support over the years, friends and Luke.

The research disclosed in this publication is partially funded by the Endeavour Scholarship Scheme (Malta). Scholarships are part-financed by the European Union – European Social Fund (ESF) – Operational Programme II – Cohesion Policy 2014-2020
“Investing in human capital to create more opportunities and promote the well-being of society”.



European Union – European Structural and Investment Funds
Operational Programme II – Cohesion Policy 2014-2020
*“Investing in human capital to create more opportunities
and promote the well-being of society”*
Scholarships are part-financed by the European Union –
European Social Funds (ESF)
Co-financing rate: 80% EU Funds; 20% National Funds



Publications

Articles

Bhangra KS, **Busuttil F***, Phillips JB, Rahim AA. Using Stem Cells to Grow Artificial Tissue for Peripheral Nerve Repair. *Stem Cells Int.* 2016;2016:7502178.

Busuttil F, Rahim AA, Phillips JB. Combining Gene and Stem Cell Therapy for Peripheral Nerve Tissue Engineering. *Stem Cells Dev.* 2017 Feb 15;26(4):231-238.

*Joint first author

Conference proceedings

Busuttil F, Hughes MP, Bhangra KS, Phillips JB, Rahim AA. An evaluation of lentiviral mediated gene deliver to Schwann cells for the purpose of tissue engineering. In: British Society for Gene and Cell Therapy Annual Conference, 15th April 2016, London, UK.

Busuttil F, Hughes MP, Bhangra KS, Kingham PJ, Phillips JB, Rahim AA. Enhancing peripheral nerve regeneration through tissue engineering and gene transfer. In: Tissue and Cell Engineering Society Annual Meeting, 4-6th July 2016, London, UK.

Busuttil F, Hughes MP, Bhangra KS, Kingham PJ, Phillips JB, Rahim AA. Enhancing peripheral nerve regeneration through combined gene therapy and tissue engineering. In: Society for Neuroscience Annual Meeting, 12-16th November 2016, San Diego, USA.

Busuttil F, Hughes MP, Kingham PJ, Phillips JB, Rahim AA. Combining tissue engineering and gene delivery to enhance peripheral nerve regeneration. In: International Symposium on Peripheral Nerve Regeneration, 6-8th July 2017, Barcelona, Spain.

Busuttil F, Hughes MP, Kingham PJ, Phillips JB, Rahim AA. Enhancing peripheral nerve regeneration through combined gene therapy and tissue engineering. In: British Society for Gene and Cell Therapy Annual Conference, 27th April 2018, London, UK.

Table of contents

Abstract	3
Impact statement	4
Acknowledgements	5
Publications	7
Table of contents	8
List of figures	15
List of tables	20
List of abbreviations	21
Chapter 1. Introduction	23
1.1 Background	23
1.2 Study rationale	23
1.3 Aims and objectives	25
1.4 Organisation of thesis.....	26
Chapter 2. Literature review	27
2.1 The peripheral nervous system	27
2.1.1 Peripheral nerves.....	28
2.1.2 Schwann cells.....	30
2.1.3 Vasculature	31
2.2 Peripheral nerve injury.....	33
2.2.1 Incidence and aetiology	33
2.2.2 Pathophysiology	34
2.2.2.1 Neuronal response.....	34
2.2.2.2 Schwann cell response	36
2.2.3 Clinical peripheral nerve repair	38
2.2.3.1 Types of injury.....	38
2.2.3.2 Surgical interventions	39
2.3 Regenerative medicine for peripheral nerve repair.....	46

2.3.1 Tissue engineering.....	46
2.3.1.1 Conduits	46
2.3.1.2 Luminal fillers	48
2.3.1.3 Vascularisation	50
2.3.2 Cell therapy.....	53
2.3.3 Gene therapy	56
2.3.3.1 Gene delivery vectors	57
2.3.3.2 <i>in vivo</i> gene delivery to Schwann cells and nerves	60
2.3.3.3 <i>ex vivo</i> gene delivery for peripheral nerve repair	62
Chapter 3. Materials and methods.....	67
3.1 Introduction.....	67
3.2 Cell culture	68
3.2.1 SCL4.1/F7 rat Schwann cell culture.....	68
3.2.2 Rat adipose derived stem cells culture and differentiation	68
3.2.3 Human foetal neural stem cell culture.....	69
3.2.4 Human umbilical vein endothelial cells culture.....	69
3.2.5 PC12 cell culture.....	70
3.2.6 HEK293T cell culture	70
3.3 Cloning of the <i>VEGF-A₁₆₅</i> gene	70
3.3.1 Polymerase chain reaction.....	72
3.3.1.1 PCR optimisation.....	73
3.3.2 Restriction enzyme digest.....	73
3.3.3 Gel electrophoresis	74
3.3.4 DNA extraction.....	74
3.3.5 Ligation	74
3.3.6 Bacterial transformation	75
3.3.7 Plasmid purification and diagnostic digest	75
3.3.8 Synthesised genes	76
3.3.9 Sequencing.....	76

3.4 Plasmid transfection	77
3.5 Lentivirus production	77
3.5.1 HEK293T cells triple transfection and virus harvest.....	78
3.5.2 Lentivirus concentration via centrifugation	79
3.5.3 Lentivirus titration.....	79
3.6 Transduction.....	79
3.6.1 Assessing transduction efficiency by flow cytometry.....	80
3.7 Protein expression analysis.....	80
3.7.1 Sample preparation.....	81
3.7.2 Western blot.....	81
3.7.3 ELISA.....	83
3.8 Cell proliferation assay	83
3.9 Cell morphology analysis.....	83
3.10 Collection and processing of conditioned media	84
3.11 Functional assays.....	84
3.11.1 Effect of VEGF-A ₁₆₅ on HUVEC viability	85
3.11.2 Endothelial tube formation assay	85
3.11.3 Scratch assay	86
3.11.4 Transwell migration assay	87
3.12 Engineered neural tissue.....	88
3.12.1 Fabrication of engineered neural tissue	88
3.12.2 Contraction assay	89
3.12.3 Distribution of cells in the EngNT	90
3.13 Cell viability assays	90
3.13.1 alamarBlue® assay.....	90
3.13.2 Live-dead stain	91
3.14 Bioluminescence imaging.....	92

3.15 <i>in vitro</i> 3D co-cultures.....	92
3.15.1 PC12 - SCL4.1/F7 co-cultures	92
3.15.2 HUVEC - SCL4.1/F7 co-cultures	92
3.16 Immunocytochemistry and imaging	93
3.17 <i>In vivo</i> experiments	93
3.17.1 Animals	93
3.17.2 Device assembly.....	94
3.17.3 Surgery	94
3.17.4 <i>in vivo</i> bioluminescence imaging	97
3.17.5 Functional tests.....	97
3.17.5.1 Von Frey	97
3.17.5.2 Static sciatic index.....	98
3.17.6 Electrophysiology.....	99
3.17.7 Tissue harvesting.....	100
3.17.8 Processing of tissue.....	101
3.17.8.1 <i>ex vivo</i> bioluminescence imaging.....	101
3.17.8.2 Tissue fixing and cryosectioning	101
3.17.9 Immunofluorescence staining of nerve sections	102
3.17.9.1 Preparation of chrome-gelatine coated slides.....	102
3.17.9.2 Immunofluorescence	102
3.17.9.2 Quantitative analysis of immunofluorescence staining.....	103
3.18 Statistical analysis	104
Chapter 4. An evaluation of lentiviral-mediated gene delivery to Schwann cells for the purpose of peripheral nerve tissue engineering	105
4.1 Introduction.....	105
4.2 Lentiviral mediated gene delivery to SCL4.1/F7 cells.....	106
4.2.1 The SFFV.Luc.2A.eGFP lentiviral vector	106
4.2.2 The SCL4.1/F7 cell line.....	106
4.2.3 Lentiviral transduction resulted in eGFP expression.....	107

4.2.4	Establishing the transduction efficiency using flow cytometry	108
4.2.5	Stability of eGFP expression.....	112
4.2.6	Effect of transduction on cell viability, proliferation and morphology	113
4.3	<i>in vitro</i> bioluminescence imaging.....	116
4.3.1	Lentiviral transduction resulted in luciferase expression	117
4.3.2	Adjusting the exposure time.....	118
4.3.3	Luciferin kinetics study.....	119
4.3.4	Correlation between bioluminescence signal strength and cell number	120
4.3.5	Luciferin toxicity study.....	121
4.3.6	Monitoring the luciferase intensity over time	123
4.4	Engineered neural tissue.....	124
4.5	Discussion	127
4.6	Conclusion.....	133
	Chapter 5. Assessing cell viability in engineered neural tissue	134
5.1	Introduction.....	134
5.2	<i>in vitro</i> bioluminescence imaging.....	135
5.2.1	<i>In vitro</i> bioluminescence kinetics study	135
5.2.2	Cell viability and proliferation assessment	136
5.3	Comparing bioluminescence imaging with cell viability assays	138
5.4	<i>in vivo</i> bioluminescence imaging	140
5.4.1	<i>In vivo</i> kinetics study	141
5.4.2	Route of luciferin administration.....	142
5.4.3	Animal position	144
5.5	<i>ex vivo</i> bioluminescence imaging	145
5.6	Fluorescence imaging	151

5.7 Monitoring cell viability in the nerve repair device	152
5.8 Discussion	155
5.9 Conclusion.....	168
Chapter 6. Lentivirus-mediated expression of VEGF-A₁₆₅ in SCL4.1/F7 cells: assessing <i>in vitro</i> effects	169
6.1 Introduction.....	169
6.2 Choice of the therapeutic gene.....	170
6.3 Cloning of the <i>VEGF-A₁₆₅</i> gene	171
6.3.1 The polymerase chain reaction.....	172
6.3.2 Inserting the <i>VEGF-A₁₆₅</i> gene into the pSFFV.IRES.eGFP transfer plasmid	174
6.3.3 Formation of the pSFFV.VEGF.IRES.eGFP transfer plasmid.....	175
6.3.4 Functionality of the pSFFV.VEGF.IRES.eGFP transfer plasmid.....	177
6.4 The lentiviral vector delivering the <i>VEGF-A₁₆₅</i> gene.....	178
6.4.1 Transduction efficiency	180
6.4.2 VEGF-A ₁₆₅ overexpression following transduction	181
6.4.3 Effect of transduction on proliferation and morphology	183
6.5 Testing the functionality of the lentiviral expressed VEGF-A ₁₆₅ protein .	187
6.5.1 Angiogenesis assays	187
6.5.1.1 Endothelial cell viability assay.....	187
6.5.1.2 Scratch wound assay.....	188
6.5.1.3 Tube formation assay.....	190
6.5.2 Effect of VEGF-A ₁₆₅ on Schwann cell migration.....	192
6.6 Constructing EngNT from SCL4.1/F7 cells overexpressing VEGF-A ₁₆₅	193
6.6.1 VEGF-A ₁₆₅ production by transduced cells in EngNT	197
6.7 Co-cultures	200
6.7.1 Neurotrophic effects.....	200
6.7.2 Angiogenic effects.....	202

6.8 Discussion	205
6.9 Conclusion.....	209
Chapter 7: Effects of EngNT containing SCL4.1/F7 overexpressing VEGF-A₁₆₅ on peripheral nerve regeneration.....	210
7.1 Introduction.....	210
7.2 VEGF-A ₁₆₅ overexpression in clinically relevant sources of therapeutic cells	211
7.2 Animal model.....	212
7.3 Outcome measures	214
7.3.1 Functional outcomes	214
7.3.1.1 Static sciatic index.....	215
7.3.1.2 Von Frey	216
7.3.1.3 Gastrocnemius muscle mass.....	217
7.3.2 Electrophysiological outcomes.....	219
7.3.3 Histological outcomes	220
7.3.3.1 Axonal counts.....	220
7.3.3.2 Vascularisation	223
7.5 Discussion	225
7.6 Conclusion.....	231
Chapter 8: Discussion	232
8.1 Overview	232
8.2 Summary of results	233
8.3 Study limitations	234
8.4 Future work	235
8.5 Conclusion.....	237
9. References.....	239

List of figures

Figure 1. The central and peripheral nervous systems.....	29
Figure 2. Peripheral nerve anatomy.....	30
Figure 3. The Schwann cell lineage.....	32
Figure 4. The vasa nervorum.....	33
Figure 5. Regenerative response after nerve injury.....	35
Figure 6. The Schwann cell injury response.....	38
Figure 7. Surgical interventions for nerve repair.....	41
Figure 8. The autologous nerve graft.....	43
Figure 9. Generations of nerve conduits.....	49
Figure 10. Schematic representation of the diffusion and transport processes in tissues <i>in vivo</i>	51
Figure 11. Issues relating to successful gene delivery.....	58
Figure 12. Gene transfer by a lentiviral vector.....	64
Figure 13. Schematic of the experimental methods used in the current project.....	68
Figure 14. Plasmid cloning by PCR.....	72
Figure 15. Lentiviral vector production.....	79
Figure 16. HUVEC tube formation assay.....	87
Figure 17. Scratch assay.....	88
Figure 18. Transwell migration assay.....	89
Figure 19. Cellular collagen gels in polyether ether ketone moulds.....	90
Figure 20. Stabilising the EngNT to produce robust hydrogels.....	90
Figure 21. Assembly of the implantable device.....	95
Figure 22. The position of the sciatic nerve in relation to the knee and hip.....	96
Figure 23. Exposing the sciatic nerve.....	96
Figure 24. Positioning the implantable device.....	97
Figure 25. Closing the muscle layer.....	97
Figure 26. Application of the von Frey filament on the rat's hind paw.....	99
Figure 27. Calculating the static sciatic index.....	100
Figure 28. Electrophysiology set up.....	101
Figure 29. The gastrocnemius muscle.....	102

Figure 30. A schematic of the lentiviral vector backbone delivering luciferase and eGFP reporter genes.....	102
Figure 31. SCL4.1/F7 cells expressing eGFP 72 hours post transduction.....	109
Figure 32. Flow cytometry analysis of eGFP expressing cells.....	110
Figure 33. Efficiency of lentiviral-mediated gene transfer to SCL4.1/F7 cells at increasing MOIs.....	113
Figure 34. Stability of lentiviral mediated eGFP expression over an 8 week period.....	115
Figure 35. Effect of transduction on cell viability.....	116
Figure 36. Effect of lentiviral transduction on SCL4.1/F7 cell proliferation.....	117
Figure 37. Effect of lentiviral transduction on SCL4.1/F7 morphology.....	119
Figure 38. Bioluminescence imaging of SCL4.1/F7 transduced with MOIs of 1, 10 and 100.....	120
Figure 39. Bioluminescence imaging of luciferase expressing SCL4.1/F7 cells to determine the optimal acquisition time.....	121
Figure 40. Luciferin kinetic curve to determine peak signal time.....	122
Figure 41. Quantitative correlation between signal strength and cell number.....	123
Figure 42. Investigating the effect of repeated and single luciferin addition on SCL4.1/F7 cells viability.....	125
Figure 43. Evaluating the stability of luciferase activity over time and after cryopreservation.....	126
Figure 44. Stereoscopic fluorescence micrograph showing even distribution of eGFP positive cells throughout the entire length and width of the EngNT.....	120
Figure 45. Lentiviral mediated eGFP expression in SCL4.1/F7 cells in EngNT.....	121
Figure 46. Z- stack through EngNT containing SCL4.1/F7 cells expressing eGFP.....	122
Figure 47. Second generation lentiviral plasmids.....	123
Figure 48. Schematic representation of the mechanism of “self-cleaving” 2A peptides.....	125
Figure 49. Kinetic profile of light emission following luciferin addition to EngNT.....	126
Figure 50. Time-course of the <i>in vitro</i> cell viability of luciferase expressing SCL4.1/F7 cells in EngNT during 10 days of culture.....	127
Figure 51. Determination of the percentage cell death in collagen gels over a 5 day period.....	128

Figure 52. alamarBlue® assay to assess cell viability in EngNT over a 5 day period....	129
Figure 53. No bioluminescence signal was obtained in the <i>in vivo</i> imaging study.....	131
Figure 54. Subcutaneous administration of luciferin did not result in a bioluminescence signal.....	137
Figure 55. Investigating the effect of animal positioning on bioluminescence imaging.....	138
Figure 56. <i>ex vivo</i> imaging of the nerve repair device 8 days post implantation.....	140
Figure 57. Segments cut from the EngNT prior to assembling the nerve repair devices.....	141
Figure 58. <i>ex vivo</i> imaging of the explanted nerve repair devices and a representative control contralateral nerve one day post implantation.....	143
Figure 59. <i>Ex vivo</i> imaging of the explanted nerve repair devices and a representative control contralateral nerve three days post implantation.....	144
Figure 60. <i>Ex vivo</i> imaging of the explanted nerve repair devices and a representative control contralateral nerve five days post implantation.....	145
Figure 61. The bioluminescence signals obtained 30 minutes after the addition of luciferin up to 5 days post implantation.....	147
Figure 62. Explanted EngNT contained eGFP positive cells.....	148
Figure 63. The silicone tube in the nerve repair device did not attenuate the emitted light.....	149
Figure 64. Assessing the impact of the silicone tube on luciferin kinetics.....	150
Figure 65. A schematic representing the structure of the <i>VEGF-A</i> gene.....	151
Figure 66. Gel electrophoresis image suggesting the presence of the <i>VEGF-A₁₆₅</i> gene.....	152
Figure 67. Gel electrophoresis image deducing the optimum PCR conditions.....	154
Figure 68. Restriction digest analysis of the pSFFV.VEGF.IRES.eGFP plasmid using <i>BamHI</i> and <i>XhoI</i>	155
Figure 69. Schematic of the pSFFV.VEGF.IRES.eGFP transfer plasmid.....	156
Figure 70. eGFP expression in HEK293T cells following transfection with the pSFFV.VEGF.IRES.eGFP transfer plasmid.....	173
Figure 71. Quantifying the amount of VEGF-A ₁₆₅ produced by transfected HEK293T cells.....	174
Figure 72. Schematic of the lentiviral vector delivering the <i>VEGF-A₁₆₅</i> gene.....	175

Figure 73. eGFP expression following lentiviral transduction.....	177
Figure 74. Efficiency of lentiviral-mediated gene transfer to SCL4.1/F7 cells.....	178
Figure 75. Western blot analysis of VEGF-A ₁₆₅ levels in SCL4.1/F7 cells following transduction compared to endogenous VEGF-A ₁₆₅ in untransduced cells.....	179
Figure 76. Quantifying the amount of VEGF-A ₁₆₅ produced by SCL4.1/F7 cells transduced by the lentiviral vector delivering VEGF-A ₁₆₅	180
Figure 77. VEGF-A ₁₆₅ overexpression resulted in a significant increase in SCL4.1/F7 cell proliferation.....	182
Figure 78. Effect of VEGF-A ₁₆₅ overexpression on SCL4.1/F7 morphology.....	183
Figure 79. Effect of VEGF-A ₁₆₅ on endothelial cell viability.....	184
Figure 80. Effect of VEGF-A ₁₆₅ on endothelial cell migration.....	185
Figure 81. Effect of VEGF-A ₁₆₅ on endothelial tube formation.....	187
Figure 82. Analysis of the effect of VEGF-A ₁₆₅ on the migration of SCL4.1/F7 cells.....	188
Figure 83. Contraction assay for control SCL4.1/F7 cells and SCL4.1/F7 cells overexpressing VEGF-A ₁₆₅	190
Figure 84. Laser scanning confocal microscopy for imaging of lentiviral mediated gene expression in SCL4.1/F7 cell constructs.....	191
Figure 85. Laser scanning confocal microscopy for imaging of lentiviral mediated VEGF-A ₁₆₅ expression in SCL4.1/F7 cell constructs.....	193
Figure 86. Quantifying the amount of VEGF-A ₁₆₅ produced by SCL4.1/F7 cells incorporated into EngNT.....	195
Figure 87. Quantifying the amount of VEGF-A ₁₆₅ produced by transduced SCL4.1/F7 cells in EngNT in a silicone tube.....	196
Figure 88. Representation of the 3D engineered co-culture.....	197
Figure 89. Effect of VEGF-A ₁₆₅ on neurite length <i>in vitro</i>	198
Figure 90. Evaluation of endothelial tube formation in the 3D co-culture system after 4 days.....	200
Figure 91. Endothelial cell network characteristics in the HUVEC - SCL4.1/F7 cell 3D co-cultures.....	201
Figure 92. Quantifying the amount of VEGF-A ₁₆₅ produced by transduced CTX0E03, ADSCs and SCL4.1/F7 cells.....	203
Figure 93. Rat body weight monitoring during the 8 week experiment.....	203
Figure 94: An explanted nerve repair device.....	205

Figure 95. Calculating the SSI.....	206
Figure 96. SSI monitoring during the study period.....	214
Figure 97. Von Frey testing.....	215
Figure 98. Gastrocnemius muscles harvest at 8 weeks.....	215
Figure 99. Gastrocnemius muscle mass following sciatic nerve repair.....	217
Figure 100. Axonal staining.....	218
Figure 101. Quantification of neurites at different positions through repaired nerves.....	219
Figure 102. Blood vessel analysis.....	220
Figure 103. Examination of vasculature within repair site.....	221

List of tables

Table 1. Seddon and Sunderland classifications for peripheral nerve injuries.....	40
Table 2. Examples of FDA approved nerve guidance conduits.....	46
Table 3. Angiogenic factors currently used in tissue engineering.....	53
Table 4. Characteristics of different viral vectors.....	60
Table 5. <i>In vivo</i> gene delivery targeting nerves and Schwann cells.....	62
Table 6. Studies enhancing the regenerative potential of therapeutic cells by over expression of neurotrophic factors.....	65
Table 7. Primers used to amplify the <i>VEGF-A₁₆₅</i> gene.....	73
Table 8. Components and volumes used in the PCR reaction.....	73
Table 9. Initial PCR conditions.....	74
Table 10. Components and volumes used in a typical restriction enzyme digest.....	74
Table 11. Components and volumes used in a typical ligation reaction.....	76
Table 12. Sequencing primers.....	77
Table 13. Primary antibodies used in western blotting.....	83
Table 14. Secondary antibodies used in western blotting.....	84
Table 15. Primary antibodies used in immunofluorescence studies.....	104
Table 16. Secondary antibodies used in immunofluorescence studies.....	104
Table 17. Use of bioluminescence imaging to monitor cell survival in tissue engineered constructs implanted in live animals.....	160
Table 18. Electrophysiological evaluation of sciatic nerve 8 weeks postoperatively.....	222

List of abbreviations

2D – two-dimensional

3D – three-dimensional

AAV – adeno-associated virus

ADSCs – adipose derived stem cells

ANOVA – analysis of variance

BCA – bicinchoninic acid

BDNF – brain-derived neurotrophic factor

bFGF – basic fibroblast growth factor

BMP7 – bone morphogenetic protein-7

BMSCs – bone marrow stem cells

bp – base pair

BrdU - 5-bromo-2'-deoxyuridine

BSA – bovine serum albumin

CDNF – conserved dopamine neurotrophic factor

CM – conditioned media

CMAP – compound muscle action potential

CNS – central nervous system

CNTF – ciliary neurotrophic factor

CO₂ – carbon dioxide

DAPI – 4',6-diamidino-2-phenylindole

dH₂O – distilled water

DMEM – Dulbecco's Modified Eagle Medium

DNA – deoxyribonucleic acid

dNTPs – deoxynucleotide triphosphates

ECM – extracellular matrix

EDTA – ethylenediaminetetraacetic acid

eGFP – enhanced green fluorescent protein

EGM – endothelial cell growth medium

ELISA – enzyme-linked immunosorbent assay

EngNT – engineered neural tissue

FBS – foetal bovine serum

FDA - Food and Drug Administration
FGF2 – fibroblast growth factor-2
GDNF – glial-cell derived neurotrophic factor
HEK – human embryonic kidney
HGF – hepatocyte growth factor
HUVECs – human umbilical vein endothelial cells
IP – intraperitoneal
IRES – internal ribosomal entry site
IVIS – *in vivo* imaging system
kb – kilo base
LB – Luria-Bertani
MOI – multiplicity of infection
NGF – nerve growth factor
ns – non-significant
NT3 – neurotrophin-3
OCT – optimal cutting temperature
PBS – phosphate buffered saline
PCR – polymerase chain reaction
PEI – polyethylenimine
PFA – paraformaldehyde
PNI – peripheral nerve injury
PNS – peripheral nervous system
RECA-1 – rat endothelial cell antibody-1
RIPA – radioimmunoprecipitation
RNA – ribonucleic acid
SC – subcutaneous
SD – standard deviation
SFFV – spleen focus-forming virus
SSI – static sciatic index
TAE – tris-acetate-EDTA
VEGF – vascular endothelial growth factor
VSG-V – vesicular stomatitis virus G glycoprotein
WPRE – woodchuck hepatitis virus posttranscriptional regulatory element

Chapter 1. Introduction

1.1 Background

Damage to the peripheral nervous system can have a serious impact on patient quality of life, resulting from loss of motor or sensory function. Despite an improved understanding of the complex neuropathophysiology following peripheral nerve injuries, clinical treatments have remained largely unchanged over the past 30 years (Faroni *et al.*, 2015). Surgical procedures aim to restore the connection between the proximal and distal stumps in transection injuries, either through a primary repair or a nerve autograft. However, these procedures often result in poor clinical outcomes, with patients unlikely to regain full function (Geuna *et al.*, 2009). This highlights the need for continued research to provide more efficacious treatment strategies.

In recent years, there has been considerable interest in developing tissue engineered constructs as an alternative to current treatment modalities (Gu *et al.*, 2014). While nerve guidance conduits have already been approved for clinical use, none of them offer complete functional recovery (Belanger *et al.*, 2016). Supplementing biomaterial conduits with therapeutic cells can provide structural and trophic support by recreating key features of nerve architecture, thus enhancing peripheral nerve engineering strategies. However, tissue engineering is limited by the inability to adequately vascularise tissues due to nutrient perfusion and mass transport limitations (Lovett *et al.*, 2009). In fact, vascularisation is currently regarded as one of the main hurdles hindering the translation of tissue engineering to clinical applications (Grounds, 2018). This has prompted the investigation of methods to successfully connect the tissue engineered construct to the host vasculature following implantation (Rouwkema and Khademhosseini, 2016).

1.2 Study rationale

Angiogenic growth factors are effective initiators of vascularisation by activating endothelial cells and stimulating them to migrate towards the factor gradient. They also promote vessel formation and maturation. The main factors in upregulating angiogenic

processes are vascular endothelial growth factor (VEGF), basic fibroblast growth factor (bFGF) and hepatocyte growth factor (HGF) (Nomi *et al.*, 2006). Angiogenic factors can be exploited as a means of inducing vascularisation in tissue engineered constructs (Novosel *et al.*, 2011) and there has been an interest in the development of strategies for the delivery of these factors to the implant site. Angiogenic factors are inherently unstable *in vivo*, precluding their administration by bolus injection (Nomi *et al.*, 2002). Furthermore, vascularisation is implicated in tumour growth and metastasis (Horch *et al.*, 2013), making the widespread and uncontrolled delivery of angiogenic factors undesirable. Consequently, efforts are being made to create a spatially restricted and stable delivery system. One such approach is the use of genetically modified cells that overexpress these factors. Once incorporated into tissue-engineered constructs, these cells can provide a local and sustained angiogenic factor release (Novosel *et al.*, 2011).

Viral gene delivery has been established as a highly effective means of genetically modifying cells for patient benefit and has been suggested as a means of enhancing peripheral nerve tissue engineering strategies (Busuttill *et al.*, 2017). The combination of gene delivery and cell therapy is an emerging strategy that has yielded clinical success in other medical conditions. A noteworthy example is the regulatory approval of Strimvelis™, the first *ex vivo* autologous stem cell gene therapy to treat patients with severe combined immunodeficiency due to adenosine deaminase deficiency (Ylä-Herttuala, 2016).

In addition to increasing cell survival in implanted tissue engineered constructs, vascularisation is also important for the process of peripheral nerve regeneration itself. Cattin *et al.* (2015) have showed that following injury, new blood vessels guide migrating Schwann cells across the injury site, a process that is essential for axonal regeneration. Further, angiogenic factors such as VEGF exhibit neurotrophic effects (Sondell *et al.*, 2000). Neurotrophic factors control the survival, migration, proliferation and differentiation of various types of cells that are involved in nerve repair (Sebben *et al.*, 2011). The overexpression of VEGF may augment peripheral nerve tissue engineering strategies by providing the optimal environment for axonal regeneration and reestablishment of functional circuits.

To fully evaluate the performance of tissue engineered constructs *in vitro* and *in vivo*, it is necessary to obtain information on cell distribution and cell fate. This has traditionally been done by histological analysis using *in vitro* samples or explanted specimens after *in vivo* applications (Leferink *et al.*, 2016). However, this requires destruction of the samples, excluding the possibility of longitudinal monitoring (Nam *et al.*, 2015). In order to overcome the limitations of destructive endpoint analysis, imaging modalities capable of monitoring the tissue engineered constructs over a period of time are being investigated (Nam *et al.*, 2015).

Molecular imaging may allow the longitudinal, non-invasive and quantitative imaging of tissue engineered constructs. This can be achieved by genetically modifying cells to express a reporter gene. Commonly used reporter genes in cell-based therapies include enhanced green fluorescent protein (eGFP) for fluorescence imaging and luciferase for bioluminescence imaging (Li *et al.*, 2018). Bioluminescence imaging is a popular means of assessing cell viability and tracking cells in pre-clinical studies (Strohschein *et al.*, 2015). Additionally, it can also provide valuable information about cell behaviour in three-dimensional (3D) tissue engineered constructs (Vila *et al.*, 2016).

1.3 Aims and objectives

The overarching hypothesis of this project is that the combination of tissue engineering and gene delivery can be used to augment peripheral nerve regeneration. This hypothesis will be tested by:

- Labelling cells with a bioluminescent tag to monitor cell viability in the tissue engineered constructs *in vitro* and *in vivo*.
- Modifying cells to overexpress VEGF-A₁₆₅, thereby improving vascularisation to the implanted tissue.
- Improving peripheral nerve regeneration by creating a microenvironment conducive to axonal regrowth as VEGF-A₁₆₅ also has neurotrophic effects.

In order to reach these aims, this project has the following specific objectives:

- To produce lentiviral vectors to deliver therapeutic and reporter genes.
- To assess the ability of the lentiviral vectors to efficiently deliver genes to a variety of cell types *in vitro*.
- To determine whether the transduced cells can produce functional proteins *in vitro*.
- To ensure that the transduced cells remain viable and can be used to produce tissue engineered constructs.
- To monitor cell viability in the tissue engineered constructs *in vitro* and *in vivo*.
- To determine whether tissue engineered constructs containing cells overexpressing VEGF-A₁₆₅ improve axonal regeneration and functional recovery in a rat model of sciatic nerve injury.

1.4 Organisation of thesis

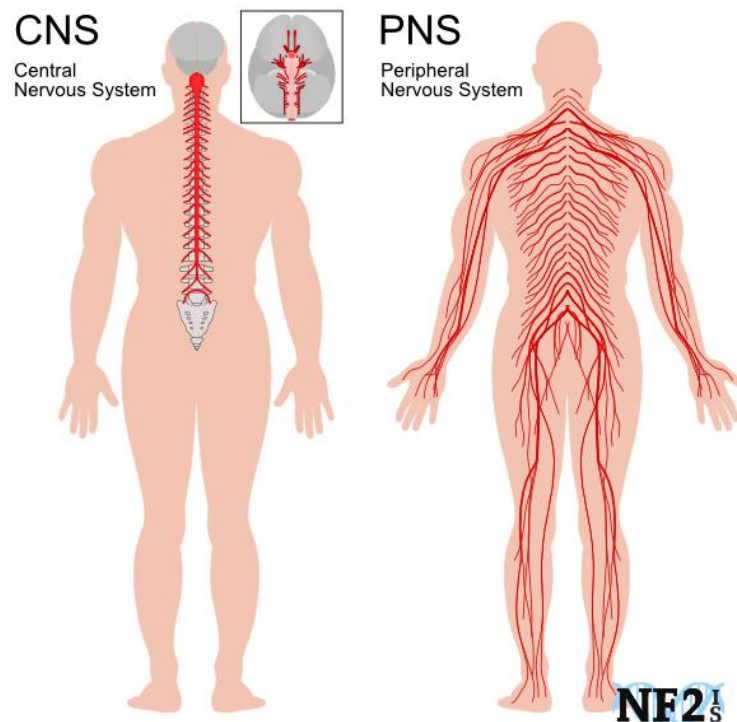
Chapter 2 provides a literature review covering peripheral nerve injury and regeneration. This chapter evaluates the use of tissue engineered constructs containing genetically modified cells in enhancing peripheral nerve regeneration as well as the importance of vascularisation of tissue engineered constructs. Chapter 3 details the materials and methods used in this study. Chapter 4 presents the results of an *in vitro* proof-of-concept study describing lentiviral mediated gene delivery to a rat Schwann cell line. Chapter 5 investigates the use of bioluminescence imaging to monitor the viability of cells in engineered neural tissue (EngNT), both *in vitro* and *in vivo*. Chapter 6 describes the genetic modification of cells to overexpress VEGF-A₁₆₅ and the assays used to assess the functionality of the protein *in vitro*. Chapter 7 explores the transduction of clinically relevant stem cells. Results from a pilot study investigating the efficacy of EngNT containing cells overexpressing VEGF-A₁₆₅ in a rat model of sciatic nerve injury are also presented. Chapter 8 summarises the main findings of this study along with the study limitations and future work.

Chapter 2. Literature review

2.1 The peripheral nervous system

The nervous system in vertebrates comprises the central nervous system (CNS) and the peripheral nervous system (PNS) (figure 1). The CNS consists of the brain and spinal cord whereas the PNS includes the cranial, spinal, autonomic, enteric and peripheral nerves. The PNS connects the CNS to the sensory and motor pathways (Raimondo *et al.*, 2011). Sensory nerves transmit impulses to the CNS from sensory receptors while motor nerves transmit neural signals from the CNS to effectors (glands, organs and muscles). These impulses are generated and directed via the sequential process of axonal depolarisation and subsequent repolarisation, a process dependent on sodium and potassium channel flux. The PNS derives from the neural crest and develops in a tightly controlled process that involves the migration of multipotent precursor cells that progressively differentiate into neurons and glial cells (Prendergast and Raible, 2014). In order to fully understand how to effectively develop strategies to enhance peripheral nerve regeneration, an understanding of peripheral nerve organisation, glial function and blood supply is needed and will be discussed in this section.

Figure 1. The central and peripheral nervous systems. The PNS includes afferent neurons that relay sensory information from receptors in the periphery toward the CNS and efferent neurons that transmit information away from the brain to the peripheral tissues. Image taken from https://www.nf2is.org/peripheral_nerve_damage.php (accessed 25th May 2019).



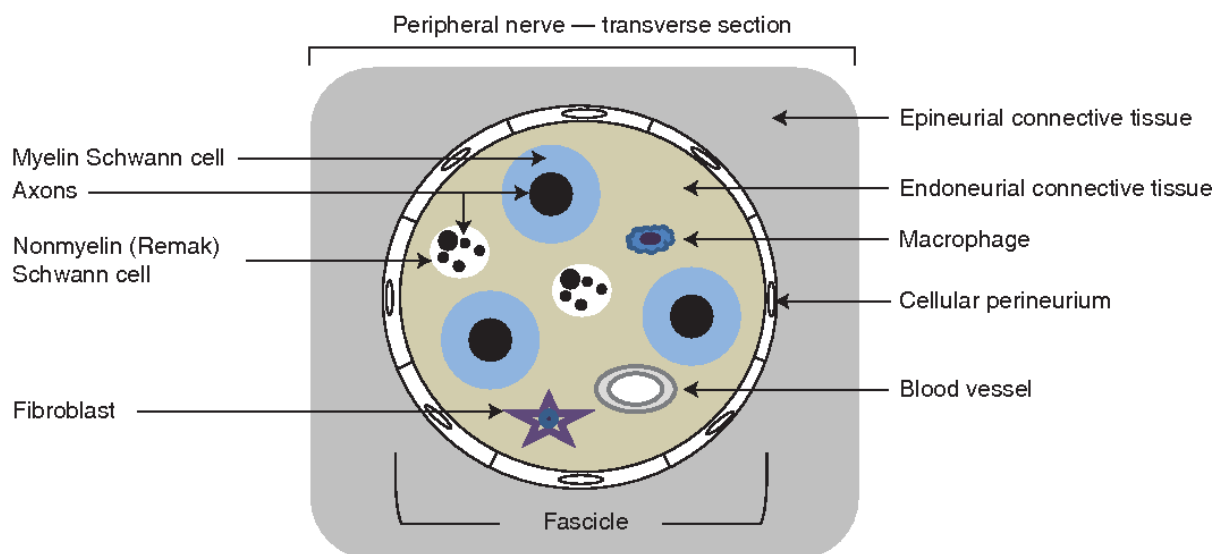
2.1.1 Peripheral nerves

Peripheral nerves extend throughout the body, forming a complex network. Sensory nerve fibres generally originate from pseudounipolar neurons located in the sensory ganglia while motor nerve fibres originate from somatic and autonomic motor neurons located in the CNS. Somatic motor fibres directly reach the target skeletal muscle fibres whereas autonomic motor fibres create synapses in an ortho- or parasympathetic ganglion where the second-order autonomic neuron is located and the axon of which reaches the target visceral organs (Geuna *et al.*, 2009).

Peripheral nerves are complex tissues composed of Schwann cells, perineurial cells and neuronal processes (axons), surrounded by connective tissue elements. The smallest functional unit of a peripheral nerve is the nerve fibre. Nerve fibres can be myelinated or unmyelinated. Large mammalian axons are myelinated whereas axons smaller than 1 μm in diameter are generally unmyelinated. Myelination allows the fast conduction of

action potentials by insulating the axons (Geuna *et al.*, 2009). Nerves in different parts of the body vary in fibre composition and in the presence and number of fascicles. However, nerve morphology (figure 2) is comparatively similar in nearly all regions.

Figure 2. Peripheral nerve anatomy. A nerve consists of axons embedded in a collagenous matrix (endoneurium), forming fascicles. Fascicles are ensheathed by connective tissue (perineurium) and wrapped by an external connective layer (epineurium). Nerves can be myelinated or unmyelinated. Image taken from Jessen *et al.* (2015).



A heterogeneous and highly specialised combination of cells and extracellular matrix (ECM) protects the nerves and provides resistance to stretch and compression forces during body movements. This intrinsic part of nerve structure is arranged in three layers, namely the epineurium, perineurium and endoneurium (figure 2) (Peltonen *et al.*, 2013). The epineurium is the outermost layer of supporting and protective tissue and surrounds the entire nerve and its individual fascicles. It contains fibroblasts, collagen (types I and II) and variable amounts of fat, and thus contributes to the tensile strength of the nerve. It carries the main intraneural vascular system, which passes across the perineurium and into the endoneurium (Geuna *et al.*, 2009).

The perineurium is a dense and mechanically strong sheath that surrounds each fascicle, consisting of alternating layers of flattened polygonal cells and collagen (Richner *et al.*, 2014). The number of perineurial cell layers varies according to the number and size of

the fascicles in the nerve (Peltonen *et al.*, 2013). The perineurium, together with the blood–nerve barrier described below, plays an essential role in maintaining the osmotic milieu and the fluid pressure within the endoneurium (Mizisin and Weerasuriya, 2011).

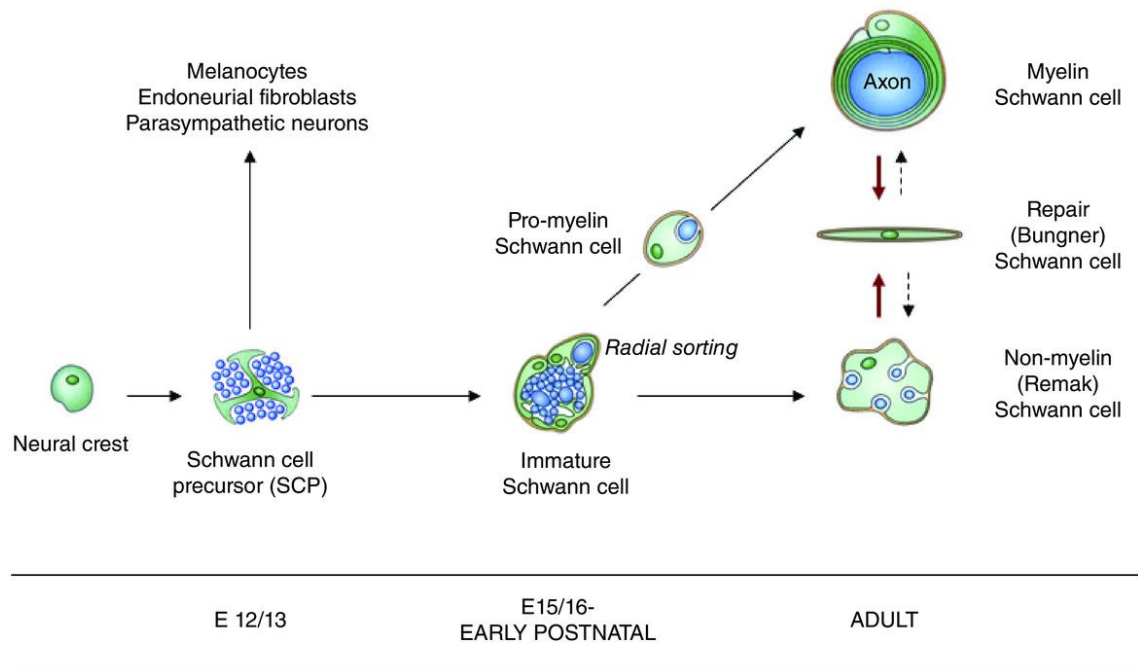
The endoneurium is a loose, soft, connective tissue that surrounds and supports the fascicles, protecting them during the movements of an extremity and from external trauma. The cell population in the endoneurium consists mostly of Schwann cells and endothelial cells that form capillary networks (Geuna *et al.*, 2009). Endoneurial blood vessels isolate the endoneurium from the circulating blood, forming the blood-nerve barrier that consists of tight junctions between endothelial cells (Mizisin and Weerasuriya, 2011). Tight control of ion and water concentrations within peripheral nerves is required to maintain the internal microenvironment needed for axonal signal transmission.

2.1.2 Schwann cells

Schwann cells and satellite glia are two types of glial cells found in the PNS (Rasband, 2016). Whereas satellite glia are found within ganglia in close association with neuronal cell bodies, Schwann cells are found in close contact with axons in peripheral nerves. Both Schwann cells and satellite glia derive embryologically from the neural crest, which comprises multipotent cells migrating away from the dorsal neural tube (Nitzan *et al.*, 2013).

Neural crest cells differentiate into Schwann cell precursors, which migrate and proliferate along tracts of axons that have already extended into the periphery. Schwann cell precursors then embark on a process of cellular differentiation into immature Schwann cells to eventually become either myelinating or nonmyelinating (Remak) Schwann cells (Jessen *et al.*, 2015) (figure 3). Only large-diameter axons, which conduct impulses at the highest speed, become myelinated. Myelinated nerve fibres consist of a single axon that is enveloped by Schwann cells. The Schwann cell membranes wrap around the nerve fibre to form a multilaminated myelin sheath. Small-diameter axons are surrounded by nonmyelinating Schwann cells, forming Remak bundles (Campana, 2007).

Figure 3. The Schwann cell lineage. The embryonic phase of Schwann cell development involves three transient cell populations: migrating neural crest cells, Schwann cell precursors and immature Schwann cells. All these cells are considered to have the same developmental potential, and their fate is determined by the axons with which they associate. Schwann cells that envelop large-diameter axons will be induced to myelinate, while those cells that ensheath small-diameter axons progress to become mature non-myelinating cells. Image taken from Jessen and Mirsky (2016).

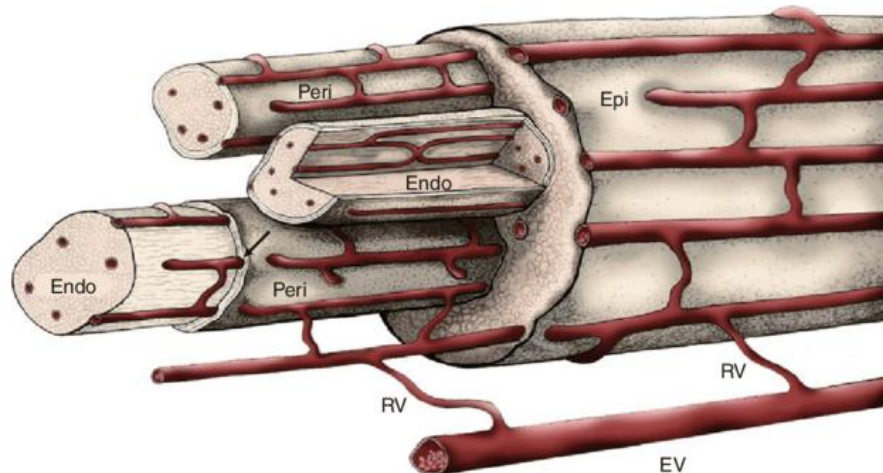


Schwann cells are able to undergo phenotypic modulation in order to support the axons they are associated with. This is most notable after peripheral nerve injury (Zhang *et al.*, 2017). The myelin and non-myelin (Remak) Schwann cells distal to the nerve injury site undergo an extensive change in gene expression, resulting in a change in function from myelinating axons to facilitating nerve regeneration (Jessen and Mirsky, 2016).

2.1.3 Vasculature

Peripheral nerves have a unique vascular network due to their anatomical compartmentalisation (Ubogu, 2013). This vascular network, the vasa nervorum, consists of two separate, functionally independent, but anastomosing, systems: an extrinsic epineurial system and an intrinsic endoneurial system (Wigley, 2008) (figure 4).

Figure 4. The vasa nervorum. The circulation of peripheral nerves derives from regional extrinsic vessels (*EV*) which give rise to branch radicular vessels (*RV*) that supply the intrinsic circulation of the vasa nervorum. The intrinsic circulation consists of longitudinally oriented vessels that run through the epineurium (*Epi*), down to the perineurium (*Peri*) and join with vessels in the endoneurium (*Endo*) via transperineurial connections (*arrow*). Image taken from Mizisin and Weerasuriya (2011).



The extrinsic system is composed of small arteries and veins from neighbouring tissue space and muscular blood vessels, which run parallel along peripheral nerves (Gao *et al.*, 2013a). The epineurial blood vessels lack tight junctions, have numerous fenestrations and are highly permeable. These vessels therefore provide nutrients, oxygen and blood flow to the intrinsic vascular system (Ubogu, 2013). The endoneurial microvasculature consists of tight junction-forming endothelial cells that, together with the perineurium, form the blood nerve barrier. This restricts the passive diffusion of macromolecules and cell entry from the blood circulation, and maintains the stability of the endoneurial microenvironment (Ubogu, 2013).

Structural and functional changes in the blood-nerve barrier are thought to be involved in the pathogenesis of peripheral neuropathies. Therefore, re-establishing blood-nerve barrier function may enhance peripheral nerve regeneration after injury by restoring the endoneurial microenvironment needed for axonal regeneration, remyelination and signal transduction (Ubogu, 2013).

2.2 Peripheral nerve injury

2.2.1 Incidence and aetiology

As the PNS lies primarily outside the skull and vertebral column, it is prone to damage from trauma. Consequently, peripheral nerve injuries (PNIs) are common and are reported in approximately 3% of all trauma patients, increasing to 5% if plexus and root avulsion cases are included (Taylor *et al.*, 2008). Scholz *et al.* (2009) reported that 81% of PNIs occur in the upper extremities, 11% in the lower extremities and the remaining 8% in other locations. The incidence of PNI is estimated to be between 13 and 23 per 100,000 persons per year in the developed countries (Li *et al.*, 2014). However, the incidence of PNI is thought to be largely underestimated (Rodrigues *et al.*, 2012), principally due its diverse aetiology and subsequent intervention from different clinical disciplines (Pfister *et al.*, 2011). Retrospective studies by Kouyoumdjian (2006) and Eser *et al.* (2009) have revealed that PNI is predominantly reported in young men of working age, which has considerable social and economic impacts (Shen and Wang, 2014).

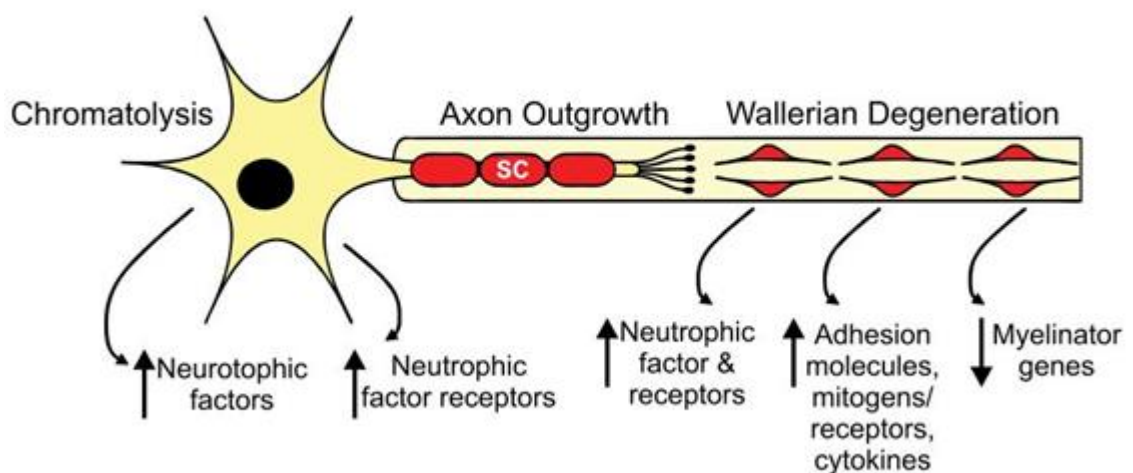
Traumatic injuries, such as collisions, motor vehicle accidents, gunshot wounds, fractures and lacerations, are the most common causes of PNI (Mukhatyar *et al.*, 2009). Stretch-related injuries are the most frequently encountered form of PNI (Campbell, 2008). Although peripheral nerves are viscoelastic because of their collagenous endoneurium, injuries can still occur if they are exposed to large strain rates (Burnett and Zager, 2004). Lacerations are another common cause of PNI (Campbell, 2008). Whereas complete transections can occur following a laceration, partial nerve continuity usually remains (Burnett and Zager, 2004). Compression is another frequently encountered cause of PNI (DeLisa *et al.*, 2005). These injuries do not involve a tearing of the neural elements and are generally reversible (Burnett and Zager, 2004). Other causes of PNI include diabetes (Callaghan *et al.*, 2012), Guillain-Barré syndrome (van den Berg *et al.*, 2014), compression syndromes (Keir and Rempel, 2005), cancer (Antoine and Camdessanché, 2007) and surgery (Kömürcü *et al.*, 2005).

2.2.2 Pathophysiology

2.2.2.1 Neuronal response

After PNI, the proximal and distal stumps of the injured nerve undergo structural and molecular changes (Menorca *et al.*, 2013) (figure 5). Within an hour of injury, dieback in both the proximal and distal stumps is mediated by channel-mediated calcium influx and activation of calpains that cleave neurofilament and microtubular-associated components such as tubulin (Sulaiman and Gordon, 2013). This stage is followed by a longer period of disassembly of cytoskeletal proteins by calcium-activated calpains and the ubiquitin-proteasome system (Zhai *et al.*, 2003).

Figure 5. Regenerative response after nerve injury. After injury, regeneration-associated genes are transiently upregulated in the neurons while genes associated with normal synaptic transmission are downregulated. Wallerian degeneration occurs in the distal nerve stump, creating a microenvironment conducive to axonal regrowth. Image taken and adapted from Sulaiman *et al.* (2013).



Proximal stump

The cell body in the proximal nerve stump undergoes chromatolysis within hours of the injury. This is characterised by the loss and dispersion of the Nissl bodies (Geuna *et al.*, 2009), enabling changes in gene expression that lead to a decrease in the synthesis of neurotransmission-related proteins (such as choline acetyltransferase, acetylcholinesterase and neurofilament) and an increase in the synthesis of neuronal growth-associated proteins (such as cytoskeletal proteins and neurotrophic factors) (Deumens *et al.*, 2010). Axotomized neurons are thus characterised by a shift from a

“transmitting” state to a “regenerative” state (Navarro *et al.*, 2007). Additionally, each injured axon produces a great number of collateral and terminal sprouts. Continuous pruning of misguided axons occurs and those that remain begin the process of elongation through the distal nerve stump (Menorca *et al.*, 2013). Long Schwann cell processes have been observed proceeding in front of the regenerating axons in the proximal stump and these processes allow axon extension across the nerve bridge following a transection injury (Dun and Parkinson, 2015). The initial stage of axonal regeneration is sustained by both the availability of locally produced cytoskeletal materials (Sulaiman and Gordon, 2013) as well as anterogradely transported cytoskeletal proteins. Axon regeneration proceeds at a rate of 1-3 mm/day (Gordon and English, 2016), the rate corresponding with the rate of transport of the cytoskeletal materials (Sulaiman and Gordon, 2013). This slow rate of regeneration implies that re-establishment of a functional motor unit may be delayed, resulting in chronic muscle denervation and atrophy (Romeo-Guitart *et al.*, 2017).

Distal stump

Immediately after PNI, the distal segment begins to undergo Wallerian degeneration (Geuna *et al.*, 2009). This process involves myelin breakdown, proliferation of Schwann cells and recruitment of macrophages (Raimondo *et al.*, 2011). Myelinophagy, a form of selective autophagy, is an important mechanism by which Schwann cells initiate the degradation of myelin proteins and lipids after nerve injury (Gomez-Sanchez *et al.*, 2015). Macrophages are also recruited to phagocytose the myelin and cellular debris in order to clear the inhibitory factors released (Hirata and Kawabuchi, 2002). Additionally, proliferating Schwann cells form columns, termed bands of Bungner, which selectively guide regrowing axons from the proximal stump (Ribeiro-Resende *et al.*, 2009). Further elongation and regeneration through the distal nerve stump are dependent on the bands of Bungner (Allodi *et al.*, 2012). Thus, Wallerian degeneration serves to create a microenvironment that favours axonal regrowth distal to the injury site (Allodi *et al.*, 2012).

2.2.2.2 Schwann cell response

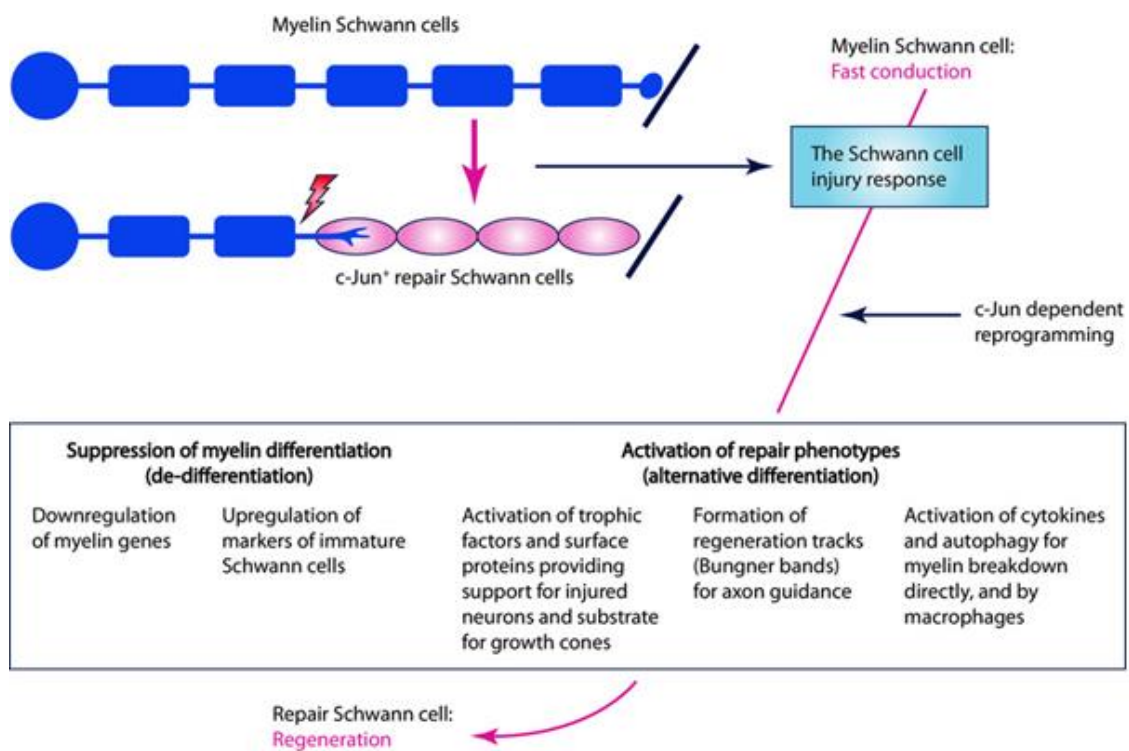
Loss of axonal contact following PNI causes Schwann cells within the distal stump to transdifferentiate to a pro-regenerative phenotype (Kim *et al.*, 2013). Schwann cells lose their differentiated morphology, downregulate myelin genes (such as *MPZ* and *MBP*), upregulate markers of immature Schwann cells and re-enter the cell cycle. They also upregulate genes implicated in promoting axon growth, neuronal survival and macrophage invasion. Thus the expression of neurotrophic factors (such as nerve growth factor, brain-derived neurotrophic factor, and glial-derived neurotrophic factor), their receptors (such as p75, GFRA-1, GFRA-2) and adhesion molecules (such as neural-cell adhesion molecule) is increased. Schwann cells also activate mechanisms to break down their myelin sheaths and transform morphologically into cells with long, parallel processes, forming the bands of Bungner, which guide regenerating axons (Arthur-Farraj *et al.*, 2012).

Schwann cells play a major role in the removal of the axonal debris. They also secrete chemoattractant factors, such as monocyte chemoattractant protein-1, which recruit macrophages into the denervated distal nerve stumps where they phagocytose remaining axon and myelin debris. The axon debris releases mitogens that promote mitotic Schwann cell division. It also results in the upregulation of cytokines and transcription factors that stimulate myelin breakdown and macrophage invasion (Sulaiman and Gordon, 2013).

Arthur-Farraj *et al.* (2012) used mice with selective inactivation of the transcription factor c-Jun in Schwann cells to show that c-Jun is a global regulator of the Schwann cell injury response (figure 6) that specifies the characteristic gene expression, structure and function of the denervated Schwann cell. c-Jun determines the expression of trophic factors, adhesion molecules, the formation of the bands of Bungner, myelin clearance and controls the distinctive regenerative potential of peripheral nerves. This was further corroborated by Hung *et al.* (2015), who used ChIP-sequencing to measure changes in histone H3K27 acetylation, a mark of active enhancers, to identify injury-induced enhancers in rat peripheral nerves following injury. Hung *et al.* (2015) also suggested

that other transcription factors, in addition to c-Jun, maintain active enhancer status after nerve injury. Epigenomic changes may thus mediate the effects of transcription factors that control Schwann cell responses following PNI. The extracellular-regulated kinase 1/2 pathway (Harrisingh *et al.*, 2004), Pax-3 (Doddrell *et al.*, 2012) STAT3 (Benito *et al.*, 2017) and Sox2 (Roberts *et al.*, 2017) have also been shown to be involved in Schwann cell injury response.

Figure 6. The Schwann cell injury response. Nerve injury triggers the conversion of myelinating and Remak Schwann cells to a cell phenotype specialised to promote repair. These repair Schwann cells provide the necessary signals and spatial cues for axonal regeneration. Image taken from Jessen and Mirsky (2016).



After prolonged denervation, Schwann cells stop maintaining the bands of Büngner and the basal lamina tubes break down and disappear (Scheib and Höke, 2013). Besides these structural changes, the upregulation of neurotrophic factors and their receptors induced by Schwann cells after injury is not maintained and declines (Hall, 2005). By 6 months in experimental animals, expression has been noted to decrease, thereby losing the growth-supportive environment for regenerating axons. This time-limited upregulation of genes supports the view that nerve repair should not be delayed following injury (Hall, 2005).

2.2.3 Clinical peripheral nerve repair

2.2.3.1 Types of injury

Seddon (1943) described three types of nerve injuries, namely neurapraxia, axonotmesis and neurotmesis. Neurapraxia is the mildest type and causes temporary conduction block without disruption of the axon or perineurium. Clinically, it results in sensory dysfunction. Recovery may occur within hours up to twelve weeks. Axonotmesis leads to axonal loss without disruption of the connective tissue layers, leading to motor and/or sensory dysfunction. Decreased nerve conduction velocity and regional muscle denervation occur. Neurotmesis is the most severe nerve injury and causes disruption of both the axon and connective tissue, resulting in compromised sensory and functional recovery. Conduction is not observed and spontaneous recovery is extremely unlikely without surgical intervention (Kaya and Sarikcioglu, 2014).

Sunderland (1951) further stratified the three injury types described by Seddon (1943) into five categories according to severity (table 1). A first-degree injury is equivalent to Seddon's neurapraxia and a second-degree injury is equivalent to axonotmesis. Third-degree nerve injuries occur when there is disruption of the axon (axonotmesis) and also partial injury to the endoneurium. Functional recovery may be possible depending on the extent of endoneurial damage. Sunderland divides Seddon's neurotmesis into fourth- and fifth-degree injuries. In a fourth-degree injury, all portions of the nerve are disrupted except the epineurium. A fifth-degree injury involves complete severance of the nerve. Recovery for fourth- and fifth-degree injuries is not possible without surgical intervention (Burnett and Zager, 2004).

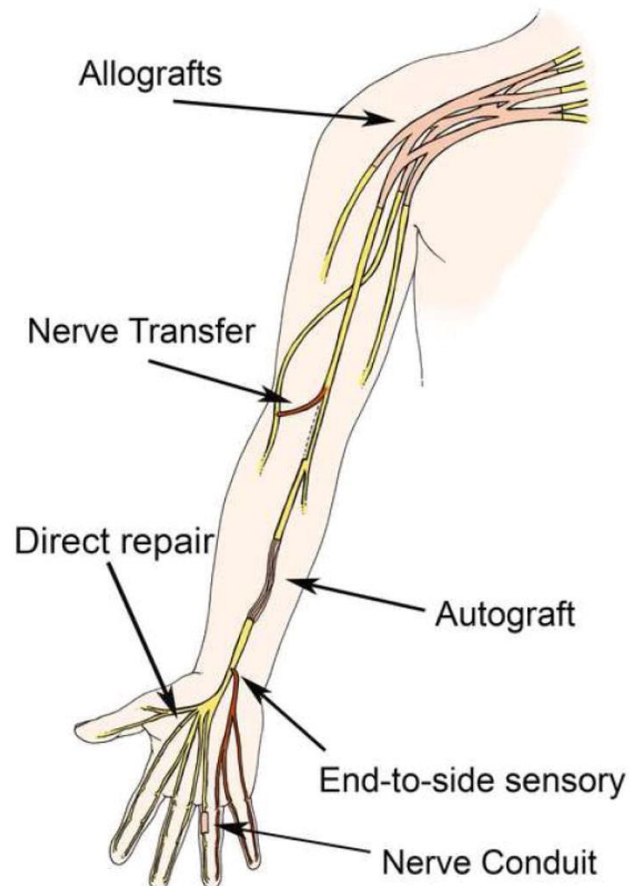
Table 1. Seddon and Sunderland classifications for peripheral nerve injuries. Taken and adapted from Mitchell *et al.* (2017).

Seddon	Sunderland	Injury type
Neurapraxia	I	Intrafascicular oedema with conduction block, possible segmental demyelination
Axonotmesis	II	Severed axon, intact endoneurium
	III	Severed axon, disruption of endoneurium
	IV	Disruption of endoneurium and perineurium
Neurotmesis	V	Complete nerve discontinuity

2.2.3.2 Surgical interventions

Unlike the adult CNS, the PNS has an intrinsic, albeit limited, ability to spontaneously regenerate after injury (Huebner and Strittmatter, 2009). However, despite this and improvements in surgical techniques for nerve repair (figure 7), functional restoration in patients is often incomplete (Rochkind and Nevo, 2014). This sub-optimal recovery is mainly associated with chronic axotomy, chronic Schwann cell denervation or severe damage of endoneurial tubes that inhibits the regenerative process. Muscular denervation often occurs secondary to the injury of the corresponding peripheral nerve and is a consequence of neurogenic atrophy and structural fibrosis (Alvites *et al.*, 2018). The clinical outcome following a peripheral nerve injury is largely dependent on the amount of cellular damage, the site of the lesion, the degree of disruption of the connective-tissue elements surrounding the nerve, the extent of associated injuries, particularly vascular injuries and the age and health of the patient (Hall *et al.*, 2005).

Figure 7. Surgical interventions for nerve repair. Nerve allografts are used for large, otherwise irreparable injuries. Nerve transfer use redundant nerve fibres for a proximal nerve injury. The autograft is used to reconstruct a nerve gap. Direct repair is used when there is no intervening nerve gap to create tension. Both end-to-side and nerve conduits are used for noncritical sensory injuries. Image taken from Ray and Mackinnon (2010).

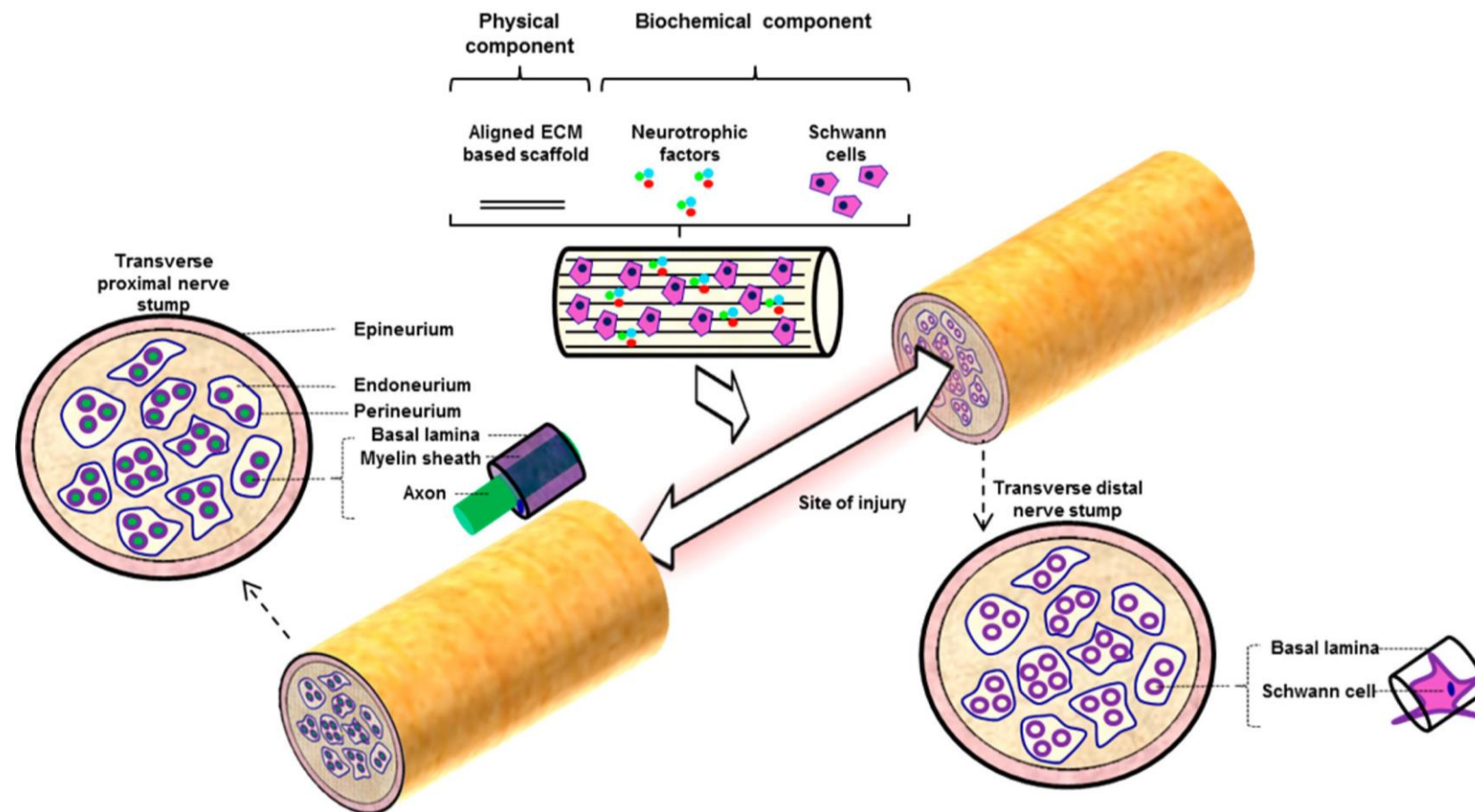


Several factors influence the choice of treatment following a peripheral nerve injury. These include the width of the nerve gap, the length of elapsed time from injury to treatment, the patient's age and comorbidities affecting the nervous and circulatory systems. Treatment options include a direct epineurial and/or group fascicular end-to-end repair or bridging the nerve defect with an autograft, allograft or nerve conduit (Gaudin *et al.*, 2016). Direct repair is only useful in small gaps since tension across the suture lines is known to inhibit regeneration, possibly due to impaired activation of Schwann cells and a higher amount of apoptotic Schwann cells (Yi and Dahlin, 2010). Further, epineurial repairs can increase the local pro-inflammatory innate immune response and tissue remodelling that results in scar tissue (Ren *et al.*, 2018). The current clinical gold standard treatment for nerve damage that extends over a few centimetres in length is the autologous nerve graft (Patel *et al.*, 2018). When a large gap cannot be repaired by anatomic reconstruction, other means of functional

reinnervation, such as nerve transfers or end-to-side coaptations, may be used. These procedures are currently limited to cases without other reconstruction options (Battiston *et al.*, 2017).

The autologous nerve graft (figure 8) bridges the nerve gap and provides a physical scaffold over which axonal outgrowth may occur. Furthermore, it supplies Schwann cells necessary for regeneration. However, it is also associated with several disadvantages. Autografts sacrifice a functioning nerve and may result in sensory loss, scarring and neuroma formation at the donor site (Battiston *et al.*, 2017). Additionally, size and fascicle mismatch, scarring and fibrosis may occur at the repair site, leading to poor regeneration (Grinsell and Keating, 2014).

Figure 8. The autologous nerve graft. For effective peripheral nerve repair, the gap resulting from injury must be structurally bridged to promote correct reinnervation and functional regeneration. The autologous nerve graft is the gold standard for gaps extending over a few centimetres in length. It provides autologous Schwann cells, aligned connective tissue as well as neurotrophic factors. Image taken from Lackington *et al.* (2017).



Cadaveric nerve allografts are abundantly available and allow size/length and motor/sensory matching. They contain both Schwann cells and the endoneurial microstructure provided by nerve autografts and support repair in the absence of sufficient autologous material (Moore *et al.*, 2011). However, they require long-term use of immunosuppressant therapy that increases the risk of infection (Daly *et al.*, 2012). In order to ensure immunotolerance, there has been an increased interest in processing nerve allografts to render them acellular while still maintaining the supportive 3D endoneurial microstructure (Thompson *et al.*, 2017).

In 2015, AxoGen received Food and Drug Administration (FDA) approval for Avance® Nerve Graft, an off-the-shelf processed human nerve allograft manufactured from donated human peripheral nerve tissue. The tissue undergoes detergent processing to selectively remove cellular components and debris and is terminally sterilised (Moore *et al.*, 2011). Brooks *et al.* (2012) reported that in a study of 76 nerve injuries in humans, the use of Avance® yielded results comparable to those reported in the literature for nerve autografts and more favourable results than those reported for nerve conduits. Despite the evidence in support of acellular allografts, the gap length over which this technology remains effective has not been established. This is because acellular allografts lack Schwann cells that are essential for nerve repair. It has been shown in animal models, that following implantation, *in vivo* host Schwann cells from the connecting nerve stumps migrate into the graft (Hayashi *et al.*, 2007). However, populating long acellular allografts places a proliferative demand on host Schwann cells, which may lead to stress and Schwann cell senescence (Saheb-Al-Zamani *et al.*, 2013). This Schwann cell senescence is thought to be the limiting factor to axonal regeneration in acellular nerve allografts (Thompson *et al.*, 2017).

Nerve guidance conduits constructed of natural or synthetic materials have been developed to eliminate the donor site morbidity and immunosuppressant therapy requirement associated with nerve autografts and allografts, respectively (Daly *et al.*, 2012). The FDA has approved several nerve guidance conduits used to repair nerve defects (Kehoe *et al.*, 2012) (table 2). According to Dixon *et al.* (2018), nerve guidance conduits should exhibit the following properties:

- Mechanical support to keep the proximal and distal nerve ends aligned
- Porosity to allow the diffusion of nutrients and waste
- Low immunogenicity to limit the inflammatory response
- Biodegradability to eliminate the need for secondary surgery for removal and to prevent the occurrence of nerve compression.

Additionally, nerve guidance conduits should prevent fibrous tissue ingrowth into the injury site to reduce scarring and retain neurotrophic factors secreted by Schwann cells and nerves (Kehoe *et al.*, 2012). Even with optimised biomaterial characteristics, hollow nerve guidance conduits do not achieve functional recovery equivalent to nerve autografts and have been unsuccessful in repairing defects over 3 cm in length (Dixon *et al.*, 2018).

Table 2. Examples of FDA approved nerve guidance conduits.

Product	Company	Material	Structure	FDA-approval	Treated nerves in humans	Study size	Outcome	Reference
NeuroTube®	Synovis Micro Companies	Polyglycolic acid	Bioabsorbable, tight-weave mesh rolled into a 2-mm diameter tube	1999	Digital nerves	98 patients	Resulted in improved sensation compared with end-to-end repair and nerve grafts for deficits <3 cm in length	Weber <i>et al.</i> , 2000
NeuraGen®	Integra LifeSciences Co.	Bovine type I collagen	Semipermeable, fibrillary tube of varying calibre	2001	Digital nerves and large-calibre nerves	96 patients	Resulted in sensory recovery in the 35–45% range	Wangensteen and Kalliainen, 2010
Neurolac®	Polyganics Innovations	Poly (DL-lactide-ε-caprolactone)	Synthetic transparent tube	2003	Nerves in the arm and hand	23 patients	Did not result in overall favourable outcomes in repairing hand nerve defects	Chiriac <i>et al.</i> , 2012
NeuraWrap™	Integra LifeSciences Co.	Bovine type I collagen	Porous conduit with a longitudinal slit in wall	2004	Median nerve	10 patients	Patients showed improvement of clinical symptoms	Kokkalis <i>et al.</i> , 2016
SaluTunnel™	Salumedica LLC	Polyvinyl alcohol	Nonresorbable hydrogel	2010	No information to date			Gaudin <i>et al.</i> , 2016

2.3 Regenerative medicine for peripheral nerve repair

According to Faroni *et al.* (2015), a purely microsurgical approach to nerve repair does not address the complex cellular and molecular events of peripheral nerve regeneration. This highlights the need for new therapeutic strategies that will maximise functional nerve regeneration and improve patient outcomes. The UK Medical Research Council (2017) defines regenerative medicine as “an interdisciplinary approach that seeks to repair or replace damaged or diseased human cells or tissues to restore normal function”. It encompasses several fields, including but not limited to soluble molecules, gene therapy, stem cell transplantation, tissue engineering and reprogramming of cell and tissue types (Greenwood *et al.*, 2006).

2.3.1 Tissue engineering

Tissue engineering aims to produce tissue replacement material purposely tailored to promote repair and regeneration at the implant site (Carletti *et al.*, 2010). In the context of peripheral nerve regeneration, tissue engineering can be used to produce devices consisting of a biomaterial-based structure as well as an array of cellular and/or molecular components which increase their regenerative potential (Gu *et al.*, 2014).

2.3.1.1 Conduits

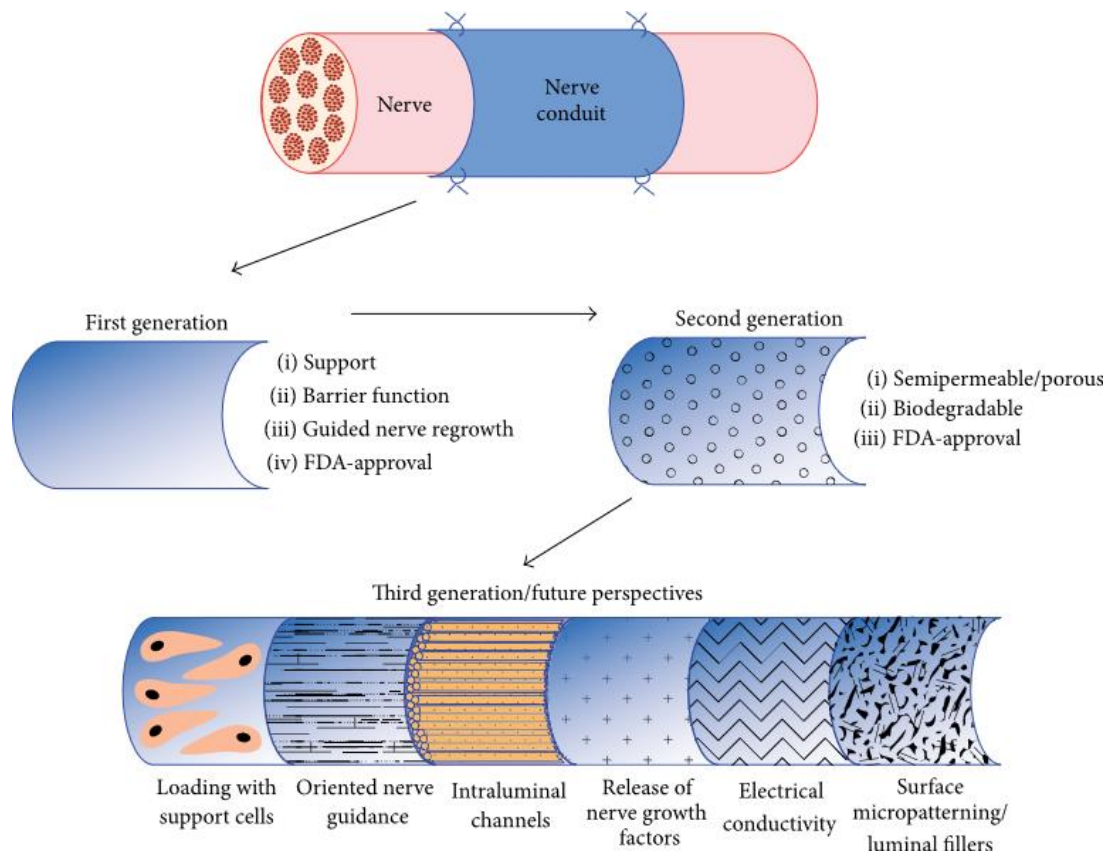
Conduits represent the space available for the tissue to develop and provide the physical support for cell growth (Carletti *et al.*, 2010). Conduits can be manufactured from a range of natural and synthetic materials. The materials used for nerve repair devices confer different physical properties that may influence repair (de Ruitter *et al.*, 2009). Synthetic materials have advantages such as a defined chemical composition and mechanical properties that can be fine-tuned (Knight and Przyborski, 2015). However, synthetic materials often lack sites for cellular adhesion. This may require coating the surface of the scaffold with ECM proteins, such as laminin or fibronectin, in order to provide a suitable environment for the cells (Subramanian *et al.*, 2009).

The main synthetic material used in early nerve repair devices was silicone (Braga-Silva, 1999). Silicone is non-degradable and can provoke a foreign body response, leading to inflammation and scarring (de Ruiter *et al.*, 2009) and can potentially cause nerve compression (Dahlin and Lundborg, 2001). It also requires surgical removal from the implant site after nerve repair occurs (Belanger *et al.*, 2016). Biodegradable synthetic polymers, including aliphatic polyesters, poly(phosphoesters), polyurethanes, piezoelectric polymers and some electrically conducting polymers are being investigated (Gu *et al.*, 2014).

Natural materials are often based on various components of the ECM such as collagen (Klein *et al.*, 2016) and fibrin (Pettersson *et al.*, 2010) but can also include other naturally derived materials such as alginate (Novikova *et al.*, 2006), silk (Wang *et al.*, 2018) and chitosan (Meyer *et al.*, 2016). Natural materials are an attractive source of material for tissue engineering as they are biocompatible, biodegradable and contain cell adhesion sites (Knight and Przyborski, 2015). Despite their advantages, clinical-grade sources of natural materials can be challenging to obtain and they tend to exhibit batch-to-batch variation. There are also limitations associated with controlling their mechanical properties. Additionally, biodegradation of natural materials may be difficult to control and may influence cell activity in unknown ways (Knight and Przyborski, 2015).

Current (first and second generation) nerve guidance conduits have yet to reach similar efficacy to the nerve autograft. However, there has been considerable interest in the development of a third generation of conduits to enhance nerve regeneration (Lin *et al.*, 2013) (Figure 9). According to Gaudin *et al.* (2016), experimental third generation conduits incorporate controlled release of neurotrophic factors, electroconductive material, therapeutic cells, surface micropatterning or luminal fillers serving as guidance structures. The use of neurotrophic factors, therapeutic cells and luminal fillers will be discussed in subsequent sections.

Figure 9. Generations of nerve conduits. Efforts are being made to develop artificial nerve guidance conduits to replace autografts. Several first- and second-generation conduits have regulatory approval while third-generation conduits are currently still in experimental stages. Third generation conduits attempt to mimic the features of a natural nerve and may include neurotrophic factors, cells and ECM molecules. Image taken from Gaudin *et al.* (2016).



2.3.1.2 Luminal fillers

Regenerating axons develop growth cones that explore and recognise growth and guidance cues within the surrounding environment. Growth cone adhesion and attachment to a solid surface is required for axon growth. Thus, the microarchitecture of the conduit interior is thought to be crucial for promoting regeneration across a gap (Sarker *et al.*, 2018). Filling hollow conduits with a substrate that supports axonal growth may enhance the regenerative process (Ezra *et al.*, 2016). The use of polysaccharides, ECM molecules, proteins and peptides to prepare a hydrogel matrix for use in hollow conduits has been documented (Carballo-Molina and Velasco, 2015). ECM proteins such as fibrin, laminin and collagen contain attachments sites that can be used by advancing axonal growth cones. The inclusion of these proteins can thus promote directional growth of axons, leading to improved nerve regeneration (Sarker *et al.*, 2018). Further,

the degradation products of ECM based materials have been demonstrated to be bioactive and chemotactic for Schwann cells (Prest *et al.*, 2018).

Around 90% of nerve ECM is composed of type I collagen, making this material a popular choice for nerve tissue engineering (Gao *et al.*, 2013b). Wei *et al.* (2013) implanted a silicone conduit filled with type I collagen into a rat model of sciatic nerve injury (10 mm gap). Compared to animals that received physiological saline as a negative control, animals that received type 1 collagen had an increased number of myelinated axons and improved electrophysiological outcomes after 8 weeks. The findings of this study were corroborated by Maturana *et al.* (2013), who reported that polycaprolactone conduits filled with a collagen matrix resulted in superior axon suprastructural organisation compared to nerve autografts and empty polycaprolactone conduits 60 days following a sciatic nerve transection in a rat model (6 mm gap).

In the early stages of peripheral nerve regeneration in a hollow conduit, Williams *et al.* (1987) noted the formation of an acellular fibrin cable between the proximal and distal stumps. Schwann cells, fibroblasts and endothelial cells then migrated into the nerve gap from both nerve stumps and aligned along the fibrin cable, guiding subsequent axonal regeneration from the proximal to the distal end. Inspired by this finding, several authors have investigated the effect of filling hollow conduits with longitudinally aligned fibrin in order to accelerate the regenerative process. Du *et al.* (2017) implanted a chitosan conduit filled with a 3D aligned fibrin nanofiber hydrogel into a rat model of sciatic nerve injury (10 mm gap). This device was found to support Schwann cell cable formation, accelerate axonal regrowth and improve motor functional recovery after 12 weeks. Morphological analysis and electrophysiological examination revealed regenerative outcomes that were comparable to those achieved by autologous nerve grafts and superior to hollow chitosan tubes or chitosan tubes filled with random fibrin nanofiber hydrogel. Similar results were previously reported by Nakayama *et al.* (2007).

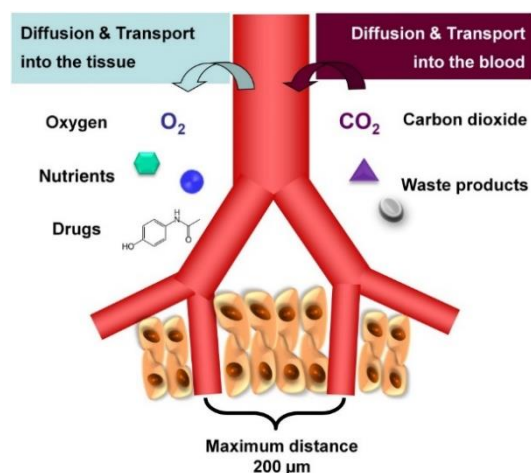
As shown in the study by Du *et al.* (2017), the longitudinal alignment of ECM based material in a nerve conduit may further enhance axonal regeneration. This is because aligned ECM can support and guide regenerating neurites from the proximal to the distal side of the repair site (de Rooter *et al.*, 2009). Additionally, failure to recreate the aligned

ECM architecture limits clinical repair and reconstruction, often leading to scarring and poor restoration of mechanical properties (Brown and Phillips, 2007). Several approaches have been used to produce aligned ECM architecture in nerve conduits, including the use of aligned fibres (Kim *et al.*, 2016) or channels (Sridharan *et al.*, 2015), magnetic or electrical fields (Gessmann *et al.*, 2016) and patterned surfaces (Hoffman-Kim *et al.*, 2010).

2.3.1.3 Vascularisation

Vascularisation refers to the process by which blood vessels, especially capillaries, develop within a tissue. It is an essential factor which determines tissue viability as well as characteristics such as size, cell density, innervation and lymphatic supply of the tissue (Jeyaraj *et al.*, 2015). *In vivo*, living cells must be within 100–200 μm from a blood capillary in order to survive due to nutrient perfusion and mass transport limitations (Lovett *et al.*, 2009) (figure 10).

Figure 10. Schematic representation of the diffusion and transport processes in tissues *in vivo*. The blood supply provides tissues with oxygen and nutrients and removes waste products. However, the efficiency of this system is only maintained over a maximum distance of 200 μm . Image taken and adapted from Novosel *et al.* (2011).



Inadequate vascularisation is still a major limitation for the clinical application of tissue-engineered constructs (Novosel *et al.*, 2011; Jundziłł *et al.*, 2017). After implantation of tissue engineered constructs, a spontaneous vascularisation of the implant is usually

seen. However, vessel growth *in vivo* is a slow process and depends on host cells colonising the construct and building a new capillary network in response to angiogenic factors at the implant site. Further problems arise if the development of the capillary network is poorly organised, leaky and does not properly integrate with the host's vascular system (Avolio *et al.*, 2017). This induced vessel ingrowth is often too slow to provide adequate nutrient transport to the cells in the interior of the transplanted tissue and can lead to improper cell integration or cell death in tissue-engineered constructs. Additional strategies for enhancing vascularisation are therefore essential to ensure the survival of large tissue-engineered grafts (Rouwkema *et al.*, 2008). Moon and West (2008) suggested that vascularisation may be increased by the coordinated use of angiogenic factors, cells and biomaterials.

Two main strategies have been suggested to increase vascularisation in tissue engineered constructs (Laschke and Menger, 2012). The first approach involves the stimulation of angiogenesis by host endothelial cells that colonise the construct post-implantation. The physical characteristics of the construct as well as the incorporation of angiogenic factors (table 3) can serve to encourage host endothelial cell invasion. The second approach relies on the creation of prevascularised tissue engineered constructs *in vitro*. Once implanted, the pre-formed vascular network can inosculate with the host vasculature. This process can be facilitated by the manufacture of biomaterials able to guide the formation of new tubular structures (Avolio *et al.*, 2017).

Table 3. Angiogenic factors currently used in tissue engineering. Table adapted from Lovett *et al.* (2009).

Growth/signalling factor	Function	Disadvantages
Vascular endothelial growth factor	Most important family of cytokines in neovascularisation; initiator of endothelial capillary formation	Rapidly degraded due to short half-life; excessive amounts cause vascular leakage
Basic fibroblast growth factor	Heparin-binding protein; induces proliferation of endothelial cells; initiator of endothelial capillary formation	Rapidly diffuses, requires controlled release; mitogen for wide variety of cell types
Hepatocyte growth factor	Mitogen of hepatocytes and other various cell types; stimulates growth of endothelial cells	Short half-life, rapid diffusion; large amounts of protein required for response
Platelet-derived growth factor	Mitogen for connective tissue cells, released from platelets; promotes vessel maturation	High levels result in vessel destabilisation; increased activity linked with several diseases
Angiopoietin-1	Plays key regulatory role in regulating vessel homeostasis; promotes endothelial cell migration and stabilisation of newly formed capillaries	Overexpression induces endothelial hyperplasia and reduced vessel leakage

The delivery of angiogenic factors has resulted in a significant improvement of vascularisation in tissue-engineered constructs in several animal models (Chang and Niklason, 2017). In spite of promising results, there remain major challenges in angiogenic factor delivery namely, their inherent instability *in vitro* and *in vivo* and limited control over their spatial and temporal distribution (Jabbarzadeh *et al.*, 2008). Gene therapy has been proposed as an alternative to conventional protein delivery strategies and has demonstrated a significant improvement of biomaterial vascularisation *in vivo* (Iwaguro *et al.*, 2002; Qu *et al.*, 2011; Cucchiari *et al.*, 2016). This will be discussed in subsequent sections.

Vascularisation is especially important in the context of peripheral nerve tissue engineering. Cattin *et al.* (2015) reported that endothelial cells guide the regeneration of peripheral nerve axons, indicating a direct relationship between nerve regeneration and blood vessels. Following a nerve transection, the two stumps are connected by a tissue structure referred to as 'the bridge' that consists of a mixture of inflammatory

cells and ECM (Jurecka *et al.*, 1975). Macrophages in the area release VEGF-A, which induces vascularisation in the bridge region. These newly established blood vessels act as a guiding path to Schwann cells, allowing them to migrate across the bridge region. The physical surface of the blood vessel allows Schwann cells to efficiently migrate and form bands of Büngner that help axonal regeneration. Regenerating axons can then use the Schwann cells to migrate from the proximal stump through to the distal stump. Misdirection of blood vessels causes Schwann cells to migrate into surrounding tissues and blood vessels have been shown to be essential to direct the migration of Schwann cells (Cattin *et al.*, 2015).

2.3.2 Cell therapy

In addition to the use of aligned ECM luminal fillers, several authors have investigated the use of cells in nerve guidance conduits to further enhance regeneration (McGrath *et al.*, 2018). Studies have shown that tissue engineered constructs seeded with Schwann cells can enhance axonal regeneration in animal models (Mosahebi *et al.*, 2002). These cells create an environment conducive to axon regeneration through the secretion of neurotrophic factors and the production of ECM molecules. However, the routine clinical use of Schwann cells is limited as their isolation requires invasive biopsies and they display limited *in vitro* expansion capability (Gu *et al.*, 2014). Therefore, one of the goals of peripheral nerve regenerative medicine is to identify therapeutic cell types that could act as supporting cells in a tissue engineered construct.

Kabiri *et al.* (2015) proposed olfactory ensheathing cells as a viable cell type for peripheral nerve engineering. Scaffolds seeded with olfactory ensheathing cells have been successfully employed in a rat model of sciatic nerve injury (10 mm gap). Functional analysis and histological assessment at 9 weeks revealed results comparable with the nerve autograft group and superior to the cell-free scaffold group. Although promising results were reported in this study, there is limited data supporting the use of olfactory ensheathing cells following peripheral nerve injury. Further, aggravation of hyperalgesia following olfactory ensheathing cell transplantation in spinal cord injuries has been reported (Nakhjavan-Shahraki *et al.*, 2018).

Therapeutic benefits of stem cell therapy have been shown in several experimental models of peripheral nerve injury (Bhangra *et al.*, 2016). Different sources of stem cells have a potential application in PNI (Walsh and Midha, 2009; Lehmann and Höke, 2016). These include adipose derived stem cells (ADSCs) (Georgiou *et al.*, 2015; Sowa *et al.*, 2016), bone marrow stem cells (Mimura *et al.*, 2004; Ding *et al.*, 2010), umbilical cord stem cells (Matsuse *et al.*, 2010; Peng *et al.*, 2011), skin-derived precursor cells (Park *et al.*, 2012; Grochmal *et al.*, 2014), hair follicle stem cells (Lin *et al.*, 2011), dental pulp stem cells (Sanen *et al.*, 2017), induced pluripotent stem cells (Liu *et al.*, 2012), embryonic stem cells (Cui *et al.*, 2008; Ziegler *et al.*, 2011) and neural stem cells (O'Rourke *et al.*, 2018). As ADSCs and neural stem cells have been used in the current study, these two cell types will be discussed in more detail.

Adipose tissue is largely comprised of adipocytes as well as a smaller stromal vascular fraction which includes ADSCs (Mizuno *et al.*, 2012). These mesenchymal stem cells have been extensively studied as an adjunct to nerve repair (Bhangra *et al.*, 2016) and have also been differentiated into Schwann cell-like cells (di Summa *et al.*, 2010). di Summa *et al.* (2010) compared adult rat ADSCs and bone marrow stem cells, each differentiated to a Schwann cell-like phenotype, for the repair of a sciatic nerve injury in a rat model (10 mm gap, 2 weeks). The cells from both sources enhanced regeneration but, unlike bone marrow stem cells, ADSCs can be harvested less invasively with a higher yield, can be rapidly expanded *in vitro* and show low immunogenicity (Faroni *et al.*, 2013). Erba *et al.* (2010) investigated the effects of undifferentiated rat ADSCs in a poly-3-hydroxybutyrate nerve conduit on peripheral nerve regeneration as well as their ability to differentiate *in situ* in a rat sciatic transection model (10 mm gap, 2 weeks). While the ADSCs increased regeneration and Schwann cell proliferation compared to controls, a lack of viable implanted cells was observed 14 days of transplantation. Consequently, the authors were unable to detect any *in situ* differentiation of ADSCs into neuronal or glial cell types. Santiago *et al.* (2009) reported that the transplantation of human ADSCs in a rat sciatic nerve defect promoted nerve regeneration and a decrease in muscle atrophy, but that the ADSCs did not differentiate to Schwann cell-like cells at the site of injury. The results of these studies suggest that the regenerative effect of transplanted ADSCs is likely due to an initial release growth factors as well as an indirect effect on host Schwann cell activity. Further evidence for peripheral nerve regeneration through

the paracrine effects of ADSCs was presented by Kingham *et al.* (2014). Georgiou *et al.* (2015) used differentiated rat ADSCs to construct engineered neural tissue through a combination of cellular self-alignment and plastic compression in a collagen hydrogel. The sheets of aligned cellular collagen supported axon regeneration over a critical length gap (15 mm, 8 weeks) in rat sciatic nerves. Interestingly, the phenotype of the cells changed when they were transferred to the 3D collagen environment from two-dimensional (2D) monolayers, with an increase in expression of key growth factors associated with the support of regeneration.

Neural stem cells have been isolated from both the embryonic and the adult central nervous system (Ernst *et al.*, 2014). Fu *et al.* (2011) used two recombinant mammalian vectors delivering the rat *GDNF* or *BDNF* genes to transfect adult mouse neural stem cells. The transfected cells were seeded onto poly(D,L-lactide) conduits and implanted into a rat model of sciatic nerve transection (15 mm gap). After 8 weeks, improved regeneration, myelination and functional recovery were observed in the animals treated with the transfected cells compared to those treated with untransfected cells. Liard *et al.* (2012) transplanted adult pig subventricular zone neural stem cells inside an autologous venous graft into a 30 mm femoral nerve gap in an adult pig model and reported improved functional recovery at 6 months compared to empty vein grafts. Post-mortem immunohistochemistry revealed that the transplanted cells survived inside the venous graft from 10 to 240 days and all displayed a neuronal phenotype. Further, the authors reported that neural stem cell transplantation resulted in activation of host Schwann cells. O'Rourke *et al.* (2018) implanted a clinically relevant human neural stem cell line (CTX0E03) in stable aligned sheets of cellular hydrogel within a collagen conduit into a 12 mm gap in a rat sciatic nerve. The nerve repair device supported growth of neurites and vasculature through the injury site and facilitated reinnervation of the target gastrocnemius muscle. The findings reported by the authors are significant, as the use of such a cell line could help overcome the limitations associated with the nerve graft or the culture of autologous cells.

A significant challenge that remains is the identification and selection of the most suitable stem cell source to enhance regeneration. The ideal cell should be easily

harvested from the patient to allow autologous therapy and prevent rejection. However, allogeneic sources may also provide a good alternative if a detrimental immunological response can be avoided. It should be readily expandable *in vitro* (Bhangra *et al.*, 2016), survive transplantation and engraft into the host tissues (Walsh and Midha, 2009). Further, it should exhibit similar phenotypic characteristics to Schwann cells and secrete factors required for peripheral nerve regeneration (Bhangra *et al.*, 2016). Additionally, in order to facilitate further opportunities to improve efficacy, it should be amenable to genetic modification (Busuttil *et al.*, 2017).

2.3.3 Gene therapy

Further to guiding axonal growth and providing support cells, nerve repair devices are also increasingly being used as a carrier for the delivery of substances which enhance the microenvironment following injury. Due to the short half-life of many of these substances as well as side effects when administered systemically, strategies for continuous local release have been developed. Acellular delivery systems include loaded crosslinked polymer scaffolds (Madduri *et al.*, 2010), incorporation of loaded microspheres into the scaffold (Kokai *et al.*, 2011) and mini osmotic pumps (Boyd and Gordon 2003). Neurotrophic factors may also be delivered naturally from cells seeded into the nerve conduits (Madduri and Gander, 2012). Further, genetically modified cells overexpressing neurotrophic factors have also been used to ensure a local and continuous release of substances required for peripheral nerve regeneration (Busuttil *et al.*, 2017). Gene therapy has also been used to transduce resident cells to overexpress neurotrophic factors (Pfister *et al.*, 2007).

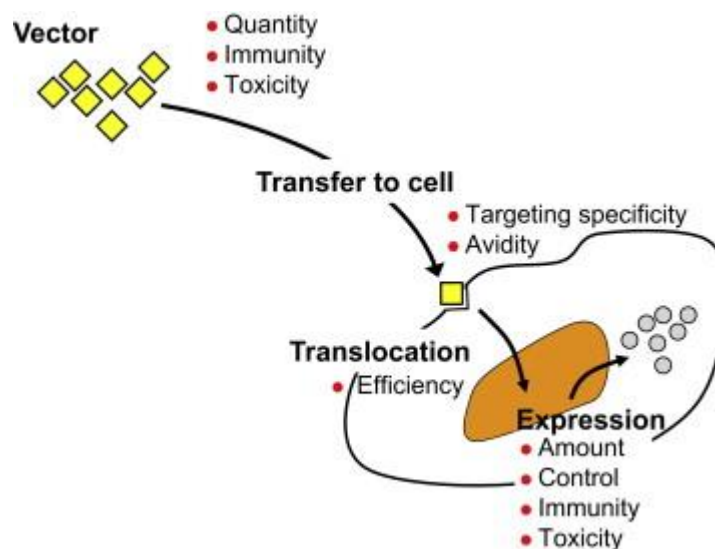
Gene therapy can be defined as the treatment of a medical disorder by the delivery of therapeutic nucleic acids into the relevant cellular targets. Gene therapy has been primarily associated with correcting the consequences of specific gene mutations in inherited diseases (Nayerossadat *et al.*, 2012). However, it can also be utilised to reprogram cells in other contexts, one of which is peripheral nerve repair (Hoyng *et al.*, 2015a). Gene therapy is unique in its ability to correct the underlying pathological mechanism of a disease process with prolonged benefits (Mohan *et al.*, 2013). Thus gene therapy could provide the damaged nerve with the prolonged regenerative support

necessary for repair. The success of gene therapy can be attested by a number high profile life-saving or life-changing clinical trials for haematological (Nathwani *et al.*, 2014; Negre *et al.*, 2016), immunological (Aiuti *et al.*, 2013; Castiello *et al.*, 2015), ophthalmic (Bainbridge *et al.*, 2015; Feuer *et al.*, 2016) and neurological conditions (Cartier *et al.*, 2009; Biffi *et al.*, 2013). These advances may become pertinent to translational research to enhance peripheral nerve repair (Busuttill *et al.*, 2017).

2.3.3.1 Gene delivery vectors

Eukaryotic cells have developed several mechanisms to prevent the entry of exogenous genetic material. These barriers include the hydrophobic plasma membrane, enzymes and the nuclear envelope. This presents a problem for efficient gene therapy, which is reliant on the delivery of genes to cells (figure 11).

Figure 11. Issues relating to successful gene delivery. In addition to the choice of vector, successful gene delivery is influenced by the quantity of vector needed and any toxicity or immunity that will limit its use. The vector has to be introduced into cells, which may require targeting specificity. Once inside the target cells, the vector's genetic payload needs to translocate to the nucleus where it is expressed. Gene expression may induce toxicity and may need to be controlled. Image taken from Worgall and Crystal (2014).



In order to circumvent the problems associated with delivering genes, gene delivery systems have been developed, with viral vectors proving to be the most efficient (de Winter *et al.*, 2013). Viral vectors result in a high rate of target cell transduction and transgene expression and recent advances have led to good safety profiles (Tannemaat

et al., 2008). Notably, around 70% of the gene therapy clinical trials for different conditions carried out so far have used viruses to deliver genes (Yin *et al.*, 2014). Further, the first licensed gene therapy product in Europe (Glybera[®]) involves an adeno-associated virus (AAV) vector for the treatment of lipoprotein lipase deficiency, indicating that viral vector-based gene therapy is becoming more relevant to translational research (Ylä-Herttuala, 2012). More recent developments in the field include the regulatory approval of Strimvelis[™], the first *ex vivo* autologous stem cell gene therapy to treat patients with severe combined immunodeficiency due to adenosine deaminase deficiency (Ylä-Herttuala, 2016), as well as FDA approval for Luxturna[®], which involves an AAV vector for the treatment of inherited retinopathies.

The efficiency of viral vectors can be attributed to the fact that viruses have developed mechanisms by which to infect cells and deliver their genetic cargo. In order to be used as a clinical tool, viral vectors have been genetically engineered to remove the pathogenic components as well as their ability to self-replicate. However, their ability to enter cells and deliver genes is preserved. Different viral vectors have been developed to target the diverse range of disease applications. These include adenovirus, adeno-associated virus, lentivirus and retrovirus (table 4). Ideal characteristics of a viral vector include the abilities to be reproducibly and stably produced, to be purified to high titres and to mediate targeted delivery and transgene expression without inducing harmful side effects (Thomas *et al.*, 2003).

Table 4. Characteristics of different viral vectors. Table taken from Chamcheu *et al.* (2015).

Vector	Packaging ability (kb)	Genetic material	Tropism	Vector genome form	Advantages	Disadvantages
Adeno-associated virus	<5	ssDNA	Dividing/non-dividing cells	Non-integrated (90 %), integrated (<10 %)	Non-inflammatory, non-pathogenic	Low production profile, low transduction efficiency, low packaging capacity
Adenovirus	7.5	dsDNA	Dividing/non-dividing cells	Non-integrated	Excellent transduction efficiency	High antigenicity, elicits immune response, transient gene expression
Lentivirus	8	RNA	Dividing/non-dividing cells	Integrated	High transduction efficiency, long term gene expression	Potential for random integration into host genome
Retrovirus	8	RNA	Dividing cells	Integrated	High transduction efficiency, long term gene expression,	Cannot transduce non-dividing cells, random integration into the host genome

Abbreviations: ss – single stranded; ds – double stranded.

2.3.3.2 *in vivo* gene delivery to Schwann cells and nerves

Successful *in vivo* gene delivery of various neurotrophic factors to the PNS in animal models has been reported with various vectors (Mason *et al.*, 2011) (table 5). Schwann cells are the main target cells for gene therapy in the injured peripheral nerve itself (de Winter *et al.*, 2013). As described in section 2.2.2.2, Schwann cells play a central role in peripheral nerve regeneration as they are responsible for secreting growth-promoting molecules, guiding the regenerating axons toward target organs and myelinating regenerated axons. However, the pro-regenerative properties of these cells can fade away after long periods of denervation (Jessen and Mirsky, 2016). Gene delivery to Schwann cells could be used to prevent down-regulation of genes associated with maintaining the repair phenotype and to keep the cells in their pro-regenerative state for a longer period of time. This makes gene therapy a potential adjuvant treatment in the reconstruction of peripheral nerves following injury.

Table 5. *In vivo* gene delivery targeting nerves and Schwann cells.

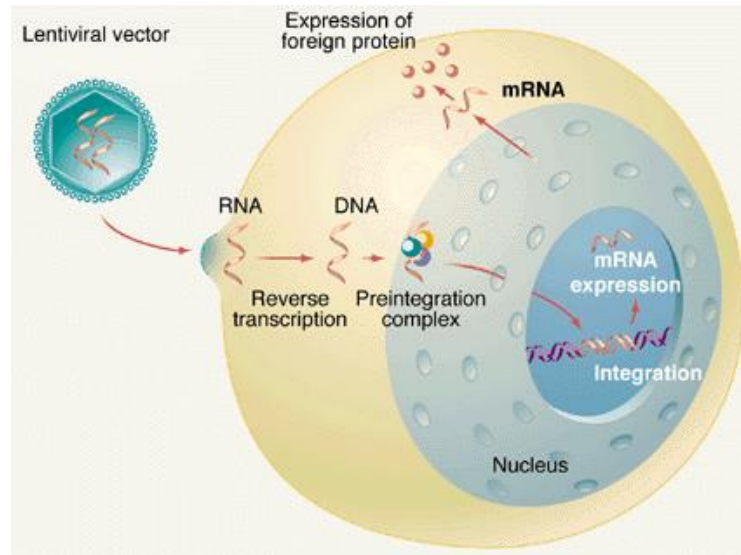
Author	Gene (s)	Vector	Mode of delivery	Animal model (length of gap, mode of repair, duration of experiment)	Outcome measures
Nikolaev <i>et al.</i>, 2014	<i>FGF2, VEGF</i>	Double-cassette plasmid	Direct injection of the vector into the sciatic nerve	Rat sciatic nerve transection, 5mm gap, poly(ϵ -caprolactone) conduit filled with fibrin hydrogel matrix, up to 30 days	Functional tests, number of myelinated fibres, immunochemistry
Cheng <i>et al.</i>, 2013	<i>CDNF</i>	Lentivirus	Direct injection of the vector into the sciatic nerve	Rat sciatic nerve transection, 3mm gap, silicone tube, up to 8 weeks	Gastrocnemius muscle weight, sciatic function index, immunohistochemistry, myelination
Hu <i>et al.</i>, 2010	<i>NGF</i>	Adenovirus	Direct injection of the vector into the femoral nerve	Rat femoral transection, 0.5 – 0.8 mm gap, silicone tube, up to 8 weeks	Retrograde tract tracing
Tsai <i>et al.</i>, 2010	<i>BMP7</i>	Adenovirus	Direct injection of the vector into the sciatic nerve	Rat sciatic nerve transection, immediate resuturing, up to 4 weeks	Behavioural tests, histological analysis
Tannemaat <i>et al.</i>, 2008	<i>NGF, GDNF</i>	Lentivirus	Direct injection of the vector into the sciatic nerve	Rat sciatic transection, immediate resuturing, up to 12 weeks	Behavioural tests, soleus and gastrocnemius muscle weight, number of neurites

Abbreviations: FGF2 - fibroblast growth factor-2; VEGF - vascular endothelial growth factor; CDNF - conserved dopamine neurotrophic factor; NGF - nerve growth factor; BMP7 - bone morphogenetic protein-7 ; GDNF - glial cell-derived neurotrophic factor.

2.3.3.3 *ex vivo* gene delivery for peripheral nerve repair

Hoyng *et al.* (2015b) compared the ability of AAV serotypes 1–9 and a lentivirus to transduce cultured rat and human Schwann cells and nerve segments. The AAV and lentiviral vectors were produced using an identical expression cassette that consisted of a cytomegalovirus promoter driving green fluorescent protein. The nine AAV serotypes tested showed differential transduction of dissociated primary rat and human Schwann cells and in rat and human nerve segments. AAV1 was the best serotype to transduce rat Schwann cells, while AAV2 and AAV6 were the best to transduce human Schwann cells. Rat nerve segments could be genetically modified equally well by AAV1, AAV5, AAV7, AAV9, whereas AAV2 was superior in human nerve segments. The lentiviral vector proved to be more effective than all the AAV serotypes tested in transducing cultured rat and human Schwann cells. In rat nerve segments, AAV5, AAV7 and AAV9 were not significantly different from the lentiviral vector while in human nerve, the lentiviral vector was superior to all AAV serotypes. According to Hoyng *et al.* (2015b), lentiviral vectors (figure 12) are considered to be the current gold standard in experimental gene therapy for peripheral nerve repair. Verrier *et al.* (2010) and Yang *et al.* (2012) have also previously reported successful *ex vivo* transduction of rat Schwann cells using lentiviral vectors.

Figure 12. Gene transfer by a lentiviral vector. After the lentiviral vector has infected a cell, the vector RNA containing the therapeutic gene is transcribed into DNA. The DNA forms a preintegration complex with the accessory protein Vpr, the enzyme integrase, and the protein matrix. This complex then enters the nucleus and the DNA is inserted into the host genome by integrase. Image taken from Amado and Chen (1999).



In addition to Schwann cells and nerve segments, lentiviruses have been used to successfully transduce human and rodent stem cells of various origin (Ye *et al.*, 2008; Lin *et al.*, 2012). The use of therapeutic cells in the context of peripheral nerve injury may be enhanced by subjecting them to *ex vivo* genetic modification prior to seeding in nerve repair devices for transplantation (table 6). This involves obtaining cells from patients or donors followed by *in vitro* manipulation to enhance the therapeutic potential of the cell and subsequent transplantation into the patient. This approach has a number of advantages over *in vivo* gene therapy mentioned in section 2.3.3.2. The delivery of genetic material can be targeted to a specific cell type, i.e. the therapeutic cell, without affecting other cells in the body. Cells can be characterised *in vitro* for successful incorporation of the transgene and only those which show biological activity are then incorporated into nerve repair devices. Further, in the cases of autologous stem cell harvest, no apparent adverse immune response has been reported, as demonstrated by Gaspar *et al.* (2004) and Aiuti *et al.* (2013).

Table 6. Studies enhancing the regenerative potential of therapeutic cells by over expression of neurotrophic factors.

Author	Gene delivery method	Gene(s)	Cell type	Mode of delivery	Animal model (length of gap, duration of experiment)	Outcome measures
Ee et al., 2017	Lentivirus	<i>GDNF</i>	Rat primary Schwann cells	Cells injected into a cellular nerve allograft	Rat sciatic transection (14 mm gap, 6 weeks)	Myelinated axon count, neural tissue
Hsu et al., 2017	Baculovirus	<i>GDNF</i>	Rat adipose derived stem cells	Adipose derived stem cell sheets wrapped around the injury site	Rat sciatic transection (direct repair, up to 8 weeks)	Electrophysiology, walking track analysis, muscle mass, axon area, angiogenesis, myelination
Man et al., 2016	Lentivirus	<i>VEGF</i>	Human bone marrow stem cells	Cells in fibrin gel seeded in a poly-L-lactide acid conduit	Mouse sciatic transection (4 mm gap, 2 weeks)	Neurite extension, Schwann cell proliferation, VEGF expression, axon regeneration, stem cell tracking
May et al., 2016	Retrovirus	<i>GDNF</i>	Rat Schwann cells	Cells seeded in silicone tubes	Rat cavernous nerve transection to (5 mm gap, 12 weeks)	Neurostimulation, and intracavernous pressure, measurement, histology, functional recovery
Meyer et al., 2016	Nucleofection	<i>GDNF, FGF2</i>	Rat Schwann cells	Cells in NVR gel seeded in a chitosan conduit	Rat sciatic nerve transection (15 mm gap, up to 17 weeks)	Functional recovery, electrophysiology, muscle weight, myelin thickness, g-ratio, total axon count, nerve fibre density, fibre diameter

Marquardt et al. (2015)	Lentivirus	<i>GDNF</i>	Rat Schwann cells	Acellular nerve allografts and cells injected into the distal nerve stump	Rat sciatic nerve transection (30 mm gap, up to 8 weeks)	Total axon count, axon density, fibre width, myelination, percent neural tissue, live tracking of regenerating axons
Tseng and Hsu (2014)	Effectene®-based transfection	<i>BDNF</i>	Rat adipose derived stem cells	Cell spheroids seeded in a poly(D,L-lactide) conduit	Rat sciatic nerve transection (10 mm gap, 31 days)	Electrophysiology, cell tracking, cross-sectional area of regenerated axons, quantification of axonal growth
Liu et al., 2014	Lentivirus	<i>CDNF</i>	Rat bone marrow stem cells	Cells in a collagen conduit	Rat sciatic nerve transection (5 mm gap, up to 12 weeks)	Protein expression, walking track analysis, muscle mass, horseradish peroxidase tracing, myelination thickness, axon diameter, G-ratio
Allodi et al., 2014	Lentivirus	<i>FGF2</i>	Rat Schwann cells	Cells in collagen matrix seeded in a silicone conduit	Rat sciatic transection (6 mm gap, up to 2 months)	Protein expression, immunohistochemistry, electrophysiology, axon regeneration, myelination, functional recovery
Godinho et al., 2013	Lentivirus	<i>BDNF, CNTF, NT3</i>	Rat Schwann cells	Cells in culture media injected into an acellular nerve sheath	Rat peroneal transection (10 mm gap, 10 weeks)	Quantification of axonal numbers, functional recovery, axonal regeneration, myelination, immunohistochemistry
Santosa et al., 2013	Lentivirus	<i>GDNF</i>	Rat Schwann cells	Cells in culture media seeded in an acellular nerve allograft	Rat sciatic transection (14	Gene expression, electrophysiology, total myelinated fibre count and

					mm gap, up to 12 weeks)	fibre width, percent neural tissue, muscle mass
Shakhbazau et al., 2013	Lentivirus	<i>GDNF</i>	Rat Schwann cells	Silicone conduit and cells injected into the distal nerve stump	Rat sciatic transection (5 mm gap, up to 11 weeks)	Electrophysiology, sensitivity testing, motor recovery, muscle mass
Fu et al. (2011)	Polyfect®-based transfection	<i>BDNF, GDNF</i>	Mouse neural stem cells	Cells in culture media seeded in a poly(D,L-lactide) conduit	Rat sciatic nerve transection (15 mm gap, 8 weeks)	Functional analysis, electrophysiology, cross-sectional area of regenerated nerve, numbers of myelinated sheaths and blood vessels
Shi et al. (2009)	Lentivirus	<i>GDNF</i>	Rat neural stem cells	Cells in Matrigel seeded in a polyglycolic/polyglycolic acid conduit	Rat facial nerve transection (8 mm gap, up to 12 weeks)	Electrophysiology, number of regenerated axons, myelin thickness
Haastert et al. (2006)	Metafectene®-based transfection	<i>FGF2</i>	Rat Schwann cells	Cells in culture media seeded in a silicone conduit	Rat sciatic nerve transection (15 mm gap, up to 6 months)	Cell tracing, analysis of protein expression, functional recovery, electrophysiology, retrograde labelling of regenerated neurons, quantification of myelinated nerve fibres

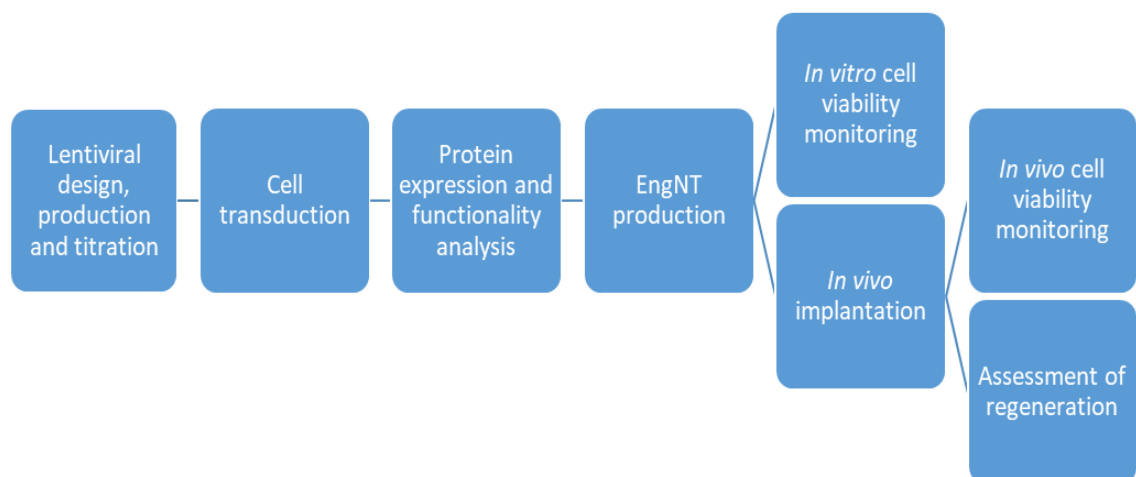
Abbreviations: FGF2 - fibroblast growth factor-2; VEGF - vascular endothelial growth factor; CNTF - ciliary neurotrophic factor; NGF – nerve growth factor; GDNF - glial cell-derived neurotrophic factor; BDNF - brain-derived neurotrophic factor; CDNF - conserved dopamine neurotrophic factor; NT3 - neurotrophin-3.

Chapter 3. Materials and methods

3.1 Introduction

The overarching goal of this project was to combine cell-based tissue engineering and gene delivery to enhance peripheral nerve regeneration following injury. Cells were initially labelled using lentiviral vectors to deliver a bioluminescent gene to monitor and further our understanding of cell viability in the tissue engineered constructs *in vitro* and *in vivo*. It was also thought that improving vascularisation to the implanted tissue engineered constructs would enhance peripheral nerve tissue engineering strategies as perfusion and oxygen transport have direct effects on cell viability. Cells used to make the tissue engineered constructs were therefore genetically modified using lentiviral-mediated gene delivery to overexpress VEGF-A₁₆₅, an angiogenic factor which also exhibits neurotrophic effects. Owing to the neurotrophic effects of VEGF-A₁₆₅, it was thought that its overexpression may further improve peripheral nerve regeneration by creating a microenvironment conducive to axonal regrowth. The experimental methods used in this project are outlined in figure 13.

Figure 13. Schematic of the experimental methods used in the current project.



3.2 Cell culture

3.2.1 SCL4.1/F7 rat Schwann cell culture

Rat Schwann cell line SCL4.1/F7 (Health Protection Agency) cells were grown in Dulbecco's Modified Eagle's Medium (DMEM) with GlutaMax™ (Gibco™, ThermoFisher), supplemented with 10 % (v/v) heat inactivated foetal bovine serum (FBS) (Gibco™, ThermoFisher) and 1 % (v/v) penicillin/streptomycin solution (Gibco™, ThermoFisher), in tissue cultured treated flasks with filters (Greiner CELLSTAR®, Sigma-Aldrich). The cultures were maintained at sub-confluent levels at 37 °C with 5 % CO₂/95 % air and passaged when required. When passaging, cells were washed with phosphate buffered saline (PBS) (Gibco™, ThermoFisher) and dissociated by the addition of 0.05 % Trypsin-EDTA (Gibco™, ThermoFisher) for 5 minutes at 37 °C. Trypsin was inactivated by the addition of complete medium and the cell suspension was centrifuged at 1200 rpm for 5 minutes at room temperature. The cell pellet was resuspended in complete medium and the total number of cells was determined using a haemocytometer. The appropriate volume of cell suspension was pipetted into new tissue culture flasks. SCL4.1/F7 cells were used up to passage 28 for *in vitro* experiments and up to passage 14 for *in vivo* work.

3.2.2 Rat adipose derived stem cells culture and differentiation

Rat ADSCs (kindly provided by Dr Paul Kingham, Department of Integrative Medical Biology, Umeå University) were grown in Minimum Essential Medium - alpha Modification (α -MEM) (Gibco™, ThermoFisher) containing 10 % (v/v) FBS and 1 % (v/v) penicillin/streptomycin solution. To differentiate the adipose stem cells into a Schwann cell-like phenotype, growth medium was supplemented with 1 mM β -mercaptoethanol (Sigma-Aldrich) for 24 hours. The cells were then washed with PBS and fresh medium supplemented with 35 ng/ml all-trans-retinoic acid (Sigma-Aldrich) was added. After 72 hours, the cells were washed and the medium was replaced with differentiation medium containing cell growth medium supplemented with 14 μ M forskolin (Sigma-Aldrich), 10 ng/ml basic fibroblast growth factor (Pepro Tech Ltd.), 5 ng/ml platelet-derived growth factor (Pepro Tech Ltd.) and 252 ng/ml neuregulin-1 (R&D Systems). The cells

were incubated for a minimum of two weeks with the differentiation medium replaced every 72 hours. Cells were maintained at subconfluent levels at 37 °C with 5 % CO₂/95 % air and passaged as described in section 3.2.1 when required. ADSCs were used up to passage 15.

3.2.3 Human foetal neural stem cell culture

The human neural stem cell line CTX0E03 (supplied by ReNeuron Ltd.) was expanded using previously described methods (Pollock *et al.*, 2006). CTX0E03 cells were cultured in DMEM:F12 medium (Gibco™, ThermoFisher) supplemented with 0.03 % human albumin solution (Grifols), 2 mM GlutaMAX™ (Gibco™, ThermoFisher), 5 µg/ml human transferrin (Sigma-Aldrich), 16.2 µg/ml putrescine dihydrochloride (Sigma-Aldrich), 5 µg/ml human insulin (Sigma-Aldrich), 60 ng/ml progesterone (Sigma-Aldrich), 40 ng/ml sodium selenite (Sigma-Aldrich), 20 ng/ml epidermal growth factor (Sigma-Aldrich), 10 ng/ml basic fibroblast growth factor (Invitrogen), and 100 nM 4-hydroxytamoxifen (4-OHT) (Sigma-Aldrich) in 20 µg/ml laminin-coated (Amsbio) tissue culture treated flasks with filters. When passaging, cells were washed with Hanks' Balanced Salt Solution (HBSS) (Gibco™, ThermoFisher), and dissociated by the addition of TrypZean® (Sigma-Aldrich) for 5 minutes at 37 °C. TrypZean® was inactivated by the addition of defined trypsin inhibitor (Gibco™, ThermoFisher) and the cell suspension was centrifuged at 1500 rpm for 5 minutes at room temperature. The cell pellet was resuspended in growth media and the total number of cells was determined using a haemocytometer. The appropriate volume of cell suspension was pipetted into new laminin coated tissue culture flasks. Cells were used between passages 25 and 33.

3.2.4 Human umbilical vein endothelial cells culture

Human umbilical vein endothelial cells (HUVECs) (PromoCell) were grown in endothelial cell growth medium (EGM) (PromoCell), supplemented with 10 % FBS, 1 % penicillin/streptomycin and SupplementMix (PromoCell). For conditions of serum starvation, HUVECs were grown in media containing 0.1 % FBS, 1 % penicillin/streptomycin and SupplementMix overnight. Cells were maintained at

subconfluent levels at 37 °C with 5 % CO₂/95 % air and passaged as described in section 3.2.1 when required. HUVECs were used up to passage 10.

3.2.5 PC12 cell culture

PC12 cells (Sigma-Aldrich) were grown in suspension in RPMI 1640 culture medium (Gibco™, ThermoFisher), supplemented with 1 % (v/v) penicillin/streptomycin solution, 2 mM l-glutamine (Sigma-Aldrich), 10 % (v/v) heat-inactivated horse serum (Sigma-Aldrich) and 5 % (v/v) heat inactivated FBS in tissue culture treated flasks with filters. Cells were maintained at subconfluent levels at 37 °C with 5 % CO₂/95 % air. When passaging, cells in culture media were centrifuged at 1200 rpm for 5 minutes. The cell pellet was resuspended in complete media and the total number of cells was determined using a haemocytometer. The appropriate volume of cell suspension was pipetted into new tissue culture flasks. Cells were used up to passage 35.

3.2.6 HEK293T cell culture

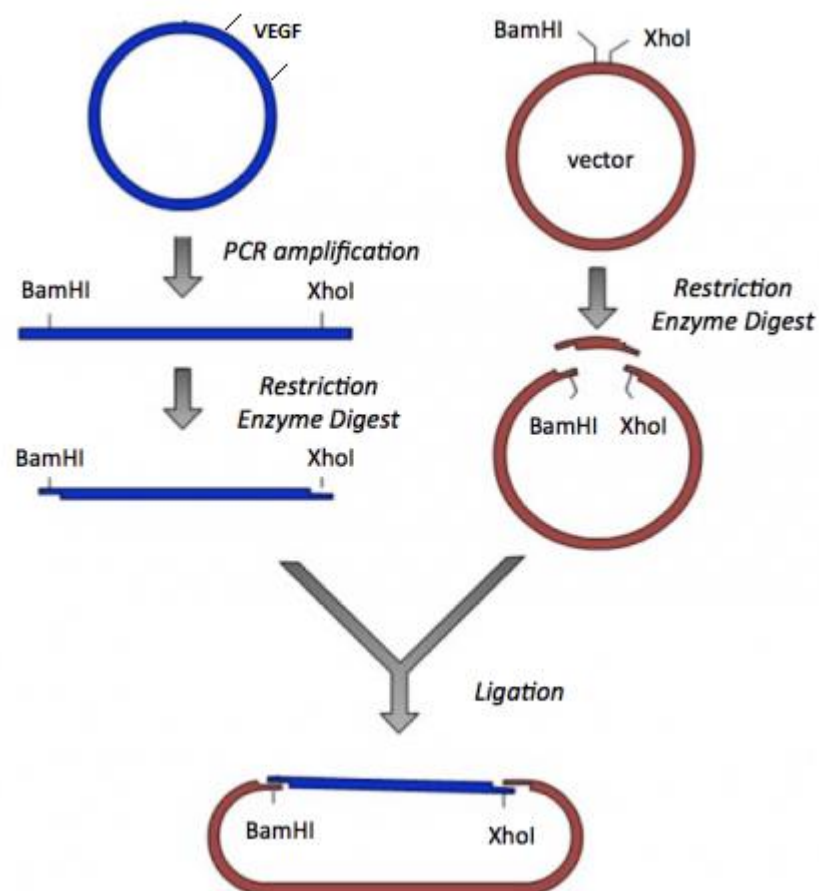
Human embryonic kidney cells (HEK293T) (ThermoFisher Scientific) were grown in DMEM GlutaMax™ supplemented with 10 % (v/v) heat inactivated FBS and 1 % (v/v) penicillin/streptomycin solution in tissue culture treated flasks with filters. Cells were maintained at sub-confluent levels at 37 °C with 5 % CO₂/95 % air and passaged when required as described in section 3.2.1. Cells were used up to passage 15 for lentivirus production.

3.3 Cloning of the *VEGF-A₁₆₅* gene

VEGF-A₁₆₅ cDNA was extracted from an adenoviral vector containing the human pro-angiogenic *VEGF-A₁₆₅* gene cDNA sequence (Swanson *et al.*, 2016) (kindly provided by Professor Anna David, UCL Institute for Women's Health). It was decided to clone the gene into the expression cassette of the pSFFV-IRES-eGFP lentiviral backbone plasmid using the polymerase chain reaction (PCR) (figure 14). Using this technique, polymerase chain reaction (PCR) primers that included restriction enzyme sites were designed for the amplification of the *VEGF-A₁₆₅* gene cDNA sequence. Following PCR amplification

and purification, the PCR product and lentiviral backbone plasmid pSFFV-IRES-eGFP were digested using restriction enzymes. The digested DNA was separated on an agarose gel and isolated. The *VEGF-A₁₆₅* gene cDNA sequence was then ligated into the pSFFV-IRES-eGFP backbone plasmid downstream of the SFFV promoter sequence and in front of the IRES sequence. The recombinant plasmid pSFFV-VEGF-IRES-eGFP was subsequently transformed into competent bacteria. Individual colonies were selected and the plasmid DNA was extracted. A diagnostic restriction digest was performed to confirm the presence of the *VEGF-A₁₆₅* gene in the backbone plasmid. The final recombinant plasmid was then verified by Sanger sequencing.

Figure 14. Plasmid cloning by PCR. The *VEGF-A₁₆₅* gene was extracted from an adenoviral vector (blue) using PCR. *Bam*HI and *Xho*I restriction enzyme sites were introduced on each end of the gene to allow insertion into the pSFFV-IRES-eGFP lentiviral backbone plasmid (red), forming the pSFFV-VEGF-IRES-eGFP recombinant plasmid (blue and red). Image taken and adapted from engineerbiology.org. Accessed on 10th October 2018.



3.3.1 Polymerase chain reaction

High fidelity proof reading PFU DNA polymerase (Promega Corporation) was used to amplify the *VEGF-A₁₆₅* gene from the adenoviral vector. Primer pairs (Sigma-Aldrich) were designed to flank the sequence at the 5' and 3' ends and to introduce *Bam*HI and *Xho*I restriction enzyme sites to allow cloning into the pSFFV-IRES-eGFP backbone plasmid. The primers used are shown in table 7.

Table 7. Primers used to amplify the *VEGF-A₁₆₅* gene.

	Sequence (5' → 3')	Length (bp)	% GC content	T _m
Forward primer	CACAGGATCCGCCACCATGAACTTTCTGCTG	31	54.8	65.4
Reverse primer	ATATCTCGAGTCACCGCCTCGGCTTGTC	28	57.1	64.7

A PCR nucleotide mix (VWR International) containing equimolar amounts of each of the four deoxyribonucleotide triphosphates (dATP, dCTP, dGTP, and dTTP) was used to generate amplified DNA. All PCR reaction mixtures were made up to a volume of 20 µl. The composition of the reaction mix is shown in table 8.

Table 8. Components and volumes used in the PCR reaction.

Component	Volume (µl)
10x enzyme buffer	2
dNTPs (10 mM)	2
Forward primer (10 µM)	1
Reverse primer (10 µM)	1
PFU DNA polymerase	0.5
Adenovirus template	5
dH₂O to a final volume of	20

The PCR was carried out using the 96-well Veriti™ thermal cycler (Applied Biosystems) using the conditions shown in table 9.

Table 9. Initial PCR conditions. Each reaction involved 25 cycles of denaturation, annealing and extension.

Step	Time (minutes)	Temperature (°C)
Initial denaturation	2	94
Denaturation	0.25	94
Annealing	1	60
Extension	5	68
Final extension	7	72
Storage	Indefinitely	4

The PCR products obtained were subsequently purified using a silica-membrane-based purification column (QIAquick PCR Purification Kit, Qiagen) according to the manufacturer's instructions.

3.3.1.1 PCR optimisation

The initial conditions described in table 8 resulted in poor PCR efficiency. In order to establish the optimum PCR conditions, the effects of changing the concentration of the template DNA and annealing temperature of the reaction were investigated. PCR efficiency was compared by running the reaction at annealing temperatures of 56 °C, 58 °C and 61 °C using serial dilutions (10^{-1} , 10^{-2} , 10^{-3} , 10^{-4} , and 10^{-5}) of the adenovirus template.

3.3.2 Restriction enzyme digest

The backbone plasmid and PCR products were digested with a restriction enzyme buffer system (New England Biolabs Inc.) for 1 hour at 37 °C. The double digest reaction mixture consisted of the components in table 10.

Table 10. Components and volumes used in a typical restriction enzyme digest.

Component	Volume (µl)
<i>Bam</i> HI	0.5
<i>Xho</i> I	0.5
DNA/plasmid vector	Equivalent to 1 µg
Enzyme buffer	2.5
dH ₂ O to a final volume of	25

3.3.3 Gel electrophoresis

The digested PCR products and backbone plasmid were separated according to size on 0.8 % agarose gel (Invitrogen) using 1x tris-acetate-EDTA (TAE) buffer. A 50x TAE buffer stock solution was prepared by dissolving 242 g Tris base (Sigma-Aldrich) in distilled water (dH₂O) followed by the addition of 57.1 ml glacial acetic acid (Sigma-Aldrich) and 100 ml of 500 mM EDTA (Sigma-Aldrich). The pH was adjusted to 8 by the addition of 1 M sodium hydroxide (Sigma-Aldrich) and the final volume up was brought up to 1 litre. The nucleic acid stain SafeView™ (Applied Biological Materials Inc.) was added to the agarose gel at a dilution of 1:10 000 prior to setting.

30 µl of each sample were loaded into the wells with 1x orange G gel loading buffer (Sigma-Aldrich) to allow visual tracking of DNA migration during electrophoresis. 10 µl of a 1 kbp plus and/or 100 bp molecular weight marker (ThermoFisher Scientific) were used to determine DNA fragment size. Gels were run at 100 V (PowerPac Basic, Biorad) for 45 minutes and visualised under an ultraviolet transilluminator at low setting and for minimal periods of time to avoid UV-mediated mutations in gene sequences.

3.3.4 DNA extraction

The DNA fragments were isolated from the agarose gel under UV light using a sterile scalpel to remove the desired bands. The DNA was subsequently purified using silica-membrane-based purification (QIAquick Gel Extraction Kit, Qiagen) following the manufacturer's instructions. DNA was eluted in a final volume of 30 µl of dH₂O and the concentration and purity determined by spectrophotometry. The concentration was measured by absorbance at 260 nm while the ratio of absorbance at 260 nm and 280 nm was used to assess the purity of the DNA.

3.3.5 Ligation

The purified *VEGF-A₁₆₅* gene was inserted into the pSFFV-IRES-eGFP lentiviral vector plasmid by cohesive-end ligation using the bacteriophage T4 DNA ligase (Promega Corporation) according to the manufacturer's instructions. Several insert: vector ratios

(3:1, 5:1 and 7:1) were tested in order to establish the optimal ratio for single insertion into the vector. The mass of insert required at the different insert: vector ratios tested was calculated using the following equation:

$$\frac{\text{ng of vector} \times \text{kb size of insert}}{\text{kb size of vector}} \times \text{molar ratio of } \left(\frac{\text{insert}}{\text{vector}}\right) = \text{ng of insert}$$

Each 10µl ligation reaction mixture contained the components in table 11.

Table 11: Components and volumes used in a typical ligation reaction.

Component	Volume (µl)
Vector	According to the ratio required
Insert	According to the ratio required
T4 DNA ligase	1
Enzyme buffer	5
dH ₂ O to a final volume of	10

3.3.6 Bacterial transformation

In order to produce multiple copies of the recombinant plasmid formed in the ligation reaction described in section 2.2.5, the plasmid was transformed into chemically competent *Escherichia coli* (One Shot™ Stbl3™, ThermoFisher), following the manufacturer's instructions. The transformation mix was streak-plated on Luria-Bertani (LB) agar (Fisher Scientific) containing 100 µg/ml of ampicillin (Sigma-Aldrich) in Petri dishes. The dishes were incubated at 37 °C overnight. The following morning, single colonies were isolated and used to inoculate 5 ml of LB broth containing 100 µg/ml ampicillin (starter cultures). The starter cultures were incubated overnight at 37 °C in a shaking incubator at 225 rpm.

3.3.7 Plasmid purification and diagnostic digest

The desired recombinant plasmid DNA was purified from the bacterial cultures in the starter cultures following a bind-wash-elute procedure (QIAprep Spin Miniprep Kit, Qiagen) according to the manufacturer's instructions. The purified plasmid DNA was

eluted in 50 µl of distilled water and the concentration was determined by spectrophotometry as described in section 3.3.4.

For larger scale plasmid DNA purification, a starter culture was grown in 500 ml of LB broth containing 100 µg/ml ampicillin overnight at 37 °C in a shaking incubator at 225 rpm. The desired recombinant plasmid DNA was purified using a QIAprep Spin Maxiprep Kit (Qiagen) according to the manufacturer's instructions. The purified plasmid DNA was eluted in 500 µl of distilled water and the concentration determined by spectrophotometry as described in section 3.3.4.

The plasmid DNA obtained was purified and subjected to a diagnostic digest and gel electrophoresis (section 3.3.3) to confirm the presence of the inserted genes.

3.3.8 Synthesised genes

The *VEGF-A₁₆₅* gene was not successfully cloned into the pSFFV-IRES-eGFP backbone plasmid using the PCR method even after multiple cloning attempts. It was decided that instead of using PCR to attach restriction enzymes sites to the gene of interest, the gene together with the restriction enzyme sites would be synthesised by Life Technologies Limited to facilitate the cloning process.

3.3.9 Sequencing

The final recombinant plasmid DNA obtained using the synthesised genes, together with sequencing primers (table 12) were sent externally to Source BioScience for Sanger sequencing.

Table 12. Sequencing primers.

Primer location (region, locus in plasmid)	Sequence (5' → 3')	Length (bp)	% GC content	T _m
SFFV promoter, 387 - 405	TGCTTCTCGCTTCTGTTCG	19	52.6	58.2
VEGF-A ₁₆₅ gene, 791 - 810	CCACTGAGGAGTCCAACATC	20	55	57

The resulting DNA electropherograms were visualised and analysed using MacVector v15.0.

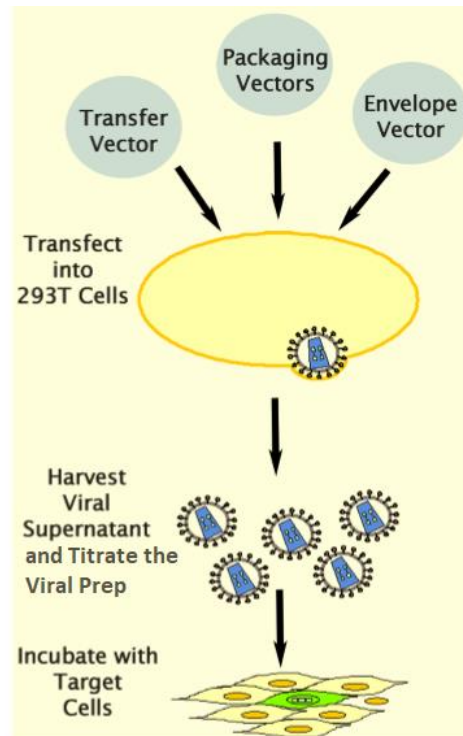
3.4 Plasmid transfection

Before the recombinant plasmid produced was used to manufacture the lentiviral vector, its functionality was tested by a transient transfection in HEK293T cells. 1.5×10^5 cells/well were seeded onto 6-well plates and grown in complete media for 24 hours. The transfection mix per sample was the following: 500 μ l of Opti-MEM (Gibco™, ThermoFisher), 2 μ g of DNA plasmid and 2.5 μ l of polyethylenimine (PEI) (Polyscience). The solution was vortexed and left at room temperature for 20 minutes to allow the formation of DNA-PEI complexes. The transfection mix was then added to the cells. The cells were incubated at 37 °C with 5 % CO₂/95 % air for 48 hours, after which proteins in the media and cell lysate were harvested and processed as described in section 3.7.1.

3.5 Lentivirus production

A second-generation lentiviral vector packaging system was used to produce the vectors described in this study. Standard lentiviral production (figure 15) typically relies on the transient transfection of HEK293T cells with a packaging plasmid, an envelope glycoprotein-encoding plasmid and a transfer plasmid. Following transfection, lentiviral particles are produced and released into the culture supernatant of the HEK293T cells (Vigna and Naldini, 2000). The particles are then harvested, purified by centrifugation and titred.

Figure 15. Lentiviral vector production. The transfer plasmid, packaging plasmid and envelope plasmid are triple transfected into HEK293T cells. After an incubation period of up to 48 hours, the media containing the viral particles is collected and centrifuged to concentrate virus. The virus is then titred and used to transduce the cells of interest. Image taken from <http://www.cellbiolabs.com/pantropic-shrna-lentiviral-expression-systems>. Accessed on 12th October 2018.



3.5.1 HEK293T cells triple transfection and virus harvest

HEK293T cells were seeded in 15 cm dishes (Nunc) at a seeding density of 7×10^6 cells/dish for a confluence of 70 - 80 % the following day. The following amounts of the three plasmids required for lentiviral production were added to 2.5 ml Opti-MEM[®] per dish:

- 40 µg of the transfer vector plasmid pSFFV.VEGF.IRES eGFP
- 10 µg of the envelope plasmid pMD2.G
- 30 µg of the packaging construct plasmid pCMV-dR8.74

42 µl of 3.5 mg/ml PEI (Sigma-Aldrich) was added to the plasmid and Opti-MEM[®] mixture. PEI is a transfection agent that works by forming positively charged complexes with target DNA, which then interact with the negatively charged host cell membrane and release DNA into the cell (Kuroda *et al.*, 2009). It has been shown to improve the

efficiency of lentiviral vector production (Tang *et al.*, 2015). The mixture was gently vortexed and incubated at room temperature for 20 minutes to allow complexation. The cells were washed with PBS and 2.6 ml of the transfection mix was added to each dish. Cells were incubated overnight, after which the media was replaced with 15 ml complete DMEM. After 48 hours, the medium was removed for the first harvest and replaced with 15 ml of fresh medium. The cells were then allowed to incubate for another 24 hours, after which the medium was collected again.

3.5.2 Lentivirus concentration via centrifugation

Media containing viral particles harvested 48 and 72 hours after transfection was centrifuged at 3000 g for 10 minutes at room temperature and filtered through a 0.22 µm filter unit (Millipore® Stericup™, Sigma-Aldrich) to remove all cell debris. The viral particles were pelleted by centrifugation overnight at 3000 x g at 4 °C. The resulting pellet was resuspended in Opti-MEM®, aliquoted and stored at -80 °C.

3.5.3 Lentivirus titration

The physical lentiviral titre was obtained by the quantification of the viral envelope protein p24 using the ZeptoMetrix p24 antigen enzyme linked immunosorbent assay (Fischer Scientific) as per the manufacturer's protocol. The assay measures the amount of p24 capsid protein present in the viral supernatant and this correlates directly with the virus titre. There are approximately 1×10^4 physical particles of lentivirus for every pg of p24 antigen.

3.6 Transduction

When the cells were growing exponentially, 1×10^5 - 1.5×10^5 cells in their respective medium were added to each well in a 6-well plate. The number varied according to cell type to accommodate a confluence of 70 - 80 % upon transduction. The cells were incubated at 37 °C with 5 % CO₂/95 % air for 24 hours. The medium was then removed from the wells. 1.5 ml fresh medium was added to each well followed by the required volume of lentiviral particles. A range of multiplicities of infection (MOIs) (MOI of 1, 10

and 100) to determine the optimal number of lentiviral particles needed for efficient transduction was tested.

The MOI was calculated using the following formula:

$\frac{\text{Total number of cells per well} \times \text{desired MOI}}{\text{Lentiviral titre (viral particles/ml)}} = \text{Total volume of lentiviral particles to add to each well (ml)}$

Following addition of the viral particles, the plates were gently swirled and incubated at 37 °C at 5 % CO₂/95 % air. Lentiviral mediated eGFP expression was assessed over a 72 hour period using a fluorescence microscope (Inverso-TC Trinocular Inverted Microscope with Epi-Fluorescence Module).

3.6.1 Assessing transduction efficiency by flow cytometry

Transduction efficiency was assessed 72 hours following transduction by flow cytometry (MACS Quant Flow Cytometer). The cells were detached and counted using a haemocytometer. Cells at a density of 7.5 x 10⁵/ml were resuspended in sterile PBS and passed through a 40 µm nylon mesh filter (Falcon®) right before sorting to ensure that only single cells were present. Fluorescent cells were separated from non-fluorescent cells by setting a minimum fluorescence value (thresholding) on the histograms generated from the cell data provided by the cytometer. By setting the threshold just to the right of the dimmest peak, cells to the left of the threshold were excluded from those counted as fluorescent within the channel.

3.7 Protein expression analysis

To confirm successful overexpression of the transgene following transfection or transduction, Western blot and ELISA were used to measure protein expression.

3.7.1 Sample preparation

48-72 hours after transfection or transduction, cells and media were collected for protein extraction. The media was centrifuged at 1500 rpm for 10 min at 4 °C. The supernatant was transferred to clean 1.5 ml microcentrifuge tubes and used immediately or stored at -80 °C. After the media was collected, the cells were washed with ice-cold PBS. The PBS was discarded and 100 µl of cold radioimmunoprecipitation assay (RIPA) buffer (ThermoFisher) with 1x protease inhibitor cocktail (ThermoFisher) were added per well. The cells were incubated on ice for 5 minutes, swirling the plate every minute. The cells were then scraped using a cold plastic cell scraper and collected in 1.5 ml microcentrifuge tubes. The cell lysate was incubated for 30 minutes at 4 °C on a tube rotator and then centrifuged at 16 000 rpm for 20 minutes at 4 °C. The supernatant was collected and transferred into clean microcentrifuge tubes and used immediately or stored at -80 °C. 15 µl of the processed cell lysate and cell media were taken to estimate the total amount of protein per sample using a bicinchoninic acid (BCA) protein assay kit (ThermoFisher) according to the manufacturer's instructions.

3.7.2 Western blot

Western blotting was used to provide semi-quantitative data on the presence and molecular weight of the VEGF-A₁₆₅ protein produced by SCL4.1/F7 cells following lentiviral transduction. 1x lithium dodecyl sulfate sample buffer (NuPAGE™, ThermoFisher) and 1x sample reducing agent (NuPAGE™, ThermoFisher) were added the volume of cell lysate or media equivalent to 20 µg of total protein as determined by the BCA assay. The sample buffer contains tracking dyes (Coomassie G250 and phenol red) which give a sharp dye front close to the moving ion front. The reducing agent completely reduces disulphide bonds present in the proteins. The solution was made up to a volume of 30 µl with RIPA buffer. The mixture was incubated at 70 °C for 10 minutes to denature the proteins. The samples were loaded into the wells of a pre-cast 8 cm x 8 cm bis-tris 4 - 12 % polyacrylamide gel (NuPAGE™, ThermoFisher), which resolves proteins in the range of 1 - 200 kDa. 10 µl of sharp pre-stained protein standard (Novex™, ThermoFisher) was added to a separate well to confirm the molecular weight of the visualised bands. 500 µl of antioxidant (NuPAGE™, ThermoFisher) was

added was added to the upper buffer chamber of the XCell SureLock™ Mini-Cell gel running tank ((NuPAGE™, ThermoFisher) to prevent sample reoxidation and maintain the proteins in a reduced state. Proteins were separated via polyacrylamide gel electrophoresis with 1x MES SDS running buffer (NuPAGE™, ThermoFisher) run at 90 V for 2 hours.

Proteins were transferred on to a methanol activated polyvinyl difluoride membrane (Thermo Fisher Scientific) via semi dry transfer. The membrane was soaked in methanol for 1 minute and rinsed with transfer buffer (48 mM Tris, 39 mM glycine, 20 % methanol, 0.04 % sodium dodecyl sulfate). Filter paper was also soaked in transfer buffer and placed in the semi dry transfer unit. A stack was formed by placing the membrane and gel on top of the filter paper and covering the gel with additional filter paper. Semi dry transferring was run at 400 mA for 1 hour. The membrane, now containing the transferred proteins, was blocked for 1 hour at room temperature using 3 % skimmed milk powder (Sigma-Aldrich) in TBST (Tris-buffered saline, 0.1 % Tween 20). The membrane was incubated with the appropriate dilutions of primary antibody (table 13) in TBST. After three 5 minute washes in 1x TBST, the membrane was incubated with horseradish peroxidase (HRP) conjugated secondary antibodies (table 14) in 3 % bovine serum albumin (BSA) (Sigma-Aldrich) in TBST at room temperature for one hour. After another three 5 minute washes in TBST, the signal was developed using an enhanced chemiluminescence system (ThermoFisher) following the manufacturer's instructions. Bands were detected using a GeneGnome imager.

Table 13. Primary antibodies used in western blotting.

Primary antibody	Host	Reactivity	Dilution	Incubation conditions
Anti-VEGFA (ab1316, Abcam)	Mouse	Mouse, rat, rabbit, dog, human	1:1000	1 hour at room temperature
Anti-tubulin (ab6161, Abcam)	Rat	Mouse, rat, dog, human, <i>Saccharomyces cerevisiae</i> , <i>Schizosaccharomyces pombe</i> , alligator	1:1000	Overnight at 4 °C

Table 14. Secondary antibodies used in western blotting.

Secondary antibody	Host	Reactivity	Dilution	Incubation conditions
Goat anti-mouse IgG H&L (HRP) (ab6789, Abcam)	Goat	Mouse	1:2000	1 hour at room temperature
Goat anti-rat IgG H&L (HRP) (ab97057, Abcam)	Goat	Rat	1:10000	1 hour at room temperature

3.7.3 ELISA

A solid-phase sandwich Enzyme-Linked Immunosorbent Assay (ELISA) (Invitrogen, ThermoFisher) was used to detect and quantify the level of human VEGF-A₁₆₅ protein in cell lysate and cell culture medium. Following transfection and lentiviral transduction, sample preparation as described in section 3.7.1, the assay was performed according to the manufacturer's instructions.

3.8 Cell proliferation assay

A colorimetric 5-bromo-2'-deoxyuridine (BrdU) cell proliferation ELISA kit (Abcam) was used to evaluate whether the transduction or the expression of the transgenes had an effect on cell proliferation. 0.5×10^4 transduced and control untransduced SCL4.1/F7 cells were seeded per well in a 96-well plate and allowed to attach overnight. The following day, 20 μ l of 1x BrdU reagent was added to each well and incubated for 18 hours. The assay protocol was followed as per manufacturer's instructions.

3.9 Cell morphology analysis

Transduced and control untransduced SCL4.1/F7 cells were analysed morphologically by light microscopy and were also characterized by immunofluorescence staining. A 0.01 % solution of poly-L-lysine (Sigma-Aldrich) made in dH₂O was used to coat the surface of circular coverslips (thickness # 1) (ThermoFisher) to ensure cell attachment. 5×10^4 SCL4.1/F7 cells in 100 μ l complete DMEM were seeded onto the coverslips and allowed to attach for 2 hours at 37 °C with 5 % CO₂/95 % air before the addition of 2 ml of

complete media per well. After 24 hours, the cells were fixed by the addition of 4 % paraformaldehyde (PFA) for 10 minutes followed by two 5 minute washes in PBS. Cells were permeabilised using 0.3% Triton X-100 (Sigma) in PBS for 30 minutes at room temperature. Following two 5 minute washes in PBS, 5 % normal goat serum in PBS was added for 30 minutes at room temperature to block non-specific binding sites. The goat serum was then removed and after two 5 minute washes with PBS, primary antibodies diluted in PBS were added and incubated for 1 hour at room temperature. The cells were washed three times for 10 minutes in PBS and incubated with secondary antibodies diluted in PBS for 1 hour in the dark. After three final 5 minute washes in PBS, the coverslips containing the cells were mounted cell side down onto microscope slides using Vectashield mounting media with 4',6-diamidino-2-phenylindole (DAPI) (Vector Laboratories) and allowed to dry before viewing under a fluorescence microscope. Circularity, serving as a cell shape descriptor, was measured using ImageJ.

3.10 Collection and processing of conditioned media

Transduced and control untransduced SCL4.1/F7 cells were seeded at a density of 2×10^4 cells/cm² in complete DMEM in a T75 flask. After 24 hours, the cells were washed with PBS. 15 ml of DMEM containing 0.1 % FBS was added to the cells. After 24 hours, the media was collected and filtered using a 0.2 µm syringe filter. The conditioned media was aliquoted and stored at -80 °C. The conditioned media was diluted with fresh EGM at a ratio of 2:3 for use in functional assays.

3.11 Functional assays

Functional assays were used to assess the angiogenic activity of the VEGFA produced by the transduced SCL4.1/F7 cells in conditioned media (CM). The following test groups were employed in the first three functional assays described in this section:

- Group 1: conditioned media from serum starved transduced SCL4.1/F7 cells overexpressing VEGF-A₁₆₅ + endothelial cell media + 1 % FBS.
- Group 2: conditioned media from serum starved control untransduced SCL4.1/F7 cells + endothelial cell media + 1% FBS.

- Group 3: DMEM + 1 % FBS (negative control).
- Group 4: EGM + 10 % FBS.
- Group 5: EGM + 1 % FBS + recombinant VEGF-A₁₆₅ protein (50 ng/ml) (positive control).

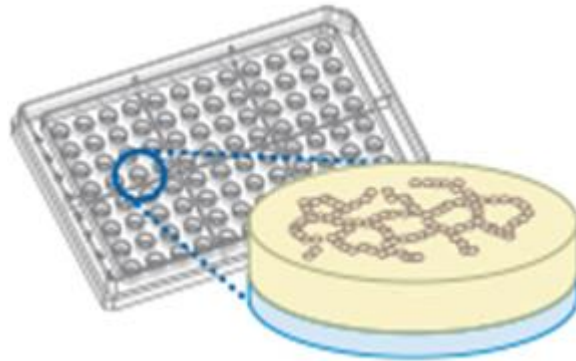
3.11.1 Effect of VEGF-A₁₆₅ on HUVEC viability

HUVECs in complete EGM were seeded in a 96-well plate at a density of 2000 cells per well and allowed to attach overnight. The complete medium was removed and the cells were washed with PBS. Cells were then incubated with the test media described in section 3.11 for up to 72 hours. Cell viability was measured every 24 hours by the addition of 10% alamarBlue® 6 hours prior to readout as described in section 3.13.1.

3.11.2 Endothelial tube formation assay

An *in vitro* angiogenesis assay kit (Chemicon®, Merck), based on a solid gel of basement proteins prepared from the Engelbreth Holm-Swarm mouse tumour, was used to evaluate tube formation by HUVECs in response to the VEGF-A₁₆₅ produced by the transduced SCL4.1/F7 cells (figure 16). The assay was carried out per manufacturer's instructions using 0.5×10^3 HUVECs per well in a 96-well plate. After a 6 hour incubation period with the test media described in section 3.11, tube formation was visualised under an inverted light microscope with magnification of 10x. Five pre-determined view fields per well were photographed and following researcher blinding, the endothelial tube visual patterns were examined. A numerical value associated with a degree of angiogenesis progression was assigned to each pattern.

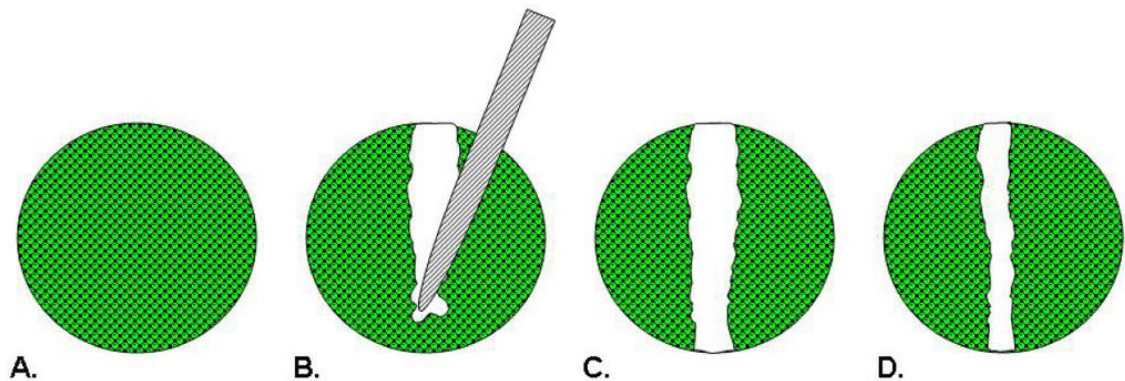
Figure 16. HUVEC tube formation assay. The assay measures the ability of endothelial cells, seeded on basement proteins, to form capillary-like structures in the presence of angiogenic signals. Image taken and adapted from ibidi application note: Tube Formation Assays in the μ -Plate Angiogenesis 96 Well. Available from: <https://ibidi.com/content/92-tube-formation-assays-in-the-plate-angiogenesis-96-well>. Accessed on 12th October 2018.



3.11.3 Scratch assay

Serum starved HUVECs were detached from T175 tissue culture flasks and counted using a hemocytometer. HUVECs at a density of 2×10^5 cells/well were plated in a 6-well plate and allowed to adhere overnight. This density was chosen to ensure a confluent monolayer the following morning. A scratch was made across the centre of the well using a P200 pipette tip (figure 17). A sterile razor blade was used as a straight edge to make the scratch as straight as possible. Cell debris was removed by washing with PBS. 2 ml of test media described in section 3.11 was added to each well. Three equidistant positions in the scratch (top, middle and bottom) were marked with reference points on the outer bottom of the plate using an ultrafine tip marker. These points were visualised using an inverted light microscope at 10x magnification and images were taken to measure the area of the scratch at time 0. The cells were then incubated at 37 °C with 5 % CO₂/95 % air for 8 hours. The predetermined positions were located using the reference points, and images were taken to measure the area of the scratch after 8 hours.

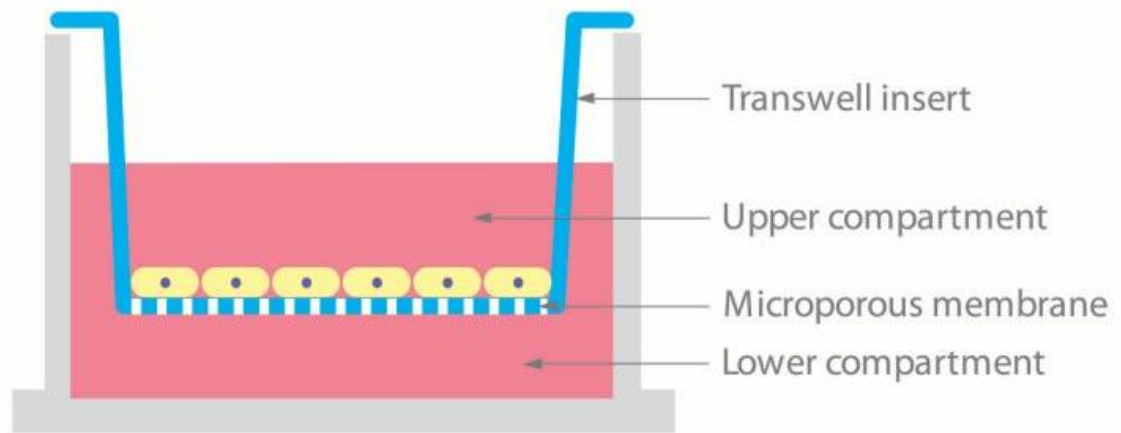
Figure 17. Scratch assay. A wound is introduced into a confluent monolayer of cells (A) by drawing a tip across the cell layer (B). The scratch is imaged to measure the area pre-migration (C) and after cell migration (D). Image taken from Hulkower and Herber (2011).



3.11.4 Transwell migration assay

SCL4.1/F7 cells were detached from T175 tissue culture flasks and counted using a haemocytometer. 3×10^5 cells in 1.5 ml of serum free DMEM were pipetted into the top compartment of a transwell insert (Sigma-Aldrich) ($8 \mu\text{m}$ pore size, placed in a 6-well plate). The contents of the lower compartments were varied across different experimental conditions. Cells were allowed to migrate for 12 hours (figure 18). At the end of the experiment, unmigrated cells on the apical side of the membrane were removed using a cotton bud soaked in PBS. Migrated cells on the basolateral side of the membrane were fixed with 4 % PFA for 10 minutes and washed three times with PBS. The membrane was cut out from the insert using a razor blade and placed onto a microscope slide, cell side facing up. Cells were stained with DAPI for 5 minutes and washed with PBS. The slides were cover slipped with Vectashield mounting media (Vector Laboratories) and allowed to dry. The number of nuclei (representing migrated cells) in 10 pre-determined view fields were counted using a fluorescent microscope.

Figure 18. Transwell migration assay. SCL4.1/F7 cells were placed in the upper compartment and their migration response to VEGF-A₁₆₅ in the lower compartment was assessed. Image taken from <https://www.corning.com/worldwide/en/products/life-sciences/products/permeable-supports/permeable-support-systems.html>. Accessed on 13th October 2018.



3.12 Engineered neural tissue

SCL4.1/F7 cells were used to create EngNT according to methods described previously (Georgiou *et al.*, 2013). EngNT is produced through self-alignment of cells within a collagen gel followed by stabilisation using plastic compression, a process whereby a biocompatible absorbent material is placed upon the gel to absorb interstitial fluid. This generates a dense robust hydrogel with a 50-fold increase in cell and collagen density (Brown *et al.*, 2005).

3.12.1 Fabrication of engineered neural tissue

100 μ l 10x minimum essential medium (Sigma) was mixed with 800 μ l type I rat tail collagen (2 mg/ml in 0.6 % acetic acid) (First Link, UK). The mixture was kept at 4 °C and was neutralised by the drop wise addition of 1 M sodium hydroxide (Sigma), indicated by a colour change from pale yellow to peach. The collagen solution was added to 100 μ l cell suspension to give a cell density of 4×10^6 cells/ml of gel. Gels were allowed to set in tethering moulds (figure 19) at 37 °C for 15 minutes and then immersed in culture medium and incubated at 37 °C in a humidified incubator with 5 % CO₂/ 95 % air for 24 hours, during which time the cells contracted the tethered gels and become aligned. RAFT™ 24-well cell culture plate biocompatible absorbers (Lonza Bioscience) were then used to stabilise the aligned gels for 15 min (figure 20).

Figure 19. Cellular collagen gels in polyether ether ketone moulds. The tethering bars are supported at each end of the rectangular moulds. Gels adopt a characteristic shape as cells contract and align.

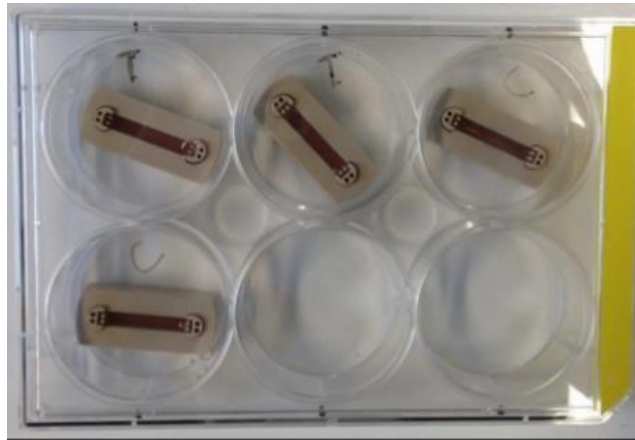
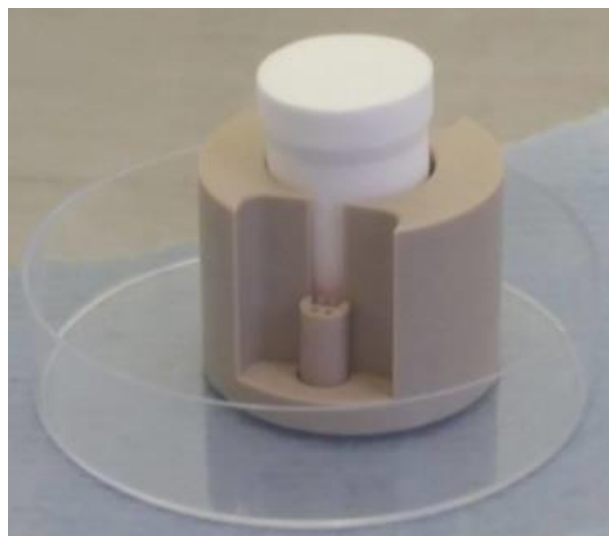


Figure 20. Stabilising the EngNT to produce robust hydrogels. A RAFT™ absorber is used to stabilise the gel by drawing out the interstitial fluid.



3.12.2 Contraction assay

75 μ l of the collagen-cell mixture (4×10^6 cells/ml of gel) described in section 3.12.1 was added to individual wells of 96-well plates and allowed to set for 10 minutes at 37 °C. The gels were immersed in culture medium and incubated at 37 °C for a further 15 minutes before detachment from well plates using a sterile needle. Gels were incubated at 37 °C in a humidified incubator with 5 % CO₂/95 % air for 24 hours. The

media was removed from the wells and the plates were placed on a black surface and photographed. Percentage contraction was calculated by comparing the area of the well occupied by each gel to the area of the well using ImageJ.

3.12.3 Distribution of cells in the EngNT

A fluorescence stereomicroscope (Leica MZ16) was used to visualise the eGFP positive cells in the EngNT at a low magnification. This permitted the visualisation of the cells distributed throughout the construct. The 3D nature of the aligned SCL4.1/F7 cells within the collagen gels was captured by means of visualising lentivirus mediated expression of eGFP using scanning confocal microscopy (Zeiss LSM 710). DAPI was used as a nuclear and chromosome counterstain for identifying nuclei as it selectively binds to DNA and shows little to no background staining of the cytoplasm.

3.13 Cell viability assays

3.13.1 alamarBlue® assay

alamarBlue® (Bio-Rad) was used to establish whether the transduction or the expression of the transgenes had an effect on cell viability. alamarBlue® is a cell viability assay reagent which contains the cell permeable and non-toxic indicator dye resazurin. Resazurin is used as an oxidation-reduction indicator that undergoes a colorimetric change from blue to pink in response to cellular metabolic reduction. The absorbance measured is proportional to the number of living cells respiring. By detecting the level of oxidation during respiration, alamarBlue® can be used to quantitatively measure cell viability.

alamarBlue® in complete DMEM at a final volume of 10 % (v/v) was added to SCL4.1/F7 cells in a 96-well plate (2000 cells per well) as per manufacturer's guidelines. Cells were allowed to incubate for 6 hours at 37 °C and the absorbance of the media was then read at 570 nm and 600 nm on a Synergy HT plate reader using Gen5 software. The percentage reduction of alamarBlue® was calculated using the equation:

Percentage reduction of alamarBlue® = $(O2 \times A1) - (O1 \times A2) \times 100$

$$\frac{\quad}{(R1 \times N2) - (R2 \times N1)}$$

Where:

O1 = molar extinction coefficient of oxidized alamarBlue® at 570 nm (80 586)

O2= molar extinction coefficient of oxidized alamarBlue® at 600 nm (117 216)

R1 = molar extinction coefficient of reduced alamarBlue® at 570 nm (155 677)

R2= molar extinction coefficient of reduced alamarBlue® at 600 nm (14 652)

A1 = absorbance of test wells at 570 nm

A2 = absorbance of test wells at 600 nm

N1 = absorbance of negative control well (media plus alamarBlue® but no cells) at 570 nm

N2 = absorbance of negative control well (media plus alamarBlue® but no cells) at 600 nm

3.13.2 Live-dead stain

Cellular gels prepared as described in section 3.12.2 were analysed by NUCLEAR-ID® Blue/Red cell viability reagent (GFP-CERTIFIED®) (Enzo Life Sciences), a mixture of a blue fluorescent cell-permeable nucleic acid dye and a red fluorescent cell-impermeable nucleic acid dye that is suited for staining dead nuclei. The staining pattern allows the determination of live and dead cell populations in GFP-expressing cell lines. The reagent was diluted in fresh cell culture media at a ratio of 1:1000 and incubated with the gels at 37 °C for 1 hour followed by three 5 minute washes in PBS. The stained gels were placed onto microscope slides and five predetermined fields were imaged using a magnification of 20x on a Zeiss Axiolab A1 Axiocam Cm1 microscope.

3.14 Bioluminescence imaging

Luciferase gene expression in transduced cells and cellular gels was assessed using live bioluminescence imaging. A 15 mg/ml (100x) solution of d-luciferin potassium salt (GoldBio) was prepared in sterile normal saline. Luciferin was used at a final concentration of 150 µg/ml in all assays. Bioluminescence images were taken using an IVIS® Lumina Series III *in vivo* imaging system (Perkin Elmer). In order to establish a kinetic curve for luciferin uptake in the cells, cells and gels were imaged immediately after the addition of luciferin and every 5 minutes for 40 minutes.

3.15 *in vitro* 3D co-cultures

3.15.1 PC12 - SCL4.1/F7 co-cultures

EngNT was made using SCL4.1/F7 cells as described in section 3.12.1. The EngNT was cut into 2 equal segments and each segment was transferred to a separate well in a 24-well plate. 1×10^5 PC12 cells suspended in 50 µl medium were seeded on top of each segment. The co-cultures were incubated for 1 hour at 37 °C to allow attachment of PC12 cells to the collagen gel. Following this, 1 ml complete DMEM was added to each well and the co-cultures were incubated at 37 °C in a humidified incubator with 5 % CO₂/95 % air for 72 hours. The co-cultures were then fixed with 4% PFA overnight for relevant analysis. Fluorescence microscopy (Zeiss AxioLab A1 AxioCam Cm1) was used to observe neurites in five pre-determined fields of each gel segment.

3.15.2 HUVEC - SCL4.1/F7 co-cultures

EngNT was made using a mixture of SCL4.1/F7 and HUVECs. Muangsanit *et al.* (unpublished) tested different culture conditions in order to establish the optimal conditions for HUVECs to form tube-like structures in collagen gels. They tested different incubation times and cell densities and it was shown that an incubation time of 4 days and a ratio of 4×10^6 HUVECs: 1×10^6 SCL4.1/F7 cells /ml yielded optimal tube formation. Therefore, these optimised conditions were also used in the current study. Confocal microscopy was used to visualise the endothelial cell network. Angiogenesis Analyzer,

a plugin in ImageJ (Carpentier, 2012), was used to measure the number of meshes, mesh area, number of junctions and total branching length of the tube-like structures per field of view formed by the HUVECs.

3.16 Immunocytochemistry and imaging

Cellular EngNT and 3D co-cultures were fixed in 4 % PFA in PBS overnight at 4 °C followed by two 10 minute washes in PBS. Gels were permeabilised using 0.5% Triton X-100 (Sigma) in PBS for 30 minutes at room temperature with agitation. Gels were washed three times with PBS for 10 minutes each. 5 % normal goat serum in PBS was added for 30 minutes at room temperature to block non-specific binding sites. The goat serum was then removed and after three 5 minute washes with PBS, primary antibodies (table 14) diluted in PBS were added and incubated at 4 °C overnight. The following day the gels were washed three times for 10 minutes in PBS and incubated with secondary antibodies (table 15) diluted in PBS. Gels were incubated for 90 minutes in a dark humidified chamber with agitation. Gels were then washed with PBS. Finally, gels were stained with DAPI with dilution factor of 1:1000 in PBS for 10 minutes and washed once more with PBS before viewing by confocal microscopy. Per cellular gels, two z-stacks were acquired in 2 side regions, each containing 10 - 30 images (depending on the intensity of the signal at various depths) every 1 mm toward the centre of the gels.

3.17 *In vivo* experiments

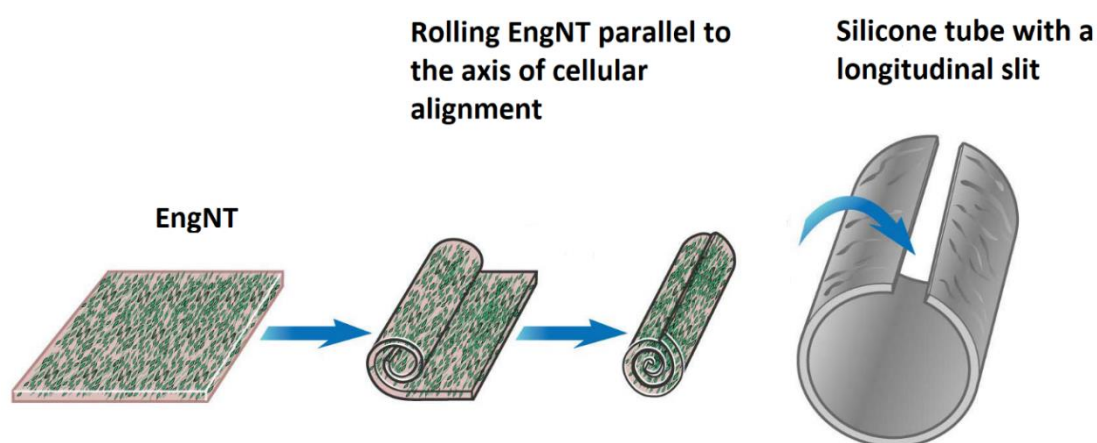
3.17.1 Animals

All surgical procedures were performed according to the Animals (Scientific Procedures) Act 1986 / the European Communities Council Directives (86/609/EEC) and approved by the UCL Animal Welfare and Ethics Review Board. Adult female Wistar rats (180 - 220 g) (Charles River Laboratories) were used for this study. Animals were housed in standard 12-hour light/dark cycles at room temperature and had continuous access to food and water.

3.17.2 Device assembly

Following stabilisation, the EngNT was thoroughly washed in PBS, cut to 15 mm in length, and rolled parallel to the axis of cellular alignment to form a tight rod (figure 21). Each rod was placed inside a sterile 17 mm silicone tube (Syndev; 1.57 mm inner diameter, 0.42 mm wall thickness). Assembled devices were stored in Hibernate™- A (Gibco™; ThermoFisher) on ice until implantation *in vivo*.

Figure 21. Assembly of the implantable device. The stabilised EngNT is rolled parallel to the axis of cellular alignment to produce a rod which is then placed into a silicone tube with a longitudinal slit. Image taken and adapted from Georgiou *et al.* (2013).

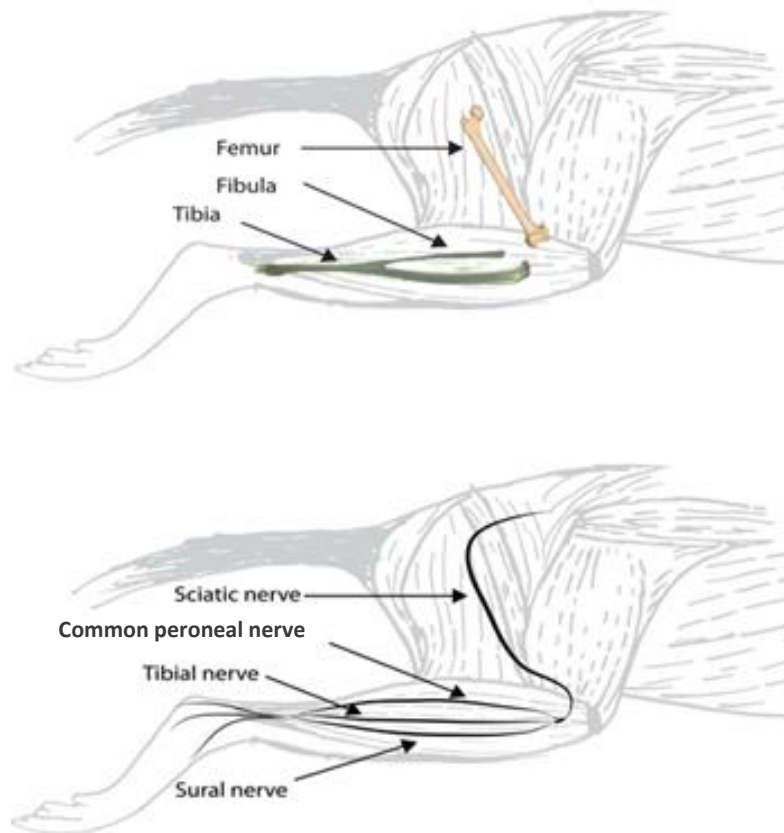


3.17.3 Surgery

The surgical procedure described in this section was carried out by Dr James Phillips (UCL School of Pharmacy). Anaesthesia was induced by inhalation of isoflurane and oxygen in an anaesthesia induction chamber and maintained using an anaesthesia gas mask throughout surgery. Surgery was carried out on a heated operating table set to 37 °C. The breathing of the animals was monitored closely and the anaesthetic dose was adjusted accordingly. Vitamin E eye ointment was applied to both eyes to prevent drying during the procedure.

The thigh was shaved and a 3 cm lateral skin incision between the knee and hip joint was made (figure 22).

Figure 22. The position of the sciatic nerve in relation to the knee and hip. The sciatic nerve innervates the posterior aspect of the thigh and the entire lower limb below the knee except for a small patch of skin on the medial aspect of the leg and ankle, which is innervated by the saphenous nerve. Image taken and adapted from Nijhuis *et al.* (2013).



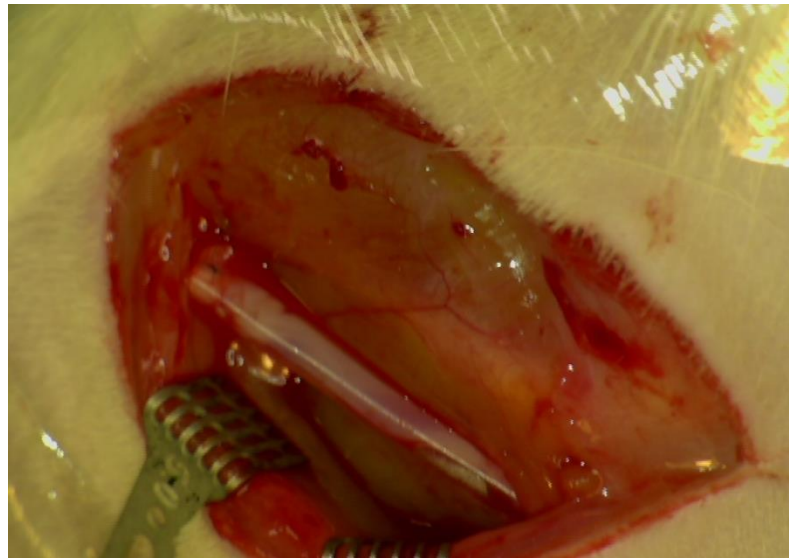
The intermuscular planes were separated using blunt dissection until the sciatic nerve was exposed (figure 23).

Figure 23. Exposing the sciatic nerve. The sciatic nerve was exposed at the mid-thigh.



The nerve was freed from the surrounding tissue under a dissecting microscope and transected mid-way between the hip and knee. The repair device was secured to the proximal and distal stumps of the transected nerve using two epineurial 10-0 non-absorbable nylon sutures (Ethicon) at each stump (figure 24).

Figure 24. Positioning the implantable device. The implantable device was positioned between the stumps to produce an inter-stump distance of 15 mm. The device was kept in place using two 10/0 epineurial sutures at each stump.



The muscle layer was closed with one 4-0 suture (figure 25) and the skin incision was closed using wound clips. 0.1 ml carprofen (5 % w/v) analgesic was administered subcutaneously to the injury site and wound powder was applied over the area to reduce the risk of infection.

Figure 25. Closing the muscle layer. The muscle layer was closed with one 4-0 suture.



Immediately after surgery, the animals were placed in a post-operative warming chamber and monitored closely until they recovered from the anaesthesia. They were then returned to their previous social group. The wound clips were removed 7 days after surgery using a wound clip remover. The animals were monitored for signs of pain, distress and weight loss until culled at the time point being investigated.

3.17.4 *in vivo* bioluminescence imaging

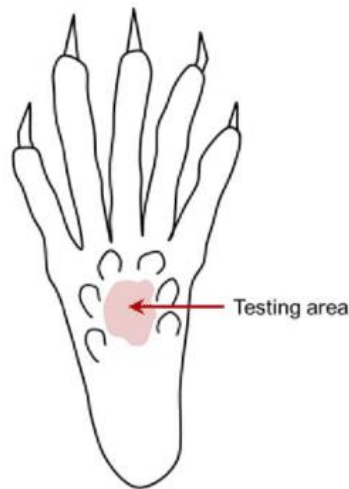
Rats were anaesthetised using an isoflurane vaporiser and 150 mg/kg of d-luciferin was injected intraperitoneally into the lower right quadrant of the abdominal region 10 minutes before imaging. The rats were placed inside the camera box of the *in vivo* imaging system. Images were taken every 10 minutes for up to 40 minutes. An exposure time of 10 minutes, f-stop of 1 and binning value at medium were used.

3.17.5 Functional tests

3.17.5.1 Von Frey

Rats were placed in acrylic chambers suspended above a wire mesh grid and allowed to acclimatise for 15 minutes prior to testing. There are different methods of measuring paw withdrawal with von Frey filaments. However, according to Bonin *et al.* (2014), the up-down method of Dixon (1965) as applied to rodents by Chaplan *et al.* (1994) is one of the most commonly used. Using this approach, the von Frey filaments were pressed against the plantar surface of the paw (figure 26) until the filament buckled. A positive response was recorded if the paw was withdrawn on application of the filament. A lack of response to a filament required stimulation with the next higher filament, while a positive response necessitated the use of the next lower filament in order to establish the lowest stimulus required to elicit a response.

Figure 26. Application of the von Frey filament on the rat's hind paw. The von Frey filaments were applied to the testing area shown. Image taken and adapted from Ferrier *et al.* (2016).



3.17.5.2 Static sciatic index

The animals were placed in an acrylic chamber and allowed to adopt a normal stance (supported by all four paws). Three images of the plantar surface of the hind paws were acquired per animal. The toe spread (distance between the tips of the first and fifth digits) and intermediate toe spread (distance between the tips of the second and fourth digits) of the injured and non-injured paws were measured using the digital images (figure 27). These values were averaged and incorporated into equations to used calculate the static sciatic index as described by Bervar (2000).

$$\text{Toe spread factor (TSF)} = (\text{ETS}-\text{NTS})/\text{NTS}$$

$$\text{Intermediary toe spread factor (ITF)} = (\text{EIT}-\text{NIT})/\text{NIT}$$

$$\text{Static sciatic function (SSF)} = 108.44 \text{ TSF} + 31.85 \text{ ITF} - 5.49$$

Where:

E= experimental side

N= normal side

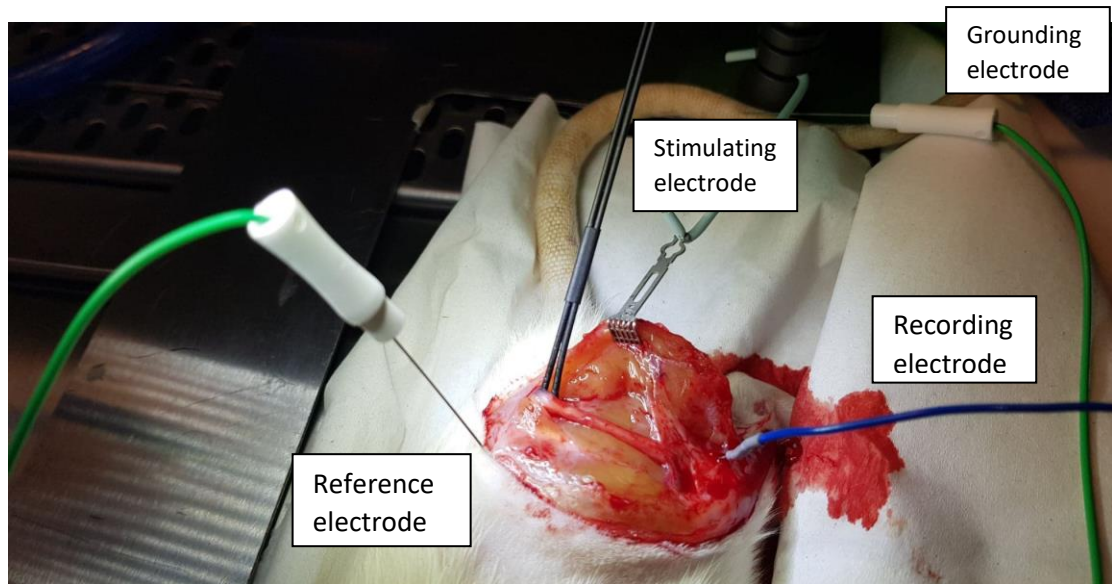
Figure 27. Calculating the static sciatic index. The toe spread and intermediate toe spread were used to determine the static sciatic index.



3.17.6 Electrophysiology

After 8 weeks, animals were anaesthetised and nerve function was assessed electrophysiologically (using a Sapphire 3ME system) by comparing the repaired nerve to the contralateral control nerve in each animal. A grounding electrode and a reference electrode (Ambu® Neuroline 710) were attached to the animal. A stimulating electrode (Neurosign Bipolar Probe 2 × 100 mm × 0.75 mm electrode) was placed proximal to the repair site on the surface of the nerve and a recording electrode (Ambu® Neuroline concentric) was placed into the gastrocnemius muscle (figure 28). The distance between the stimulating and recording monopolar electrodes was standardised. Electrophysiological stimulation of the nerve was performed in a bipolar stimulation constant voltage configuration and muscle response was recorded. The stimulation threshold was determined by increasing the stimulus amplitude in 0.1 V steps (200 µs pulse) up to 10 V, until a reproducible, stimulus-correlated muscle action potential was recorded. The latency was measured from the time of stimulus to the first deviation from the baseline, and the amplitude of the compound muscle action potential was measured from baseline to the greatest positive peak. Recordings were conducted in triplicate for the repaired nerve and contralateral control nerve in each animal.

Figure 28. Electrophysiology set up. Electrophysiological stimulation of the nerve was performed in a bipolar stimulation constant voltage configuration and the muscle response recorded.

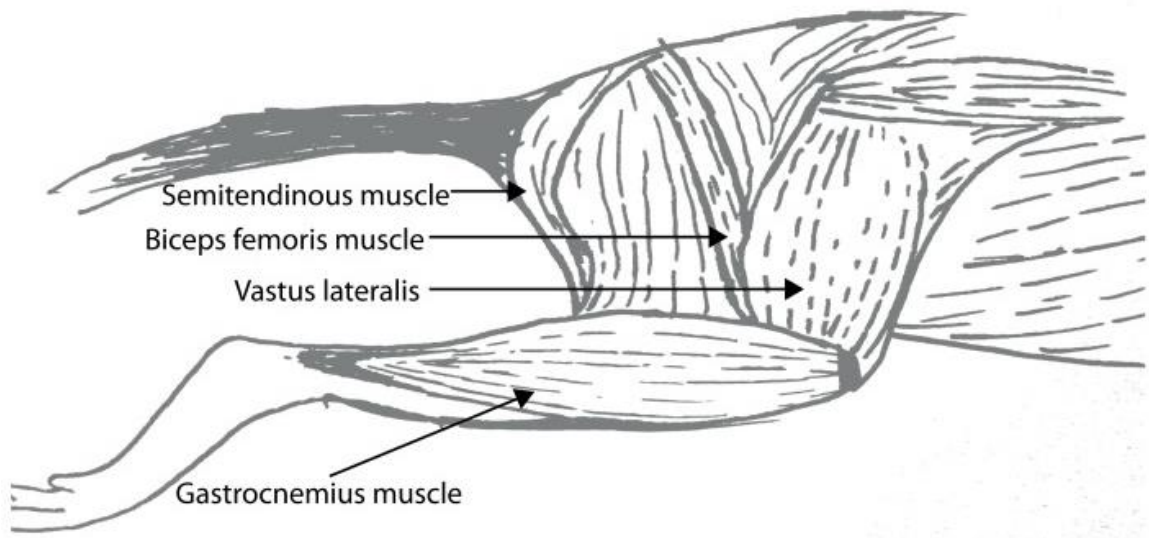


2.17.7 Tissue harvesting

Immediately following electrophysiological analysis, animals were culled by cervical dislocation according to Schedule I in the Animals (Scientific Procedures) Act 1986. The sciatic nerve was cut above and below the repair device and mounted onto a cardboard frame, indicating the proximal and distal stumps, and immersion-fixed in 4 % PFA. The contralateral nerve was also harvested and processed in the same way.

In order to evaluate the degree of muscle atrophy, the gastrocnemius muscle (figure 29) on each side were also harvested. An incision was made in the hind paw between the hip and the paw, exposing the gastrocnemius muscle which was then separated from the soleus muscle and collected. The wet muscle weight was measured immediately using a digital scale.

Figure 29. The gastrocnemius muscle. The gastrocnemius muscle undergoes significant atrophy in a rat sciatic nerve transection model. Thus, wet gastrocnemius muscle mass measurements may reflect the recovery of gastrocnemius muscle innervation and overall neuromuscular function recovery. Image taken from Nijhuis *et al.* (2013).



3.17.8 Processing of tissue

3.17.8.1 *ex vivo* bioluminescence imaging

150 $\mu\text{g/ml}$ luciferin substrate was added to the excised nerves which had been repaired by EngNT containing transduced SCL4.1/F7 cells expressing luciferase. Bioluminescence images were taken using the *in vivo* imaging system immediately after the addition of the substrate and every 5 minutes for 30 minutes.

3.17.8.2 Tissue fixing and cryosectioning

Excised nerves were immersion-fixed in 4 % PFA at 4 °C overnight after which they were washed with PBS and transferred to 30 % sucrose (Sigma-Aldrich) in PBS overnight. Nerves were embedded in a 50:50 solution of 30 % sucrose and optimal cutting temperature (OCT) compound (Leica Biosystems) in moulds and allowed to set at room temperature for 2 hours. The nerves were then snap frozen in liquid nitrogen and stored at -20 °C until required.

Transverse cryostat sections (10 μm thick) were prepared from the middle of the device and the proximal and distal parts of the nerve stumps at a constant temperature of -20

°C. The transverse sections that were used for analysis were from positions 1 mm into the proximal and distal stumps, measured from the end of the nerve stump in each case, and from the middle of the device.

3.17.9 Immunofluorescence staining of nerve sections

3.17.9.1 Preparation of chrome-gelatine coated slides

In order to increase tissue adhesion and allow downstream washes in immunofluorescent studies, all microscope slides (Superfrost, VWR) were double coated with a thin layer of gelatine. 2.5 g of gelatine powder (VWR) and 0.25 g of chromium (III) potassium sulfate 12-hydrate (VWR) were added to 500 ml dH₂O. The mixture was warmed to 45 °C and constantly stirred until a uniform solution was obtained. Slides in slide racks were briefly immersed in the solution and allowed to dry at 56 °C overnight. The process was repeated a second time the following day.

3.17.9.2 Immunofluorescence

Nerve sections were washed in immunostaining buffer (PBS, 0.2 % Triton-X (Sigma-Aldrich), 0.002 % sodium azide (Sigma-Aldrich) and 0.25 % BSA) before the addition of normal goat serum (Vector Laboratories) (1:20 in immunostaining buffer) for 45 min. The blocking serum was then removed and sections were incubated with the relevant primary antibodies (diluted in immunostaining buffer) (table 15) overnight at 4 °C. The sections were then washed with immunostaining buffer before addition of the fluorescence-tagged secondary antibody (table 16), and incubated at room temperature for 90 min. Sections underwent a final wash with immunostaining buffer before mounting with Vectashield.

Table 15. Primary antibodies used in immunofluorescence studies.

Primary antibody	Host	Reactivity	Dilution	Incubation conditions
Anti-VEGFA (ab1316, Abcam)	Mouse	Mouse, rat, rabbit, dog, human	1:1000	Overnight at 4 °C
Anti-CD31 (M0823, Dako)	Mouse	Human	1:50	
Anti-S100 (Z0311, Dako)	Rabbit	Mouse, human, rat, zebrafish	1:400	
Anti-RECA1 (MCA970R, Bio-Rad)	Mouse	Rat	1:200	
Anti-BIII-Tubulin (T8578, Sigma-Aldrich)	Mouse	Human, mouse rat	1:400	
Anti-Neurofilament (SMI-35P-050, Eurogentec)	Mouse	Mammalian	1: 1000	

Table 16. Secondary antibodies used in immunofluorescence studies.

Secondary antibody	Host	Reactivity	Dilution	Incubation conditions
Alexa Fluor®488 conjugated anti-rabbit IgG (A-11008, LifeTechnologies)	Goat	Rabbit	1:200	90 minutes at room temperature
DyLight® 549 conjugated anti-mouse IgG (STAR117D549GA)	Goat	Mouse	1:200	

3.17.9.2 Quantitative analysis of immunofluorescence staining

Tile scans were used to capture the entire nerve cross-section using a Zeiss LSM 710 confocal microscope and images were analysed using Volocity™ 6.4 (PerkinElmer) running automated image analysis protocols to determine the number of neurofilament-immunoreactive neurites in each transverse nerve section. RECA-1 was used to visualise blood vessels, which were also counted. Blood vessel diameter was measured from images captured (Zeiss AxioCam) using ImageJ.

3.18 Statistical analysis

All statistical analyses were carried out using GraphPad Prism software (version 5). A Shapiro-Wilk normality test was conducted on all data to determine appropriate statistical tests. For normally distributed data, two sample comparisons were performed using the student's t-test and multiple comparisons were analysed by analysis of variance (ANOVA) followed by a Tukey's post-test. Data which did not follow a normal distribution was analysed by a Kruskal-Wallis test followed by a Dunn's post-test. For all tests, $*p < 0.05$, $**p < 0.01$, $***p < 0.001$ and $****p < 0.0001$ were considered to be significant. All graphs are plotted as individual data points with error bars representing the standard deviation unless otherwise stated.

Chapter 4. An evaluation of lentiviral-mediated gene delivery to Schwann cells for the purpose of peripheral nerve tissue engineering

4.1 Introduction

Nerve regeneration following injury can be enhanced by the implantation of tissue-engineered constructs consisting of cells and biomaterials. It is thought that the presence of living cells is required for providing the signals necessary for optimal neurite extension and repair (de Luca *et al.*, 2015). Therefore, tissue-engineering strategies focusing on biomaterials with aligned cells which can direct axon growth are favourable. These constructs can mimic the natural environment that consists of cell-cell interactions, ECM molecules and growth factors.

Georgiou *et al.* (2013) developed aligned cellular biomaterials for the purpose of peripheral nerve repair. The technique involved cellular self-alignment in collagen gels with a stabilisation step involving removal of interstitial fluid. The engineered neural tissue (EngNT) produced consisted of aligned cells distributed evenly throughout a stable aligned matrix. Testing of this device for repair of a critical-sized 15 mm gap in a rat model of sciatic nerve injury showed that robust neuronal regeneration across the gap had occurred at eight weeks. As promising results had already been obtained using this tissue engineering strategy, the overall aim of the current project was to retain the aligned cellular architecture achieved in the EngNT and to enhance the efficacy of the technology by gene delivery.

Vascularisation of tissue-engineered constructs that are too thick to be sustained by diffusive nutrient transport alone (>100–200 μm) remains a major challenge in the field of tissue engineering (Chang and Niklason, 2017). An experimental approach for enhancing vascularisation to tissue engineered constructs following implantation is the use of genetically modified cells expressing angiogenic factors. Thus the genetic modification of cells used in EngNT in the current study may further aid peripheral nerve regeneration by providing the biological cues required to induce rapid vascularisation.

Prior to designing and producing a lentiviral vector delivering angiogenic factors, an initial proof-of-concept study was conducted. The aims of this initial study were to:

- Use a lentiviral vector to deliver the reporter genes luciferase and eGFP to a rat Schwann cell line (SCL4.1/F7) previously used to construct EngNT (Georgiou *et al.*, 2013).
- Evaluate the transduction efficiency and assess whether transduction affected cell health.
- Investigate the ability of the genetically modified cells to form EngNT.

4.2 Lentiviral mediated gene delivery to SCL4.1/F7 cells

4.2.1 The SFFV.Luc.2A.eGFP lentiviral vector

A lentiviral vector delivering luciferase and eGFP (figure 30) was used for the initial proof-of-concept study. This vector was designed, produced and titred by Dr Michael Hughes from Dr Ahad Rahim's research group at the UCL School of Pharmacy. Titration of the viral preparation by P24 assay revealed a high titre of 1×10^9 viral particles/ml.

Figure 30. A schematic of the lentiviral vector backbone delivering luciferase and eGFP reporter genes. LTR – long terminal repeats; RRE – Rev response element; SFFV - spleen focus forming virus promoter; Luc – luciferase; 2A – self cleaving element; eGFP enhanced green fluorescent protein; WPRE - woodchuck hepatitis virus post-transcriptional regulatory element.



4.2.2 The SCL4.1/F7 cell line

An important step in this project was the identification of a cell type which could be used to investigate whether gene therapy augmented tissue engineering can enhance peripheral nerve regeneration. Georgiou *et al.* (2013) showed that EngNT made from SCL4.1/F7 cells enhanced nerve regeneration when implanted into a rat model of sciatic nerve injury. Based on these promising results and the group's experience with culturing SCL4.1/F7 cells, it was decided that this cell line would be a good starting point for the

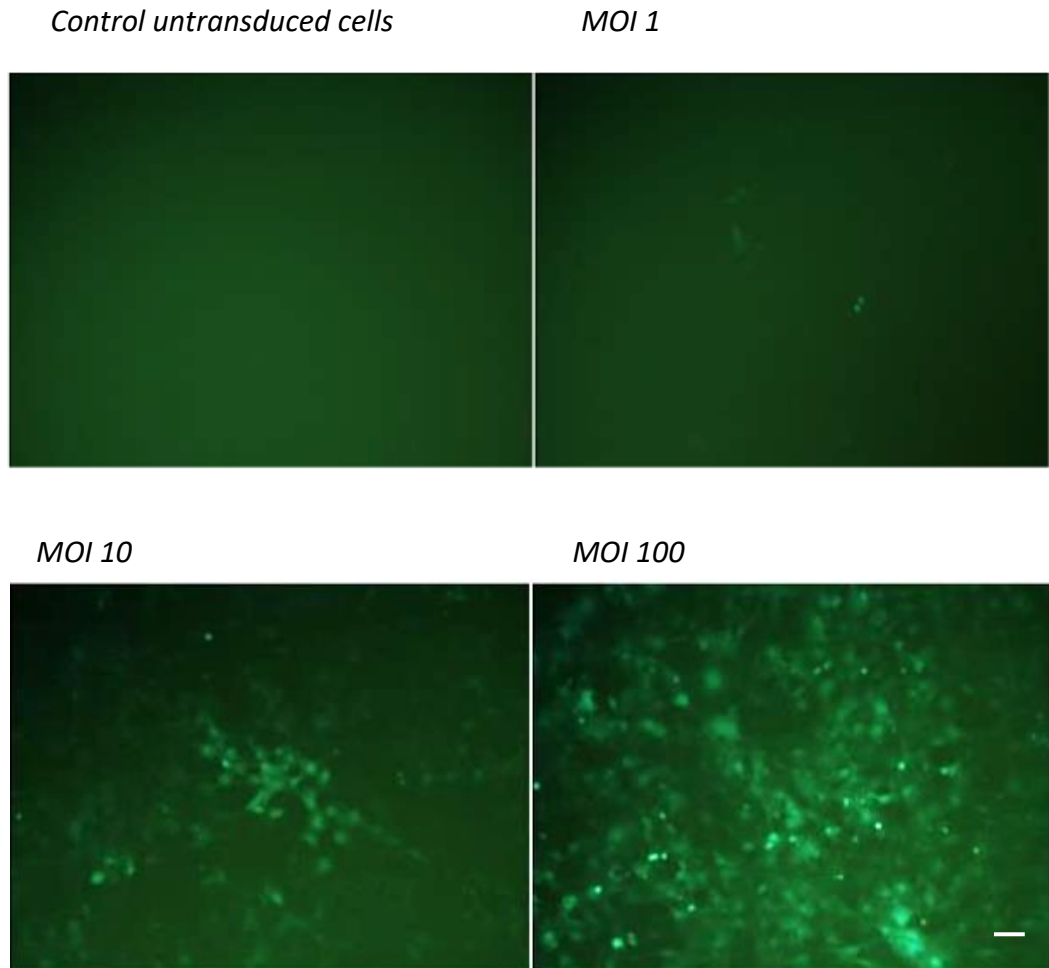
current project. Additionally, it is a reliable, cost efficient and reproducible cell line which can be cultured to produce the large number of cells required for tissue engineering purposes. Further, it is a rat Schwann cell line and would avoid immunosuppression treatment in subsequent *in vivo* experiments.

4.2.3 Lentiviral transduction resulted in eGFP expression

SCL4.1/F7 cells were transduced with the lentiviral vector at a MOI of 1, 10 and 100 to determine the optimal ratio of viral particles to cells for efficient transduction. Research has shown that a MOI which is too low may result in insufficient gene transfer and transgene expression. On the other hand, a very high MOI may cause several copies of transgene to integrate into the chromosomes of the target cells, leading to chromosomal instability (Woods *et al.* 2003).

Using fluorescence microscopy, eGFP expression was observed in the transduced cells 48 hours post transduction and the number of eGFP positive cells continued to increase over the next 24 hours. No eGFP expression was seen in the control untransduced cells. As expected, the MOI of 100 resulted in the greatest proportion of eGFP positive cells (figure 31).

Figure 31. SCL4.1/F7 cells expressing eGFP 72 hours post transduction. Representative fluorescence micrographs of control untransduced SCL4.1/F7 cells and cells transduced with the lentiviral vector delivering luciferase and eGFP at MOIs of 1, 10 and 100. No fluorescence was observed in the control untransduced cells. A higher proportion of eGFP positive cells was observed with increasing MOI (n = 3 per group). Scale bar: 50 μ m.



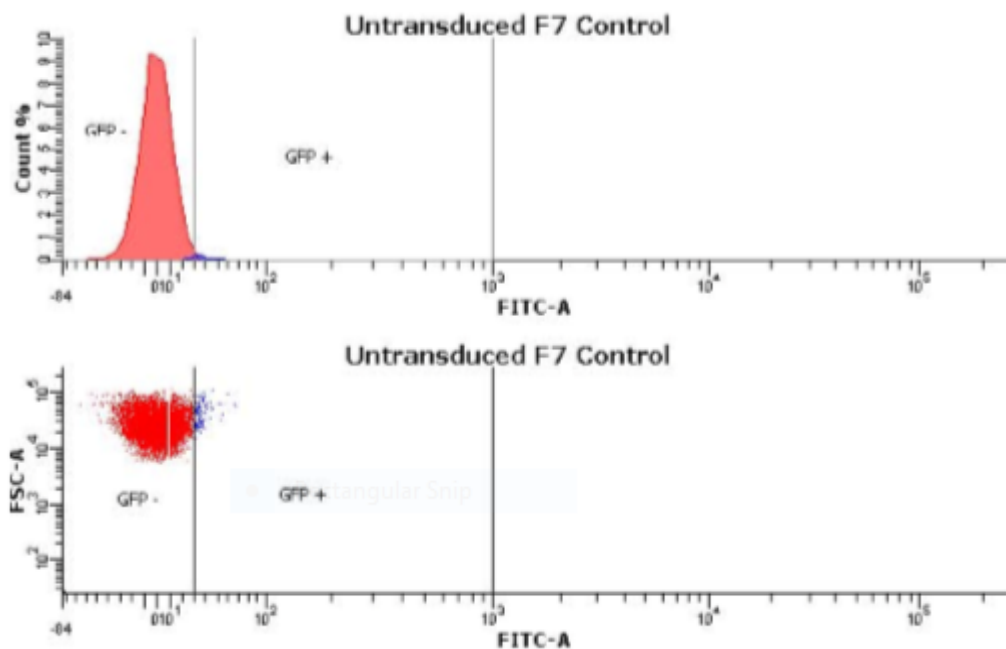
4.2.4 Establishing the transduction efficiency using flow cytometry

After establishing that the SCL4.1/F7 cells were transduced using fluorescence microscopy, flow cytometry was used to determine the percentage of transduced cells, thus establishing the transduction efficiency for each MOI. To establish the background for fluorescence and to set gates for data acquisition, control untransduced cells were used. Two figures were generated for each MOI (figure 32). The first figure is a histogram which displays the relative fluorescence on the x-axis and cell count on the y-axis. The histogram shows the total number of cells in a sample which express the marker of interest, i.e., it shows the number of eGFP positive cells for each MOI. Fluorescent cells were identified by setting a minimum fluorescence value (thresholding) on the

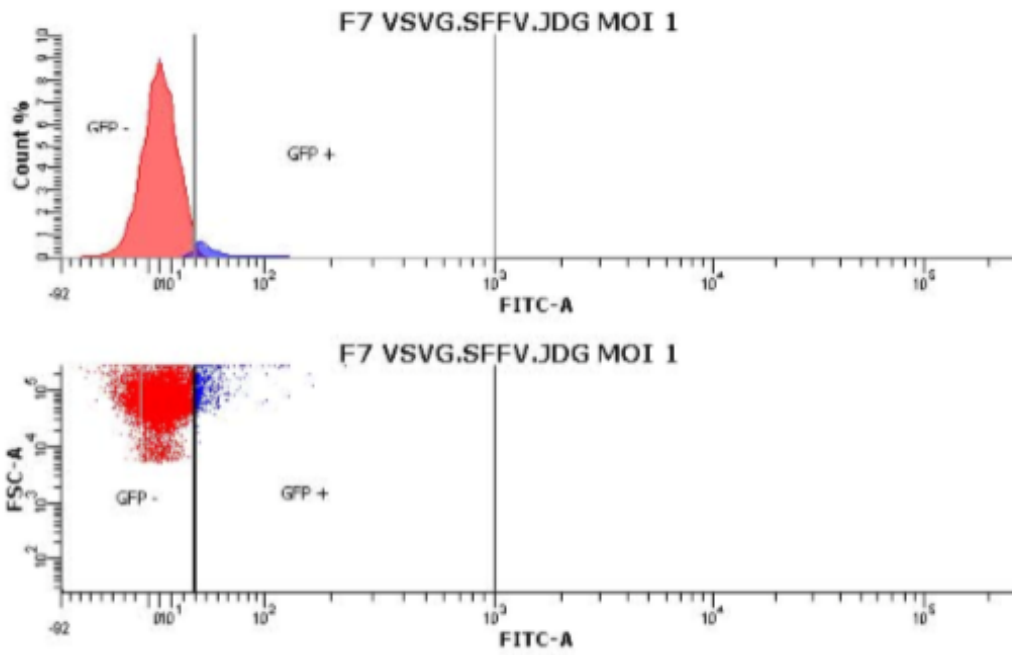
histogram. By setting the threshold just to the right of the dimmest peak, cells to the left of the threshold were excluded from those counted as fluorescent. The second figure is a density plot or a plot of forward scatter. Each dot or point represents an individual cell that has passed through the instrument. Care was taken to analyse cells that were in the required gate as indicated by forward scatter characteristics.

Figure 32. Flow cytometry analysis of eGFP expressing cells. Typical flow cytometry analysis data showing the proportion of eGFP positive and eGFP negative cells at the different MOIs. eGFP positive cells are shown in blue and eGFP negative cells are shown in red.

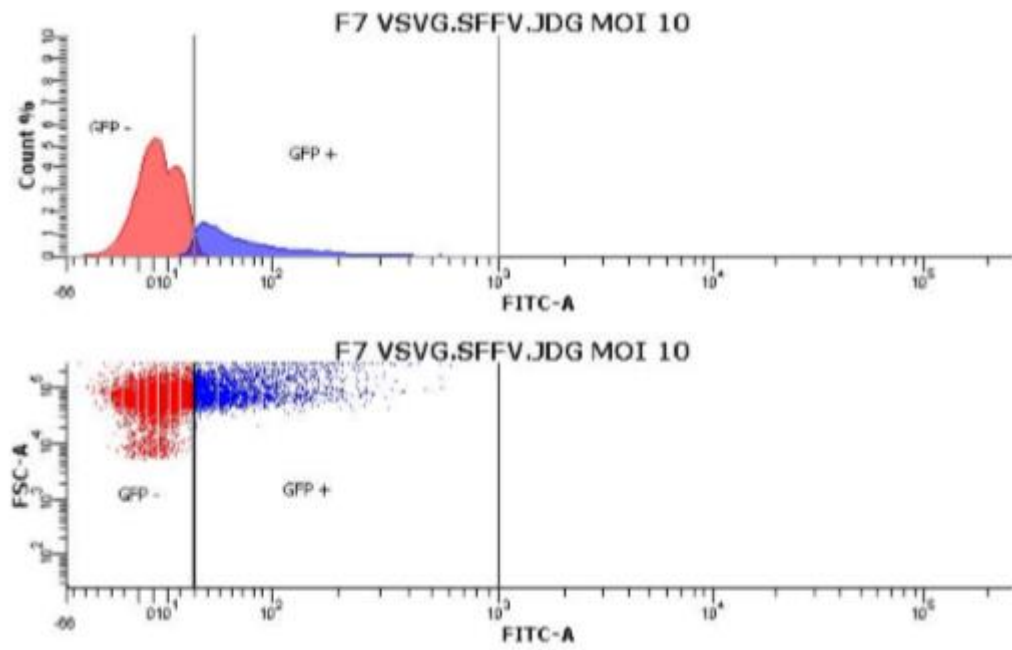
Control untransduced cells



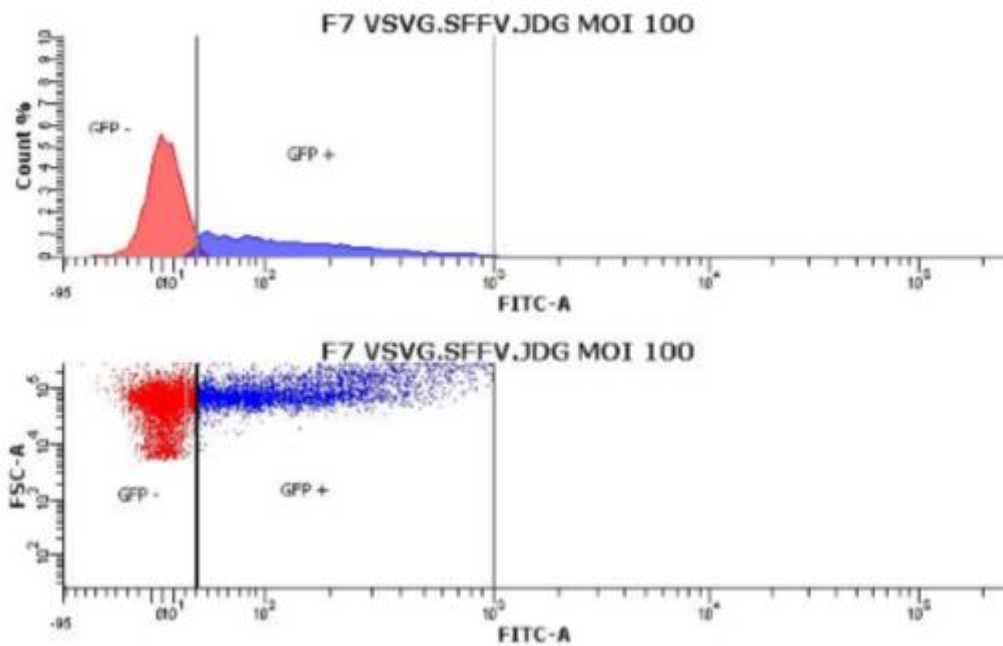
MOI 1



MOI 10

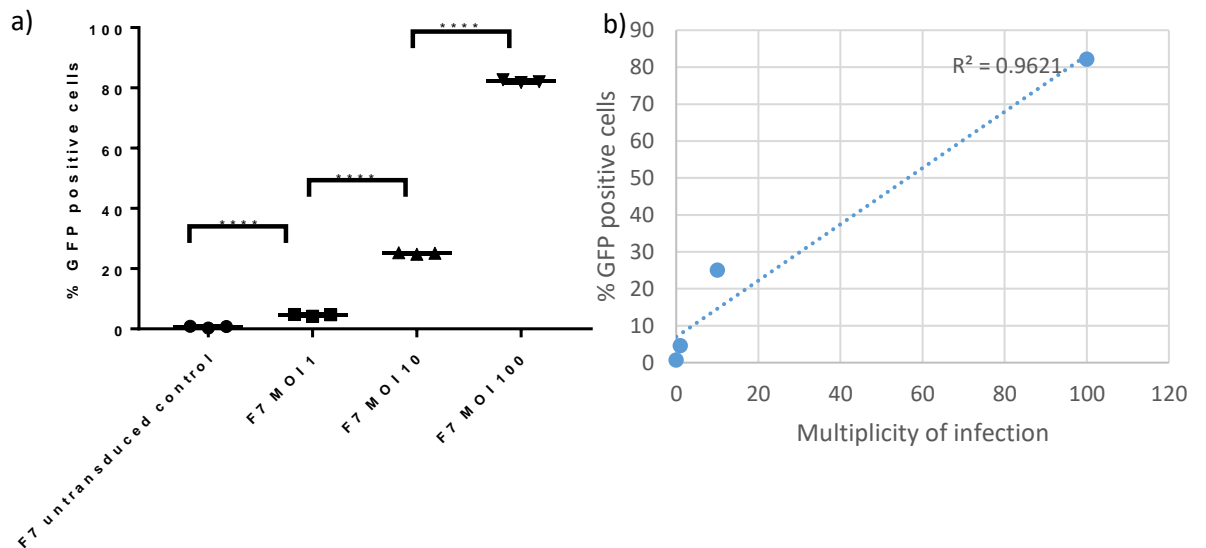


MOI 100



As expected from the fluorescence microscopy data (section 4.2.3), the percentage of eGFP positive cells increased with increasing MOI (figure 33). However, the increase in eGFP positive cells was not proportionate to the increase in MOI. A MOI of 1 resulted in an average of 4.57 % eGFP positive cells, while a MOI of 10 and 100 resulted in an average of 25.07 % and 82.17 % respectively.

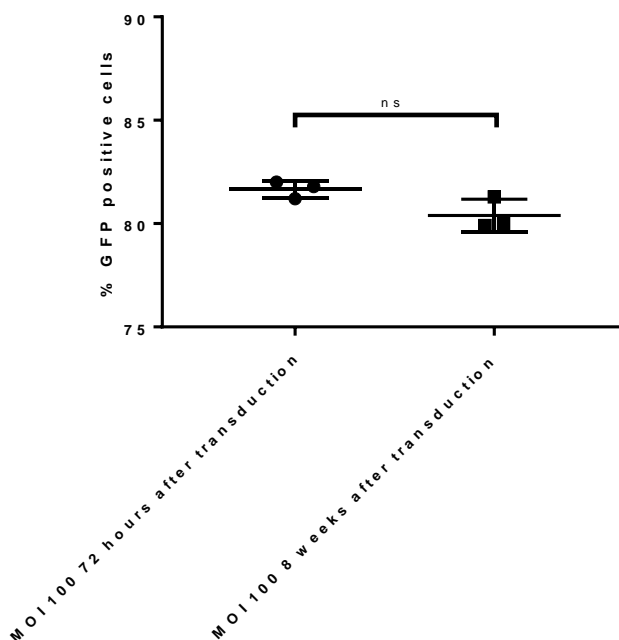
Figure 33. Efficiency of lentiviral-mediated gene transfer to SCL4.1/F7 cells at increasing MOIs. a) The percentage of eGFP positive cells significantly increased with increasing MOI (one-way ANOVA, Tukey's multiple comparisons test, 95 % confidence interval, p value = <0.0001). b) A scatter plot of the mean value of the runs shown in a) with a line of best fit to represent the trend between MOI and percentage of eGFP positive cells. Each data point represents an individual flow cytometry run with 750 000 cells per sample (n = 3 per group). * $p < 0.05$, ** $p < 0.01$, *** $p < 0.001$ and **** $p < 0.0001$.



4.2.5 Stability of eGFP expression

To assess the stability of eGFP expression, cells transduced with a MOI of 100 were maintained in culture for 8 weeks (> 25 passages) and flow cytometry analysis was repeated. The mean number of eGFP positive cells decreased by around 1.3% (figure 34). However, this change was not significant and indicated that eGFP expression remained stable during this period. Additionally, eGFP positive cells could be observed using a fluorescence microscope until the cells were discarded due to high passage number.

Figure 34. Stability of lentiviral mediated eGFP expression over an 8 week period. While slightly lower than at 72 hours after transduction, eGFP expression was not significantly lower at 8 weeks post transduction (two-tailed unpaired T test, 95 % confidence interval, p value = 0.0108). Each data point represents an individual flow cytometry run with 750 000 cells per sample (n = 3 per group). * $p < 0.05$, ** $p < 0.01$, *** $p < 0.001$ and **** $p < 0.0001$.



4.2.6 Effect of transduction on cell viability, proliferation and morphology

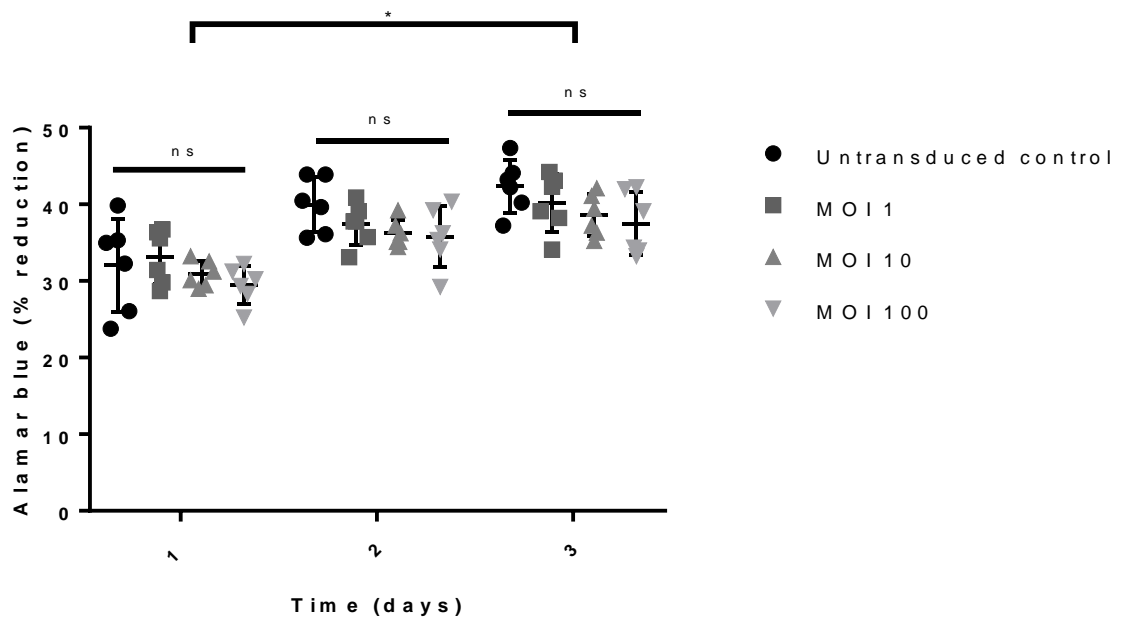
After establishing high-level gene expression in transduced SCL4.1/F7 cells, it was important to test whether lentiviral transduction resulted in cytotoxic effects as highly concentrated vesicular stomatitis virus G glycoprotein (VSG-V) pseudotyped lentiviral vectors have been previously reported to cause cytotoxicity (Castellani *et al.*, 2010; Joglekar and Sandoval, 2017). In depth analysis was carried out by assessing cell viability, proliferation rate and morphology.

Cell viability

AlamarBlue® was used to detect any changes in the metabolic activity of cells following transduction at MOIs of 1, 10 and 100. Mitochondrial enzymes present in viable cells reduce resazurin (blue) present in AlamarBlue® to resorufin (red). The extent of reduction is a reflection of cellular activity and can be quantified using absorbance (Rampersad *et al.*, 2012). After 3 days, the percentage reduction of AlamarBlue® in

control untransduced cells increased by an average of 36.73 %, whereas the percentage reduction of alamarBlue® in cells transduced with a MOI of 1, 10 and 100 increased by an average of 23.49, 24.95 and 27.98 % respectively (figure 35).

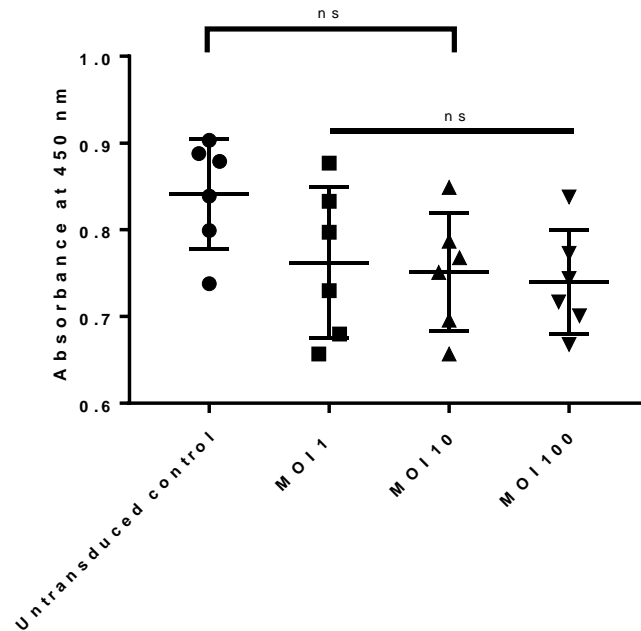
Figure 35. Effect of transduction on cell viability. There was no significant difference between the groups on each day (two-way ANOVA, Tukey's multiple comparison test, 95 % confidence interval, p value = >0.4111). However, the % reduction for all the groups was significantly higher on day 3 when compared to day 1 (p value = <0.0391). Each point represents the percentage reduction by control cells and cells transduced with the different MOIs over 3 days, $n = 6$ per group. * $p < 0.05$, ** $p < 0.01$, *** $p < 0.001$ and **** $p < 0.0001$.



Proliferation

BrdU is a synthetic thymidine analog that incorporates into the DNA of dividing cells during the S-phase of the cell cycle. The amount of BrdU incorporated into cultured cells can be quantified colorimetrically by ELISA and is a commonly employed method to assess cell proliferation (Vega-Avila and Pugsley, 2011). In the present study, a BrdU ELISA kit was used to assess whether lentiviral mediated gene delivery to SCL4.1/F7 cells had an effect on cell proliferation. Control untransduced cells had a mean absorbance of 0.84, while cells transduced with MOIs of 1, 10 and 100 had a mean absorbance of 0.76, 0.75 and 0.74 respectively. This was equivalent to an approximately 1.12 fold difference in proliferation between the control untransduced cells and the transduced cells, irrespective of MOI. However, this difference did not prove to be significant (figure 36).

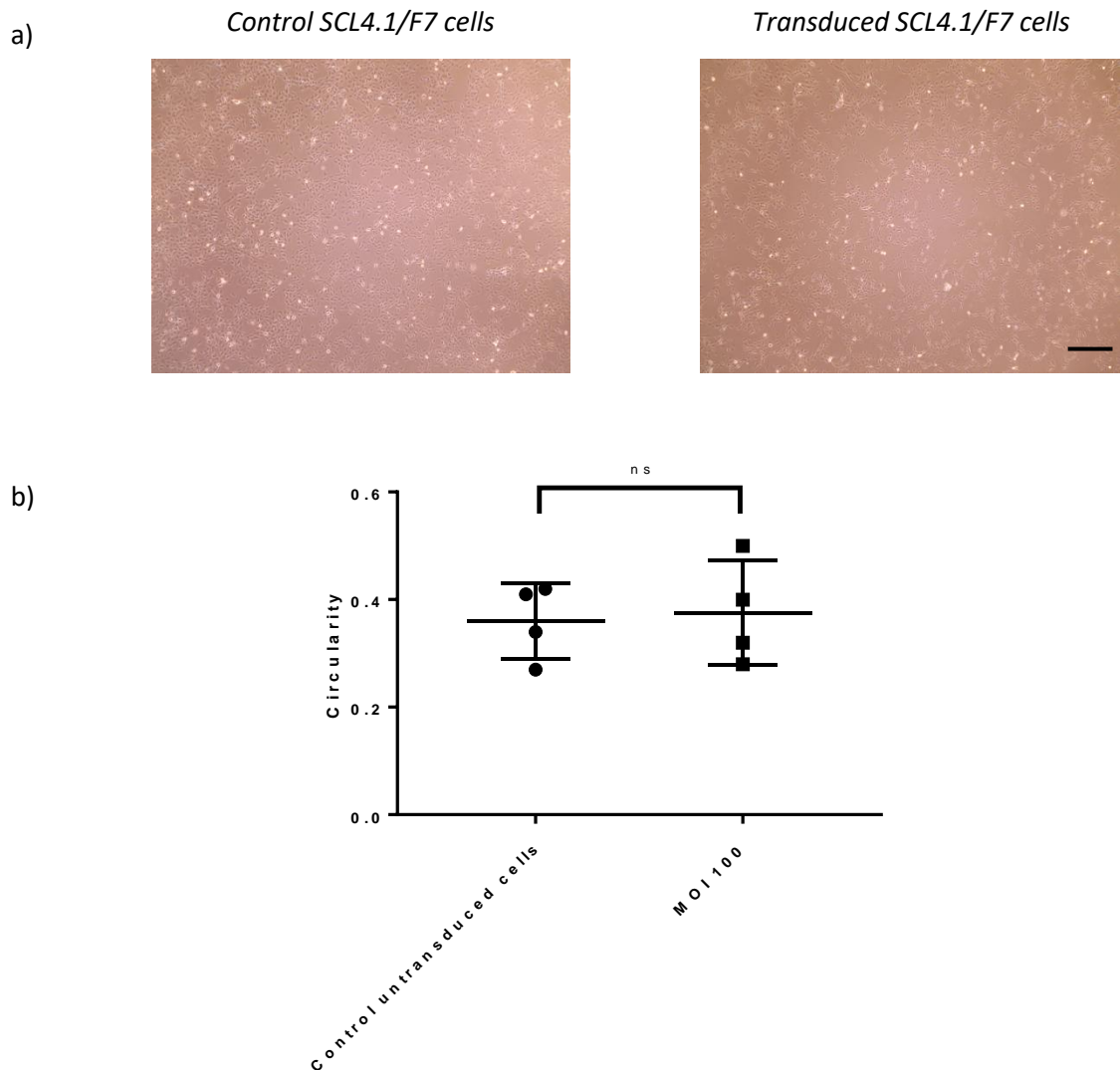
Figure 36. Effect of lentiviral transduction on SCL4.1/F7 cell proliferation. Transduction with the lentiviral vector at different MOIs did not have a significant effect on proliferation (two-way ANOVA, Tukey's multiple comparison test, 95 % confidence interval, p value = >0.9467). There was no significant difference between the transduced cells and the control untransduced cells (p value = >0.0939). Each data point represents the absorbance for control cells and cells transduced with different MOIs (n = 6 for each group). *p < 0.05, **p < 0.01, ***p < 0.001 and ****p < 0.0001.



Morphology

Morphology is an important large-scale manifestation of the physiological state of cells, and is commonly used as a qualitative measure of toxicity (Pincus and Theriot, 2007). Morphology was observed using light microscopy and cell shape was analysed by measuring circularity with ImageJ (figure 37). Circularity is a normalised ratio of area to perimeter and was defined as $4\pi \times (\text{area}/\text{perimeter}^2)$. A circle has a circularity value of 1 and lines have a circularity value of 0 (Hart *et al.*, 2018). Control untransduced cells had a mean circularity factor of 0.36 while cells transduced with a MOI of 100 had a mean circularity factor of 0.38 (figure 37).

Figure 37. Effect of lentiviral transduction on SCL4.1/F7 morphology. a) Representative light microscopy images of SCL4.1/F7 control untransduced cells and SCL4.1/F7 cells transduced with a MOI of 100 at the same passage number (p 15). Scale bar: 150 μ m. No gross changes in morphology were observed. b) The circularity factor was used to analyse morphology. No significant difference between the two groups was observed (two-tailed unpaired T test, 95 % confidence interval, p value = 0.8103). Each data point represents the mean circularity factor of 40 cells from one image (n = 4 independent images for each group).



4.3 *in vitro* bioluminescence imaging

In the field of tissue engineering, there is a need for methods that allow the monitoring of tissue engineered constructs noninvasively *in vitro* and *in vivo*. Bioluminescence imaging has been widely used for non-invasive and highly sensitive visualisation of implanted cell localisation, proliferation and migration *in vivo* (Hwang *et al.*, 2014a). It is also a well-established method for monitoring cell viability (Peeters *et al.*, 2015), using a luminometer or an *in vivo* imaging system (IVIS). One of the aims of the current study

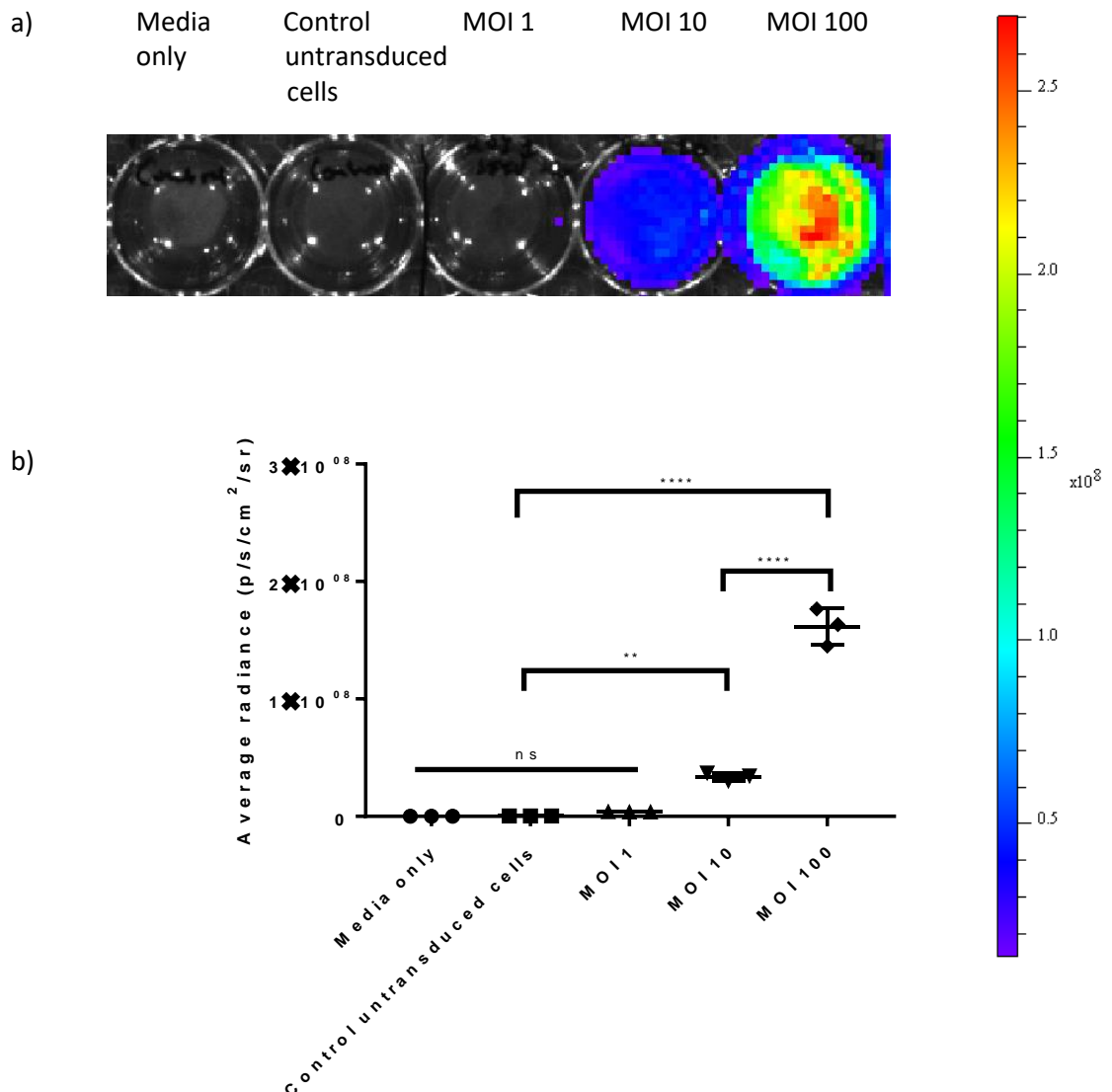
was to establish whether bioluminescence imaging can be used to monitor cell viability in EngNT used for peripheral nerve engineering. Prior to constructing EngNT, lentiviral-mediated luciferase expression in 2D monolayers was studied to identify signal strength, luciferin kinetics, possible luciferin toxicity and stability of the luciferase signal over time and after cryopreservation.

4.3.1 Lentiviral transduction resulted in luciferase expression

The bioluminescence signal produced by SCL4.1/F7 cells *in vitro* was measured using an IVIS. The bioluminescence images were overlaid on black and white photographs of the well plates that were taken just before bioluminescence imaging, allowing the precise location of the light emission to be determined. The intensity of light emission was represented using a pseudo-colour scale, with red areas showing the highest amount of light emission and blue areas showing the least. A circular region of interest was drawn around each well on the well plates and the bioluminescence values were measured in absolute units of radiance (photons/sec/cm²/steradian). This unit refers to the photons per second of light that radiate in a unit area (1 cm²) and unit angle (1 steradian) and enables data comparison between different systems and experiments (Zinn *et al.*, 2008).

Control untransduced cells had a mean bioluminescence signal of 2.85×10^5 which was similar to the signal given by culture media only (1.36×10^5). As expected, the bioluminescence signal increased with increasing MOI. Compared to the control, cells transduced with MOIs of 1, 10 and 100 showed a 13.38, 114.48 and 547.18 fold increase in signal respectively. The signal emitted by the SCL4.1/F7 cells transduced with a MOI of 1 was not statistically different to the control untransduced cells (figure 38). Based on this data, together with the results generated from fluorescence microscopy, flow cytometry analysis and cell proliferation and viability assays described earlier, it was decided that a MOI of 100 will be used throughout the study.

Figure 38. Bioluminescence imaging of SCL4.1/F7 transduced with MOIs of 1, 10 and 100. a) Representative bioluminescence images of Luciferase expressing SCL4.1/F7 transduced with different MOIs imaged 72 hours post transduction. A well containing media with no cells was used to determine the background bioluminescence. The rainbow pseudocolour scale was adjusted for all images. b) There was no statistical significance between the signal given off by the media only, the control untransduced cells and the cells transduced with a MOI of 1 (one-way ANOVA, Tukey's multiple comparisons test, 95 % confidence interval, p value = >0.9634). The bioluminescence signal increased with increasing MOI, with a MOI of 100 producing the strongest signal (p value = <0.0001). Each data point represents the average radiance measured in one well (n = 3 for each group). * $p < 0.05$, ** $p < 0.01$, *** $p < 0.001$ and **** $p < 0.0001$.

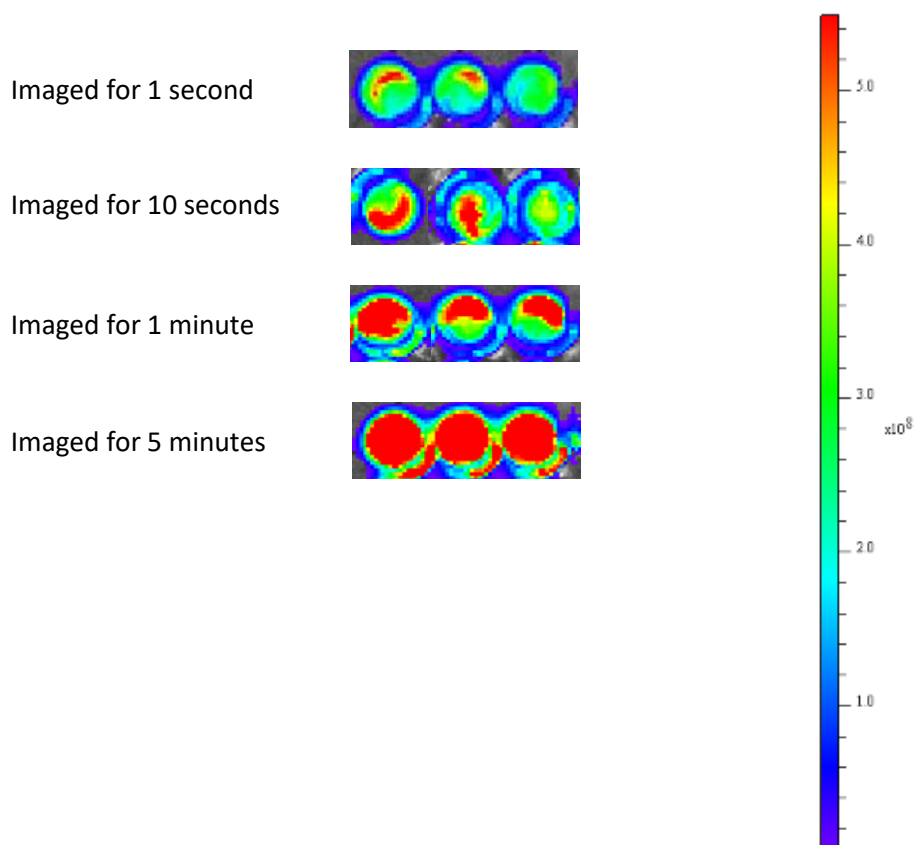


4.3.2 Adjusting the exposure time

As exposure times using the IVIS can range from 1 second to several minutes depending on signal strength, the cells were initially imaged for 5 minutes. However, the signal was extremely high and resulted in pixel saturation. The imaging time was reduced to 1 minute and 10 seconds but this still resulted in saturation. The cells could only be imaged

for the minimal amount of time (1 second) to prevent saturation (figure 39). This was consistent with the high levels of transduction achieved as well as the strong viral promoter driving the expression of luciferase.

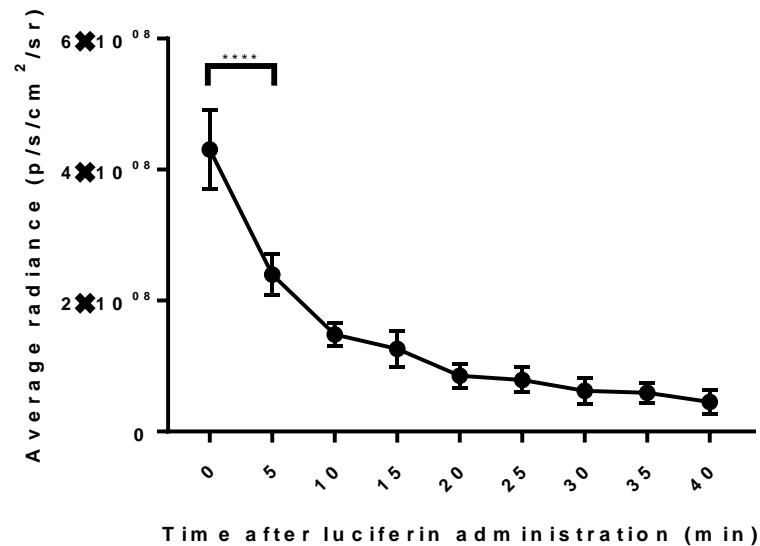
Figure 39. Bioluminescence imaging of luciferase expressing SCL4.1/F7 cells to determine the optimal acquisition time. Bioluminescence images showing the signal emitted from SCL4.1/F7 cells transduced with a MOI of 100 imaged for 1 second, 10 seconds, 1 minute and 5 minutes in triplicate. Saturated pixels were observed when the cells were imaged for more than 1 second. The rainbow pseudocolour scale was adjusted for all images (n = 3 wells for each group).



4.3.3 Luciferin kinetics study

In order to determine the kinetic curve and find the peak imaging time point for luciferase expressing SCL4.1/F7 cells in 2D monolayers *in vitro*, the cells were imaged for 10 seconds every 5 minutes up to 40 minutes after the addition of luciferin. The bioluminescence intensity was maximum immediately after luciferin addition and then decayed over time (figure 40). Five minutes after addition of luciferin, the signal had already decreased 1.8 fold. By 40 minutes, the signal had decreased 9.49 fold. Based on this data, it was decided that bioluminescence images would be acquired immediately after luciferin addition.

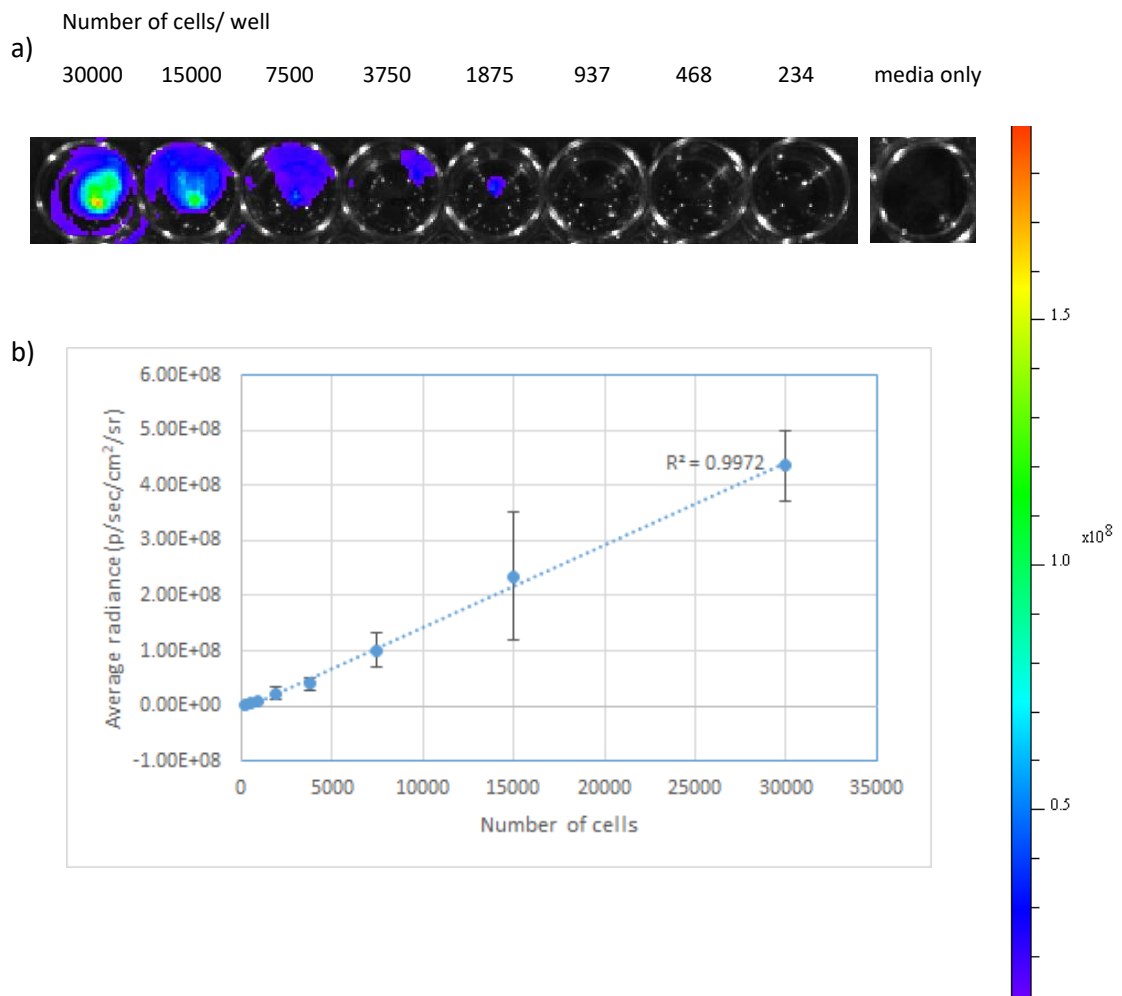
Figure 40. Luciferin kinetic curve to determine peak signal time. The signal obtained 5 minutes after the addition of luciferin was significantly lower than the signal obtained immediately after luciferin addition (one-way ANOVA, Tukey's multiple comparisons test, 95 % confidence interval, p value = <0.0001). Each point represents the mean \pm SD of three independent experiments ($n = 3$). * $p < 0.05$, ** $p < 0.01$, *** $p < 0.001$ and **** $p < 0.0001$.



4.3.4 Correlation between bioluminescence signal strength and cell number

A suspension of cells was serially diluted into a 96-well plate and the bioluminescence intensity for a given volume of cell suspension was measured. The bioluminescence intensity increased proportionally with increasing cell numbers (figure 41). A strong linear correlation between number of cells and light emission was obtained ($R^2 = 0.9972$). Bioluminescence imaging was able to detect at least 234 transduced SCL4.1/F7 cells *in vitro*, illustrating the high sensitivity of bioluminescence imaging. This result was encouraging as it suggested that bioluminescence imaging would be suitable for monitoring luciferase expressing SCL4.1/F7 cells following implantation *in vivo*.

Figure 41. Quantitative correlation between signal strength and cell number. a) Transduced SCL4.1/F7 cells were serially diluted in wells from 30000 to 234 cells/well and imaged. b) The correlation between mean radiance flux and cell numbers is indicated by the R^2 values. Each point represents the mean \pm SD of three independent experiments ($n = 3$).



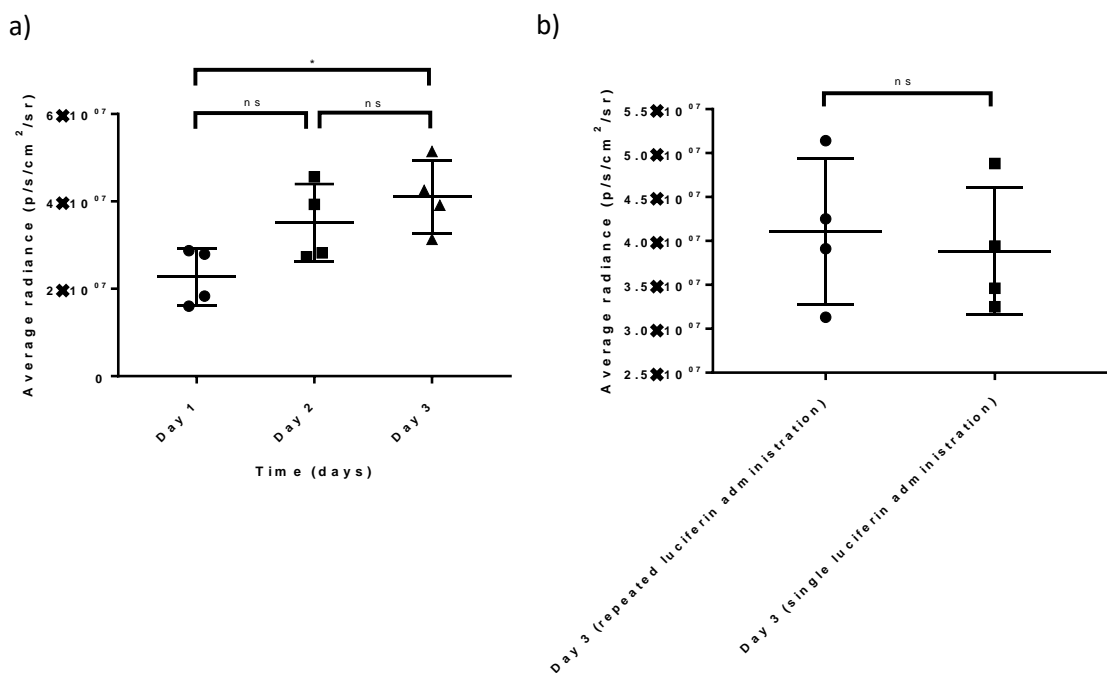
4.3.5 Luciferin toxicity study

Bioluminescence-mediated longitudinal monitoring requires the repeated administration of luciferin. It has been suggested that the build-up of oxyluciferin in long term imaging might cause oxidative damage to the cells. Further, as bioluminescence requires the presence of oxygen and ATP, repeated imaging may increase the energy requirements of the cells, leading to decreased growth (Tiffen *et al.*, 2010). It was therefore decided to investigate the possible toxic effect of repeated luciferin administration on SCL4.1/F7 cells. Luciferase expressing SCL4.1/F7 cells in a 96-well plate were imaged daily over a 3 day period. Following imaging, the cells were washed with PBS and fresh media was added. Additionally, the effect of repeated luciferin addition compared to a one off single administration was investigated. For the latter

experiment, luciferase expressing SCL4.1/F7 cells were plated in the same 96-well plate, but luciferin was only added on day 3.

The bioluminescence signal increased over the three day period. By day 3, the signal had increased 1.81 fold, indicating that the cells were healthy and viable (figure 42). Further, the mean bioluminescence signal of these cells on day 3 was comparable to the signal observed in the cells which had received a single dose of luciferin on day 3, with means of 4.11×10^7 and 3.88×10^7 p/sec/cm²/sr respectively (figure 42).

Figure 42. Investigating the effect of repeated and single luciferin addition on SCL4.1/F7 cells viability. a) The bioluminescence signal produced by cells subjected to repeated luciferin administration over a 3 day period was measured. The signal increased over the 3 days, with a significant increase observed between days 1 and 3 (one-way ANOVA, Tukey's multiple comparisons test, 95 % confidence interval, p value = 0.0243). b) The bioluminescence signal of cells subjected to repeated luciferin addition was comparable to the signal observed in the cells which had received a single dose of luciferin on day 3 (two-tailed unpaired T test, 95 % confidence interval, p value = 0.6978). Each data point represents the bioluminescence signal obtained from one individual well ($n = 4$ for each group). * $p < 0.05$, ** $p < 0.01$, *** $p < 0.001$ and **** $p < 0.0001$.



4.3.6 Monitoring the luciferase intensity over time

In the current study, it was hypothesised that the inclusion of the luciferase gene in the lentiviral expression cassette will allow for longitudinal monitoring of the cells in the EngNT *in vitro* and *in vivo*. It was therefore essential to ensure that the bioluminescence observed reflects true luciferase expression and that luciferase activity does not diminish over time.

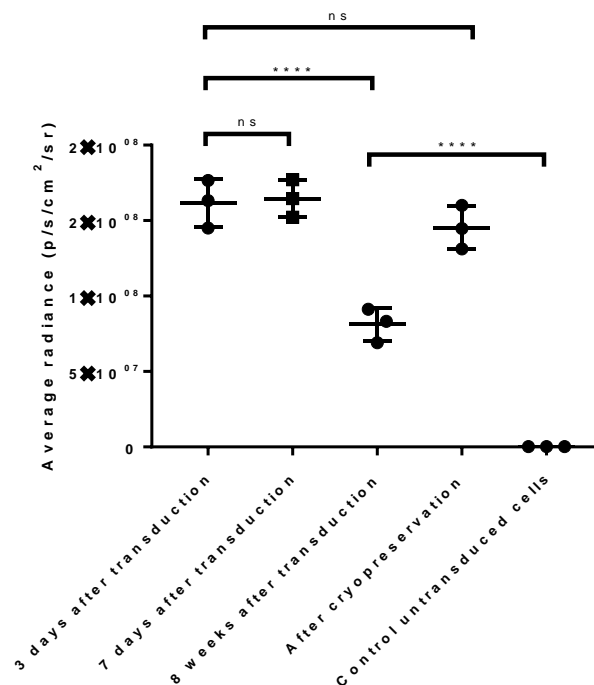
Pseudotransduction has been described as a process that may lead to the expression of foreign proteins, without delivering integrating proviral DNA, and has been reported in several studies (Haas *et al.*, 2000; Geering *et al.*, 2011). Nash and Lever (2004) postulated that during the formation of a lentiviral vector particle, some protein is passively incorporated into the viral particle and transferred to the target cell, leading to an overestimation of transduction at early time points. Gallardo *et al.* (1997) reported that VSG-S pseudotyped lentiviral vectors could result in pseudotransduction in the first 5 days after infection. Similar results were also reported by Nash and Lever (2004). In order to investigate possible pseudotransduction in the current study, luciferase expressing SCL4.1/F7 cells were imaged 72 hours and 7 days after transduction. A similar bioluminescence signal was obtained at both time points, with means of 1.62×10^8 and 1.65×10^8 p/sec/cm²/sr respectively (figure 43).

In order to assess the stability of luciferase activity over an extended period of time, the transduced SCL4.1/F7 cells were cultured for 8 weeks (>25 passages) and imaged. While the signal after 8 weeks was 1.99 fold lower than at 72 hours after transduction, it was still approximately 275 fold higher than the control untransduced cells (figure 43). This indicated that although the signal had dropped, bioluminescence imaging could still be used to monitor cell viability.

Transduced cells were frozen and used to replenish cell stocks when the passage number exceeded 25. Cells were frozen in 90% FBS and 10% dimethyl sulfoxide and stored in a cryogenic freezing container at -80 °C overnight and then transferred to -150 °C for long term storage. Three months later, the cells were thawed and allowed to proliferate before imaging. The signal produced by cells that had been cryopreserved

was similar to the signal produced 72 hours after transduction, with means of 1.45×10^8 and 1.62×10^8 p/sec/cm²/sr respectively (figure 43). This indicated that cryopreservation did not have an effect on luciferase activity, eliminating the need to continually transduce new batches of cells.

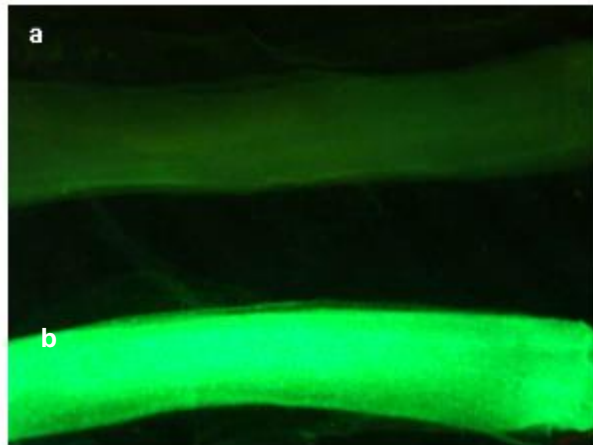
Figure 43. Evaluating the stability of luciferase activity over time and after cryopreservation. No significant difference in luciferase activity was observed 72 hours and 7 days after transduction (one-way ANOVA, Tukey's multiple comparisons test, 95 % confidence interval, p value = 0.9979). While significantly lower at 8 weeks compared to 72 hours after transduction (p value = <0.0001), the signal was still significantly higher compared to control untransduced cells (p value = <0.0001). No statistical difference between the signal produced by cells which had been cryopreserved and the signal obtained 72 hours after transduction was observed (p value = 0.5090). * $p < 0.05$, ** $p < 0.01$, *** $p < 0.001$ and **** $p < 0.0001$.



4.4 Engineered neural tissue

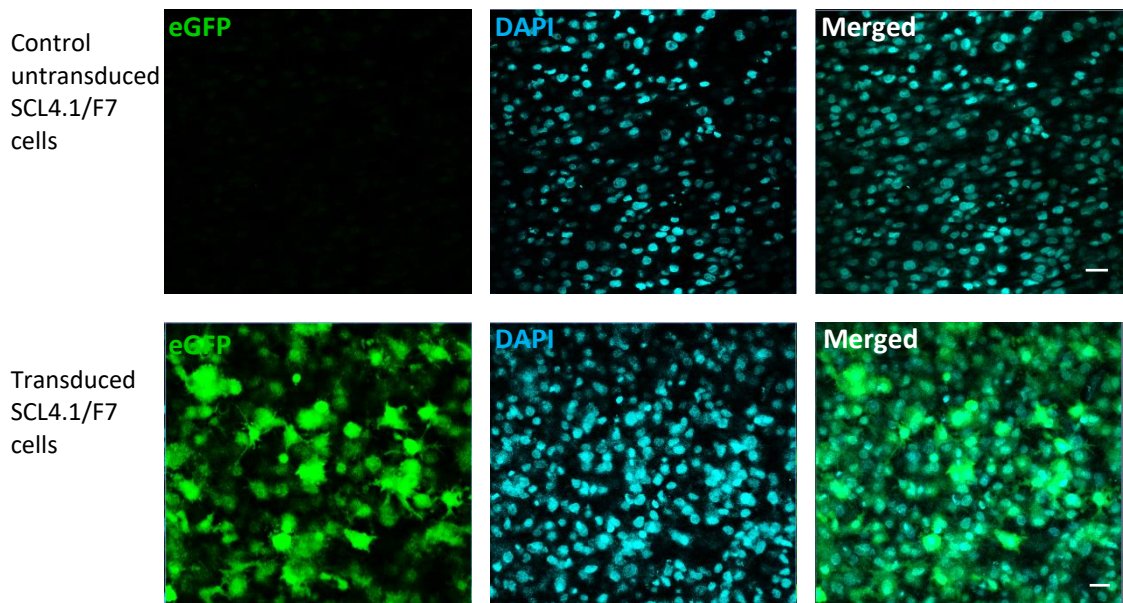
Having established that SCL4.1/F7 cells could be transduced to high efficiency using a lentiviral vector and that robust gene delivery was possible without affecting cell viability, the transduced cells were used to construct EngNT used in peripheral nerve repair. Fluorescence stereoscopic microscopy was used to visualise the eGFP positive cells throughout the entire length and width of the EngNT (figure 44). Fluorescence was observed throughout the construct, indicating even distribution of the cells. EngNT made from control untransduced cells did not display any fluorescence.

Figure 44. Stereoscopic fluorescence micrograph showing even distribution of eGFP positive cells throughout the entire length and width of the EngNT. EngNT constructed from a) transduced SCL4.1/F7 cells expressing eGFP and b) control untransduced SCL4.1/F7 cells. No fluorescence was seen in the EngNT made from control untransduced cells.



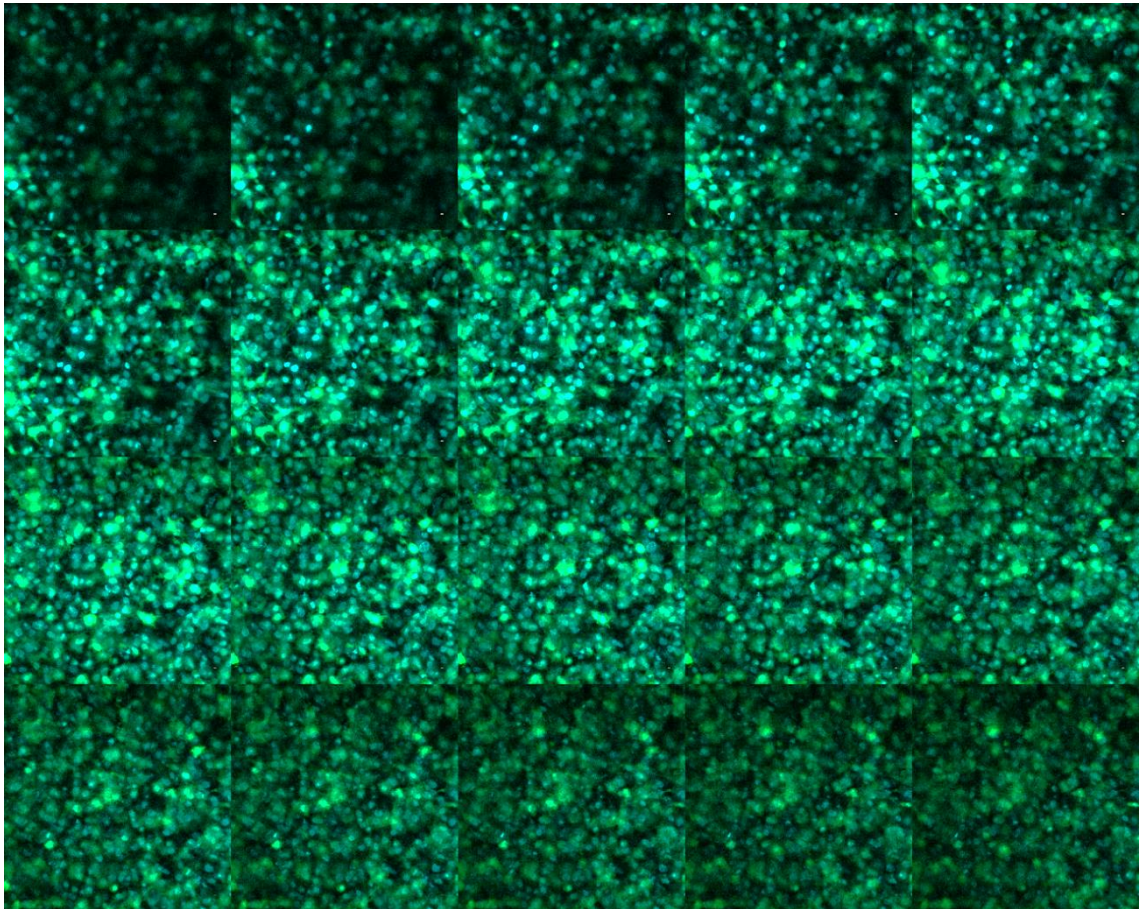
Scanning confocal microscopy was used to observe the cellular architecture in the EngNT. SCL4.1/F7 cells in the EngNT were counterstained with DAPI and images were taken from a single plane through the constructs (figure 45). No eGFP signal was detected in the constructs containing control untransduced SCL4.1/F7 cells. This ensured that any eGFP signal that was detected in the transduced cells was not autofluorescence or background signal. Colocalisation of cyan and green in the nucleus of many eGFP expressing SCL4.1/F7 cells was observed, indicating the presence of nuclear eGFP in addition to cytoplasmic eGFP.

Figure 45. Lentiviral mediated eGFP expression in SCL4.1/F7 cells in EngNT. Representative confocal micrographs showing eGFP expression in transduced SCL4.1/F7 cells in EngNT. No eGFP expression was seen in control untransduced cells. eGFP expression is shown in green and DAPI as cyan (n = 3 for each group). Scale bar: 75 μ m.



In order to confirm that the eGFP distribution was uniform throughout the 3D constructs, a series of 20 images was taken through the depth of the constructs along the Z-axis (figure 46). The Z stack corroborated the images obtained from stereoscopic fluorescence microscopy, i.e. the cells were evenly distributed throughout the EngNT.

Figure 46. Z- stack through EngNT containing SCL4.1/F7 cells expressing eGFP. eGFP expression was seen throughout the EngNT, indicating that the cells had distributed evenly through the construct. eGFP expression is shown in green and DAPI as cyan. Magnification, x20. Z-distance 20 μm , step size 1 μm .



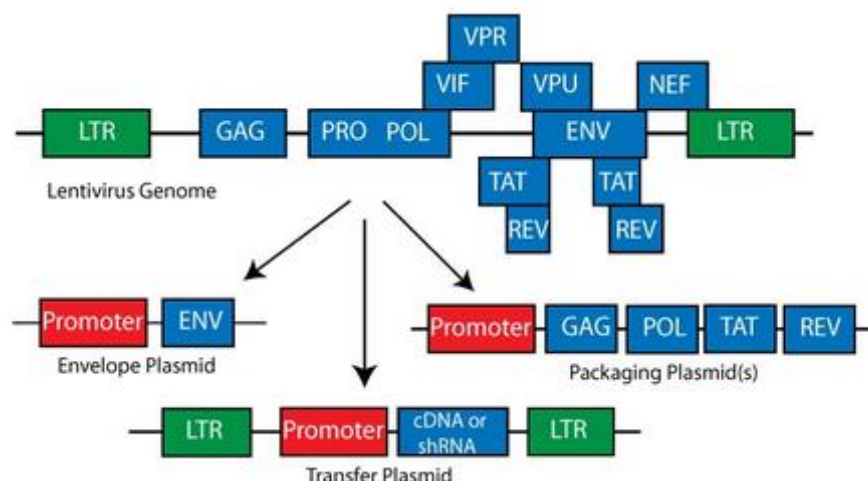
4.5 Discussion

This chapter described the results obtained from the lentiviral mediated gene delivery to SCL4.1/F7 cells. A lentiviral gene delivery mediated approach was used in this study for several reasons. Firstly and most importantly, a precedent for using lentiviral vectors has been set in clinical trials. Lentiviral vectors have been used in a range of successful gene therapy clinical trials for a number of conditions such as X-linked severe combined immunodeficiency (Hacein-Bey-Abina *et al.*, 2010) and X-linked adrenoleukodystrophy (Cartier *et al.*, 2009). Secondly, lentiviral vectors have broad species and cell tropism, allowing the transduction of different cell types with a potential application in peripheral nerve engineering. Finally, lentiviral mediated delivery of therapeutic genes in animal models of peripheral nerve injury has been shown to improve regeneration (de Winter

et al., 2013). In fact, Hoyng *et al.* (2015b) suggested that lentiviral vectors are to be considered the current gold standard in experimental gene therapy for peripheral nerve injuries. Lentiviral vectors permit stable gene expression as transgenes integrate into the target cell genome (Nightingale *et al.*, 2006). In the context of peripheral nerve regeneration, stable expression ensures a continuous provision of growth factors, thus maintaining the pro-regenerative environment needed for regeneration. Additionally, this long-term expression may be beneficial when reporter genes have applications in longitudinal cell fate tracking in tissue engineering studies.

Different generations of lentiviral vector systems have been produced due to the pathogenicity of the Human Immunodeficiency Virus-1, on which they are based. (Merten *et al.*, 2016). A second generation lentiviral packaging system (Zufferey *et al.*, 1997) was used in this study. In this system, the lentiviral genome is modified and spread among three plasmids: the packaging plasmid, the transfer plasmid and the envelope plasmid (figure 47).

Figure 47. Second generation lentiviral plasmids. Splitting the vector components into three plasmids means at least two recombination events are required to produce a replication-competent lentivirus during vector production, which is highly unlikely. Additionally, this design has evolved to increase the transgene capacity size. Image taken from: Addgene – Lentiviral Guide. Available from: <https://www.addgene.org/viral-vectors/lentivirus/lenti-guide/>. Accessed on 20th October 2018.



The envelope plasmid (pMD2.G) used in this study encodes the envelope protein VSV-G. This envelope protein is commonly used in many basic research applications as it permits very broad species and tissue tropism (Hastie *et al.*, 2013). This is useful in the context of peripheral nerve engineering as cells of different origin have been used to improve regeneration in animal models of nerve injury (Bhangra and Busuttill, 2016). Additionally, VSV-G provides high stability, allowing for concentration of viral particles by centrifugation (Cronin *et al.*, 2005).

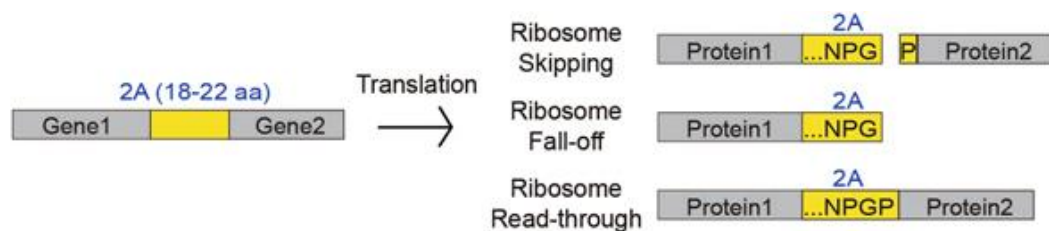
The packaging plasmid (pCMV-dR8.74) used in this study contains the structural *Gag* and *Pol* genes as well as the regulatory *Rev* and *Tat* genes (Dull *et al.*, 1998). In order to create a safe and efficient vector system, viral genes that are not required for the production, transduction and integration of the vector were deleted in this plasmid (Kim *et al.*, 1998). The *Vif*, *Vpu*, *Vpr* and *Nef* genes encode for proteins that are essential for efficient HIV-1 propagation/virulence in primary cells or *in vivo* (Rücker *et al.*, 2004). Therefore, as these genes are only important for HIV as a pathogen, they are not present in second-generation lentiviruses to enhance safety (Schlimgen *et al.*, 2016).

The transfer plasmid contains the only genetic material transferred to the target cells and consists of the lentiviral backbone containing the transgene expression cassette flanked by elements necessary for reverse transcription and integration (Merten *et al.*, 2016). Viral long terminal repeats facilitate integration of the transfer plasmid sequences into the host genome. Second-generation transfer plasmids have a wildtype 5'LTR, which requires the presence of the *Tat* gene on the packaging plasmid to work. The Psi packaging signal is placed immediately downstream of the 5' LTR and is required for viral genomic RNA packaging as well as gene delivery efficiency (Kim *et al.*, 2012). In order to reduce safety concerns, Zufferey *et al.* (1998) proposed the use of self-inactivating lentiviral vectors, which rely on a deletion in the U3 region of the 3' LTR. This deletion prevents full-length viral RNA from being produced in target cells and minimises the risk of producing RCLs.

The lentiviral vector used in the current study contained an expression cassette consisting of the ubiquitous spleen focus forming virus (SFFV) promoter driving the expression of the luciferase gene and the downstream eGFP gene. The luciferase and

eGFP reporters allow *in vivo* and *in vitro* monitoring of labelled cells as well as the analysis of transduction efficiency by flow cytometry. The woodchuck hepatitis virus post-transcriptional regulatory element (WPRE) was present after the genes since it has been shown to stabilise mRNA expression and enhance gene expression (Zufferey *et al.*, 1999). The bicistronic expression of two genes from the same promoter was provided by inclusion of the self-cleaving 2A element (figure 48) between the two genes. This has been shown to allow for multigene products from the same vector (Szymczak *et al.*, 2004). The mechanism of 2A-mediated self-cleavage was described by Donnelly *et al.* (2001) and involves ribosome skipping from one codon to the next without the formation of a peptide bond. This in turn allows the synthesis of a discrete downstream translation product to proceed.

Figure 48. Schematic representation of the mechanism of “self-cleaving” 2A peptides. 2A peptides are 18–22 amino acid - long viral oligopeptides that mediate “cleavage” of polypeptides during translation in eukaryotic cells. The term 2A refers to a specific region of the viral genome. Image taken from Liu *et al.* (2017).



In the current study, lentiviral mediated gene delivery resulted in high level gene expression. Generally, the higher the MOI, the higher the efficiency of gene transfer and the level of gene expression. In the current study, the level of gene expression following lentiviral transduction increased with increasing MOI. However, this increase was not directly proportional (section 4.2.4). *in vitro* experiments employing MOIs greater than 1000 have still resulted in less than 100% of cells transduced (Hamaguchi *et al.*, 2000), indicating the presence of unknown variables. Theoretically, a MOI of 2 should result in every single cell experiencing two gene transfer events in a given transduction experiment. However, the efficiencies of transduction are lower than the theoretical outcomes and are thought to be influenced by factors such as target cell type, cell membrane composition and Brownian motion which allows the viral vector to reach the target cell (Zhang *et al.*, 2004).

It was particularly important to establish the effect of transduction on cell viability and proliferation as a downstream application of the transduced cells was to use bioluminescence imaging to monitor the cells in EngNT. Therefore if transduction compromised viability and proliferation, the data generated by bioluminescence imaging would not be a true representation of the cell health in the EngNT. A reduction in cell viability following lentiviral transduction has been noted by some authors (Castellani *et al.*, 2010). Maunder *et al.* (2017) suggested that the presence of the transgene may impact the metabolism and viability of the transduced cells. Lee *et al.* (2004) reported that lentiviral vectors can cause a transient arrest at the S phase of the cell cycle in transduced cells, resulting in a marked decrease in proliferation of the cells. According to Millington *et al.* (2009), this effect is less likely to be observed if low MOIs are used. In the current study, lentiviral transduction did not have an effect on the viability or proliferation rate of SCL4.1/F7 cells irrespective of the MOI used (section 4.2.6). This may be explained by the relatively low range of MOIs used, which is markedly lower than those reported in other studies (Mostoslavsky *et al.*, 2005; Castellani *et al.*, 2010). Transduction of cells using lower MOIs may be preferable to decrease the risk of insertional mutagenesis and toxicity.

As mentioned in section 2.1.2, Schwann cells are the principal mediators of nerve regeneration in the PNS. It is therefore desirable for nerve repair devices to contain a cellular component that can simulate the regenerative roles of Schwann cells (Johnson *et al.*, 2013). While allogeneic or autologous Schwann cells may seem like an attractive choice, there are numerous disadvantages associated with their sourcing and culturing. Their harvesting requires invasive nerve biopsies (Gersey *et al.*, 2017) while *in vitro* culture is laborious and time consuming due to their slow growth rate and potential overgrowth of fibroblasts over time (Jiang *et al.*, 2012). Several models of immortalized Schwann cell lines, including JS-1 (Kimura *et al.*, 1990) and S16Y (Toda *et al.*, 1994) have been used to study peripheral nerve regeneration (Geuna *et al.*, 2016). However, it has been noted that Schwann cell lines tend to undergo rapid transformation and lose normal Schwann cell properties, such as myelination capacity at later passages (Porter *et al.*, 1987) and the ability to downregulate their own growth (Eccleston *et al.*, 1991).

The clonally derived diploid rat Schwann cell line SCL4.1/F7 developed by Haynes *et al.* (1994) used in this study does not undergo rapid transformation and therefore retains some normal Schwann cell phenotypic properties. In order to prevent genetic instability and phenotypic drift, two frequently encountered problems with the use of cell lines (Geraghty *et al.*, 2014), SCL4.1/F7 cells were frozen at the lowest passage number possible and used to replace stocks at regular intervals. However, while SCL4.1/F7 cells are ideal for the current study, it must be noted that interpretation of results from these model cells cannot necessarily be extrapolated to represent Schwann cell behaviour more broadly.

In vitro quantification of bioluminescence from luciferase expressing SCL4.1/F7 cells demonstrated a 547 fold increase in signal compared to the control untransduced cells (section 4.3.1). According to Lim *et al.* (2009), a high expression level *in vitro* is required to ensure that the luciferase expressing cells can be imaged successfully *in vivo*. This was especially important in the current study as one of the aims was to demonstrate that luciferase expressing SCL4.1/F7 cells in EngNT implanted into a rat model of sciatic nerve injury can be monitored using an *in vivo* imaging system. Similar to eGFP expression, luciferase expression was demonstrated over an 8 week period *in vitro*, confirming long term gene expression (sections 4.2.5 and 4.3.6). A luciferin toxicity study (section 4.3.5) indicated that neither luciferin nor luciferase activity was detrimental to the health of transduced SCL4.1/F7 cells.

The nerve autograft contains aligned Schwann cells which support and guide regenerating neurites from the proximal to the distal side of the repair site, and recreating this anisotropic 3D cellular architecture is the focus of much research in the area of peripheral nerve repair. East *et al.* (2010) have shown that aligned astrocytes within a collagen gel can support and guide neuronal regeneration *in vitro*, and that aligned astrocyte gels can be stabilised through removal of interstitial fluid. Georgiou *et al.* (2013) applied this stabilisation technique to Schwann cell-populated collagen gels after cellular self-alignment, increasing cell and collagen density to a sufficient extent that tethering could be removed from the gels without subsequent loss of cell and matrix alignment. The resulting EngNT consisting of stable aligned cellular material guided regenerating neurons and was robust enough to withstand being rolled and

wrapped to form an implantable construct. In the current study, genetically modified SCL4.1/F7 cells were used to construct EngNT and stereoscopic fluorescence and confocal microscopy confirmed that cell distribution was uniform throughout the entire length and width of the EngNT. This suggests that EngNT can be constructed from genetically modified SCL4.1/F7 cells overexpressing factors required for nerve regeneration following injury. The presence of these factors may further increase the extent of regeneration currently supported by the cellular EngNT.

4.6 Conclusion

Fluorescence microscopy revealed that SCL4.1/F7 cells were successfully transduced by the lentiviral vector delivering luciferase and eGFP. Flow cytometry revealed that the greatest transduction efficiency (>80%) was obtained using a MOI of 100. Long term eGFP expression (8 weeks) was observed *in vitro*. No detrimental effects on cell viability, proliferation or morphology were noted following transduction. High luciferase expression was also observed in transduced cells and the cells could only be imaged for the minimum period of time to prevent signal saturation (1 second). Similar to eGFP expression, luciferase expression persisted over 8 week of *in vitro* culture. Cryopreservation was found to have no effect on luciferase expression. The genetically modified cells were used to construct EngNT used in peripheral nerve repair. Stereoscopic fluorescence and confocal microscopy confirmed that cell distribution was uniform throughout the entire length and width of the EngNT. No fluorescence was observed in EngNT made with control untransduced cells. This *in vitro* proof-of-concept study paves the way for a novel combination of tissue engineering and gene therapy. This is because the combination of nerve repair devices containing cells that overexpress neurotrophic or angiogenic factors could provide a microenvironment that enhances peripheral nerve regeneration after injury.

Chapter 5. Assessing cell viability in engineered neural tissue

5.1 Introduction

Results from the previous chapter showed that a lentiviral vector can be used to successfully deliver reporter genes to SCL4.1/F7 cells. One of the reporter genes delivered encoded firefly luciferase, an enzyme which catalyses the oxidation of luciferin in the presence of oxygen and ATP. This reaction produces oxyluciferin, a highly unstable compound that emits light upon relaxation to its ground state (Rowe *et al.*, 2009). This emitted light peaks at 562 nm (Rice *et al.*, 2001) and forms the basis of bioluminescence imaging, which detects visible light produced during the luciferase-mediated oxidation of luciferin by cells expressing luciferase (Sadikot and Blackwell, 2005). A major advantage of bioluminescence imaging is inherently low background, as mammalian cells and tissues do not emit endogenous light (Oudina *et al.*, 2011).

Although not directly translational to the clinic, bioluminescence imaging has become a popular method of imaging small animals in the research environment (Chen and Thorne, 2012). In fact, bioluminescence imaging has been applied in a range of preclinical studies including monitoring of transgene expression (Fan *et al.*, 2011), progression of infection (Warawa and Lawrenz, 2014), tumor growth and metastasis (Giubellino *et al.*, 2012), toxicology (Xu *et al.*, 2013) and gene therapy (He *et al.*, 2016).

Another potential application of bioluminescence imaging is in tissue engineering (Bagó *et al.*, 2013). Monitoring the distribution and viability of cells in tissue engineered constructs *in vitro* and *in vivo* is key to ensuring the success of tissue engineering strategies. Most methods currently available to assess the number and distribution of viable cells within tissue engineered constructs have limited *in vivo* application as they require destruction of the sample and cannot be used for repeated monitoring. They may also not distinguish between implanted cells and host cells which can confound findings. Additionally, the scaffold material may interfere with the assays used. Therefore, there is an increasing need for methods which can nondestructively and noninvasively assess the performance of tissue-engineered constructs (Close *et al.*,

2011). This chapter describes the feasibility of bioluminescence imaging to monitor luciferase expressing SCL4.1/F7 cells in EngNT and to establish whether this technique is useful for studying cell survival and distribution in peripheral nerve engineering. This part of the study had the following aims:

- To use bioluminescence imaging to monitor cell viability in EngNT *in vitro*.
- To use bioluminescence imaging to monitor cell viability in EngNT following implantation in a rat model of sciatic nerve injury.
- To determine how long the implanted cells survive *in vivo*.

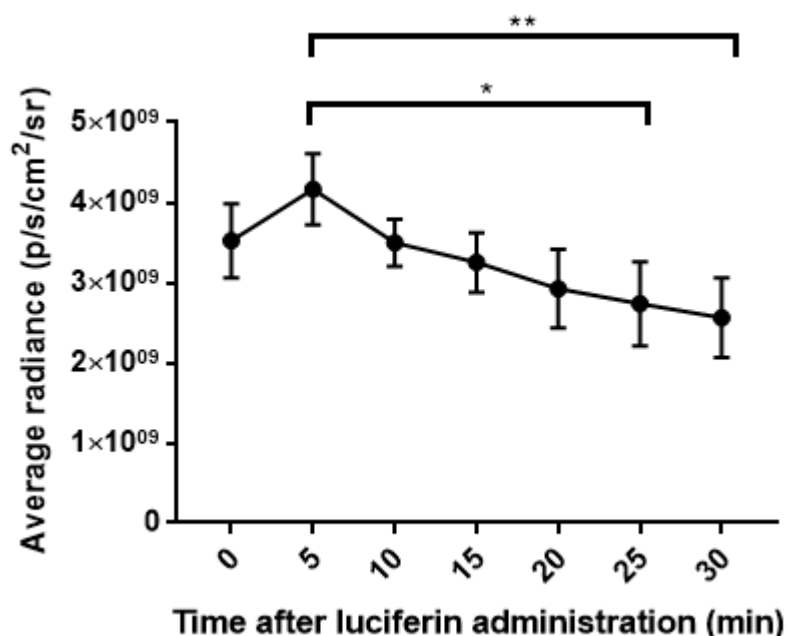
5.2 *in vitro* bioluminescence imaging

Steady state imaging allows luciferase expressing cells to be imaged over time in order to determine if the signal increases or decreases, providing valuable information on cell survival and proliferation (Close *et al.*, 2011). Longitudinal monitoring of lentiviral-mediated luciferase expressing SCL4.1/F7 cells in EngNT *in vitro* was carried out non-destructively using an IVIS bioluminescence imaging system.

5.2.1 *In vitro* bioluminescence kinetics study

The material of tissue-engineered constructs can influence the biodistribution kinetics of luciferin (Oudina *et al.*, 2011). It is therefore important to carry out a kinetic study to determine the time at which light emission peaks. A series of imaging captures starting immediately after luciferin addition and then every 5 minutes for 30 minutes was taken using the IVIS and the signal emitted was quantified at each time point (figure 49). Similar to SCL4.1/F7 cells in monolayers, SCL4.1/F7 cells in the EngNT could only be imaged for 1 second to prevent signal saturation. The signal increased during the first 5 minutes and then gradually declined over time. Although higher than immediately after the addition of luciferase, the signal after 5 minutes was not statistically different. However, based on this trend, it was decided that all subsequent readings would be taken 5 minutes after luciferin addition.

Figure 49. Kinetic profile of light emission following luciferin addition to EngNT. The graph shows a peak signal at 5 minutes which goes down steadily over the next 25 minutes. A statistical significance was seen between the signal obtained 5 minutes after addition and 25 minutes and 30 minutes after addition (one-way ANOVA, Tukey's multiple comparisons test, 95 % confidence interval, p value = <0.0201). No statistical significance was seen at any other time point (p value = >0.0515). Data presented as the mean \pm SD (n = 3). * p < 0.05, ** p < 0.01, *** p < 0.001 and **** p < 0.0001.

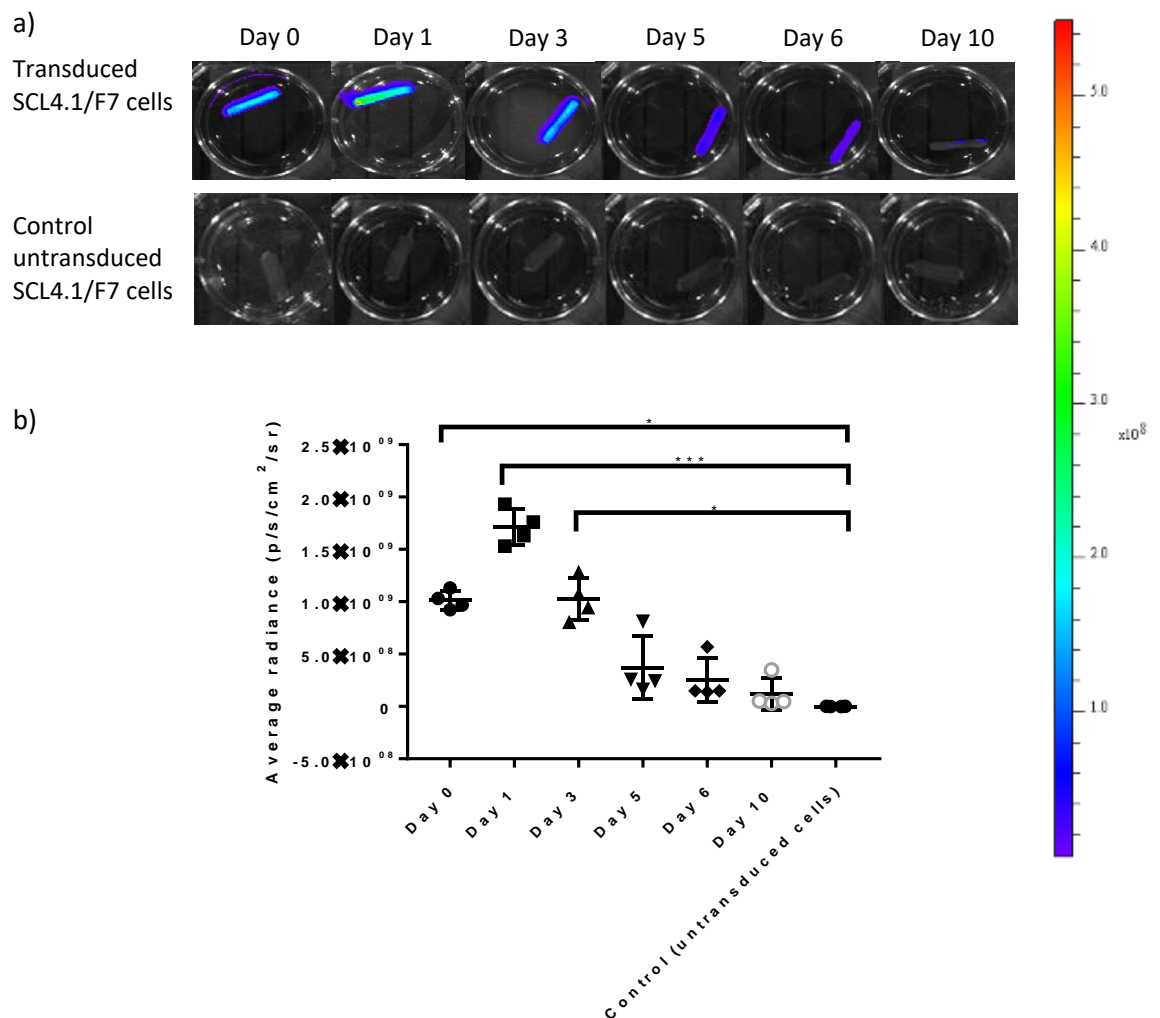


5.2.2 Cell viability and proliferation assessment

Bioluminescence imaging can be used to study cell viability, as the bioluminescence signal is dependent on the presence of ATP in metabolically active cells (Lomakina *et al.*, 2015). In order to demonstrate the ability of bioluminescence imaging to measure cell viability in EngNT *in vitro* over time, changes in signal were evaluated by repeated imaging of EngNT over 10 days. Upon addition of luciferin, the light generated by the luciferase expressing SCL4.1/F7 cells was transmitted through the collagen hydrogel and was monitored externally using the IVIS. The imaging revealed signal throughout the entire EngNT, supporting previous observations about cell distribution obtained through stereoscopic fluorescence and confocal microscopy (section 4.4). As expected, no bioluminescence was emitted from EngNT made with control untransduced SCL4.1/F7 cells. When regions of interest were measured, a 1.69 fold increase in the bioluminescence signal was observed between days 0 and 1. However, this did not prove to be significant (figure 50). After this increase, the signal began to decrease and by day 5 there was no significant difference between the signals obtained and the control. The

bioluminescence signal decreased from a mean of 1.01×10^9 p/s/cm²/sr on day 0 to a mean of 1.18×10^8 p/s/cm²/sr on day 10, equivalent to a 8.57 fold difference.

Figure 50. Time-course of the *in vitro* cell viability of luciferase expressing SCL4.1/F7 cells in EngNT during 10 days of culture. a) Representative bioluminescent images of luciferase expressing and control SCL4.1/F7 cells in EngNT using the IVIS. The rainbow pseudocolour scale was adjusted for all images. b) The bioluminescence signals (p/s/cm²/sr) from luciferase expressing SCL4.1/F7 cells in EngNT. An increase in signal was observed on day 1, however, this was not statistically significant (Kruskal-Wallis test, Dunn's multiple comparisons test, p value = >0.9999). Only the bioluminescence signals on days 0, 1 and 3 were significantly higher than the control (p value = >0.0008). The signal dropped to control level by day 5 (p value = >0.9999). Each data point represents the signal emitted from an individual EngNT (n = 4). *p < 0.05, **p < 0.01, ***p < 0.001 and ****p < 0.0001.

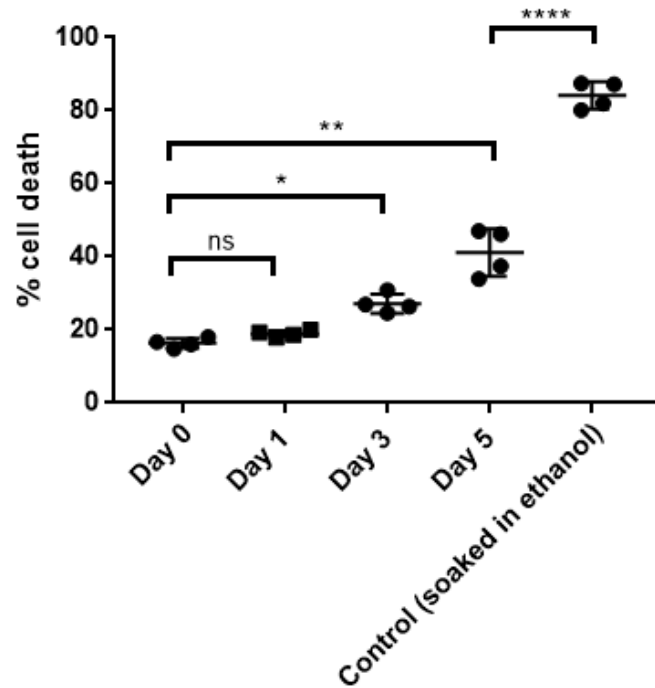


5.3 Comparing bioluminescence imaging with cell viability assays

Two cell viability assays, namely live-dead staining and the alamarBlue[®] assay, were compared to bioluminescence imaging in terms of their sensitivity in assessing cell viability in the EngNT. The assays used measured the integrity of three different cellular compartments, namely the cell membrane (live-dead staining), mitochondrial reducing agents (the alamarBlue[®] test) and the presence of ATP (bioluminescence imaging). Live-dead staining is an endpoint approach and unlike the alamarBlue[®] assay and bioluminescence imaging, cannot be used for monitoring cell viability over time.

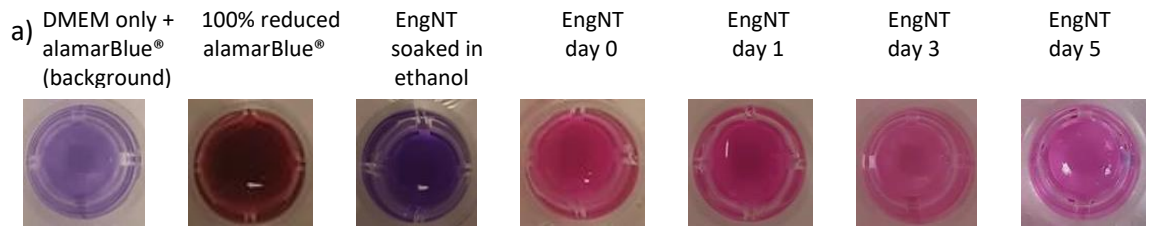
The NUCLEAR-ID[®] blue/red cell viability reagent, which consists of a mixture of a blue fluorescent cell-permeable nucleic acid dye and a red fluorescent cell-impermeable nucleic acid dye, was used to determine the percentage of dead cells in the collagen gels by fluorescence microscopy (figure 51). The percentage of dead cells on days 0 and 1 was similar ($\leq 20\%$). By days 3 and 5, the percentage of dead cells increased from a mean of 16.38% on day 0 to 27.191 and 41.15% respectively. This was equivalent to a 1.7 and 2.5 fold difference respectively. However, the percentage of dead cells on day 5 was still significantly lower than that observed in the collagen gels soaked in ethanol. Collagen gels were soaked in ethanol for 10 minutes to serve as a positive control, with a cell death of $\geq 80\%$.

Figure 51. Determination of the percentage cell death in collagen gels over a 5 day period. The percentage cell death was similar on days 0 and 1 (one-way ANOVA, Tukey's multiple comparisons test, 95 % confidence interval, p value = 0.8438). Compared to day 0, the percentage cell death was significantly higher on day 3 (p value = 0.0055) and 5 (p value = <0.0001). The percentage cell death on day 5 was significantly lower than the positive control of ethanol soaked collagen gels (p value = <0.0001). Each data point represents the percentage cell death in an individual collagen gel ($n = 4$ for each group). * $p < 0.05$, ** $p < 0.01$, *** $p < 0.001$ and **** $p < 0.0001$.

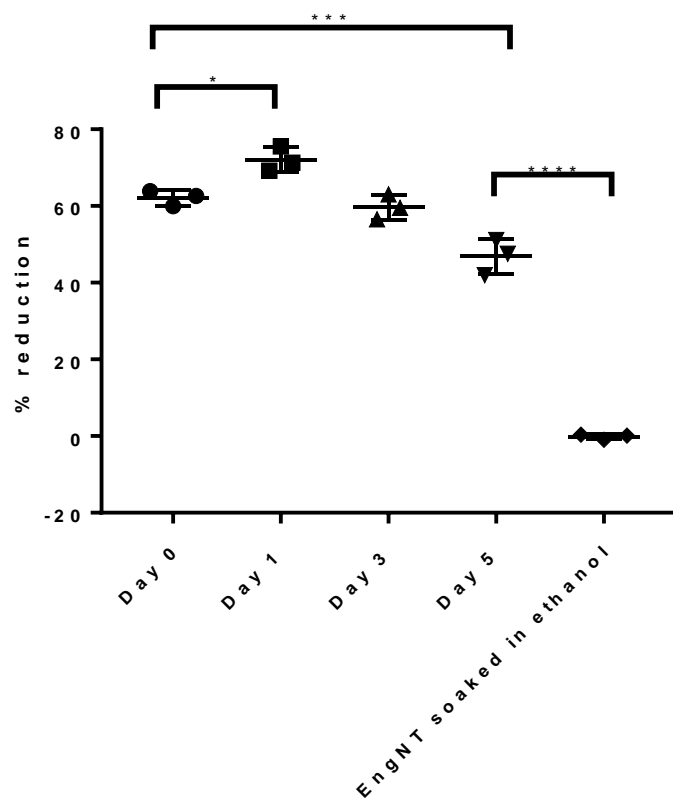


The alamarBlue® assay was also used to assess the viability of the cells in the EngNT over a 5 day period. When incubated with viable cells, the reagent undergoes a colorimetric change from blue to pink in response to cellular metabolic reduction. The absorbance measured is proportional to the number of living cells respiring. Similar to the data obtained from bioluminescence imaging, there was an increase in cell viability between days 0 and 1. However, this increase was significant. After day 1, the percentage reduction of alamarBlue® decreased steadily, indicating a decline in cell viability (figure 52). Similar to the live-dead staining results, the cell viability on day 5 was still significantly higher than that observed in the EngNT soaked in ethanol. EngNT soaked in ethanol for 10 minutes served as a negative control. A solution of 100% reduced alamarBlue® in DMEM (prepared by autoclaving for 15 minutes) was used as a positive control.

Figure 52. alamarBlue® assay to assess cell viability in EngNT over a 5 day period. a) Representative images of alamarBlue® colour changes. Viable cells result in the reduction of alamarBlue®, which is accompanied by a colour change from blue to red. b) alamarBlue® percentage reduction. There was a significant increase in cell viability between days 0 and 1 (one-way ANOVA, Tukey's multiple comparisons test, 95 % confidence interval, p value = 0.0008). The percentage reduction was significantly lower on day 5 compared to day 0 (p value = 0.0187), however it was still significantly higher than the percentage reduction seen in ethanol soaked EngNT (p value = <0.0001). Each data point represents the percentage reduction in alamarBlue® produced by the cells in an individual EngNT ($n = 4$). * $p < 0.05$, ** $p < 0.01$, *** $p < 0.001$ and **** $p < 0.0001$.



b)



5.4 *in vivo* bioluminescence imaging

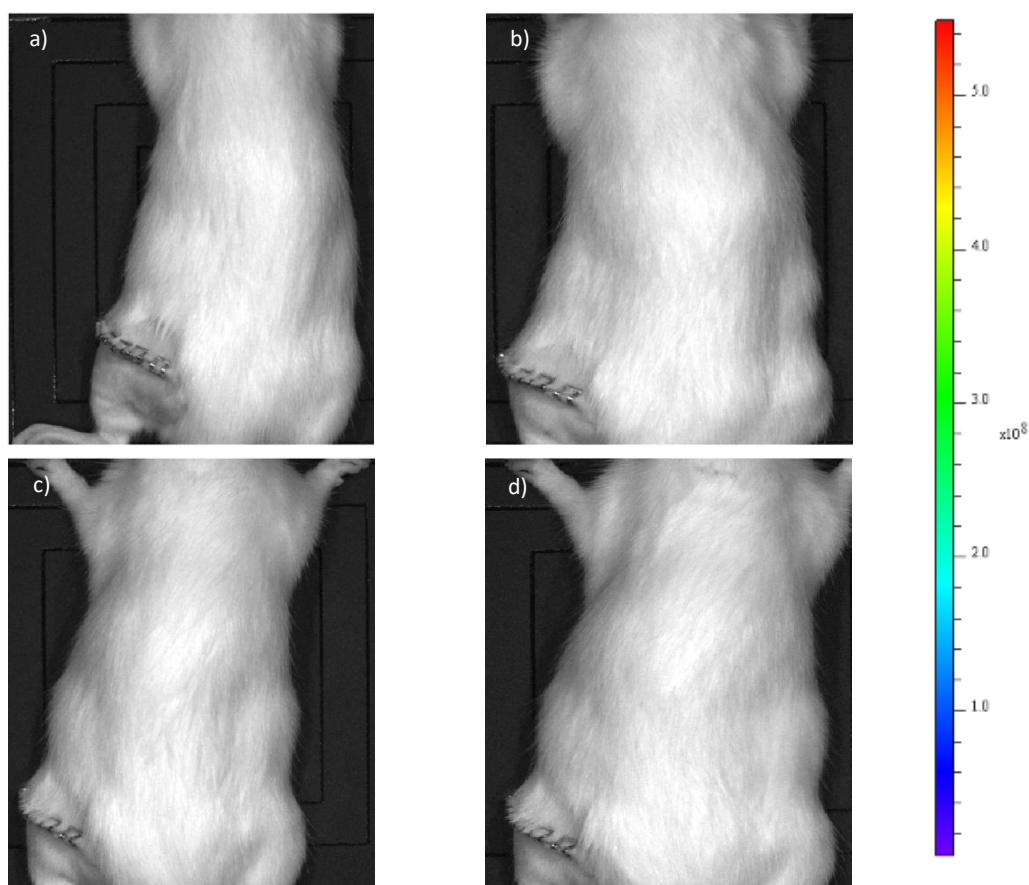
Physical defects caused by injury can result in the loss of specialised cells within tissues, compromising repair and impairing function. Cell-based therapies are being developed to promote repair and regeneration of damaged tissues. However, several obstacles, including low retention of transplanted cells, have been encountered and are a major

focus for improving cell-based therapy (Yang *et al.*, 2013). Before moving onto clinical trials, the behaviour and mechanism of action of transplanted cells must be understood *in vivo*. Bioluminescence imaging can be used to provide repetitive, non-invasive and quantitative measurements of transplanted cells, providing information on cell survival, proliferation and migration over time in the same living subject (Close *et al.*, 2011). Additionally, because of its high sensitivity, bioluminescence imaging has been recently applied to tracking cells in cellular constructs transplanted in live animals for tissue engineering purposes (Leferink *et al.*, 2016). Having established that bioluminescence could be used to monitor cell viability in EngNT *in vitro*, it was decided to determine whether similar results would be obtained *in vivo*.

5.4.1 *In vivo* kinetics study

EngNT made from luciferase expressing SCL4.1/F7 cells was rolled and inserted into a silicone tube to form an implantable device which was used to repair a 10 mm gap in the rat sciatic nerve. A sequence of images was taken starting 10 minutes after intraperitoneal administration of luciferin and then every 10 minutes for 30 minutes in order to establish the optimal timing of imaging. Badr *et al.* (2014) suggested that an incubation step of 5-15 minutes following intraperitoneal luciferin administration would allow its absorption through the peritoneum and result in a better tissue distribution. Data acquisition was also continued until 30 minutes after injection on days 3, 5 and 7 post surgery. Unexpectedly, a signal was not obtained on any of the days the animal was imaged (figure 53). The exposure time was increased from 5 to 10 minutes, but this did not have an effect on the signal produced.

Figure 53. No bioluminescence signal was obtained in the *in vivo* imaging study. Representative images showing that no signal was obtained throughout the course of the kinetic study following intraperitoneal injection of luciferin on a) day 1, b) day 3, c) day 6 and d) day 7. The rainbow pseudocolour scale was adjusted for all images (n = 1).



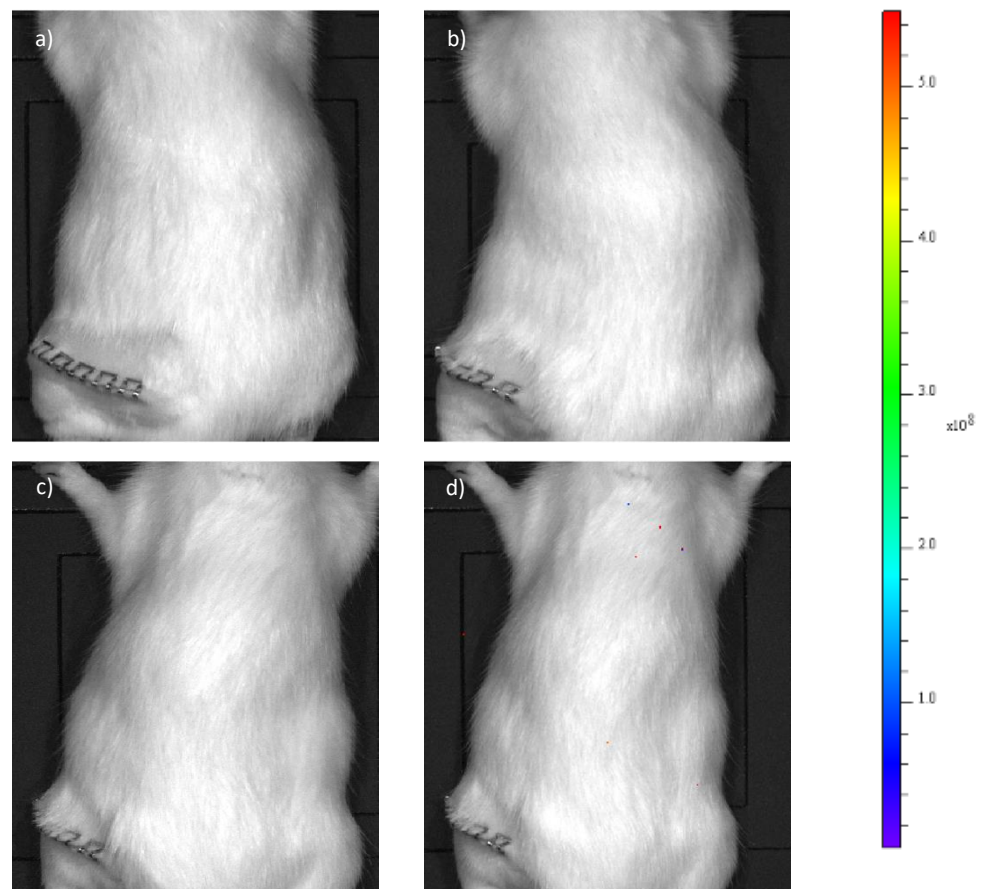
5.4.2 Route of luciferin administration

The optimal route of administration of luciferin should be determined for every *in vivo* bioluminescence imaging experiment as this can influence the bioluminescence signal (Badr *et al.*, 2014). Intraperitoneal administration of luciferin is a popular choice for many researchers. However, following this route of injection, luciferin must be absorbed through the peritoneum and reach the luciferase expressing cells via the bloodstream. Variations in the rate of absorption can influence the signal and confound results (Keyaerts *et al.*, 2008). Further, luciferin may be inadvertently injected into the bowel, resulting in a weak or non-existent signal that may be misinterpreted as a negative result (Baba *et al.*, 2007).

Subcutaneous injection of luciferin has been proposed as an alternative to intraperitoneal injection (Inoue *et al.*, 2009; Khalil *et al.*, 2013). Khalil *et al.* (2013) suggested that subcutaneous injection may be preferable to intraperitoneal administration when weak signals are obtained or when greater precision is required.

In the current study, luciferin was initially administered via intraperitoneal injection. However, no signal was obtained following this route of administration. It was then decided to inject luciferin subcutaneously in the thigh, close to the implantation site. Luciferin (15 mg/ml) in sterile saline solution was administered at a dose of 150 mg/kg for both routes. It was thought that a local injection would result in greater availability of the luciferin to the luciferase expressing cells. However, a signal was still not obtained (figure 54).

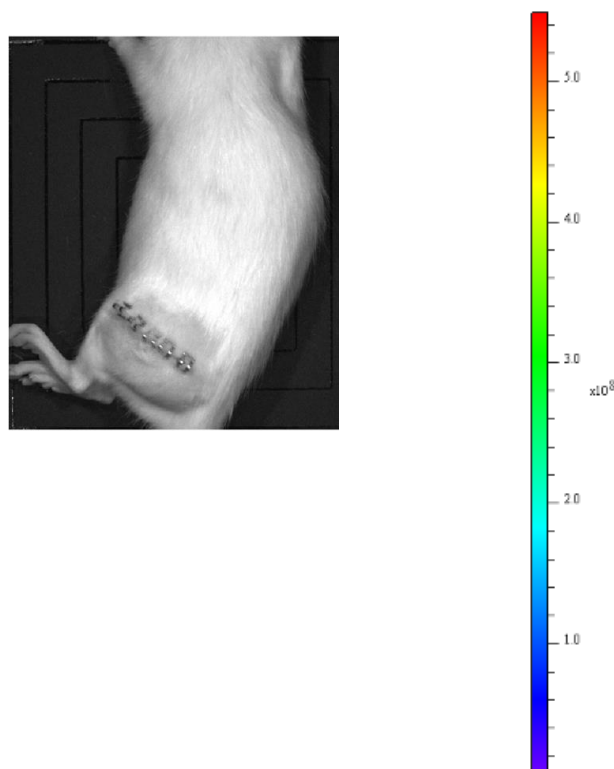
Figure 54. Subcutaneous administration of luciferin did not result in a bioluminescence signal. Representative images showing that no signal was obtained throughout the course of the kinetic study following subcutaneous injection of luciferin on a) day 1, b) day 3, c) day 6 and d) day 7. The rainbow pseudocolour scale was adjusted for all images (n = 1).



5.4.3 Animal position

Bioluminescence measurements can be affected by rotation of the sample as the detected photon emission depends on the angle the surface makes with the optical axis of the camera. Virostko *et al.* (2004) investigated the effect of subject positioning on bioluminescence measurements by imaging a constant emission bioluminescent bead implanted at a renal and hepatic site. Supine orientation was used as normal placement for hepatic bead imaging, whereas lateral orientation was used for renal imaging. At rotations of 50° from normal, the signal decreased to approximately a quarter compared to the normal measurement for renal beads. For hepatic beads, a 50° rotation resulted in intensity less than half of the normal measurement. This implies that the exact position of the subject relative to the camera must be carefully controlled and can result in signal variations that are not representative of the biological processes for which bioluminescence is being measured. As no signal was obtained when the animal was in the prone position, it was decided to image the rat in a lateral orientation. However, a signal was still not obtained (figure 55).

Figure 55. Investigating the effect of animal positioning on bioluminescence imaging. A representative image showing that a bioluminescence signal was still not obtained when the rat was imaged in a lateral orientation.

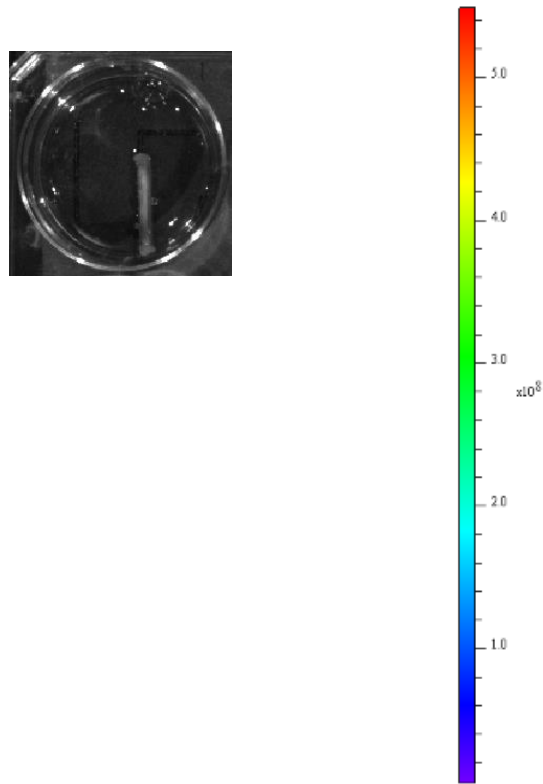


5.5 *ex vivo* bioluminescence imaging

It was thought bioluminescence imaging would be useful to monitor the survival of luciferase expressing SCL4.1/F7 cells in the nerve repair device in a rat model of sciatic nerve injury. However, a signal was not obtained throughout the *in vivo* imaging study, even after parameters such as the route of administration of luciferin and animal positioning were adjusted. This could be due to a number of biologic variables and imaging parameters which influence bioluminescence, such as the size and composition of the device, the thickness and optical properties of overlying tissue, perfusion and luciferin availability (Virostko *et al.*, 2004).

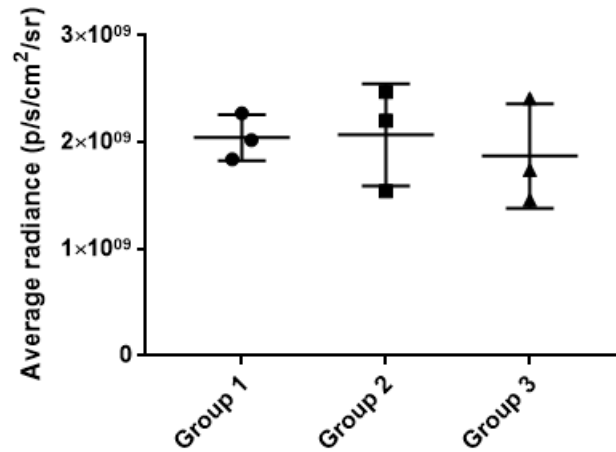
On day 8 of the *in vivo* imaging study, it was decided to cull the animal and explant the EngNT in the silicone tube. The explant was placed in PBS and imaged in a 6-well plate following the addition of luciferin. Even though confounding factors, such as the overlying tissue and luciferin availability, were removed a signal was not obtained (figure 56). This indicated that the majority of the cells in the nerve repair device had not survived 8 days post implantation.

Figure 56. *Ex vivo* imaging of the nerve repair device 8 days post implantation. The nerve repair device was explanted and imaged *ex vivo* in a 6-well plate. Following the addition of luciferin, the device was imaged every 5 minutes for 30 minutes. A representative image showing that a signal was not obtained at any time point (n = 1).



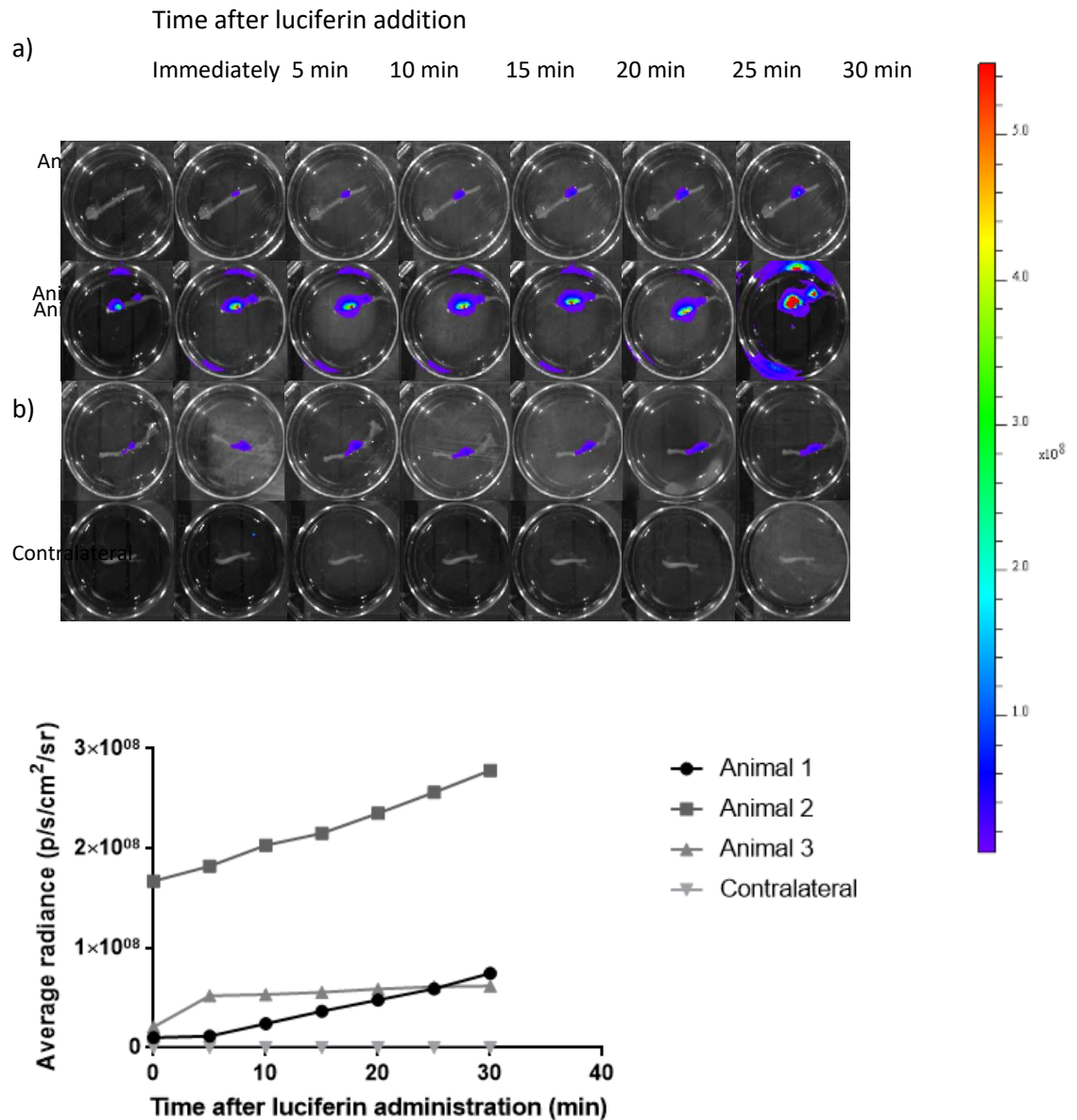
In order to establish whether cells survived at earlier time points, and to eliminate confounding factors, it was decided to repeat the experiment and explant and image the nerve repair device 1, 3 and 5 days post implantation. To ensure that the cells in the EngNT were viable on the day of implantation, a 2mm segment was cut from the EngNT prior to assembling the device and imaged. A high signal was obtained for all the segments (figure 57), indicating that the cells in the EngNT were healthy prior to implantation.

Figure 57. Segments cut from the EngNT prior to assembling the nerve repair devices. Groups 1, 2 and 3 refer to segments removed from EngNT implanted to the animals and explanted and imaged *ex vivo* on days 1, 3 and 5 respectively. The cells in each segment emitted a high bioluminescence signal and no statistical difference between any of the groups was obtained (one-way ANOVA, Tukey's multiple comparisons test, 95 % confidence interval, p value = >0.9235). Each data point represents the signal obtained from one segment in the different groups (n = 3 for each group).



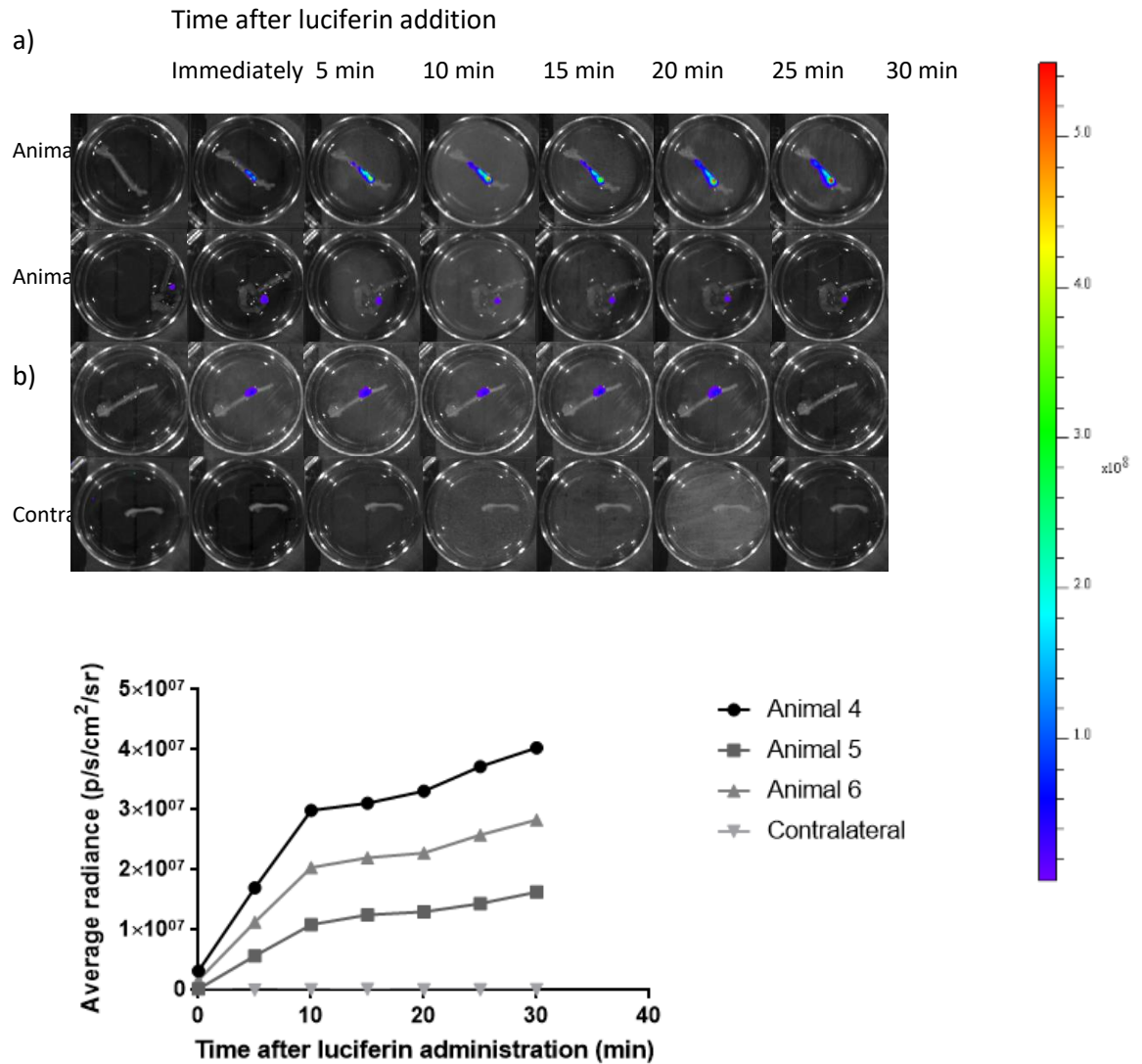
On day 1, bioluminescence imaging revealed that the signal obtained from the nerve repair devices explanted from the three rats varied greatly (figure 58). The highest signal was obtained 30 minutes after the addition of luciferase and ranged from 6.19×10^7 p/s/cm²/sr in the EngNT explanted from rat 3, to 7.47×10^7 and 2.78×10^8 p/s/cm²/sr in the EngNT explanted from rat 1 and 2 respectively. This was equivalent to a 4.49 fold difference in bioluminescence intensity.

Figure 58. *Ex vivo* imaging of the explanted nerve repair devices and a representative control contralateral nerve one day post implantation. a) Bioluminescence images showing the emitted light immediately after the addition of luciferin up to 30 minutes after addition. The rainbow pseudocolour scale was adjusted for all images. b) The bioluminescent signals ($\text{p/s/cm}^2/\text{sr}$) were plotted for each explant ($n = 3$).



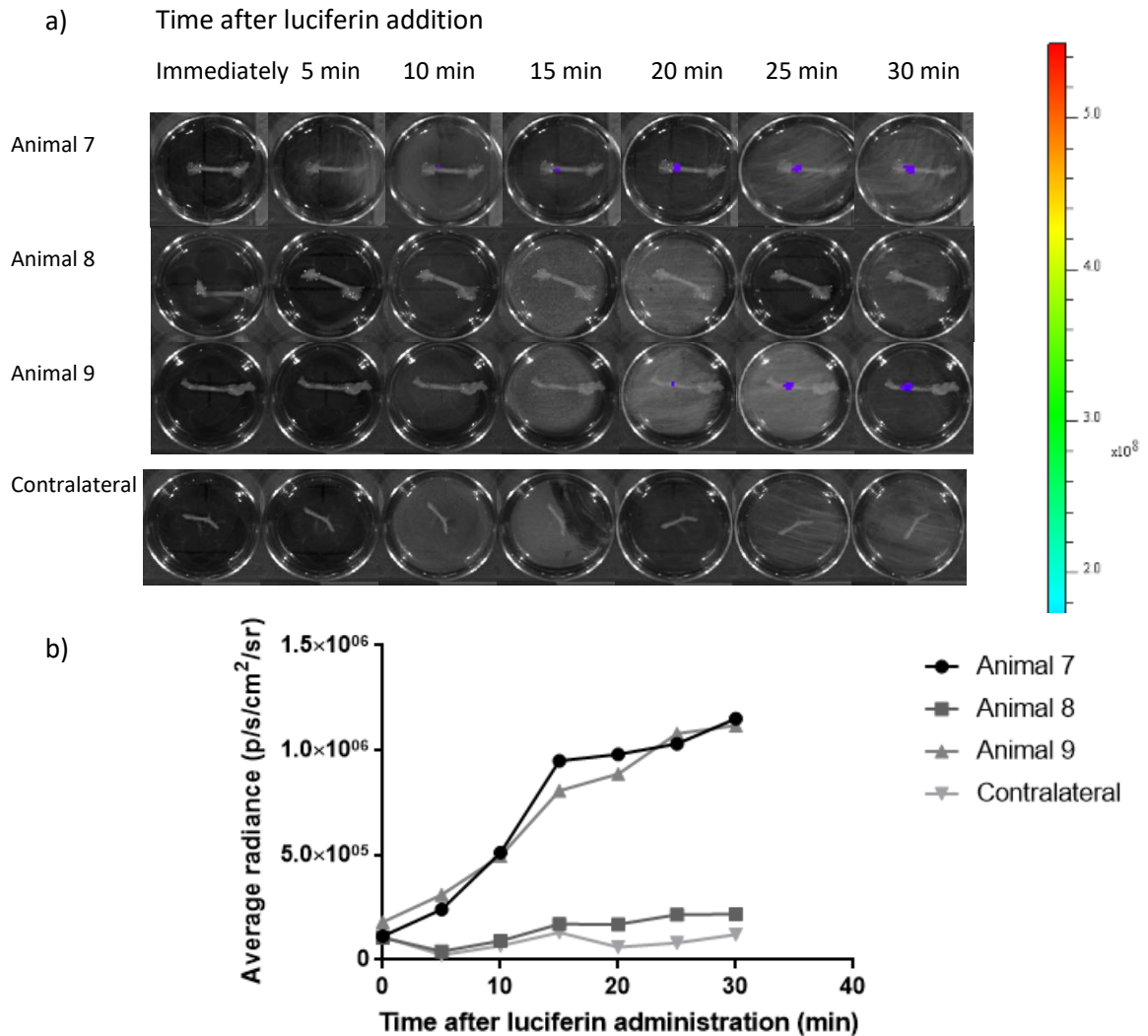
On day 3, the bioluminescence signal obtained from the EngNT explanted from the three rats varied greatly again (figure 59). The signal obtained 30 minutes after the addition of luciferase ranged from $1.63 \times 10^7 \text{ p/s/cm}^2/\text{sr}$ in the EngNT explanted from rat 5, to $2.83 \times 10^7 \text{ p/s/cm}^2/\text{sr}$ and $4.03 \times 10^7 \text{ p/s/cm}^2/\text{sr}$ in the EngNT explanted from rat 6 and 4 respectively. This was equivalent to a 2.47 fold difference in bioluminescence intensity.

Figure 59. Ex vivo imaging of the explanted nerve repair devices and a representative control contralateral nerve three days post implantation. a) Bioluminescence images showing the emitted light immediately after the addition of luciferin up to 30 minutes after addition. The rainbow pseudocolour scale was adjusted for all images. b) The bioluminescent signals (p/s/cm²/sr) plotted for each explant (n = 3).



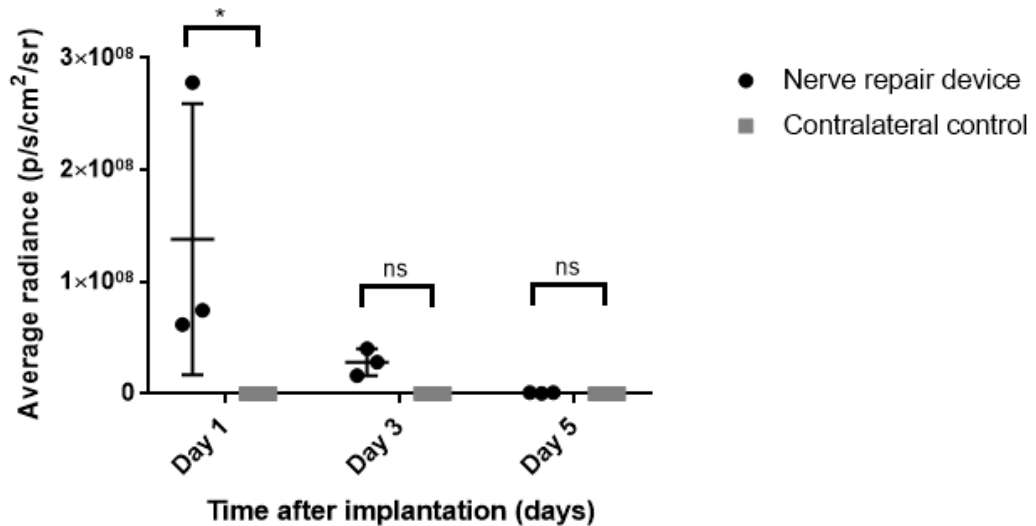
On day 5, the signal obtained 30 minutes after the addition of luciferase ranged from 1×10^6 p/s/cm²/sr in the EngNT explanted from rats 7 and 9, to 2.18×10^5 p/s/cm²/sr in the EngNT explanted from rat 8 (figure 60). This was equivalent to a 5.32 fold difference in bioluminescence intensity.

Figure 60. *Ex vivo* imaging of the explanted nerve repair devices and a representative control contralateral nerve five days post implantation. a) Bioluminescence images showing the emitted light immediately after the addition of luciferin up to 30 minutes after addition. The rainbow pseudocolour scale was adjusted for all images. b) The bioluminescent signals (p/s/cm²/sr) plotted for each explant (n = 3).



The highest bioluminescence signal obtained 30 minutes after the addition of luciferin on day 1 was 2.78×10^8 p/s/cm²/sr. By day 5, the highest signal obtained had decreased to 2.18×10^5 p/s/cm²/sr, equivalent to a 1000 fold difference. As the kinetic study revealed that the highest signal was obtained 30 minutes after the addition of luciferin, the bioluminescence signal at 30 minutes obtained for each explanted nerve repair device and control contralateral nerve on different days post implantation was plotted (figure 61). Only the bioluminescence signal obtained from the nerve repair devices explanted on day 1 was significantly higher than the control nerves.

Figure 61. The bioluminescence signals obtained 30 minutes after the addition of luciferin up to 5 days post implantation. Only the bioluminescence signal obtained from the nerve repair devices explanted on day 1 was significantly higher than the control nerve (two-way ANOVA, Tukey's multiple comparisons test, 95 % confidence interval, p value = 0.0465). Each data point represents the signal obtained from each individual nerve repair device and contralateral nerve 1, 3 and 5 days post implantation ($n = 3$ for each group). * $p < 0.05$, ** $p < 0.01$, *** $p < 0.001$ and **** $p < 0.0001$.

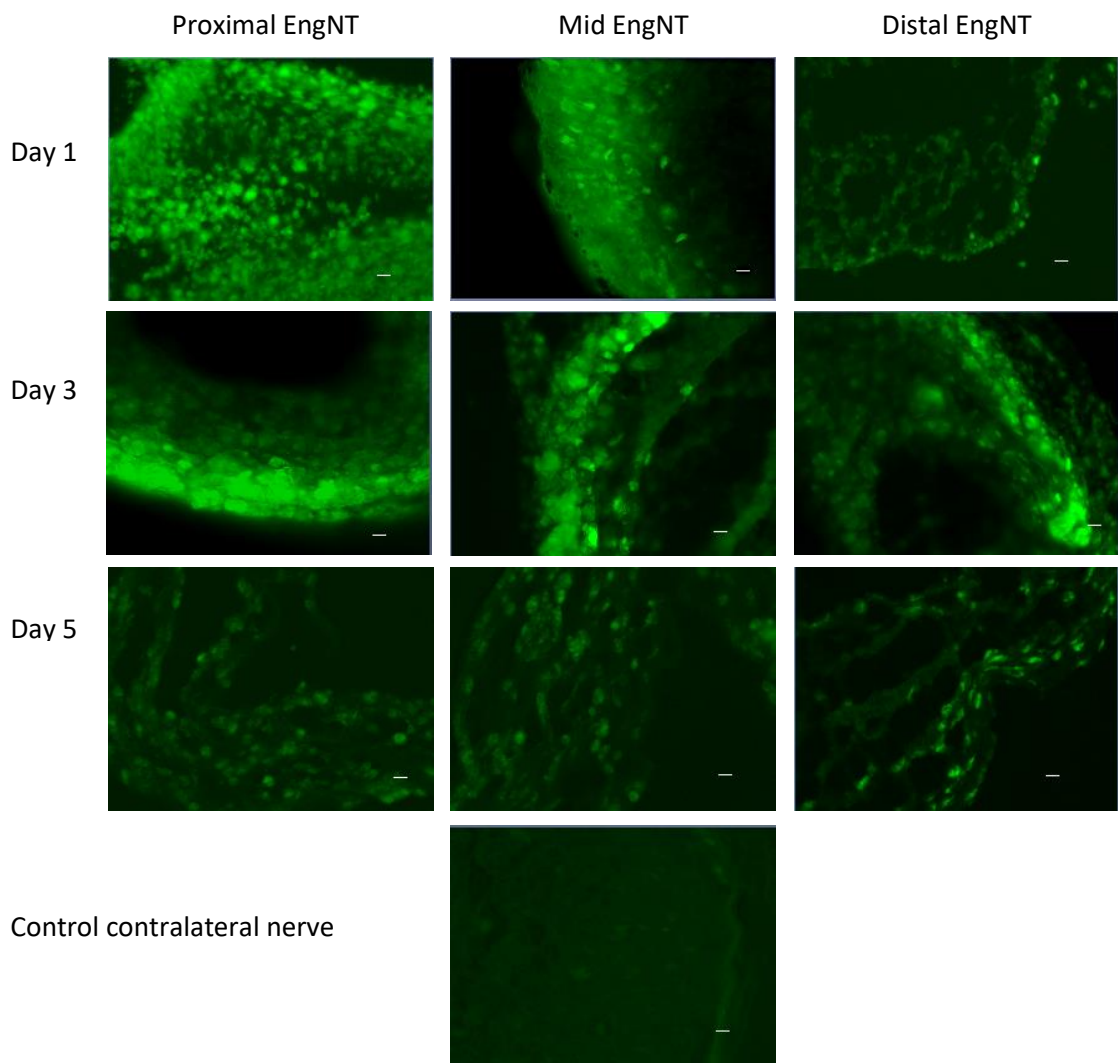


5.6 Fluorescence imaging

As described in the previous chapter, the lentiviral expression cassette consisted of a gene encoding eGFP in addition to one encoding luciferase. As *ex vivo* bioluminescence imaging gave highly variable results, it was decided to investigate whether eGFP cells were present in the explanted nerve devices and to establish whether fluorescence microscopy data would reflect bioluminescence data.

Following *ex vivo* bioluminescence imaging, the nerve repair devices were fixed and cryoprotected. The silicone tube was removed and the EngNT was subsequently placed in OCT compound. Transverse cryostat sections were cut from the proximal, middle and distal parts of the EngNT. Following mounting onto microscope slides, a Zeiss Axio Lab A1 fluorescence microscope at 20x magnification was used to directly visualise eGFP positive cells in predetermined areas in the sections. A qualitative analysis revealed that eGFP positive cells were still visible on day 5 (figure 62), indicating the presence of live cells. Sections through contralateral nerves were used as a negative control, as no eGFP positive cells should be present.

Figure 62. Explanted EngNT contained eGFP positive cells. Representative images showing eGFP expressing cells at different positions in the explanted EngNT, 1, 3 and 5 days post implantation. A section from a control contralateral nerve is also shown, no eGFP expressing cells are seen (n = 3 for each day). Scale bar: 50 μ m.

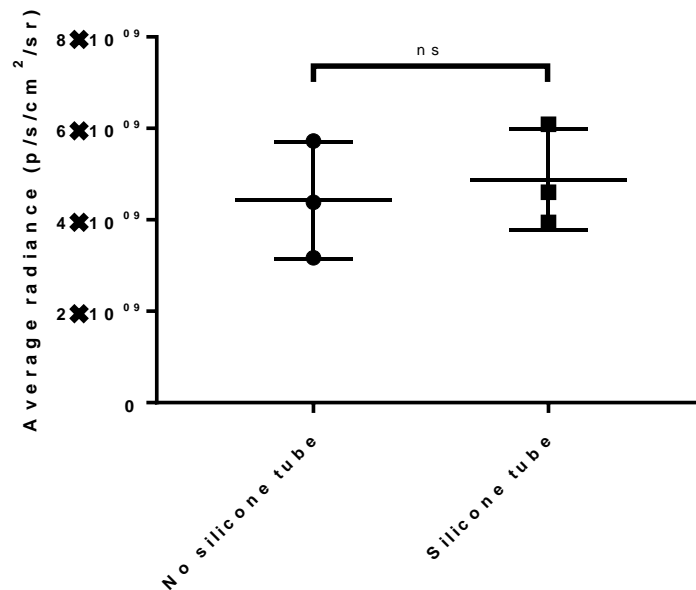


5.7 Monitoring cell viability in the nerve repair device

Following the results obtained in the *ex vivo* imaging study, it was decided to investigate the effect of the silicone tube on bioluminescence imaging. The first step was to determine whether the silicone tube attenuated the emitted light. EngNT was imaged immediately after the addition of luciferin, then rolled and inserted into a silicone tube and imaged again. In the absence of light attenuation, it was expected that the bioluminescence will continue to increase in the first 5 minutes after luciferin addition (section 5.2.1). Both measurements were taken within 2 minutes of each other and as

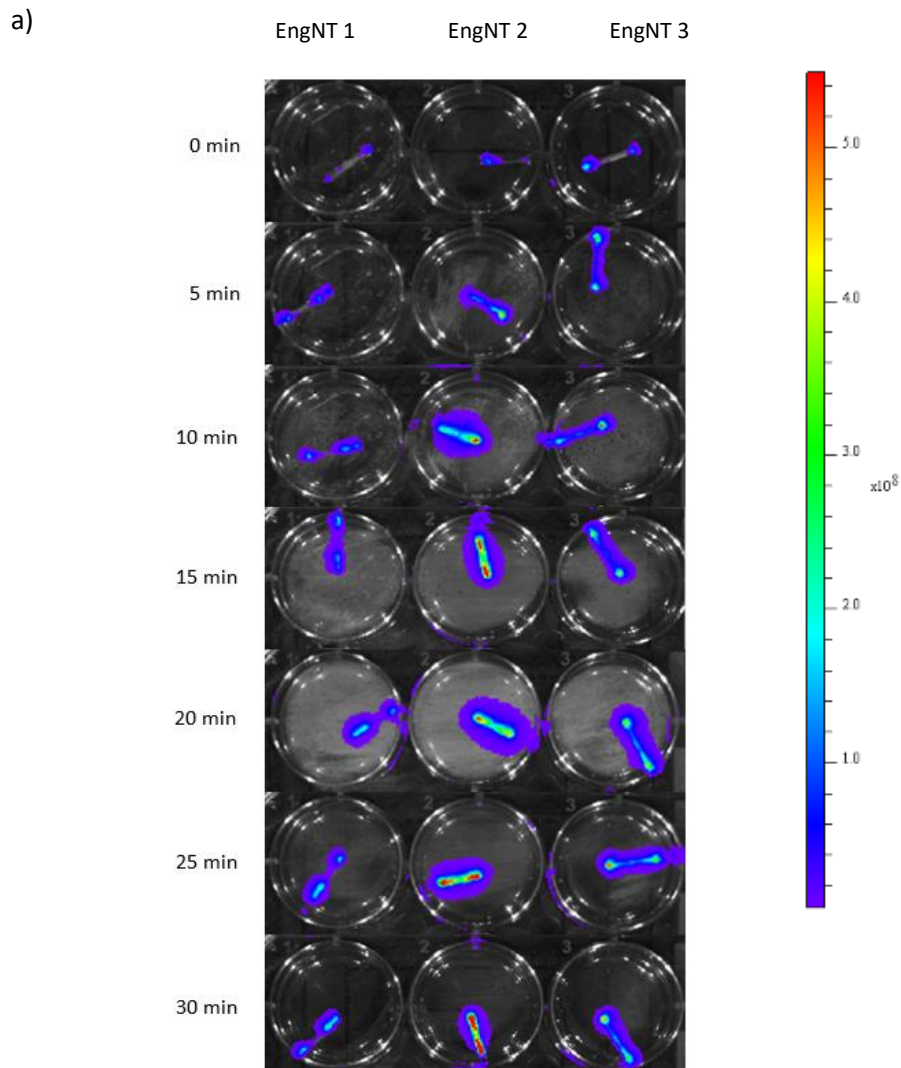
can be seen in figure 63, the presence of the silicone tube did not attenuate the emitted light.

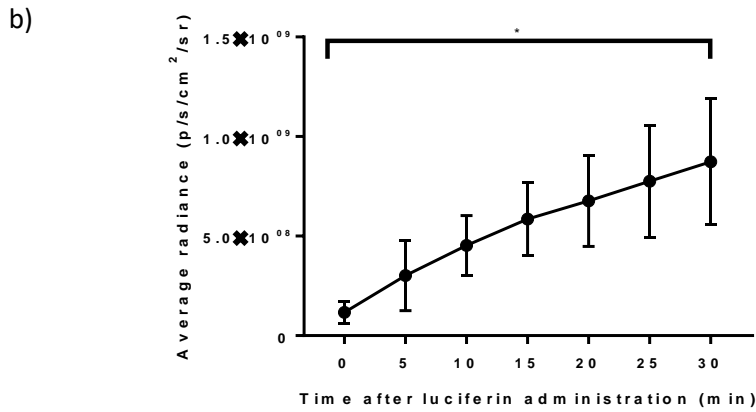
Figure 63. The silicone tube in the nerve repair device did not attenuate the emitted light. While the signal emitted from the EngNT in the silicone tube appeared to be slightly, no statistical difference was observed between the two groups (two-tailed unpaired T test, 95 % confidence interval, p value = 0.6655). Each data point represents the signal emitted from an individual EngNT with and without a silicone tube (n = 3).



Having established that the silicone tube does not attenuate the emitted light, it was then decided to investigate whether the silicone tube influenced luciferin kinetics and impeded contact of luciferin with the cells in the EngNT (figure 64). The highest signal (a mean of 8.73×10^8 p/s/cm²/sr) was obtained 30 minutes after the addition of luciferin. When imaging EngNT without a silicone tube, the highest signal was obtained 5 minutes after the addition of luciferin and had a mean value of 4.16×10^9 p/s/cm²/sr (section 4.2.1). This was equivalent to a 4.77 fold difference in bioluminescence intensity. In addition to a lower bioluminescence intensity, another difference was observed between EngNT in a silicone tube and EngNT without a silicone tube. At the early time points, a bioluminescence signal was only seen at the ends of the EngNT in silicone tubes. The bioluminescence signal in EngNT without a silicone tube was evenly distributed throughout the entire construct at all time points (image 50). The silicone tube has two open ends and this data indicated that the luciferin could only penetrate the EngNT through the ends, suggesting that the silicone tube does influence the penetration of luciferin.

Figure 64. Assessing the impact of the silicone tube on luciferin kinetics. a) Bioluminescent images showing the emitted light in 3 individual EngNT in silicone tubes up to 30 minutes after luciferin addition. The rainbow pseudocolour scale was adjusted for all images. b) The bioluminescent signals plotted for the EngNT in silicone tubes. The signal at 30 minutes was significantly higher than the signal obtained immediately after the addition of luciferin (Kruskal-Wallis test, Dunn's multiple comparisons test, p value = 0.0148). No other significant differences were observed (p value = >0.0510). Data presented as the mean \pm SD ($n = 3$). * $p < 0.05$, ** $p < 0.01$, *** $p < 0.001$ and **** $p < 0.0001$.





5.8 Discussion

A major parameter of interest following implantation of tissue engineered constructs is tracking cell fate. Bioluminescence imaging has emerged as a valuable tool for monitoring cell populations *in vivo* and has been used to assess cell survival and proliferation in tissue engineered constructs (Logeart-Avramoglou *et al.*, 20010; Hwang *et al.*, 2014b). In the current study, the efficacy of bioluminescence imaging to monitor luciferase expressing SCL4.1/F7 cells in EngNT *in vitro* and *in vivo* was assessed.

The survival of cells in 3D constructs may present a challenge when compared to culture in 2D monolayers (Ren *et al.*, 2015). This is because the presence of the scaffold may influence oxygen and nutrient availability. Further, the size, thickness, and complexity of these models can complicate the monitoring of cell viability of cells inside the constructs (Goliwas *et al.*, 2017). In the current study, cell viability in the EngNT *in vitro* was monitored by bioluminescence imaging, live-dead staining and the alamarBlue[®] assay. A decrease in cell viability in the EngNT over time was observed regardless of the method used. However, some differences in the sensitivity of the methods was noticed. When bioluminescence imaging was used, the signal emitted by the cells in the EngNT was similar to the signal emitted by the negative control by day 5, suggesting that the majority of the cells were no longer viable. However, when live-dead staining and the alamarBlue[®] assay were used, a significantly higher number of viable cells compared to the negative control was observed on day 5. Further, while an increase in cell viability between day 0 and day 1 was noted in both bioluminescence imaging and the alamarBlue[®] assay, the increase was only significant in the latter. The reduced sensitivity of bioluminescence imaging was possibly attributed to the fact that only around 80% of

the cells in the EngNT expressed luciferase (section 4.2.4). As bioluminescence imaging depends on the emission of light by luciferase expressing cells, viable cells which did not express luciferase were not detected by the imaging system.

It was thought that the relationship between emitted light intensity and the number of luciferase expressing cells would be useful for monitoring the survival of cells in the EngNT *in vivo*, as cell survival may be critical for achieving satisfactory regenerative outcomes. Further, a comprehensive literature review carried out in June 2018 revealed that a number of studies had reported the use of bioluminescence imaging to monitor cell survival in tissue engineered constructs implanted in live animals (table 16).

As can be seen in table 16, limited persistence of the bioluminescence signal has been observed extensively, with several studies reporting signal attenuation within the first two weeks (Kutschka *et al.*, 2006; Manassero *et al.*, 2016; Speidel *et al.*, 2017). However, this trend is unclear as Hwang *et al.* (2014b) reported an increase in signal in the first 3 weeks period and Schmitt *et al.* (2013) reported that the signal persisted for 4 weeks. Interestingly, Takaku *et al.* (2014) reported that a bioluminescence signal was still obtained at 21 months. It is important to note that simply quantifying the emitted light may not provide a true representation of cell viability *in vivo*. This is because the intensity of the bioluminescence signal is influenced by the number of metabolically active luciferase expressing cells, the concentration of luciferin, ATP and oxygen levels and the depth and optical properties of the tissue (Rice *et al.*, 2001).

Allen *et al.* (2014) found that lower cell doses (0.25×10^6 cells) survived better than high cell doses (2×10^6 cells) after 1 week. They suggest that following implantation, cells compete for nutrients and in the absence of an integrated vasculature, only a fraction of the implanted cells can be supported *in vivo*. Similar findings were described by Becquart *et al.* (2012). However, both authors reported that the signal decreased rapidly after 6-7 days irrespective of the cell number. Becquart *et al.* (2012) proposed that ischaemia in the core of the constructs resulted in cell death, leading to a reduced bioluminescence signal. However, they also suggested that other factors, such as cell migration, could have contributed to the reduced signal. The likelihood of ischaemia increases in larger tissue engineered constructs (Gholipourmalekabadi *et al.*, 2016).

However, while the authors cited in table 17 used constructs of varying sizes, it is not possible to compare the effect of construct size on the bioluminescence signal as different cell types, construct materials and implantation sites were used.

Table 17. Use of bioluminescence imaging to monitor cell survival in tissue engineered constructs implanted in live animals.

Author	Animal model	Cell type and seeding density	Scaffold material and size	Implantation site	Dose of luciferin injected, route of injection and timing of imaging	Exposure time and imaging protocol	Imaging time points	Vascularisation	<i>In vivo</i> bioluminescence results
Speidel et al., 2017	Healthy mice	Adult mouse cardiac stem cells; 3.5 x 10 ⁵ cells	Poly(ethylene glycol) network cross-linked with heparin-binding peptide; no information on size	Myocardium	10 µl per g of body weight; IP; 20 min before imaging	No information given	Days 0, 1, 3, 7 and 14	No information given	Signal increased up to day 3 and decreased on days 7 and 14.
Manassero et al., 2016	Immunodeficient NMRI mice	Human BMSCs; 1 x 10 ⁶ cells	Coral exoskeleton; 3.5 x 2 mm cylinders	Subcutaneous pocket in back and in a defect in the left femoral bone	75 mg/kg, IM; no information given	No information given; images were taken every 3 min during a 40 min period	Day 1, then twice a week for 5 weeks and then once a week for another 5 weeks	No information given	85% signal decrease over the first 2 weeks in both locations.

Prins <i>et al.</i>, 2016	Immunodeficient Balb/c mice	Human and goat BMSCs; 0.2 x 10 ⁶ cells	Hydroxyapatite or β -tricalcium phosphate ceramics; 2-3 mm	Subcutaneous pocket in back	2.5 mg; IP; 5 min before imaging	10 min	Day 2 then weekly for 6 weeks	No information given	Goat BMSCS – signal doubled after 1 week, declined to 60% of input after 3 weeks and remained constant until week 6. Human BMSCs - constant signal decrease to 25% of input.
Allen <i>et al.</i>, 2014	Athymic nude rats	Human BMSCs; 0.25, 0.5, 1 or 2 x 10 ⁶ cells	Alginate or agarose hydrogels in a PCL tube; 12 x 5 x 1 mm	Subcutaneous pocket in back	300 μ l; SC (2 – 4mm from the implant site); 10 min before imaging	10 sec; animals were imaged 10, 20 and 30 min post luciferin injection	Days 0 and 7	Vascularisation was observed	Decrease in signal on day 7. The survival efficiency of the cells was highest for the lower cell doses embedded within alginate matrix.
Hwang <i>et al.</i>, 2014a	Sprague-Dawley rats, immunosuppressed with cyclosporine	HB1.F3 human neural stem cells transduced with a retroviral vector; 2 x 10 ⁶ cells	Poly-L-lactic acid; no information on size	Cavity in the corticectomized rat brain	0.6 mg, injected into the brain; no information given	5 min; no information given	Days 0, 1, 3, 5, 8, 11 and 14	No information given	Gradual increase in signal up to day 8 followed by a dramatic decline after day 11.

Hwang et al., 2014b	BALB/c nude mice	HB1.F3 human neural stem cells transduced with a retroviral vector; 0.5 x 10 ⁶ cells	Gelatin-polyethylene glycol-tyramine hydrogel; no information on size	Subcutaneous region in thigh	150 mg/kg; IP; no information given	5 min; animals were imaged for 90 min at 5 min intervals	Days 0, 8 and 21	No information given No information given	Signal increased over the 21 day period.
Takaku et al., 2014	Wildtype Lewis rats	Luciferase expressing synovial cells and chondrocytes from transgenic Lewis rats	Chondrocyte and synovial cell sheets; no information on size	Defect in the patellar groove of the femur	150 mg/kg; SC; no information given	No information given; animals were imaged at 1 min intervals for 40 min	Days 0 and 4, and at 3, 6, 12, 18 and 21 months	No information given	Signal peaked on day 4 then decreased over the first month, after which it stabilised at approximately 1/10 of the intensity on day 0 and persisted for 21 months.
Schmitt et al., 2013	Rowett nude rats	Human ADSCs; 1-2 x 10 ⁶ cells	Decellularized cadaveric human flexor tendon grafts; 2 cm	Subcutaneous pocket in back	150 mg/kg; IP; 15 min before imaging	No information given	Days 7, 14, 21 and 28	Vascularisation of the construct observed after 4 weeks <i>in vivo</i>	Signal persisted for 4 weeks.
Yang et al., 2013	Sprague Dawley rats	Rat ADSCs; 5 x 10 ⁶ cells	Fibrin; no information on size	Border of infarcted myocardium	400 mg/kg luciferin; IP; no	No information given; animals	Days 1, 3, 7, 14 and 28	Vascularisation in the implanted	Signal decreased during the first week. A plateau phase was

					information given	were imaged at 2 min intervals until peak signal occurred		areas was observed	observed between days 7-14. Further decline in signal on day 28, but still present.
Becquart et al., 2012	Nude mice	Human immortalized multipotent stromal line; 5 x 10 ⁶ , 1 x 10 ⁶ , 1 x 10 ⁵ or 1 x 10 ⁴ cells	Coral particles; 600 – 900 µm diameter	Subcutaneous pocket in back	50 µl; SC at the implant site; 10 min before imaging	No information given	Days 1, 2, 6, 9, 12, 15, 21 and 30	Vascularisation was observed in the outer cells located in the outer regions of the constructs	<1% of the initial cell numbers remained at 30 days.
Geuze et al., 2010	Immunodeficient BALB/c mice and nude Sprague Dawley rats	Goat BMSCs; 0.5 x 10 ⁶ , 1 x 10 ⁶ or 3 x 10 ⁶ cells	Biphasic calcium phosphate porous particles; 2-3 mm diameter	Subcutaneous pocket in back (mice) and the spine (rats)	125 mg/kg; IP; no information given	10 min	Day 1 and then weekly for 6-7 weeks	No information given	Mice - From day 7 to 21, signal increased 5.3-fold. After day 21, signal gradually decreased to a level 1.2-fold higher at day 42 than at day 7. Rats - signal increased from day 1 to 7, after which it decreased. Signal decreased to

									baseline on day 21.
Logeart-Avramoglou et al., 2010	Nude mice	C3H10T1/2 mouse embryonic stem cells transduced with a retroviral vector; 0.1 x 10 ⁶ cells	AN69 hydrogels (acrylonitrile and sodium methallyl sulfonate copolymer); diameter 6 mm height 2 mm or coral scaffolds; (3x3x3 mm ³)	Subcutaneous pocket in back	50 µl; SC in the implant site; 10 min before imaging	10 min	Day 0 and then twice weekly for 8 weeks	No information given	Signal during days 3-6 decreased by approximately 70% (AN69 scaffold) and 80% (coral scaffold). Signal increased during the first week. The average final (at day 59) cell population was 2.5-fold higher than the initial seeding number for AN69 scaffold. For coral scaffolds, a 12-fold increase at day 59 was observed.
Dégano et al., 2008	Nude BALB/c mice	Human ADSCs and human BMSCs; 2.5 x 10 ⁶ cells	Arginine–glycine–aspartate crosslinked PEG hydrogel; no information on size	Calvarial bone defect	50 µl; SC in the implant site; 5 min before imaging	5 min; animals were imaged at 5 min intervals for 20 min	Days 0, 7, 14, 30, 45 and 90	No information given	A 63% drop in the number of the implanted BMSCs was observed and only 5% of the implanted ADSCs survived.

Olivo et al., 2008	Immunodeficient mice	Goat BMSCs transduced by a retroviral vector; 0.05 x 10 ⁶ , 0.125 x 10 ⁶ , 0.25 x 10 ⁶ , 0.5 x 10 ⁶ or 1 x 10 ⁶ cells	Biphasic calcium phosphate; 4 x 4 x 4 mm	Subcutaneous pocket in back	125 mg/kg; IP; no information given	5 min; animals were imaged over a 20 min period	Day 1, 4, 11, 18, 25, 32, 39 and 46	Blood vessels were present in and around the scaffold at day 46	Until day 46, the signal continued to increase in the scaffolds seeded with 1, 0.5, 0.25, and 0.125 x 10 ⁶ cells. In scaffolds seeded with 0.05 x 10 ⁶ cells, the signal progressively dropped to a background value.
Kutschka et al., 2006	Lewis rats, immunosuppressed with cyclosporine	Rat cardiomyoblasts; 1 x 10 ⁶ cells	Collagen or collagen with Matrigel; 3x3x1 mm	Infarcted myocardium	400 mg/kg; IP; no information given	5 min; animals were imaged 8 times	Days 1, 5, 8, 14 and 28	Capillary ingrowth into the scaffold was observed	Signal decreased during the first 8 days. Signal in collagen graft reached background level on day 14. Signal in the collagen with Matrigel graft was detectable on day 28.

Abbreviations: ADSCs – adipose derived stem cells; BMSCs – bone marrow stem cells; IP – intraperitoneal; SC - subcutaneous

All cells used in these studies expressed luciferase after transduction with lentiviral vectors unless stated otherwise.

As mentioned earlier, the efficacy of bioluminescence imaging can be influenced by several factors. This was particularly evident in the current study, as no bioluminescence signal was obtained *in vivo*, despite a very strong bioluminescence being obtained *in vitro* (section 5.2.1). It was thought that bioluminescence imaging was compromised by the exogenous and endogenous factors that will be discussed in this section. The impact of confounding factors in 2D monolayer systems is relatively limited and the bioluminescence signal tends to show a linear relationship with viable cell number. This has been reported by others (Kim *et al.*, 2010) and was also observed in the current study (section 4.3.4). However, in 3D tissue engineered constructs, bioluminescence imaging may be affected by luciferin transport kinetics and light scattering properties of the construct (Allen *et al.*, 2014). Further, following implantation, insufficient vascularisation of the newly implanted tissue engineered constructs may further confound bioluminescence imaging. These factors will be discussed below.

The strength of the promoter driving the expression of luciferase in the transduced cells is an important consideration in bioluminescence imaging, as weak promoters may not produce sufficient luciferase. This is especially important for *in vivo* studies tracking cell fate since low levels of bioluminescence may not be detected (Chen and Thorne, 2012). The strength of the promoter can be predicted based on *in vitro* quantification of cell signal. The SFFV promoter used in the study has been shown to confer a strong transcriptional ability in a variety of cell types following lentiviral transduction (Gautam *et al.*, 2016; Winiarska *et al.*, 2017). *In vitro*, the transduced SCL4.1/F7 cells in monolayers and in the EngNT could only be imaged for the minimal amount of time (1 second) to prevent saturation, indicating the production of a high level of luciferase. Despite the high levels of luciferase expression, bioluminescence imaging could not be used to monitor the cells following implantation as no signal was obtained. In addition to luciferase expression, efficient bioluminescence imaging also depends on the availability of the luciferase substrate luciferin as well as oxygen.

Cells implanted within tissue-engineered constructs may experience physiologically abnormal oxygen tension due to insufficient vascularisation following implantation (Muschler *et al.*, 2004). As well as affecting oxygen availability, a lack of vascularisation may also affect the amount of luciferin reaching the luciferase expressing cells. Allen *et*

al. (2014) investigated the association between development of vasculature and bioluminescence signal 7 days following subcutaneous implantation of luciferase expressing human bone marrow stem cells in alginate constructs in athymic nude rats. They found that construct vasculature was significantly correlated to the bioluminescence signal obtained and suggested that a lack of vasculature may reduce the bioluminescence signal obtained by limiting luciferin and oxygen availability to the luciferase expressing cells. A significant association between vasculature and bioluminescence signal in 3D tissues has also been reported by Olivo *et al.* (2008) and Sekine *et al.* (2013). Further evidence supporting the importance of vascularisation in bioluminescence imaging came from a study by Levenberg *et al.* (2005), who compared the bioluminescence signal in pre-vascularised skeletal muscle grafts to muscle grafts without endothelial cells. They observed an increased bioluminescence signal in the pre-vascularised samples that they suggested was due to increased perfusion, resulting in a higher amount of luciferin and oxygen reaching the luciferase expressing cells.

A lack of vasculature has been implicated in the availability of luciferin, but the luciferin molecule itself is associated with a number of shortcomings *in vivo*, primarily relating to its low cell permeability (Shinde *et al.*, 2006) and its heterogeneous tissue distribution (Berger *et al.*, 2008). Limited luciferin uptake in several tissues, including the brain (Lee *et al.*, 2003, Berger *et al.*, 2008), has been reported. It is thought that the presence of the blood brain barrier prevented the entry of luciferin to the brain and limited the use of bioluminescence imaging (Mofford and Miller, 2015; Iwano *et al.*, 2018). The blood brain barrier is a neurovascular unit essential for preserving CNS homeostasis. It is formed by highly specialised endothelial cells that interact directly with astrocytes, neurons and pericytes to regulate the movement of molecules, ions and cells between the blood and the CNS (Abbott, 2013).

The presence of physical barriers preventing access of luciferin to the luciferase expressing cells is especially relevant in the current study. In the PNS, endoneurial microvessels are in direct contact with circulating blood, and form the blood-nerve barrier. The endoneurial microvessels share their basement membrane with pericytes and limit the diffusion of substances in and out of the endoneurium (Palladino *et al.*, 2017). A comprehensive literature search revealed that no researchers have yet

reported that the blood nerve barrier impeded the entry of luciferin. However, the blood nerve barrier is widely regarded as the second most restrictive microvascular barrier after the blood-brain barrier in mammals (Palladino *et al.*, 2017), and therefore such an effect cannot be excluded.

It was also decided to investigate whether the collagen hydrogel and the silicone tube used in the nerve repair device served as barriers to the entry of luciferin. Hwang *et al.* (2014b) suggested the mechanical strength of hydrogels used as cell scaffolds in tissue engineering applications may influence luciferin kinetics due to reduced permeability. The current study determined that the collagen hydrogel used did not affect bioluminescence imaging, as EngNT made from luciferase expressing SCL4.1/F7 cells could only be imaged for 1 second to prevent signal saturation, similar to luciferase expressing SCL4.1/F7 cells in monolayers. Further *in vitro* investigation revealed that the silicone tube influenced luciferin kinetics, resulting in an uneven distribution of luciferin in the EngNT leading to an inconsistent signal. Based on the pattern of bioluminescence signals obtained from the *in vitro* imaging of EngNT in silicone tubes (section 4.6), the luciferin entered the EngNT through the open ends of the silicone tube. This is an important consideration as small arteries and veins from neighbouring tissue space and muscular blood vessels run parallel along peripheral nerves *in vivo* (Gao *et al.*, 2013a). A nerve repair device will consequently interrupt the vasculature and this can only be restored by angiogenesis. A lack of vasculature may therefore impede the entry of luciferin through the open ends of the silicone tube. It was therefore thought that a combination of the lack of vasculature and the impermeable nature of the silicone tube resulted in an insufficient amount of luciferin reaching the luciferase expressing cells in the EngNT.

While Tögel *et al.* (2008) suggests that bioluminescence imaging has the distinct advantage of detecting only viable cells, a lack of bioluminescence signal is not necessarily indicative of cell death as photon emission is dependent on the availability of luciferin and oxygen. In the current study, a qualitative immunofluorescence analysis revealed that eGFP positive cells in the EngNT were still visible 5 days post implantation (figure 61). Therefore a correlation between bioluminescence imaging and fluorescence was not established in the current study. This is contrary to the results reported by

Dégano *et al.* (2008), who implanted 2.5×10^6 luciferase and eGFP expressing human bone marrow stem cells and adipose derived stem cells seeded in an arginine–glycine–aspartate (RGD) crosslinked hydrogel scaffold in a mouse calvarial bone defect. While no information on the vascularisation of the constructs was given, fluorescence microscopy revealed that eGFP positive cells were present throughout the light emitting implants, while few fluorescent cells were detected in implants that produced little or no light, in correlation with the *in vivo* BLI results.

While the biomaterials used in tissue engineered constructs can affect the bioluminescence signal emitted by cells (Logeart-Avramoglou *et al.*, 2010), Hwang *et al.* (2014a) used bioluminescence imaging to select the optimal biomaterials for tissue engineering purposes. They implanted 2×10^6 luciferase expressing human neural stem cells encapsulated within a poly-L-lactic acid scaffold and unencapsulated cells in a corticectomized rat model. Following implantation, the bioluminescence signal increased gradually up to 5 days without the scaffold, and up to 8 days with the scaffold. This was followed by a decline in the signal after 5 days without the scaffold, and after 11 days with the scaffold. They related the increase in signal to cell proliferation and the decline in signal to cell death. They suggested that the decline in survival was because of the environment around the cortical lesion, where the implanted cells are subjected to immunological insults and a necrotic environment. They postulated that the encapsulated cells survived longer as the scaffold protected them from the hostile environment.

The final aim of this chapter was to determine how long the implanted cells survive *in vivo*. This was because a major goal of this study was to investigate whether EngNT made of SCL4.1/F7 cells overexpressing VEGF-A₁₆₅ improved regeneration in a rat model of sciatic nerve injury. Cell survival is essential to ensure that the genetically modified cells are able to produce VEGF-A₁₆₅ and potentially enhance regeneration. Although the data obtained from bioluminescence imaging suggested that cell death was prevalent from 3 days post implantation, fluorescence imaging revealed the presence of eGFP positive cells throughout the nerve repair device up to at least 5 days post implantation. Nishida *et al.* (2018) investigated the expression of VEGF-A following an inferior alveolar nerve transection in mice. They found that compared to an intact nerve, the level of

VEGF-A in the injured nerve started to increase one day post injury and reached its highest level on day 2. VEGF-A levels began to decrease after day 3 and became undetectable by day 7. The authors suggest that VEGF-A is therefore crucial in the early stages of nerve regeneration and vascularisation. Based on the results obtained in this chapter and the observations made by Nishida *et al.* (2018), SCL4.1/F7 cells overexpressing VEGF-A₁₆₅ should persist long enough to bring about a therapeutic effect.

5.9 Conclusion

A peripheral nerve injury often requires interventions to augment normal healing. Tissue engineered constructs containing therapeutic cells may offer an alternative to autologous nerve grafts for enhancing repair. However, the behaviour of implanted cells is still not fully understood. Such information is crucial for the optimal application of tissue engineering. To this end, gene-reporter technologies (involving, e.g., the labeling of cells with a bioluminescent reporter gene) are promising because they permit the noninvasive detection of cells in tissue engineered constructs. As seen from the results obtained in this chapter, bioluminescence imaging was not a suitable imaging modality for the current study and further work needs to be done to establish whether bioluminescence imaging is applicable to peripheral nerve tissue engineering. Specifically, work should be directed on enhancing vascularisation following implantation of nerve repair devices as well as selecting conduits with properties that mimic the natural epineurium. Additionally, increasing vascularisation may lead to enhanced peripheral nerve regeneration and this will be the focus of the next chapters.

Chapter 6. Lentivirus-mediated expression of VEGF-A₁₆₅ in SCL4.1/F7 cells: assessing *in vitro* effects

6.1 Introduction

An *in vitro* proof-of-concept study determined that SCL4.1/F7 cells were amenable to lentiviral transduction and that the transduced cells were still viable for the construction of EngNT that can be used to enhance nerve repair (chapter 4). Transduction did not affect cell morphology, viability or proliferation and long term transgene expression was observed in the transduced cells. It was initially thought the presence of the luciferase gene in the expression cassette would allow real-time and sustained imaging of the cells in the EngNT. Bioluminescence imaging provided an indication of the viability of the cells in EngNT *in vitro* but proved to be ineffective for *in vivo* imaging and yielded inconsistent data for *ex vivo* imaging. Further, a qualitative fluorescence study revealed the presence of the eGFP positive cells in explanted EngNT up to 5 days after implantation, revealing that bioluminescence imaging is not a suitable means of tracking cell fate in EngNT following implantation.

In addition to tracking cell fate, another challenge in tissue engineering is the inability to adequately vascularise implants due to nutrient perfusion and mass transport limitations (Lovett *et al.*, 2009). After implantation of tissue-engineered constructs, a spontaneous vascularisation of the implant is usually seen. However, this induced vessel ingrowth is often too slow to provide adequate nutrient transport to the cells in the interior of the transplanted tissue. Therefore, additional strategies for enhancing vascularisation are essential to ensure the survival of large tissue-engineered grafts as insufficient vascularisation can lead to improper cell integration or cell death (Rouwkema *et al.*, 2008). VEGF is a potent angiogenic factor that stimulates proliferation and migration of endothelial cells, formation of new blood vessels and enhances vascular permeability (Brockington *et al.*, 2004). Additionally, VEGF increases axonal outgrowth, Schwann cell proliferation and Schwann cell invasion following injury (Sondell *et al.*, 1999a; Haninec *et al.*, 2012). As VEGF exhibits both angiogenic and neurotrophic properties, there has been an interest in the development of strategies for

delivering VEGF in peripheral nerve tissue engineering (Ma *et al.*, 2014; Gnani *et al.*, 2017).

Based on the results obtained in the current study, it was hypothesised that a lentiviral vector could be used to deliver the *VEGF-A₁₆₅* gene to SCL4.1/F7 cells, which would then overexpress the protein. Once seeded in the EngNT, the *VEGF-A₁₆₅* overexpression could potentially encourage quicker vascularisation of the implant. Prior to implanting the EngNT containing the transduced cells into a rat model of sciatic nerve injury and assessing the effects on peripheral nerve regeneration, it was important to establish the functionality of the lentiviral vector expressing the VEGF protein produced *in vitro* as described in this chapter. The aims of this chapter were as follows:

- To produce a lentiviral vector delivering the *VEGF-A₁₆₅* gene.
- To transduce SCL4.1/F7 cells with the lentiviral vector and to confirm that the cells overexpress the *VEGF-A₁₆₅* protein.
- To confirm the functionality of the *VEGF-A₁₆₅* protein produced by assessing its angiogenic and neurotrophic effects.

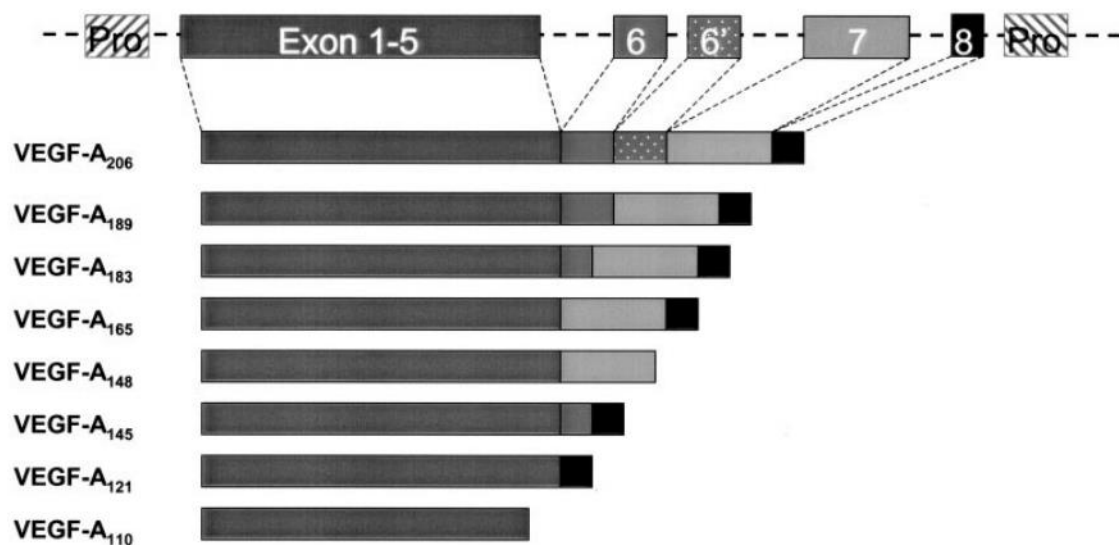
6.2 Choice of the therapeutic gene

The VEGF family consists of seven members, namely VEGF-A, VEGF-B, VEGF-C, VEGF-D, VEGF-E, VEGF-F and placental growth factor (Hoeben *et al.*, 2004). VEGF-A is the single most important regulator of blood vessel formation (Holmes and Zachary, 2005) and will be discussed in greater detail. VEGF-A is a dimeric glycoprotein and is approximately 34-42kDa in size (Hoeben *et al.*, 2004). As shown in figure 65, alternative splicing of the human *VEGF-A* gene gives rise to at least six different transcripts, with monomers consisting of 121, 145, 148, 165, 183, 189 or 206 amino acids. A common VEGF homology domain consisting of a cysteine knot motif, participating in the formation of the disulfide bridges between the VEGF monomers can be observed in all VEGF family members (Hoeben *et al.*, 2004).

The *VEGF-A* gene encodes eight exons, of which the amino acids determined by exons 1-5 and 8 are conserved in all VEGF-A isoforms. Exons 6 and 7 undergo alternative

splicing encoding two discrete heparin-binding domains (Hoeben *et al.*, 2004). The presence or absence of the heparin-binding domains influences the solubility and receptor affinity of the proteins. VEGF-A₁₂₁ is an acidic polypeptide that does not bind heparin and is thus freely diffusible. VEGF-A₁₈₉ and VEGF-A₂₀₆ are basic and bind to heparin with high affinity. As a result, they are almost completely bound in the ECM and do not diffuse (Houck *et al.*, 1992). VEGF-A₁₆₅ has intermediate properties, being both diffusible as well as having the ability to bind loosely to the heparin-containing proteoglycan receptors in the ECM (Park *et al.*, 1993). Ferrara *et al.* (2003) suggested that VEGF-A₁₆₅ is the isoform which exhibits the optimal bioavailability and biological potency and was therefore taken forward in this study.

Figure 65. A schematic representing the structure of the VEGF-A gene. The VEGF-A gene contains 8 exons of which, through differential splicing, give rise to seven isoforms named after their amino acid lengths (VEGF-A 121, 145, 148, 165, 183, 189 and 206). An additional isoform, VEGF-A₁₁₀, is produced by proteolytic cleavage by plasmin. Taken from Hoeben *et al.* (2004).



6.3 Cloning of the VEGF-A₁₆₅ gene

Having established that SCL4.1/F7 cells were successfully transduced using a lentiviral vector delivering marker genes, it was decided to insert the gene of interest, VEGF-A₁₆₅, into a lentiviral transfer plasmid. The pro-angiogenic VEGF-A₁₆₅ gene was supplied in an adenovirus, kindly provided by Professor Anna David (UCL Institute for Women's Health). Professor David's group has previously shown increased angiogenesis in a guinea pig model of foetal growth restriction following delivery of the adenovirus into

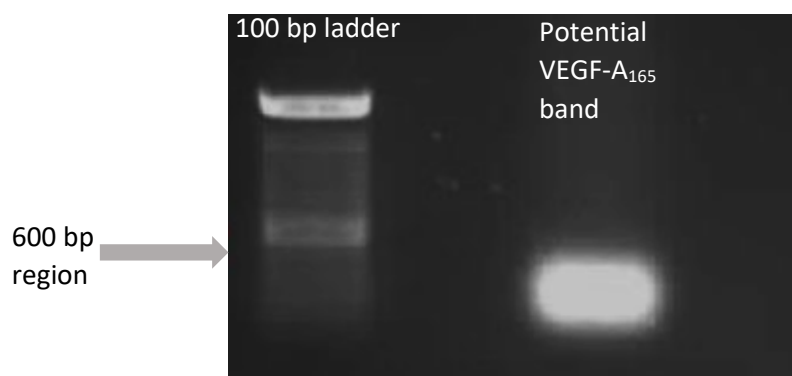
the uterine circulation (Swanson *et al.*, 2016). The sequence of the *VEGF-A₁₆₅* gene used in this study is 576 base pairs (bp) in length and is as follows:

```
5' - ATGAACTTTCTGCTGTCTTGGGTGCATTGGAGCCTTGCCTTGCTGCTCTATGCCAAGTGGT
CCCAGGCTGCACCCATGGCAGAAGGAGGAGGGCAGAATCATCACGAAGTGGTGAAGTTCAT
GGATGTCTATCAGCGCAGCTACTGCCATCCAATCGAGACCCTGGTGGACATCTCCAGGAGTA
CCCTGATGAGATCGAGTACATCTTCAAGCCATCCTGTGTGCCCTGATGCGATGCGGGGGCTG
CTGCAATGACGAGGGCCTGGAGTGTGTGCCCACTGAGGAGTCCAACATCACCATGCAGATTA
TGCGGATCAAACCTCACCAAGGCCAGCACATAGGAGAGATGAGCTTCTACAGCACAACAAA
TGTGAATGCAGACCAAAGAAAGATAGAGCAAGACAAGAAAATCCCTGTGGGCCTTGCTCAGA
GCGGAGAAAGCATTGTGTTGTACAAGATCCGCAGACGTGTAATGTTCTGCAAAAACACAGA
CTCGCGTTGCAAGGCGAGGCAGCTTGAGTTAAACGAACGTACTTGCAGATGTGACAAGCCGA
GGCGGTGA - 3'
```

6.3.1 The polymerase chain reaction

PCR based cloning was used to amplify the *VEGF-A₁₆₅* gene in the adenovirus and to add restriction sites to each end to allow cloning into the transfer plasmid. Gel electrophoresis was used to detect the purified PCR product. Initial PCR conditions employing an annealing temperature of 60°C and using the neat concentration of the adenovirus resulted in a large and bright band in the 600 base pair region of the DNA ladder (figure 66).

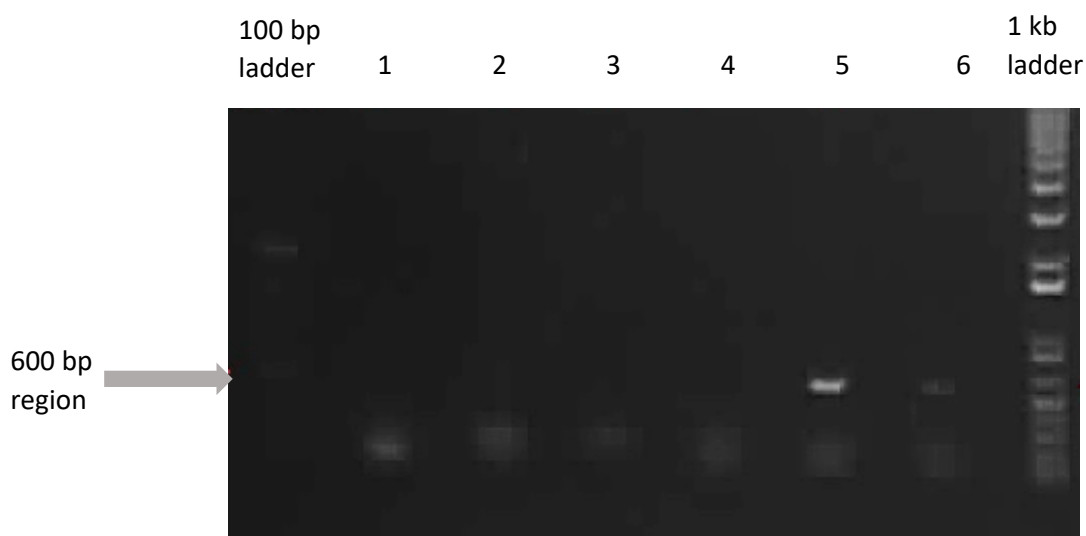
Figure 66. Gel electrophoresis image suggesting the presence of the *VEGF-A₁₆₅* gene. A 100 bp ladder was used with the 600 bp region highlighted in the image.



However, this data was not reproduced during subsequent PCR runs. PCR optimisation, whereby the annealing temperature and the concentration of the template DNA were changed, was carried out. It is commonly suggested to use an annealing temperature of around 5-10°C below the melting temperatures of the primers as this increases the probability of primer binding. The forward and reverse primers had a melting temperature of 65.4 °C and 64.7 °C respectively. It was therefore decided to run the PCR reaction using an annealing temperature of 56 °C, 58 °C and 61 °C. Optimisation of template DNA concentration is required as high concentrations may increase the risk of nonspecific amplification whereas low concentrations result in poor yield. The adenovirus was serially diluted to generate 5 dilutions (10^{-1} , 10^{-2} , 10^{-3} , 10^{-4} , and 10^{-5}) of the original template DNA.

Using these conditions, no bands were observed for the annealing temperature of 61°C and for the 10^{-3} , 10^{-4} , and 10^{-5} dilutions of the original template DNA. A reproducible band was obtained when an annealing temperature of 56°C and a dilution of 10^{-1} was used (figure 67).

Figure 67. Gel electrophoresis image deducing the optimum PCR conditions. The far left and right hand lanes were 100bp and 1Kb ladders, respectively, with the 600bp band highlighted. Lanes 1, 2 and 3 were PCR products ran at an annealing temperature of 58°C and using the original template DNA concentration, 10^{-1} and 10^{-2} dilutions, respectively. Lanes 4, 5 and 6 were PCR products ran at an annealing temperature of 56°C and using the original template DNA concentration, 10^{-1} and 10^{-3} dilutions respectively. The clearest band was seen in lane 5 (annealing temperature of 56°C, 10^{-1} dilution) and hence the optimum condition. The bands towards the bottom of the gel were assumed to be primer dimers.



6.3.2 Inserting the *VEGF-A*₁₆₅ gene into the pSFFV.IRES.eGFP transfer plasmid

As the PCR reaction had introduced the *Bam*HI and *Xho*I restriction enzyme sites on either end of the *VEGF-A*₁₆₅ gene, the next step was to subclone the gene into the pSFFV.IRES.eGFP transfer plasmid, which also contained the same restriction enzyme sites. A double digest was set up both for the *VEGF-A*₁₆₅ gene and pSFFV.IRES.eGFP transfer plasmid. This was followed by a ligation reaction to fuse the *VEGF-A*₁₆₅ gene to the transfer plasmid, creating a recombinant plasmid.

The ligation product was transformed into One Shot® Stbl3™ Chemically Competent *E. coli* cells. However, this did not result in the formation of colonies. A positive control plasmid which was also transformed into the bacterial cells indicated that the transformation procedure had worked. This suggested that the ligation reaction had not resulted in a functional recombinant plasmid. The initial insert: vector ratio used for the ligation reaction was 5:1. As the insert:vector ratio can be modified to maximise the yield of the recombinant plasmid, the ligation reaction was repeated using ratios of 1:1, 3:1 and 7:1. However, these still proved to be unsuccessful.

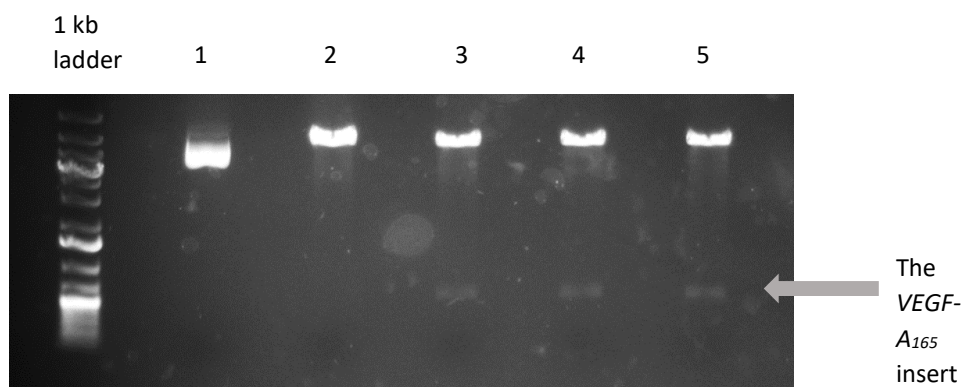
The initial subcloning approach did not result in the formation of a functional recombinant plasmid. It was therefore decided that *VEGF-A*₁₆₅ gene together with the restriction enzyme sites on each end would be synthesised by Life Technologies Limited to facilitate the cloning process. The sequence generated for the synthesised gene is as follows:

TACGTAGGTACCGGATCCGCCACCATGAACTTTCTGCTGTCTTGGGTGCATTGGAGCCTTGCCT
 TGCTGCTCTACCTCCACCATGCCAAGTGGTCCCAGGCTGCACCCATGGCAGAAGGAGGAGGG
 CAGAATCATCACGAAGTGGTGAAGTTCATGGATGTCTATCAGCGCAGCTACTGCCATCCAATC
 GAGACCCTGGTGGACATCTTCCAGGAGTACCCTGATGAGATCGAGTACATCTTCAAGCCATCC
 TGTGTGCCCTGATGCGATGCGGGGGCTGCTGCAATGACGAGGGCCTGGAGTGTGTGCCAC
 TGAGGAGTCCAACATCACCATGCAGATTATGCGGATCAAACCTACCAAGGCAGCACATAGG
 AGAGATGAGCTTCTACAGCACAACAAATGTGAATGCAGACCAAAGAAAGATAGAGCAAGAC
 AGAAAATCCCTGTGGGCCTTGCTCAGAGCGGAGAAAGCATTGTGTTGTACAAGATCCGCAGAC
 GTGTAAATGTTCTGCAAAAACACAGACTCGCGTTGCAAGGCGAGGCAGCTTGAGTTAAACG
 AACGTACTIONGAGATGTGACAAGCCGAGGCGGTGACTCGAGGTCGACAAGCTTTACGT

6.3.3 Formation of the pSFFV.VEGF.IRES.eGFP transfer plasmid

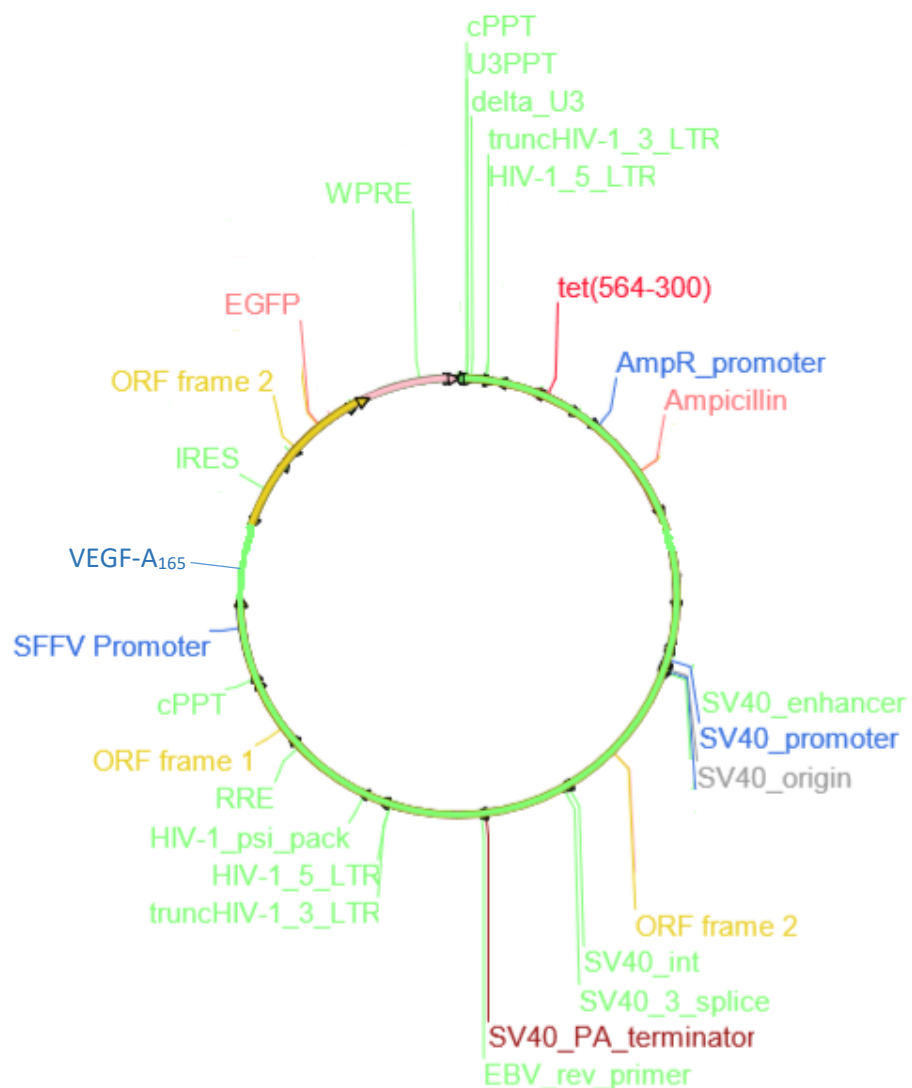
A double digest was set up for the synthesised *VEGF-A₁₆₅* gene and the pSFFV.IRES.eGFP transfer plasmid to produce a gene fragment and a linearised plasmid. This was followed by a ligation reaction that allowed the sticky ends of the insert and plasmid to stick together. An insert: vector ratio of 3:1 was used. The ligation mixture was transformed into competent bacteria and a single colony was isolated and used to generate a liquid bacterial culture. A diagnostic digest was carried out on purified plasmid DNA extracted from the bacterial culture. The resulting fragments were then analysed by gel electrophoresis. Digestion with both *Bam*HI and *Xho*I resulted in two bands: the 577 base pair *VEGF-A₁₆₅* insert and the 10427 base pair plasmid (figure 68).

Figure 68. Restriction digest analysis of the pSFFV.VEGF.IRES.eGFP plasmid using *Bam*HI and *Xho*I. Lane 1 shows the 1kb ladder. Lane 2 shows the undigested pSFFV.IRES.eGFP plasmid. Lane 3 shows the pSFFV.IRES.eGFP plasmid cut with *Bam*HI. Lanes 4-6 show the digested pSFFV.VEGF.IRES.eGFP plasmid and the *VEGF-A₁₆₅* insert at roughly the 600bp mark.



Restriction digest analysis produced bands of the predicted sizes. Before proceeding with functional experiments, it was important to sequence the plasmid by automated Sanger sequencing in order to fully confirm the successful construction of the pSFFV.VEGF.IRES.eGFP plasmid. Sanger sequencing confirmed that the *VEGF-A₁₆₅* gene had been successfully cloned into the plasmid, creating a transfer plasmid which could be used to construct a lentiviral vector. A schematic of this plasmid is shown in figure 69.

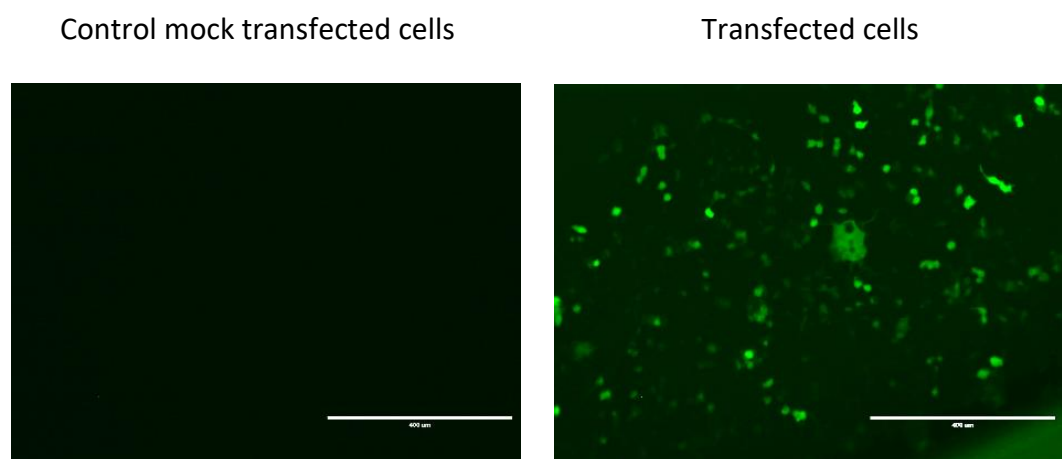
Figure 69. Schematic of the pSFFV.VEGF.IRES.eGFP transfer plasmid.



6.3.4 Functionality of the pSFFV.VEGF.IRES.eGFP transfer plasmid

Following sequencing of the pSFFV.VEGF.IRES.eGFP transfer plasmid, it was important to confirm that the plasmid was capable of expressing its transgenes and respectively encoded proteins. The plasmid was transfected into HEK293T cells, which are highly amenable to transient transfection by PEI (Aydin *et al.*, 2012). Using fluorescence microscopy, eGFP expression was observed in the cells 48 hours post transfection (figure 70). Cells transfected with the plasmid exhibited positive whole cell eGFP fluorescence, indicating functional transgene and downstream protein expression. No background eGFP expression was observed in untransfected control cells.

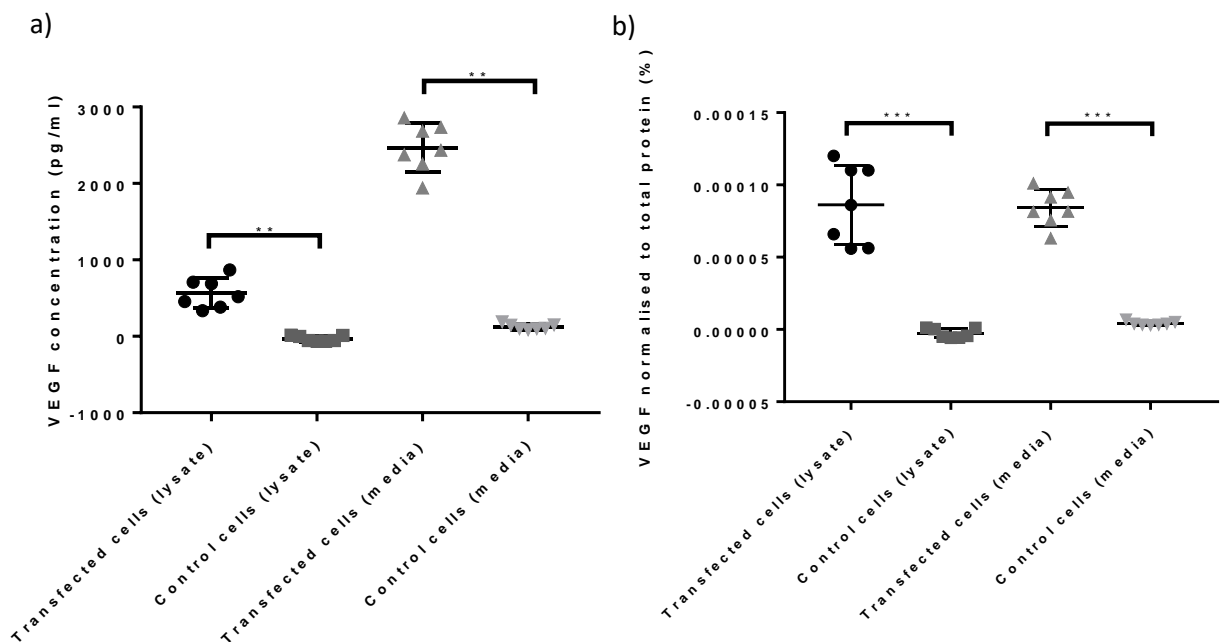
Figure 70. eGFP expression in HEK293T cells following transfection with the pSFFV.VEGF.IRES.eGFP transfer plasmid. Representative fluorescence micrographs of control mock transfected HEK293T cells (left) and cells transfected with the pSFFV.VEGF.IRES.eGFP plasmid (right) resulting in eGFP expression 48 hours after transfection (n = 3 per group). Scale bar: 400 μ m.



After establishing that delivery of the plasmid resulted in eGFP expression, it was decided to transfect SCL4.1/F7 cells and quantify the VEGF-A₁₆₅ produced using a commercially available ELISA kit. A significant fraction of VEGF-A₁₆₅ produced by cells remains bound to the cell surface and the ECM, however, some is also secreted. (Ferrara *et al.*, 1997). In fact, cells transfected with cDNA encoding VEGF-A₁₆₅ secrete bioactive VEGF-A₁₆₅ into the medium (Park *et al.*, 1993). It was therefore decided to measure the VEGF-A₁₆₅ concentration in both the cell lysate and the cell media (figure 70).

The VEGF-A₁₆₅ concentration was over 500 fold higher in the transfected cell lysate than in the control cell lysate. The VEGF-A₁₆₅ concentration was almost 20 fold higher in the transfected cell media compared to the control cell media (figure 71). The VEGF-A₁₆₅ concentration was normalised to total protein concentration, determined by a BCA assay (figure 71). A higher percentage of VEGF-A₁₆₅ protein was found in the transfected cell lysate compared to the control cell lysate and transfected cell media compared to the control cell media.

Figure 71. Quantifying the amount of VEGF-A₁₆₅ produced by transfected HEK293T cells. a) The VEGF-A₁₆₅ concentration in the lysate and media of control and transfected cells as determined by ELISA. A statistical significance was found between the transfected and control cell lysate (Kruskal-Wallis test, Dunn's multiple comparisons test, p value = 0.0087) as well as the transfected and control cell media (p value = 0.0087). b) VEGF-A₁₆₅ concentration normalised to total protein concentration. A statistical significant was found between the transfected and control cell lysate (Kruskal-Wallis test, Dunn's multiple comparisons test, p value = 0.0003) as well as the transfected and control cell media (p value = 0.0005). Each data point represents the mean of duplicate wells evaluated for VEGF-A₁₆₅ concentration and VEGF-A₁₆₅: total protein concentration (n = 7 per group). *p < 0.05, **p < 0.01, ***p < 0.001 and ****p < 0.0001.



6.4 The lentiviral vector delivering the VEGF-A₁₆₅ gene

As a result of *in vitro* confirmation of the pSFFV.VEGF.IRES.eGFP transgene expression capability, the plasmid was used to produce a bicistronic second generation lentiviral vector for subsequent testing. The lentiviral vector contained an expression cassette consisting of the SFFV promoter driving the expression of the VEGF-A₁₆₅ gene and the

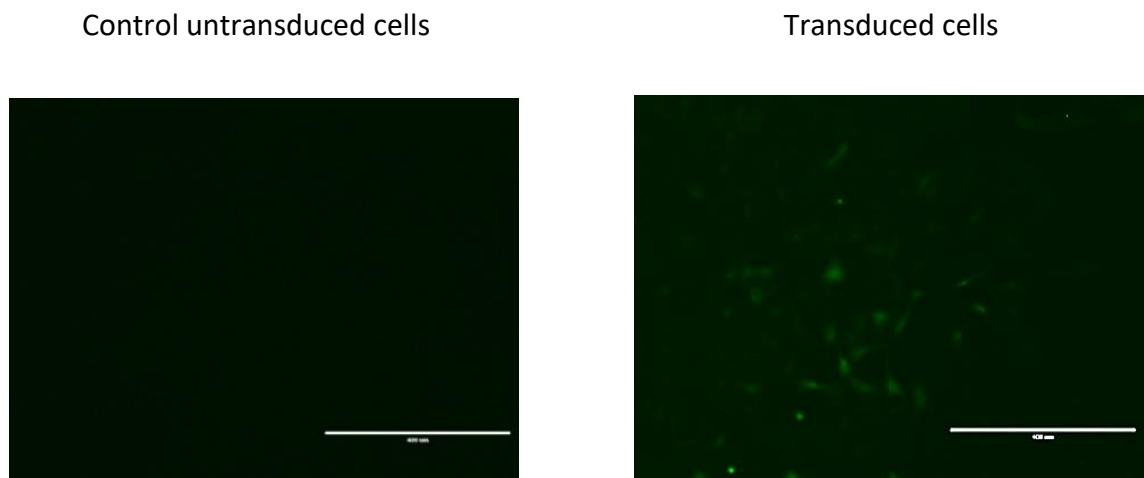
downstream eGFP gene (figure 72). Similar to the lentiviral vector described in chapter 4, this vector also had a WPRE present after the genes to enhance gene expression (Zufferey *et al.*, 1999). The bicistronic expression of two genes from the same promoter was provided by inclusion of an internal ribosomal entry site (IRES) element between the two genes. The IRES sequence mediates protein synthesis of the second gene product from an internal translational starting site within a single mRNA transgene (Yu *et al.*, 2003). The lentiviral vector was found to have a high titre of 1.9×10^9 vp/ml using a P24 ELISA.

Figure 72. Schematic of the lentiviral vector delivering the VEGF-A₁₆₅ gene. LTR – long terminal repeats; RRE – Rev response element; SFFV - spleen focus forming virus; Luc – luciferase; 2A – self cleaving element; eGFP enhanced green fluorescent protein; WPRE - woodchuck hepatitis virus post-transcriptional regulatory element.



To confirm the production of a functional lentiviral vector, SCL4.1/F7 cells were transduced at a MOI of 100. Using fluorescence microscopy, eGFP expression was observed in the transduced cells 48-post transduction and the percentage of eGFP positive cells continued to increase over the next 24 hours. No eGFP expression was seen in the control untransduced cells (figure 73). While an IRES sequence has the capacity to specify translation of the second gene from a bicistronic transcript, Sugimoto *et al.* (1995) reported that in several cases, only the gene transcribed upstream of the IRES element is expressed strongly. This was not observed in the current study, as whole cell eGFP fluorescence was observed following both plasmid transfection and lentiviral transduction.

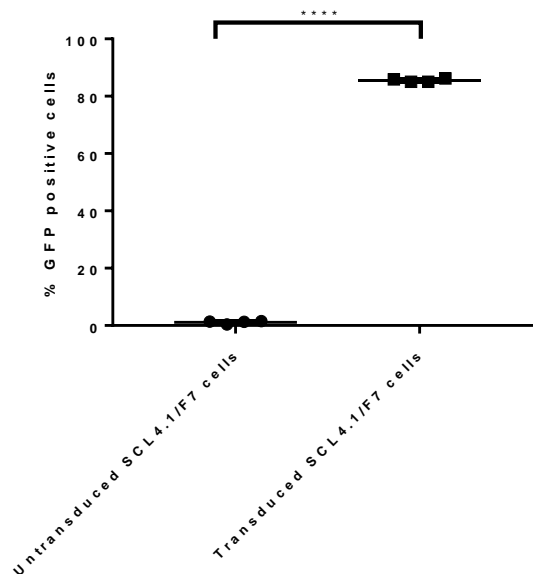
Figure 73. eGFP expression following lentiviral transduction. Representative fluorescence micrographs of control untransduced SCL4.1/F7 cells (left) and cells transduced with the lentiviral vector delivering VEGF-A₁₆₅ and eGFP (right) resulting in eGFP expression 72 hours after transduction (n = 3 per group). Scale bar: 400 μ m.



6.4.1 Transduction efficiency

After establishing that the SCL4.1/F7 cells were transduced using fluorescence microscopy, flow cytometry was used to determine the transduction efficiency as described in section 3.6.1. This showed that over 80% of the transduced cells were eGFP positive. An insignificant number of eGFP positive cells was observed in the control samples (figure 74).

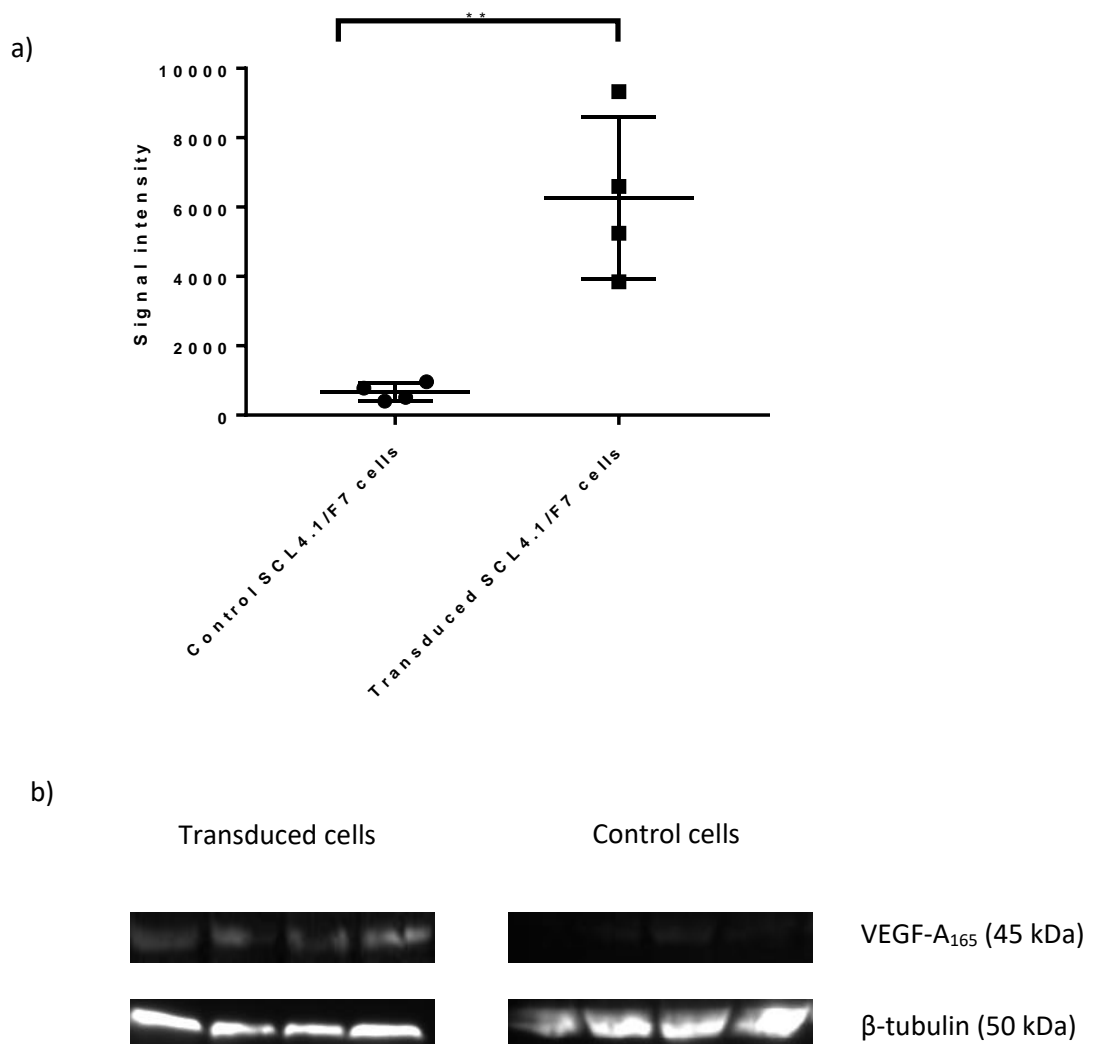
Figure 74. Efficiency of lentiviral-mediated gene transfer to SCL4.1/F7 cells. There was a significantly higher percentage of eGFP positive cells in the transduced cell population than in the control cells (two-tailed unpaired T test, 95 % confidence interval, p value = <0.0001). Each data point represents an individual flow cytometry run with 750 000 cells per sample (n = 4 for each group). * $p < 0.05$, ** $p < 0.01$, *** $p < 0.001$ and **** $p < 0.0001$.



6.4.2 VEGF-A₁₆₅ overexpression following transduction

The protein expression of VEGF-A₁₆₅ following lentiviral transduction was examined by Western blot analysis (figure 75). Densitometry analysis using ImageJ software was used to quantify the size of the bands. A very low constitutive production of VEGF-A₁₆₅ was observed in the control untransduced cells. This was expected as VEGF-A₁₆₅ is expressed and secreted at low physiological levels by most normal cells (Shellman *et al.*, 2003). The expression of VEGF-A₁₆₅ was increased over 9 fold in the transduced cells compared to the control cells (figure 75).

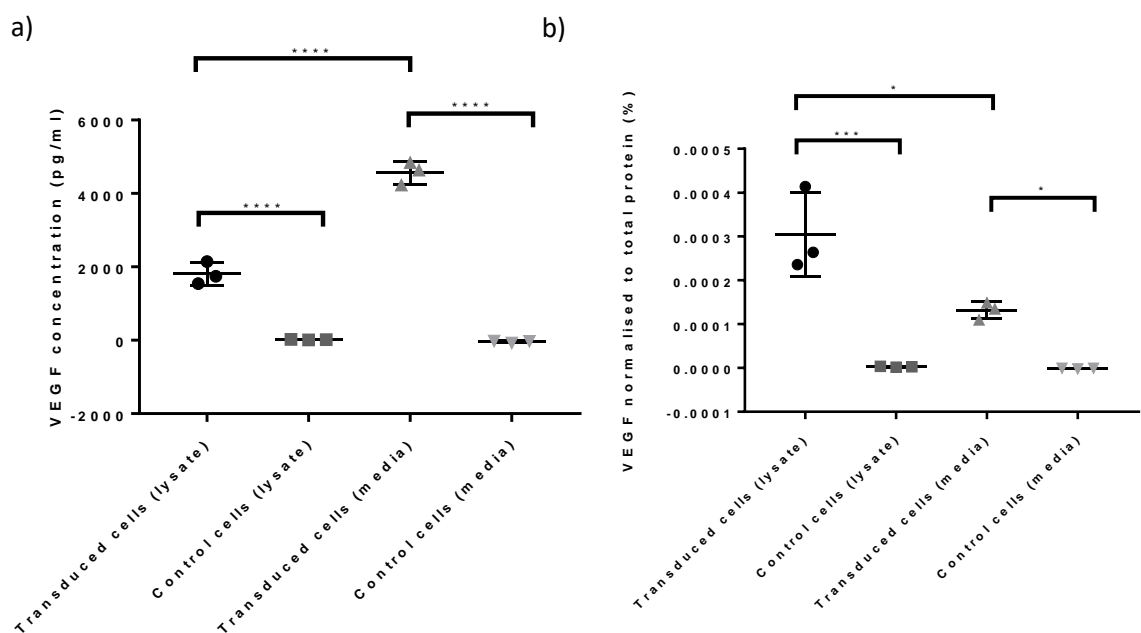
Figure 75. Western blot analysis of VEGF-A₁₆₅ levels in SCL4.1/F7 cells following transduction compared to endogenous VEGF-A₁₆₅ in untransduced cells. a) Densitometric quantification of VEGF-A₁₆₅ bands normalised against the β -tubulin loading control and expressed as signal intensity. A significantly higher signal intensity was detected in the transduced cells compared to the control cells (two-tailed unpaired T test, 95 % confidence interval, p value = <0.0031). b) The 45 kDa band represents VEGF-A₁₆₅ protein and the 50 kDa band represents the β -tubulin loading control (n = 1 blot with 4 samples per group). **p* < 0.05, ***p* < 0.01, ****p* < 0.001 and *****p* < 0.0001.



After establishing that VEGF-A₁₆₅ was overexpressed in transduced cells, the concentration of the protein was measured using an ELISA kit. The VEGF-A₁₆₅ concentration was over 100 fold higher in the transduced cell lysate than in the control cell lysate. The VEGF-A₁₆₅ concentration was over 4000 fold higher in the transduced cell media compared to the control cell media. Furthermore, it was noted that the VEGF-A₁₆₅ concentration in the transduced cell media was 2.5 fold higher than in the transduced cell lysate (figure 76). The VEGF-A₁₆₅ concentration was normalised to total

protein concentration, determined by a BCA assay (figure 76). A higher percentage of VEGF-A₁₆₅ protein was found in the transduced cell lysate of compared to the control cell lysate and transduced cell media compared to the control cell media.

Figure 76. Quantifying the amount of VEGF-A₁₆₅ produced by SCL4.1/F7 cells transduced by the lentiviral vector delivering VEGF-A₁₆₅. a) The VEGF-A₁₆₅ concentration in the lysate and media of control and transduced cells as determined by ELISA. A statistical significance was found between the transduced and control cell lysate as well as the transduced and control cell media (one-way ANOVA, Tukey's multiple comparisons test, 95 % confidence interval, p value = <0.0001). The amount of VEGF-A₁₆₅ in the transduced cell media was significantly higher than that in the transduced cell lysate (p value = <0.0001). b) VEGF-A₁₆₅ concentration normalised to total protein concentration. A statistical significance was found between the transduced and control cell lysate (one-way ANOVA, Tukey's multiple comparisons test, 95 % confidence interval, p value = 0.0420) as well as the transduced and control cell media (p value = <0.0002). Each data point represents the mean of duplicate wells evaluated for VEGF-A₁₆₅ concentration and VEGF-A₁₆₅: total protein concentration (n = 3 for each group). *p < 0.05, **p < 0.01, ***p < 0.001 and ****p < 0.0001.



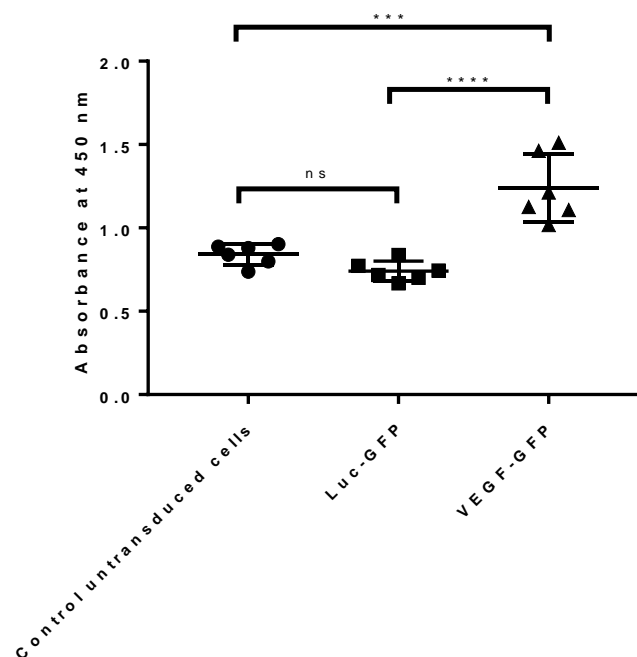
6.4.3 Effect of transduction on proliferation and morphology

After establishing high-level gene expression in transduced SCL4.1/F7 cells, it was important to test whether the overexpression of VEGF-A₁₆₅ resulted in cytotoxic effects. Previous experiments in section 4.2.6 showed that transduction with the lentiviral vector delivering luciferase and eGFP did not have any adverse effects on the cells and therefore cells transduced by this lentiviral vector were used as a control.

Proliferation

A BrdU ELISA kit was used to assess whether lentiviral mediated VEGF-A₁₆₅ delivery to SCL4.1/F7 cells had an effect on their proliferation. BrdU is a pyrimidine analog which is incorporated into the newly synthesized DNA of proliferating cells in place of thymidine. The incorporated BrdU can be detected by anti-BrdU antibody. A horseradish peroxidase-conjugated secondary antibody is then used to detect the anti-BrdU antibody bound to BrdU, followed by the addition of a horseradish peroxidase substrate. The extent of colour development is proportional to the quantity of BrdU incorporated into the cells and can be used directly as an indicator of cell proliferation (Vega-Avila and Pugsley, 2011). SCL4.1/F7 cells overexpressing VEGF-A₁₆₅ proliferated 1.5 fold more than untransduced cells and cells expressing luciferase and eGFP (figure 77). This suggested that the increase in proliferation was not due to the transduction process, but rather due to the effect of VEGF-A₁₆₅ overexpression.

Figure 77. VEGF-A₁₆₅ overexpression resulted in a significant increase in SCL4.1/F7 cell proliferation. Cell proliferation in untransduced cells and cells transduced by a lentiviral vector delivering VEGF-A₁₆₅ was measured using a BrdU ELISA. Cells transduced by a lentiviral vector delivering luciferase and eGFP were used as a control to ensure that the increased cell proliferation was not due to the transduction process. A significant difference in proliferation rate was observed between the cells overexpressing VEGF-A₁₆₅ and the untransduced cells (one-way ANOVA, Tukey's multiple comparison test, 95 % confidence interval, P value = 0.0002) as well as between the cells overexpressing VEGF-A₁₆₅ and cells expressing luciferase and eGFP (p value = <0.0001). No significant difference was observed between the untransduced cells and the cells expressing luciferase and eGFP (P value = 0.3770). Each data point represents the mean of duplicate wells evaluated for absorbance at 450 nm (n = 6 for each group). **p* < 0.05, ***p* < 0.01, ****p* < 0.001 and *****p* < 0.0001.



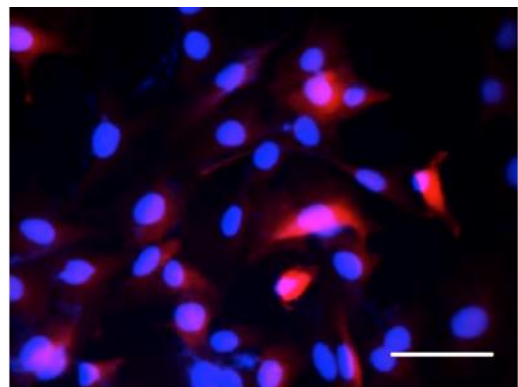
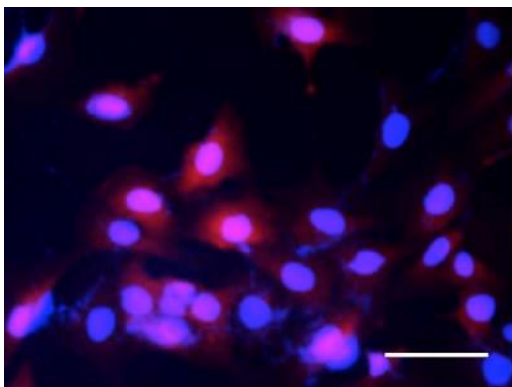
Morphology

Morphology was observed using fluorescence microscopy and cell shape was analysed by measuring circularity with ImageJ (figure 78). Control untransduced SCL4.1/F7 cells and SCL4.1/F7 cells overexpressing VEGF-A₁₆₅ were immunolabelled with S100 antibodies to delineate the cell shape. Circularity was defined as $4\pi \times (\text{area}/\text{perimeter}^2)$. Transduction with a lentiviral vector delivering luciferase and eGFP did not have an effect on cell morphology (chapter 4) and so any differences in cell morphology could be attributed to VEGF-A₁₆₅ overexpression. While the transduced SCL4.1/F7 cells appeared to be less rounded than the control cells, statistical analysis revealed that overexpression of VEGF-A₁₆₅ did not influence the morphology of SCL4.1/F7 cells.

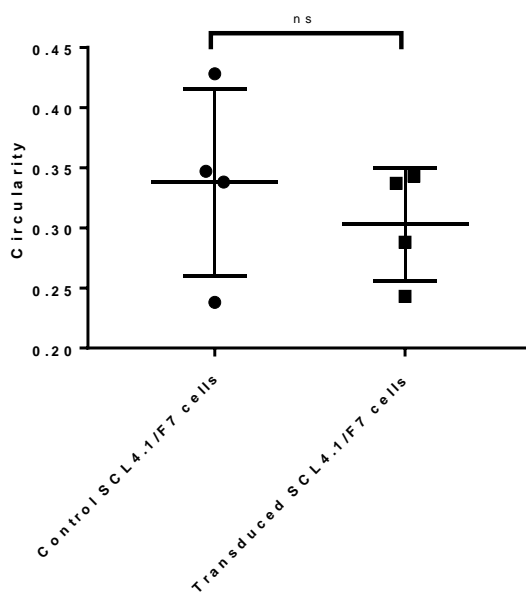
Figure 78. Effect of VEGF-A₁₆₅ overexpression on SCL4.1/F7 morphology. Immunofluorescence staining revealed that the majority of the cells were S100-positive. However, a percentage of the cells did not express the protein, suggesting the presence of a potentially mixed population of cells. a) Control untransduced cells and cells overexpressing VEGF-A₁₆₅ were immunostained to detect S100 (red) to allow visualisation of the cells. Cells were also counterstained with DAPI (blue). No gross changes in morphology were observed. Scale bar = 50 μ m. b) The circularity factor was used to analyse morphology. No significant difference between the two groups was observed (two-tailed unpaired T test, 95 % confidence interval, p value = 0.4702). Each data point represents the mean circularity factor of 10 cells from one image (n = 10 cells from 4 independent images for each group).

a) Control SCL4.1/F7 cells

SCL4.1/F7 cells overexpressing VEGF-A₁₆₅



b)



6.5 Testing the functionality of the lentiviral expressed VEGF-A₁₆₅ protein

6.5.1 Angiogenesis assays

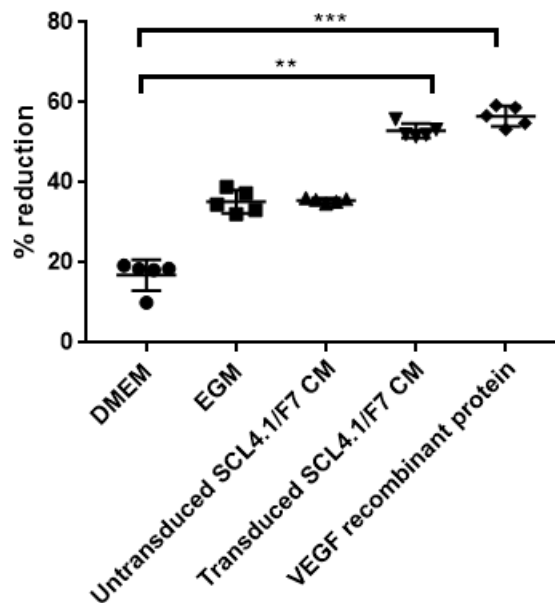
Angiogenesis is the process by which new vessels are made from existing vessels. During angiogenesis, endothelial cells begin to proliferate, migrate and undergo tubulogenesis to form functional vessels. Numerous *in vitro* assays have been developed to help understand the individual steps in this complex process. Despite significant progress in the field, none of the assays successfully recapitulates the complexity of angiogenesis and researchers must rely on the selection of multiple assays (Irvin *et al.*, 2014). Therefore, in order to investigate the angiogenic behaviour of the VEGF-A₁₆₅ produced in this study, a number of assays which mimic different steps in angiogenesis were chosen and will be discussed in this section.

6.5.1.1 Endothelial cell viability assay

In adults, endothelial cells in blood vessels tend to exist in a quiescent state. However, they are able to respond to pro-angiogenic cues and begin to proliferate and migrate. This angiogenic switch is accompanied by an increased metabolic state (Zecchin *et al.*, 2017). In order to establish whether the VEGF-A₁₆₅ produced had an effect on endothelial cell viability, alamarBlue® was used to detect changes in the metabolic activity of HUVECs following a 72 hour incubation period with the test media described in section 3.11.

While a 1.4 fold increase in cell viability was observed in cells incubated with diluted conditioned media from transduced SCL4.1/F7 cells compared to diluted conditioned media from untransduced SCL4.1/F7 cells, this difference did not prove to be significant (figure 79). No difference in cell viability was observed between diluted conditioned media from transduced SCL4.1/F7 cells compared to media containing recombinant VEGF-A₁₆₅ protein or EGM used as positive controls.

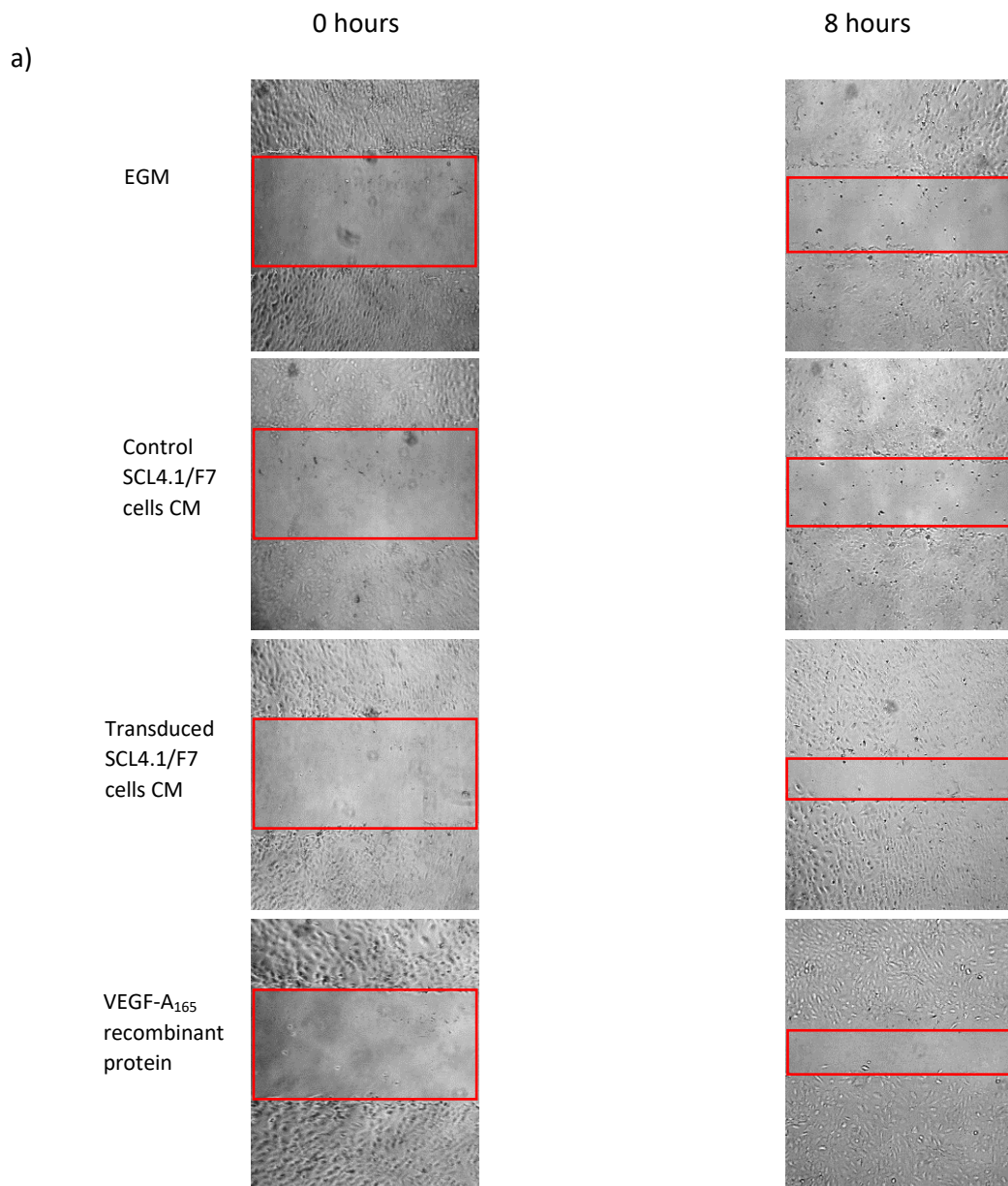
Figure 79. Effect of VEGF-A₁₆₅ on endothelial cell viability. No significant increase in alamarBlue® reduction was observed between HUVECs incubated with diluted conditioned media from transduced SCL4.1/F7 cells and those incubated with conditioned media from untransduced SCL4.1/F7 cells (Kruskal-Wallis test, Dunn's multiple comparisons test, p value = >0.9999). No difference in cell viability was observed between diluted conditioned media from transduced SCL4.1/F7 cells compared to media containing recombinant VEGF-A₁₆₅ protein or EGM (p value = >0.7114). The only statistical difference observed was between the DMEM negative control and the diluted conditioned media from transduced SCL4.1/F7 cells and media containing recombinant VEGF-A₁₆₅ protein (p value = <0.0094). Each data point represents the percentage reduction by HUVECs in wells (n = 5 wells for each group). * p < 0.05, ** p < 0.01, *** p < 0.001 and **** p < 0.0001.



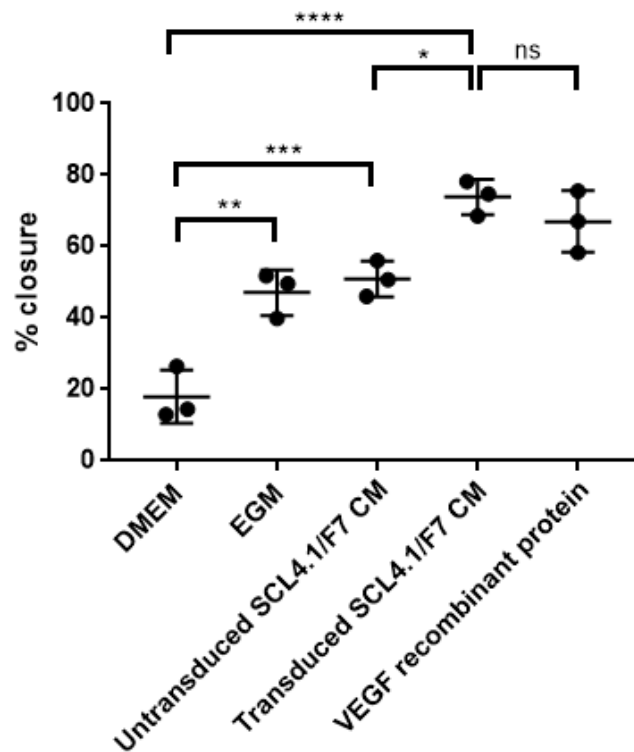
6.5.1.2 Scratch wound assay

Since cell migration is one of the major processes underlying angiogenesis, it was decided to assess the effect of the VEGF-A₁₆₅ produced on the migration of HUVECs, as measured by the scratch wound assay. HUVECs were grown to confluence and a scratch was introduced using a pipet tip followed by incubation with the test media described in section 3.11. Cell filling of the cleared space initially occurs by migration, although the cells will eventually start to proliferate. In order to minimise cell proliferation, HUVECs were serum starved overnight and the assay was carried out over a period of 8 hours. The diluted conditioned media from untransduced SCL4.1/F7 cells resulted in around 50% wound closure while the diluted conditioned media from SCL4.1/F7 cells overexpressing VEGF-A₁₆₅ protein and media containing the recombinant VEGF-A₁₆₅ protein resulted in around 70% wound closure, a roughly 1.4 fold increase (figure 80).

Figure 80. Effect of VEGF-A₁₆₅ on endothelial cell migration. a) Representative images of a scratch assay performed using HUVECs incubated with the test media. The red box represents the scratch area immediately after scratching and after 8 hours. b) % closure was calculated using the area of the scratch at time 0 hours and at 8 hours. A significant difference in wound closure was observed compared with the diluted conditioned media from untransduced SCL4.1/F7 cells (one-way ANOVA, Tukey's multiple comparison test, 95 % confidence interval, p value = 0.0116). No difference in wound closure was observed between diluted conditioned media from transduced SCL4.1/F7 cells compared to media containing recombinant VEGF-A₁₆₅ protein (p value = 0.7145). Each data point represents the percentage closure in one well, n = 3 per group. **p* < 0.05, ***p* < 0.01, ****p* < 0.001 and *****p* < 0.0001.



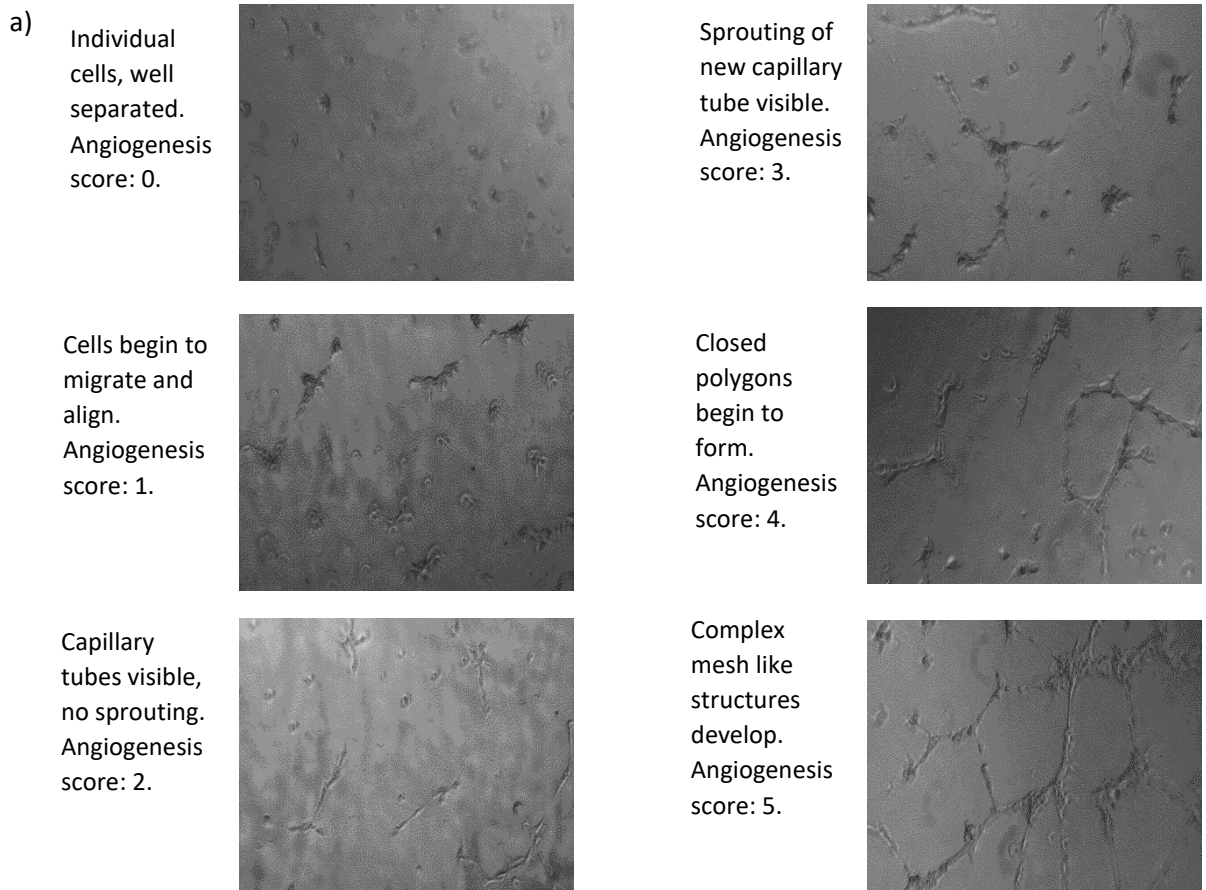
b)



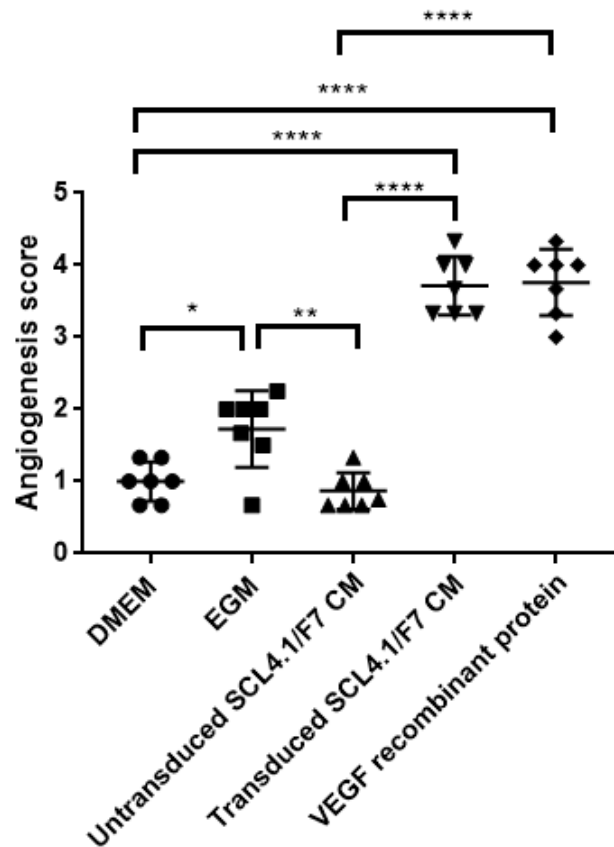
6.5.1.3 Tube formation assay

Having established that the lentiviral-mediated VEGF-A₁₆₅ produced had positive effects on both HUVEC viability and migration, it was decided to carry out a tube formation assay, as endothelial cells form capillary like structures in response to angiogenic signals. Tube formation involves several steps, including cell adhesion, migration, differentiation and growth. HUVECs were plated on a basement membrane matrix and incubated with the test media described in section 3.11 for 8 hours. HUVECs began to align themselves within 1 hour and tubules appeared after 2 hours. HUVECs incubated with diluted conditioned media from transduced SCL4.1/F7 cells formed several capillary-like tubes which were indistinguishable from the HUVECs incubated with positive control VEGF-A₁₆₅ recombinant protein (figure 81). HUVECs incubated with diluted media from untransduced SCL4.1/F7 cells formed significantly fewer tube-like structures.

Figure 81. Effect of VEGF-A₁₆₅ on endothelial tube formation. a) Representative images of HUVECs showing the degree of angiogenesis progression together with the associated angiogenesis score. b) Quantification of tube formation assay. HUVECs incubated with diluted conditioned media from transduced SCL4.1/F7 cells formed several capillary-like tubes which were indistinguishable from the HUVECs incubated with positive control VEGF-A₁₆₅ recombinant protein (one-way ANOVA, Tukey's multiple comparison test, 95 % confidence interval, p value = 0.9994). HUVECs incubated with diluted media from untransduced SCL4.1/F7 cells formed significantly fewer tube-like structures p value = <0.0001). Each point represents the tube formation score in one well, n = 7 wells for each group. **p* < 0.05, ***p* < 0.01, ****p* < 0.001 and *****p* < 0.0001.



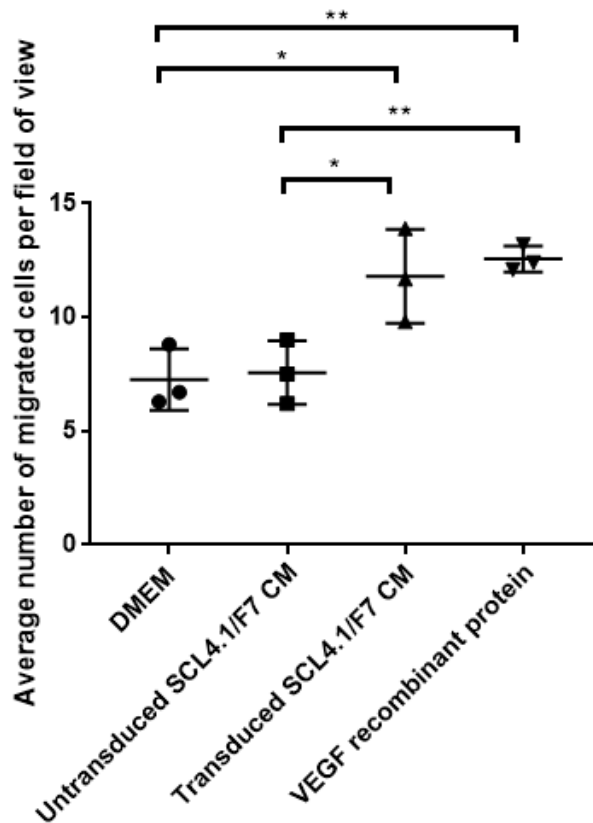
b)



6.5.2 Effect of VEGF-A₁₆₅ on Schwann cell migration

Following peripheral nerve injury, Schwann cells migrate to the site of injury to provide a supportive environment for axonal regeneration (Han *et al.*, 2007). To determine whether the VEGF-A₁₆₅ produced from lentiviral transduction increased migration of Schwann cells, a transwell assay was performed. Untransduced SCL4.1/F7 cells were pipetted into the upper compartment of a transwell insert. The contents of the lower compartments were varied across different experimental conditions. After 12 hours of incubation, SCL4.1/F7 cells incubated with conditioned media from transduced SCL4.1/F7 cells overexpressing VEGF-A₁₆₅ showed a migration rate 1.6 fold higher compared to SCL4.1/F7 cells incubated with conditioned media from untransduced SCL4.1/F7 cells (figure 82). Similar migration rates (around 12 migrated cells per field of view) were observed with SCL4.1/F7 cells incubated with positive control recombinant VEGF-A₁₆₅ protein.

Figure 82. Analysis of the effect of VEGF-A₁₆₅ on the migration of SCL4.1/F7 cells. A transwell assay with SCL4.1/F7 cells seeded in the upper chamber and different media in the lower chamber. After 12 hours, SCL4.1/F7 cells incubated with conditioned media from transduced SCL4.1/F7 cells overexpressing VEGF-A₁₆₅ showed a significantly higher migration rate compared to SCL4.1/F7 cells incubated with conditioned media from untransduced SCL4.1/F7 cells (one-way ANOVA, Tukey's multiple comparison test, 95 % confidence interval, p value = 0.0287). Similar migration rates were observed with SCL4.1/F7 cells incubated with positive control recombinant VEGF-A₁₆₅ protein (p value = 0.9120). Each point represents the mean of 10 predetermined fields of view per transwell, n = 3 for each group. *p < 0.05, **p < 0.01, ***p < 0.001 and ****p < 0.0001.

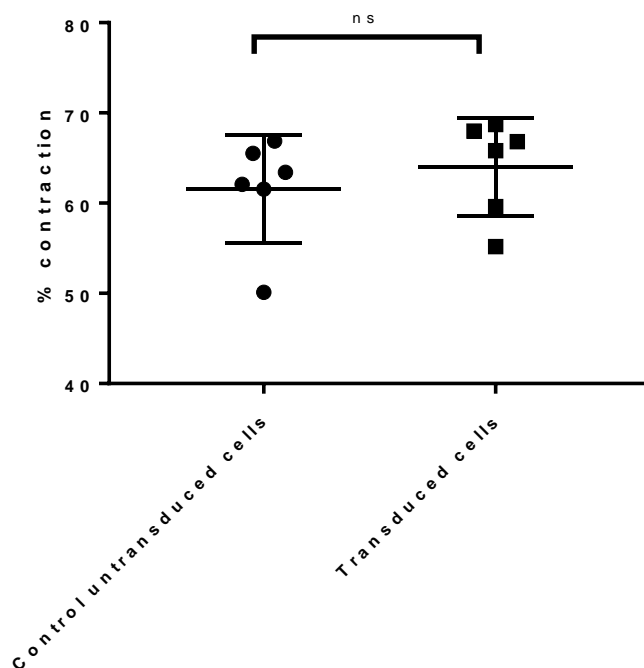


6.6 Constructing EngNT from SCL4.1/F7 cells overexpressing VEGF-A₁₆₅

Having established that VEGF-A₁₆₅ produced by the transduced SCL4.1/F7 cells had angiogenic effects and increased Schwann cell migration and proliferation (sections 6.5 and 6.4.3) *in vitro*, it was decided to construct EngNT using the SCL4.1/F7 cells overexpressing VEGF-A₁₆₅ for subsequent *in vivo* use. Prior to constructing the EngNT, it was important to ensure that the overexpression of VEGF-A₁₆₅ did not influence the contraction profile of the cellular collagen gel. Cellular self-alignment in the EngNT involves cells exerting forces that contract and deform the surrounding matrix and

different cell types vary in their ability to contract collagen gels (Bellows *et al.*, 1981). O'Rourke *et al.* (2015) developed an assay based on contraction of free-floating cellular gels in 96-well plates to investigate cell–matrix interactions. This assay was used to quantify contraction in the current study. As can be seen in figure 83, over 60% contraction was obtained for both control untransduced and transduced SCL4.1/F7 cells. O'Rourke *et al.* (2015) found that 60–80% contraction in the 96-well plate assay corresponded to alignment throughout tethered gels made using the same parameters. Gels made from control SCL4.1/F7 cells and SCL4.1/F7 cells overexpressing VEGF-A₁₆₅ had a mean percentage contraction of 62 and 64% respectively.

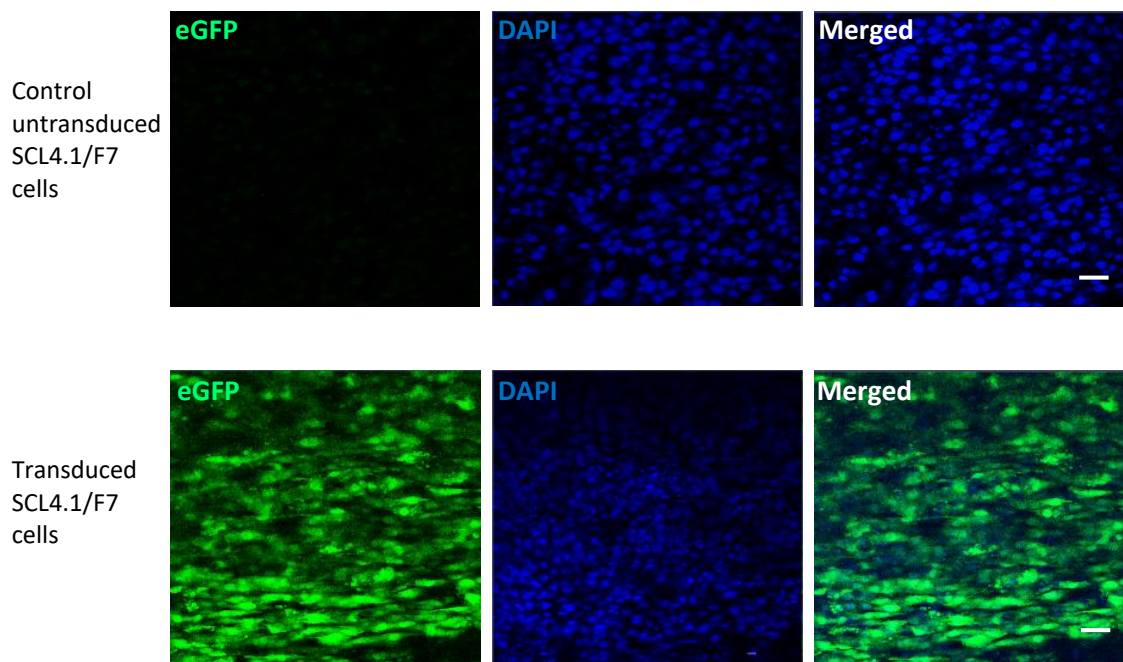
Figure 83. Contraction assay for control SCL4.1/F7 cells and SCL4.1/F7 cells overexpressing VEGF-A₁₆₅. The percentage contraction of free-floating gels was calculated. No significant difference in contraction was observed between the control and transduced cells (two-tailed unpaired T test, 95 % confidence interval, p value = 0.4784). Each point represents the percentage contraction of one individual free-floating gel, n = 6 for each group.



Transduced SCL4.1/F7 cells were then used to construct EngNT. Scanning confocal microscopy was used to observe the cellular architecture in the EngNT. eGFP expressing SCL4.1/F7 cells in the EngNT were counterstained with DAPI and images were taken from a single plane through the constructs (figure 84). No eGFP signal was detected in the constructs containing control untransduced SCL4.1/F7 cells. This ensured that any eGFP signal that was detected in the transduced cells was not autofluorescence or

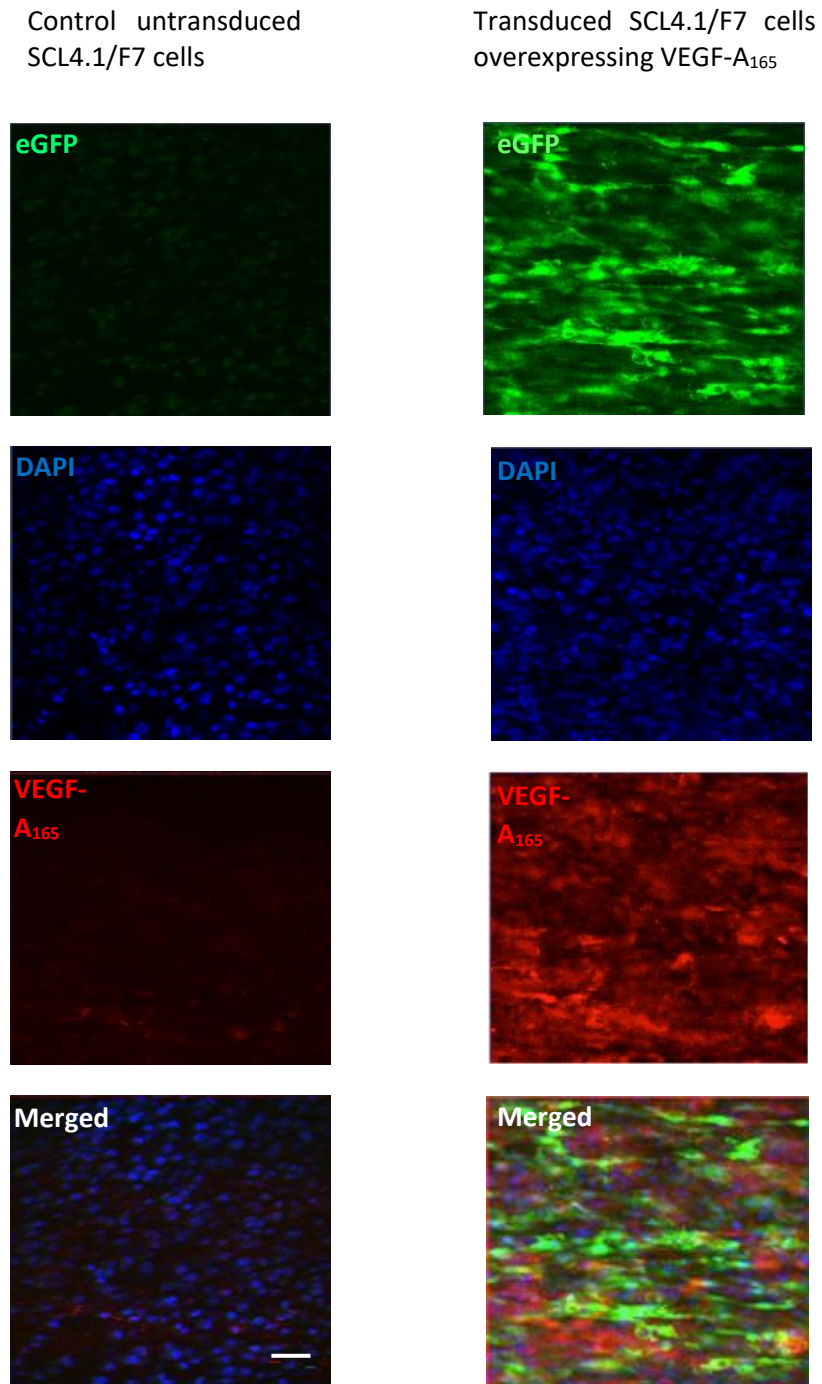
background signal. Colocalisation of blue channel (DAPI) and green channel (eGFP) in the nucleus of many eGFP expressing SCL4.1/F7 cells was observed. This indicated the presence of nuclear eGFP in addition to cytoplasmic eGFP.

Figure 84. Laser scanning confocal microscopy for imaging of lentiviral mediated gene expression in SCL4.1/F7 cell constructs. Representative images of the nuclear stain DAPI (blue channel) and eGFP (green channel) were taken from stabilised constructs and from control constructs containing untransduced SCL4.1/F7 cells. eGFP is shown in green and DAPI in blue. N = 3 individual EngNT for each group. Scale bar = 100 μ m. Z-distance = 20 μ m, step size = 1 μ m.



Additionally, VEGF-A₁₆₅ distribution in the EngNT was visualised by immunofluorescence staining using a monoclonal anti-VEGF-A antibody. Diffuse VEGF staining was observed in and around the cells in the EngNT (figure 85).

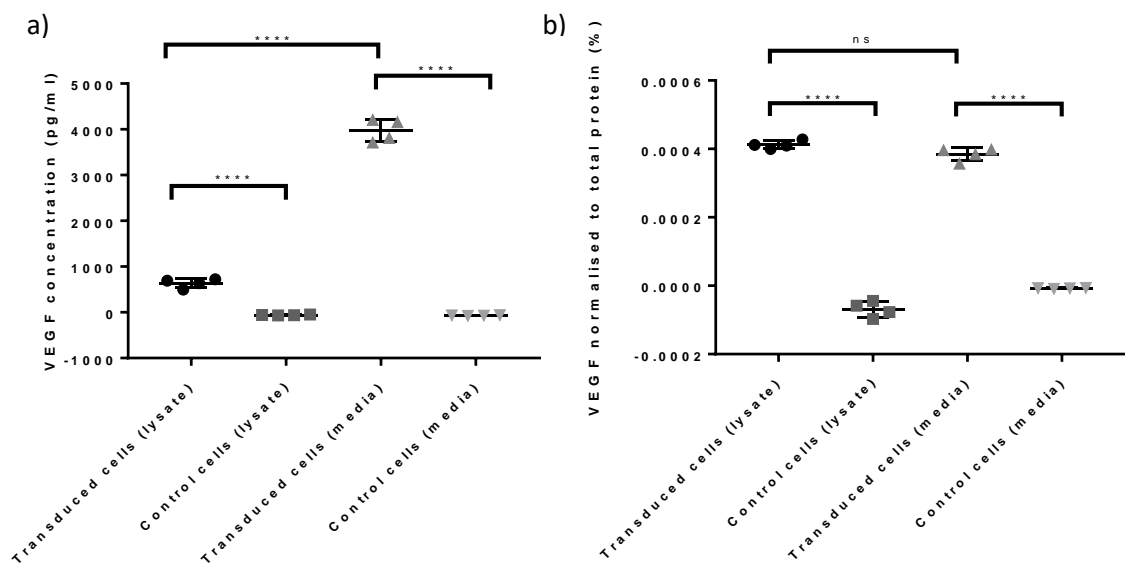
Figure 85. Laser scanning confocal microscopy for imaging of lentiviral mediated VEGF-A₁₆₅ expression in SCL4.1/F7 cell constructs. Representative images of the nuclear stain DAPI and eGFP were taken from stabilised constructs and from control constructs containing untransduced SCL4.1/F7 cells. eGFP is shown in green, DAPI in blue and VEGF-A₁₆₅ in red. N = 3 individual EngNT for each group. Magnification, x20. Z-distance = 20 μ m, step size = 1 μ m.



6.6.1 VEGF-A₁₆₅ production by transduced cells in EngNT

Immunofluorescence staining in the previous section revealed the presence of VEGF-A₁₆₅ throughout the EngNT constructed from transduced SCL4.1/F7 cells. The next step was to quantify the amount of the protein produced by the cells in the EngNT using an ELISA kit. Similar to cells in monolayer, the VEGF-A₁₆₅ concentration in both the EngNT cell lysate and media was measured. The concentration of VEGF-A₁₆₅ in the transduced cell lysate was around 700 fold higher than in the control cell lysate while the concentration in the transduced cell media was around 4000 fold higher than in the control cell media (figure 86). It was also noted that the VEGF-A₁₆₅ concentration in the transduced cell media was 5.5 fold higher than the in the transduced cell lysate. The VEGF-A₁₆₅ concentration was normalised to total protein concentration, determined by a BCA assay. As expected, the percentage of VEGF-A₁₆₅ to total protein in transduced cell lysate and media was higher compared to a negligible amount in the control cell lysate and media (figure 86).

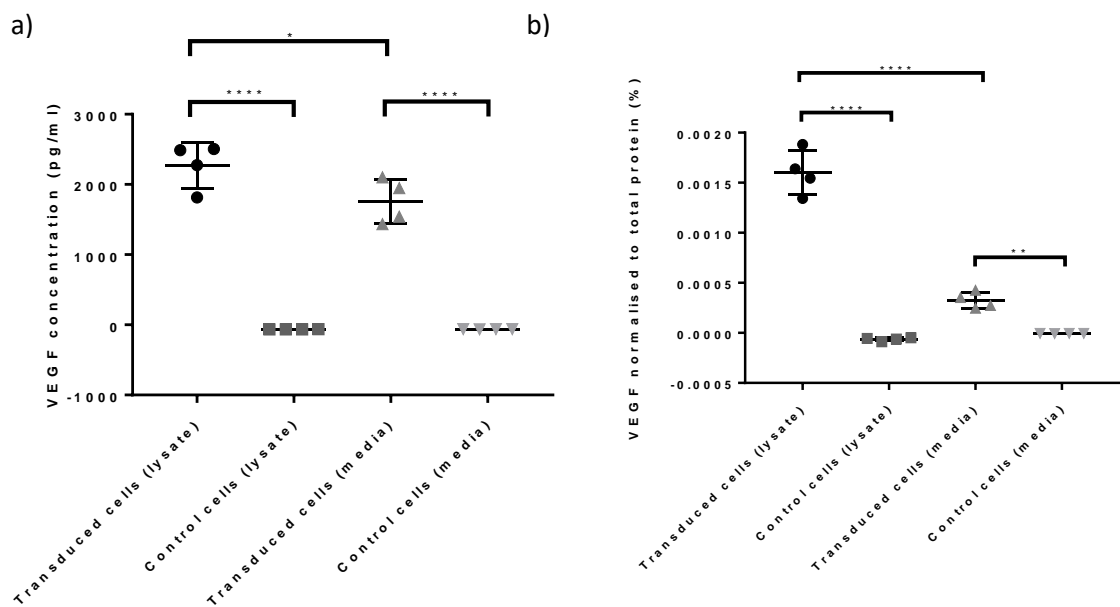
Figure 86. Quantifying the amount of VEGF-A₁₆₅ produced by SCL4.1/F7 cells incorporated into EngNT. a) The VEGF-A₁₆₅ concentration in the lysate and media of control and transduced cells as determined by ELISA. A statistical significance was found between the transduced and control cell lysate as well as the transduced and control cell media (one-way ANOVA, Tukey's multiple comparisons test, 95 % confidence interval, p value = <0.0001). The amount of VEGF-A₁₆₅ in the transduced cell media was significantly higher than that in the transduced cell lysate (p value = <0.0001). Each data point represents the mean of duplicate wells evaluated for VEGF-A₁₆₅ concentration (n = 4 individual EngNT per group). b) VEGF concentration normalised to total protein concentration. A statistical significant was found between the transduced and control cell lysate (one-way ANOVA, Tukey's multiple comparisons test, 95 % confidence interval, p value = <0.0001) as well as the transduced and control cell media (p value = <0.0001). No statistical difference was found between the transduced cell media and transduced cell lysate (p value = 0.1108). Each data point represents the mean of duplicate wells evaluated for VEGF-A₁₆₅ concentration and VEGF-A₁₆₅: total protein concentration (n = 4 individual EngNT for each group). *p < 0.05, **p < 0.01, ***p < 0.001 and ****p < 0.0001.



As the implantable device consisted of EngNT in a silicone tube, it was decided to also measure the VEGF-A₁₆₅ concentration in such a device (figure 86). The concentration of VEGF-A₁₆₅ in the transduced cell lysate was around 2200 fold higher than in the control cell lysate while the concentration in the transduced cell media was around 1700 fold higher than in the control cell media (figure 87). It was also noted that unlike the EngNT without the silicone tube, the VEGF-A₁₆₅ concentration in the transduced cell lysate was 1.3 fold higher than in the transduced cell media. Once again, the VEGF-A₁₆₅ concentration was normalised to total protein concentration, determined by a BCA assay. The percentage of VEGF-A₁₆₅ to total protein in transduced cell lysate and media was around 0.0016 and 0.0003% respectively and compared to a negligible amount in the control cell lysate and media (figure 87). The percentage of VEGF-A₁₆₅ to total

protein in the transduced cell lysate was around 4.9 fold higher than in the transduced cell media.

Figure 87. Quantifying the amount of VEGF-A₁₆₅ produced by transduced SCL4.1/F7 cells in EngNT in a silicone tube. a) The VEGF-A₁₆₅ concentration in the lysate and media of control and transduced cells as determined by ELISA. A statistical significance was found between the transduced and control cell lysate as well as the transduced and control cell media (one-way ANOVA, Tukey's multiple comparisons test, 95 % confidence interval, p value = <0.0001). The amount of VEGF-A₁₆₅ in the transduced cell lysate was significantly higher than that in the transduced cell media (p value = <0.0332). Each data point represents the mean of duplicate wells evaluated for VEGF-A₁₆₅ concentration (n = 4 individual EngNT for each group). b) VEGF concentration normalised to total protein concentration. A statistical significance was found between the transduced and control cell lysate (one-way ANOVA, Tukey's multiple comparisons test, 95 % confidence interval, p value = <0.0001) as well as the transduced and control cell media (p value = 0.0096). A statistical difference was found between the transduced cell media and transduced cell lysate (p value = <0.0001). Each data point represents the mean of duplicate wells evaluated for VEGF-A₁₆₅ concentration and VEGF-A₁₆₅: total protein concentration (n = 4 individual EngNT for each group). *p < 0.05, **p < 0.01, ***p < 0.001 and ****p < 0.0001.



It was observed that compared to EngNT without a silicone tube, the VEGF-A₁₆₅ protein concentration in the EngNT in the silicone tube contributed to a larger percentage of the total protein in the cell lysate. This difference (an average of 0.0016% in the EngNT in the silicone tube and 0.0004% in the EngNT without the silicone tube) proved to be significant (two-tailed unpaired T test, 95 % confidence interval, p value = <0.0001, n = 4). The opposite was observed in the media, where a higher percentage of VEGF-A₁₆₅ protein was observed in the EngNT without the silicone tube (p value = 0.0004).

6.7 Co-cultures

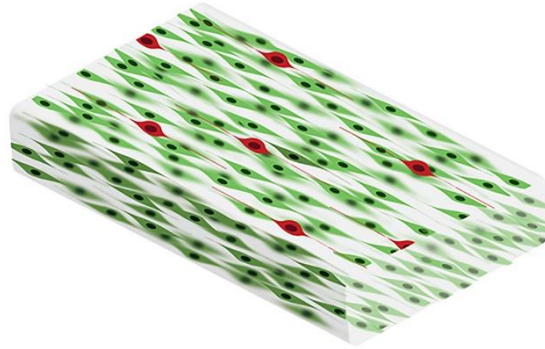
With the functionality of the VEGF-A₁₆₅ protein proven in monolayer SCL4.1/F7 cell culture models, it was decided to test its efficacy in 3D cell culture models. This was especially important as the ELISA assay revealed that in EngNT in a silicone tube, a large proportion of the VEGF-A₁₆₅ produced is found in the cells in the collagen gel. Further, despite their ease of use, monolayer cell culture models generally do not represent the complex 3D characteristics of living tissues (Ko and Frampton, 2016). It is generally agreed that the development of 3D cell models could potentially allow researchers to bridge between results obtained in *in vitro* models and *in vivo* studies more effectively. Additionally, *in vitro* monolayer studies tend to incorporate single cell types without considering the effect of other cells present in living tissue. It was therefore decided to test the effect of the neurotrophic and angiogenic effects of transduced SCL4.1/F7 cells overexpressing VEGF-A₁₆₅ on PC12 cells and HUVECs in 3D co-culture models.

6.7.1 Neurotrophic effects

Neuron-EngNT co-cultures have been previously used as a means of testing potential drug compounds that could increase regeneration following peripheral nerve injury (Rayner *et al.*, 2018). This is because when neurons are co-cultured with EngNT, neurite growth is supported and guided by the aligned Schwann cells in a 3D ECM environment, mimicking the key features of the peripheral nerve environment in the distal nerve segment. In order to establish whether the overexpression of VEGF-A₁₆₅ would increase

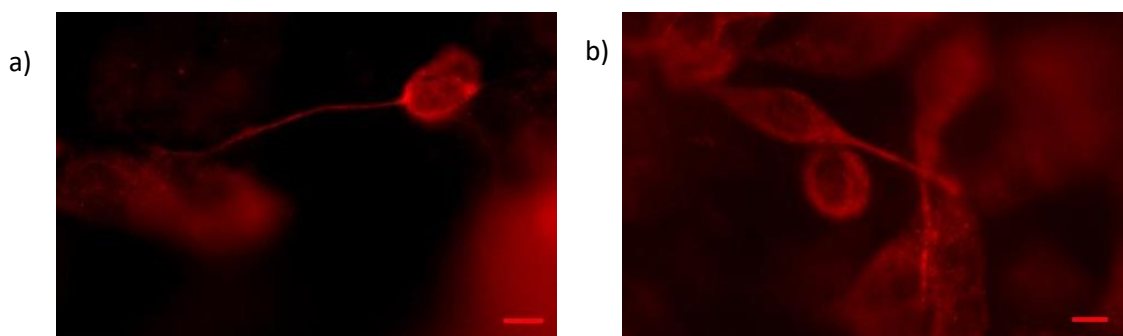
neurite length *in vitro*, it was decided to construct EngNT made from SCL4.1/F7 cells overexpressing VEGF-A₁₆₅ and culture PC12 cells on top of the EngNT (figure 88).

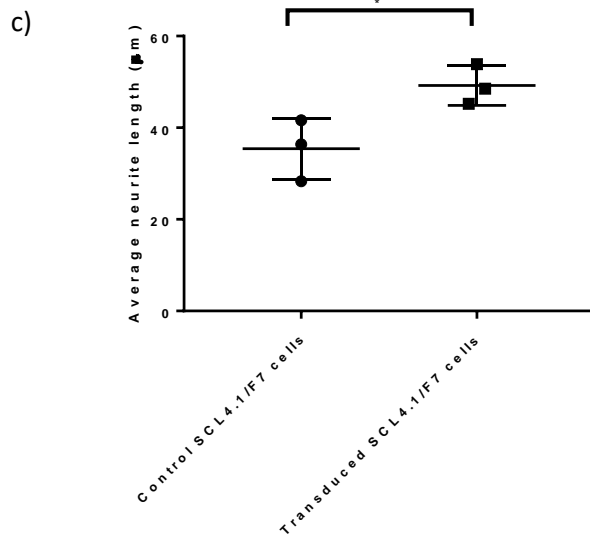
Figure 88. Representation of the 3D engineered co-culture. EngNT containing aligned Schwann cells (green) and neurons seeding on the gel surface (red). Image taken from Rayner *et al.* (2018).



Compared to EngNT made from control untransduced SCL4.1/F7 cells, EngNT made from SCL4.1/F7 cells overexpressing VEGF-A₁₆₅ resulted in a 1.39 fold increase in PC12 neurite length (figure 89).

Figure 89. Effect of VEGF-A₁₆₅ on neurite length *in vitro*. Representative fluorescence micrographs of PC12 neuronal cells seeded on EngNT made with a) transduced SCL4.1/F7 cells and b) control untransduced cells. Cultures were immunostained to detect β -III tubulin (red). Scale bar = c) VEGF-A₁₆₅ significantly increases PC12 neurite growth in the 3D EngNT co-culture model after 72 hour exposure (two-tailed unpaired T test, 95 % confidence interval, P value = <0.0404). Each data point represents the mean neurite length from 5 predetermined fields of view in one individual co-culture, n = 3 co-cultures for each group. Scale bar = 200 μ m. **p* < 0.05, ***p* < 0.01, ****p* < 0.001 and *****p* < 0.0001.



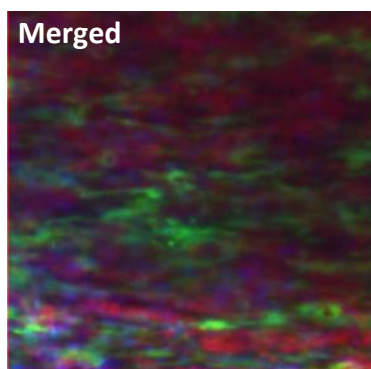
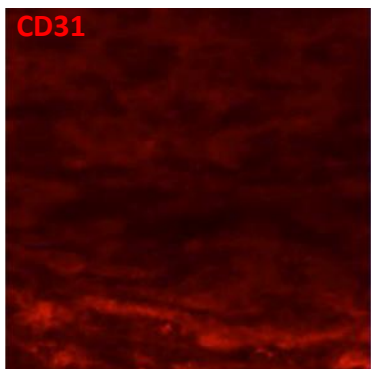
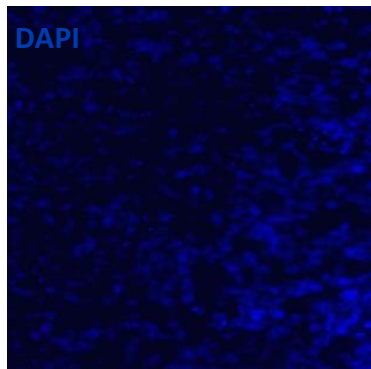
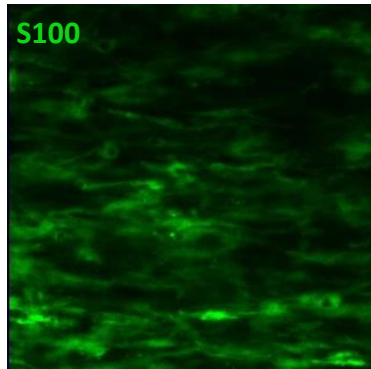


6.7.2 Angiogenic effects

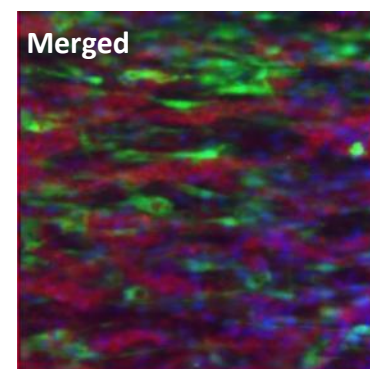
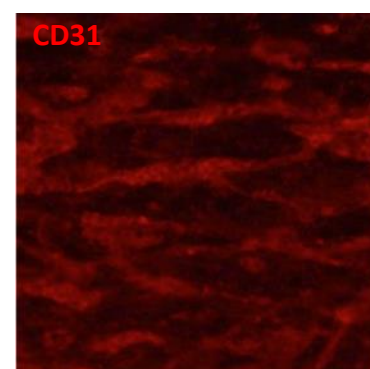
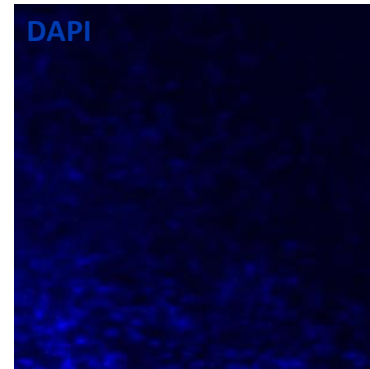
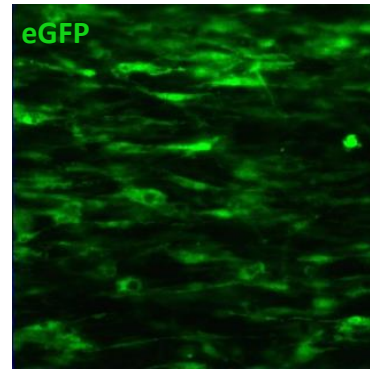
Muangsanit *et al.* (unpublished) constructed EngNT from a mixture of HUVECs and SCL4.1/F7 and found that HUVECs formed tube-like structures within the 3D matrix. A co-culture of HUVECs and SCL4.1/F7 cells was set up to investigate whether transduced SCL4.1/F7 cells overexpressing VEGF-A₁₆₅ would increase the extent of HUVEC tube formation in the collagen gel. Previous experiments by Muangsanit *et al.* (unpublished) have shown that an incubation time of 4 days and a ratio of 4×10^6 HUVECs: 1×10^6 SCL4.1/F7 cells /ml yielded optimal tube formation and so these conditions were used in the current study (figure 90).

Figure 90. Evaluation of endothelial tube formation in the 3D co-culture system after 4 days. The co-culture consisted of a ratio of 4×10^6 HUVECs: 1×10^6 SCL4.1/F7 cells /ml Representative immunofluorescence images show HUVECs forming tube-like structures and Schwann cell alignment. HUVECs were immunolabelled with CD31 (red) and control untransduced Schwann cells were immunofluorescently stained to detect S100 (green) to allow visualisation of the cells. The cells were counterstained with DAPI (blue). N = 3 individual 3D co-cultures per groups. Magnification, x20. Z-distance = 20 μ m, step size 1 = μ m.

Control SCL4.1/F7 cells and HUVECs

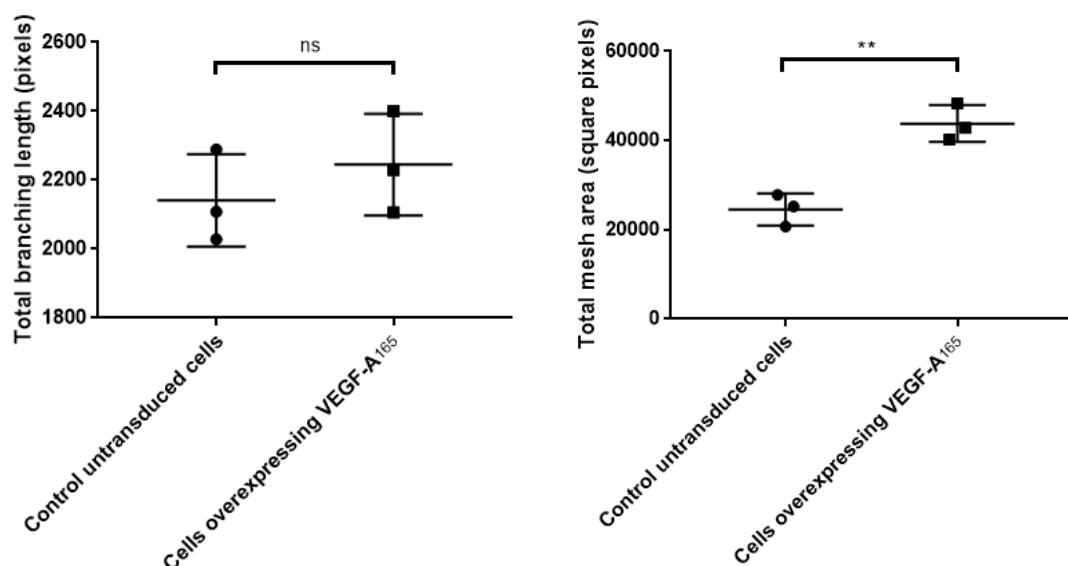


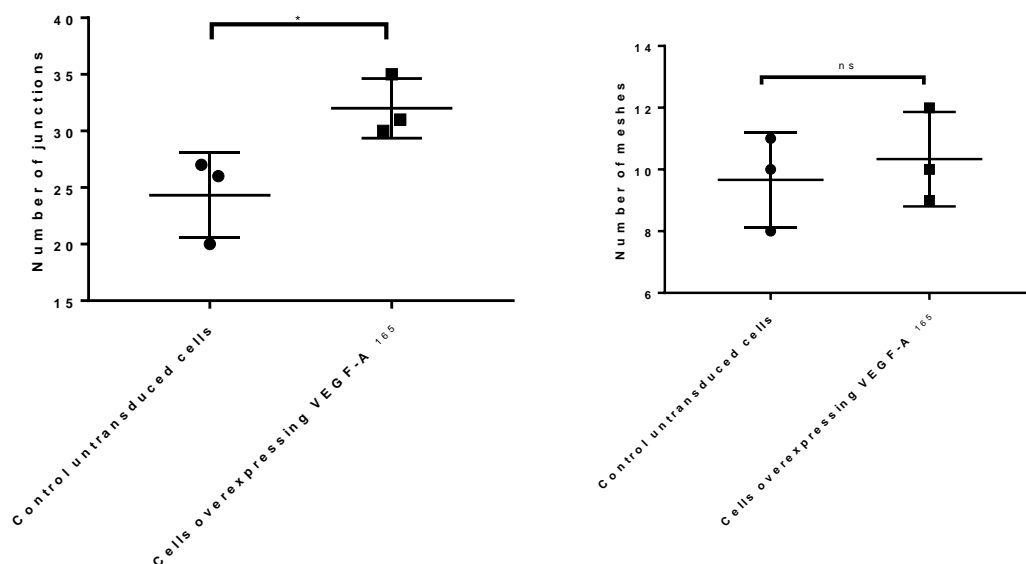
Transduced SCL4.1/F7 cells and HUVECs



Angiogenesis Analyzer, a plugin in ImageJ (Carpentier, 2012), was used to visualise endothelial network formation in the co-cultures. The parameters evaluated were number of junctions, number of meshes, total mesh area and total branching length (figure 91). The number of meshes was similar in the co-cultures made with control SCL4.1/F7 cells and transduced SCL4.1/F7 cells, with means of 9.6 and 10.3 meshes per group. However, the total mesh area was 1.78 fold higher in the co-cultures with SCL4.1/F7 cells overexpressing VEGF-A₁₆₅. Similarly, the number of junctions was 1.32 fold higher in the co-cultures with SCL4.1/F7 cells overexpressing VEGF-A₁₆₅. The total branching length of the HUVECs was 1.05 fold higher in the co-cultures with SCL4.1/F7 cells overexpressing VEGF-A₁₆₅ compared to the co-cultures with the untransduced cells, however, this was not a significant increase.

Figure 91. Endothelial cell network characteristics in the HUVEC - SCL4.1/F7 cell 3D co-cultures. The number of meshes was similar in the co-cultures made with control SCL4.1/F7 cells and transduced SCL4.1/F7 cells (two-tailed unpaired T test, 95 % confidence interval, p value = 0.6213). However, the total mesh area was significantly higher in the co-cultures with SCL4.1/F7 cells overexpressing VEGF-A₁₆₅ (p value = 0.0037). Similarly, the number of junctions was significantly higher in the co-cultures with SCL4.1/F7 cells overexpressing VEGF-A₁₆₅ (p value = 0.0452). The total branching length of the HUVECs the co-cultures with SCL4.1/F7 cells overexpressing VEGF-A₁₆₅ was similar to the co-cultures with the untransduced cells (p value = 0.4197). Each data point represents a value from an individual co-culture (n = 3 individual co-cultures for each group). * $p < 0.05$, ** $p < 0.01$, *** $p < 0.001$ and **** $p < 0.0001$.





6.8 Discussion

Having established that SCL4.1/F7 cells can be successfully transduced by a lentiviral vector delivering marker genes (chapter 4), it was decided to design and produce a lentiviral vector delivering the *VEGF-A₁₆₅* gene. The first step involved subcloning the *VEGF-A₁₆₅* gene into a lentiviral transfer plasmid. However, this proved to be unsuccessful. Due to the nature of cloning and recombinant DNA technology, it could take multiple attempts before successfully cloning a candidate gene into a transfer plasmid. While it is unclear why the initial cloning attempts were unsuccessful, several factors could have contributed to the failed attempts, including inefficient transformation, incompatible DNA ends and poor DNA quality.

No colonies were observed after the ligation mixture was transformed into the One Shot® Stbl3™ Chemically Competent *E. coli*. However, the transformation efficiency of the bacteria was confirmed as a pUC19 control plasmid yielded several colonies. This excluded the possibility of low transformation efficiency of the bacteria. A cloned sequence which is not tolerated by *E. coli* can lead to toxicity, resulting in no colonies being produced. However, this possibility was eliminated as the *VEGF-A₁₆₅* gene has been subcloned several times in literature (Ellison *et al.*, 2013; Luo *et al.*, 2017). Further, this proved not to be the case when the synthesised genes were used as colonies were formed.

Incomplete cleavage of the *VEGF-A₁₆₅* gene and pSFFV-IRES-eGFP backbone plasmid during the double digest could have also contributed to the cloning failure. However, new high quality restriction enzymes were used for the double digest to ensure optimal enzyme activity and exclude the possibility of endo-, exo-nuclease and phosphatase contamination in the enzyme preparations. Incomplete cleavage can result in vector self-ligation. However, no colonies were obtained when the bacteria were transduced with the digested pSFFV.IRES.eGFP vector plasmid control, excluding self-ligation. Further, the synthesised genes were successfully digested with the same enzymes.

The most likely explanation for the unsuccessful cloning is poor DNA quality. The *VEGF-A₁₆₅* gene and pSFFV-IRES-eGFP backbone plasmid were gel purified prior to ligation to remove the presence of contaminants. The bands were excised using an UV transilluminator at a low setting and for minimal periods of time to avoid UV-mediated mutations in gene sequences and to prevent DNA damage. However, both these measures still did not result in successful cloning. Following unsuccessful troubleshooting of the cloning process, it was decided to commercially synthesise the *VEGF-A₁₆₅* gene. The synthesised gene was subcloned into the pSFFV-IRES-eGFP backbone plasmid and a recombinant transfer plasmid was formed. This transfer plasmid was then used to produce the lentiviral vector delivering the *VEGF-A₁₆₅* gene.

Following transduction with the lentiviral vector delivering the *VEGF-A₁₆₅* gene, the amount of VEGF-A₁₆₅ produced by SCL4.1/F7 cells was quantified by ELISA. After confirming that the transduced cells produced a significantly larger amount of VEGF-A₁₆₅ compared to control untransduced cells, several bioassays were carried out to test the biological activity of the VEGF-A₁₆₅ produced. Angiogenesis is a well-coordinated process involving endothelial cell proliferation, migration and differentiation. Therefore, the potential effects of VEGF-A₁₆₅ on each of these endothelial cell behaviours were evaluated using an alamarBlue® assay, a scratch wound assay and a tube formation assay respectively.

Recombinant VEGF-A₁₆₅ protein was used a positive control in the *in vitro* bioassays. Authors cite the use of different concentrations of the protein when used as a control,

ranging from 5 - 100 ng/ml. Silva and Mooney (2010) found that doses ranging from 5 – 20 ng/ml of VEGF-A₁₆₅ resulted in the same level of endothelial cell proliferation. They also reported that the cell proliferation rate increased in a dose dependent manner and reached a plateau at 50 ng/ml. No further increase was observed with a dose of 100 ng/ml. Similarly, Hanjaya-Putra *et al.* (2010) reported that concentrations of VEGF-A₁₆₅ up to 25 ng/ml increased endothelial cell tube formation but optimal results were obtained with 50 ng/ml. It was therefore decided to use recombinant VEGF-A₁₆₅ at a concentration of 50 ng/ml as a positive control in the current study.

Conditioned media from the SCL4.1/F7 cells overexpressing VEGF-A₁₆₅ improved endothelial cell viability, migration and tube formation to levels comparable to the positive control (VEGF-A₁₆₅ recombinant protein at a concentration of 50 ng/ml). In order to determine that this effect was due to the VEGF-A₁₆₅ in the conditioned media, conditioned media from control untransduced SCL4.1/F7 cells was also tested. This had a significantly lower effect on endothelial cell viability, migration and tube formation compared to the conditioned media from the transduced cells. These results are similar to others reported in the literature. VEGF-A₁₆₅ has been shown to endothelial cell growth (Ferrara, 2004; Domigan *et al.*, 2015), migration (Wang *et al.*, 2011) and tube formation (Makarevich *et al.*, 2012) *in vitro*. Makarevich *et al.* (2012) evaluated the angiogenic activity of VEGF-A₁₆₅ produced by HEK293T cells following transfection with a plasmid delivering the VEGF-A₁₆₅ gene. HUVECs on a Matrigel-coated surface were incubated with the conditioned media and the induction of tube formation was assessed after 12-14 hours. Similar to the current study, HUVECs incubated with conditioned media from the cells overexpressing VEGF-A₁₆₅ showed comparable tube formation to HUVECs incubated with positive control recombinant human VEGF-A₁₆₅.

Conditioned media from the SCL4.1/F7 cells overexpressing VEGF-A₁₆₅ also had a significant effect on Schwann cell migration *in vitro*. Similar results were obtained by Muratori *et al.* (2018) who carried out a transwell assay showing that VEGF-A₁₆₅ increased primary Schwann cell migration. This was a significant finding as the VEGF-A₁₆₅ produced by the transduced SCL4.1/F7 cells could potentially influence the migration of Schwann cells *in vivo*, which is an important step during the regeneration process. It was also observed that SCL4.1/F7 cells overexpressing VEGF-A₁₆₅ had an increased

proliferation rate compared to control untransduced cells and cells transduced with a lentiviral vector delivering luciferase and eGFP. Similarly, Sondell *et al.* (1999b) reported that the addition of human recombinant VEGF-A₁₆₅ (50 ng/ml) to explanted adult mouse superior cervical ganglia and dorsal root ganglia resulted in Schwann cell proliferation. This is another important result in the context of peripheral nerve regeneration. Following injury the surviving Schwann cells being to proliferate and this is a significant feature of Wallerian degeneration (Atanasoski *et al.*, 2006). In addition to directing Schwann cell migration to the injury site, the secreted VEGF-A₁₆₅ could also increase the proliferation rate of resident Schwann cells.

Encouraging results were obtained from the *in vitro* studies testing the functionality of the VEGF-A₁₆₅ produced by the transduced cells. It was decided that prior to *in vivo* testing, the functionality of the VEGF-A₁₆₅ would be assessed in a 3D hydrogel, which provides a more tissue-like spatial and mechanical environment. There is increasing evidence suggesting that 3D assays offer a model which mimics the natural *in vivo* environment more closely than 2D assays (Edmondson *et al.*, 2014). Another important consideration was that Chen *et al.* (2010) have shown that VEGF-A₁₆₅ is retained and remains active within a collagen matrix. In the current study, an ELISA revealed that a significant proportion of the VEGF-A₁₆₅ was retained in the collagen based EngNT and not secreted into the media. It was therefore important to determine that the VEGF-A₁₆₅ in the current study retained its functionality within a 3D environment. This is because following implantation, host cells including axons and endothelial cells, infiltrate the EngNT and will come into contact with the VEGF-A₁₆₅ in the collagen. In order to understand how VEGF-A₁₆₅ may modulate the activity of cells in 3D cultures, SCL4.1/F7 cells overexpressing VEGF-A₁₆₅ were co-cultured with endothelial cells and PC12 cells in two separate 3D models. This is especially relevant in the context of peripheral nerve regeneration, where there is the interplay of several cell types, including neurons, Schwann cells and endothelial cells.

Chen *et al.* (2009) found that HUVECs formed sprouts with longer processes when co-cultured with glioma cells that secrete VEGF-A₁₆₅. In agreement with this data, the presence of SCL4.1/F7 cells overexpressing SCL4.1/F7 cells increased the number of junctions and meshes as well as the total mesh area formed by HUVECs in the co-culture.

The increased presence of meshes confirmed the formation of a more extended endothelial network in the co-culture with the SCL4.1/F7 cells overexpressing VEGF-A₁₆₅ (Gholobova *et al.*, 2015). However, no improvement in the total branching length compared to the co-cultures with the control SCL4.1/F7 cells was seen. Previous experiments by Muangsanit *et al.* (unpublished) have shown that an incubation time of 4 days and a ratio of 4×10^6 HUVECs: 1×10^6 SCL4.1/F7 cells /ml yielded optimal tube formation. This suggests that for the given system and conditions tested, maximal branching length was reached independent of the additional VEGF-A₁₆₅ supplied by the transduced SCL4.1/F7 cells.

Genetos *et al.* (2010) showed that exogenous VEGF-A₁₆₅ (50 ng/mL) increased the frequency of PC12 cells elaborating neurites under 2D culture. The positive effect of VEGF-A₁₆₅ on PC12 neurite length was replicated in a 3D culture in the current study. EngNT made with SCL4.1/F7 cells overexpressing VEGF-A₁₆₅ increased PC12 neurite length compared to control SCL4.1/F7 cells. This confirmed the neurotrophic effect in addition to the angiogenic effect of the VEGF-A₁₆₅ produced by the transduced cells. VEGF-A₁₆₅ has also been reported to increase neurite length in other cell types, including chicken embryonic dorsal root ganglia (Zupanc *et al.*, 2017), adult mouse dorsal root ganglia (Sondell *et al.*, 1999a) and adult mouse trigeminal ganglia (Pan *et al.*, 2013).

6.9 Conclusion

This study showed that SCL4.1/F7 cells transduced with a lentiviral vector delivering the VEGF-A₁₆₅ gene results in the production of functional VEGF-A₁₆₅ protein. Further, transduced SCL4.1/F7 cells incorporated into EngNT still produced the functional protein. As previously discussed, tissue engineered constructs seeded with genetically modified cells have the potential to enhance peripheral nerve regeneration. The next stage of this study is to therefore carry out an *in vivo* assessment of EngNT made with SCL4.1/F7 cells overexpressing VEGF-A₁₆₅ to determine whether this promotes neuronal regeneration in a rat model of sciatic nerve injury.

Chapter 7: Effects of EngNT containing SCL4.1/F7 overexpressing VEGF-A₁₆₅ on peripheral nerve regeneration

7.1 Introduction

The previous chapter showed that conditioned media from SCL4.1/F7 cells transduced with a lentiviral vector delivering the *VEGF-A₁₆₅* gene improved HUVEC viability and induced HUVEC migration and tube formation *in vitro*. The conditioned media also increased SCL4.1/F7 migration *in vitro*. Further, SCL4.1/F7 cells overexpressing VEGF-A₁₆₅ showed an increased proliferation rate. The transduced cells were used to construct EngNT and it was confirmed that the cells were able to produce VEGF-A₁₆₅ in a 3D environment. When co-cultured with PC12 cells, EngNT made with SCL4.1/F7 cells overexpressing VEGF-A₁₆₅ was shown to increase neurite length. Finally, a co-culture of HUVECs and SCL4.1/F7 cells overexpressing VEGF-A₁₆₅ revealed that the presence of VEGF-A₁₆₅ increased the number of junctions, meshes and mesh area formed by HUVECs within 3D hydrogels. Having demonstrated that the lentiviral vector successfully transduced SCL4.1/F7 cells, it was then decided to transduce clinically relevant cell types, namely CTX0E03 cells and ADSCs, with the vector. As the VEGF-A₁₆₅ produced by the transduced SCL4.1/F7 cells was proven to have neurotrophic and angiogenic properties in 2D monolayers and 3D cultures *in vitro*, EngNT made with SCL4.1/F7 cells overexpressing VEGF-A₁₆₅ was implanted into a rat model of sciatic nerve injury. The aims of this chapter were as follows:

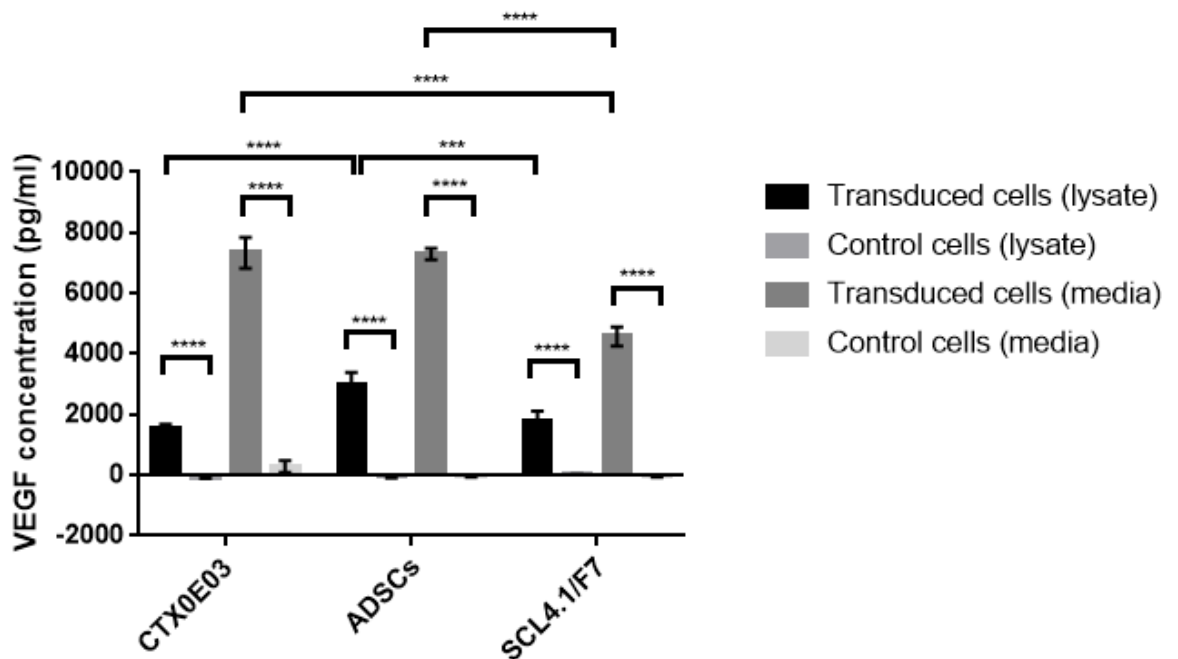
- To transduce clinically relevant sources of stem cells with the lentiviral vector delivering VEGF-A₁₆₅.
- To carry out a pilot study to assess whether EngNT made with SCL4.1/F7 cells overexpressing VEGF-A₁₆₅ improved axonal regeneration and functional recovery in a model of rat sciatic nerve injury.

7.2 VEGF-A₁₆₅ overexpression in clinically relevant sources of therapeutic cells

Having transduced SCL4.1/F7 cells with the lentiviral vector delivering VEGF-A₁₆₅, clinically relevant sources of therapeutic cells were sought. It was decided to transduce ADSCs and CTX0E03 cells as these had been previously used by the group (Georgiou *et al.*, 2015; O'Rourke *et al.*, 2017). CTX0E03 cells are manufactured according to Good Manufacturing Practice and are currently in phase II clinical trials for ischaemic stroke (Sinden *et al.*, 2017). ADSCs have been extensively studied as an adjunct to nerve repair (Faroni *et al.*, 2013) and various authors have reported improved regeneration following transplantation of ADSCs (di Summa *et al.*, 2010. Georgiou *et al.*, 2015, Masgutov *et al.*, 2018).

As expected, a higher VEGF-A₁₆₅ concentration in the transduced ADSCs and CTX0E03 cell lysate and media was seen compared to the control cell lysate and media, indicating that the cells had been successfully transduced. The VEGF-A₁₆₅ concentration in the transduced CTX0E03 cell media was 1.6 fold higher than in the transduced SCL4.1/F7 cell media. A similar VEGF-A₁₆₅ concentration was measured in transduced CTX0E03 cell lysate and transduced SCL4.1/F7 cell lysate, with means of 1552.2 and 1808.1 pg/ml respectively. In the case of the transduced ADSCs, the VEGF-A₁₆₅ concentration in the cell lysate and media were both 1.6 fold higher than the transduced SCL4.1/F7 cell lysate and media. Compared to the transduced CTX0E03 cell lysate, the VEGF-A₁₆₅ concentration in the transduced ADSC lysate was 1.9 fold higher. A similar VEGF-A₁₆₅ concentration was measured in transduced CTX0E03 cell media and transduced ADSC cell media, with means of 73337.3 and 7298.3 pg/ml respectively. The concentration of VEGF-A₁₆₅ in the transduced cell media was 2.5 fold higher than in the transduced cell lysate for the transduced SCL4.1/F7 and ADSC and 4.7 fold higher for the transduced CTX0E03 (figure 92).

Figure 92. Quantifying the amount of VEGF-A₁₆₅ produced by transduced CTX0E03, ADSCs and SCL4.1/F7 cells. The VEGF-A₁₆₅ concentration in the lysate and media of control and transduced cells was measured by ELISA. A statistical significance was found between the transduced and control cell lysate as well as the transduced and control cell media for each cell type (two-way ANOVA, Tukey's multiple comparisons test, 95 % confidence interval, p value = <0.0001). The amount of VEGF-A₁₆₅ in the transduced cell media was significantly higher than that in the transduced cell lysate for all 3 cell types (p value = <0.0001). The VEGF-A₁₆₅ concentration in the transduced ADSC cell lysate was significantly higher than in the transduced SCL4.1/F7 and CTX0E03 cell lysate (p value = <0.0004). Data is presented as the means ± SD (n = 4 for each group). *p < 0.05, **p < 0.01, ***p < 0.001 and ****p < 0.0001.



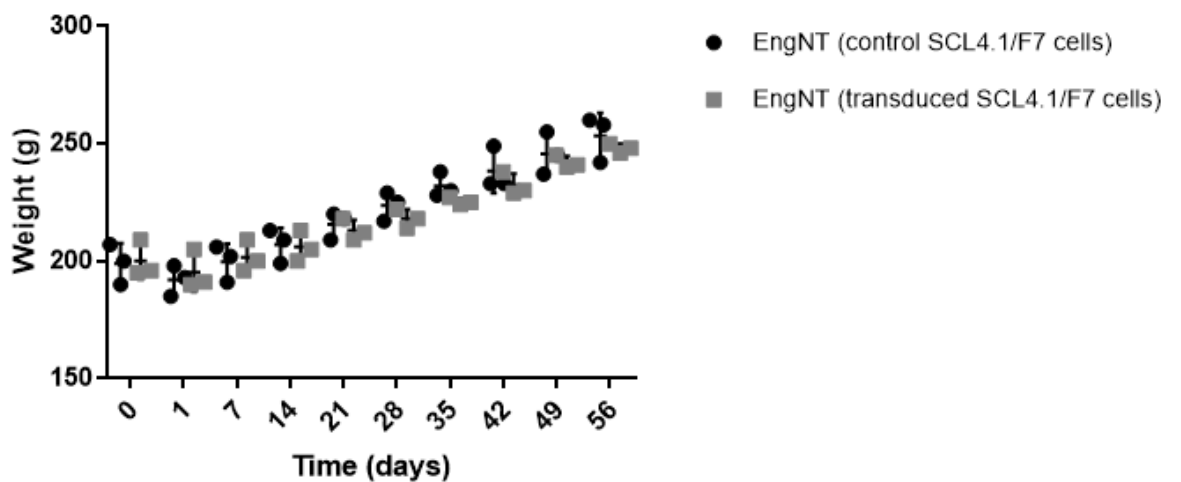
7.2 Animal model

A long gap (15 mm), 8 week experiment was used to establish whether EngNT made from SCL4.1/F7 cells overexpressing VEGF-A₁₆₅ would increase regeneration compared to EngNT made from untransduced SCL4.1/F7 cells. For each experimental group, one EngNT rod (15 mm in length) was placed into a silicone tube to create an implantable device. The device was positioned in the gap of the rat sciatic nerve following a single transection and sutured at each end as described in section 3.17.3.

The animals were monitored daily and showed no signs of distress. The animals were weighed weekly and continued to gain weight steadily over the course of the experiment. Continuous tracking of animal body weight is considered to be a sensitive and objective way of assessing the stress experienced by animals after surgical procedures and treatments and is useful method of monitoring the general health of

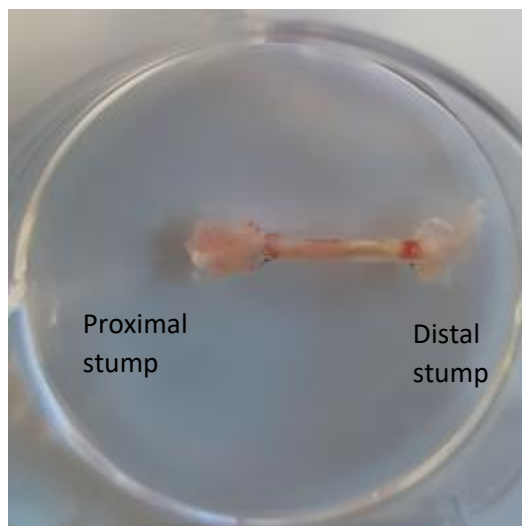
the animal (Brenneis *et al.*, 2017). The animals in both groups had similar weights at all time points (figure 93). All animals survived the entire period of recovery post-implantation (8 weeks). One animal displayed very mild autotomy which resulted in the removal of one toenail. This did not progress to more severe mutilation and so this animal was not excluded from the study.

Figure 93. Rat body weight monitoring during the 8 week experiment. The rats gained weight throughout the 8 week period and animals in both groups had similar weights at all time points.



After 8 weeks, the repaired nerves were excised under a dissecting microscope (figure 94) and cryopreserved and processed as described in section 3.17.8.2.

Figure 94: An explanted nerve repair device. EngNT in a silicone outer tube showing the proximal and distal nerve stumps after 8 weeks *in vivo*.



7.3 Outcome measures

Complete rat sciatic nerve transection is a well-established animal model used to study various aspects of nerve regeneration following injury (Kaplan *et al.*, 2015). The degree of nerve regeneration is generally evaluated and quantified through three types of measures: histological analysis, electrophysiological studies and functional assessment. Nerve fibres may regenerate without making functional connections and axonal sprouting without pruning may result in an overestimation of functional connections. This implies that histological and electrophysiological data may not necessarily correlate with recovery of function (Nichols *et al.*, 2005). In order to provide a complete picture of nerve regeneration in the current study, all three measures were evaluated. It was noted that the small sample size used in this pilot study generated difficulty in comparing the effects of EngNT made from SCL4.1/F7 cells overexpressing VEGF-A₁₆₅ and EngNT made from control SCL4.1/F7 statistically due to variation in the outcome measures. It was therefore decided not to perform statistical tests to establish significance between the two groups, instead a qualitative description of the results obtained is provided.

7.3.1 Functional outcomes

Varejão *et al.* (2004) argued that there is no general consensus on the type of assessment tool that provides the most accurate description of functional recovery following injury in animal models. Consequently, they suggest that several tests should be used in combination to give a more comprehensive picture of nerve function. According to Nichols *et al.* (2005), functional analysis may offer the most indisputable evidence to show that a nerve has regenerated and also made successful end organ connections. This section will describe the results obtained from three functional outcome measures tested in the current study, namely the SSI, von Frey analysis and gastrocnemius wet muscle mass.

7.3.1.1 Static sciatic index

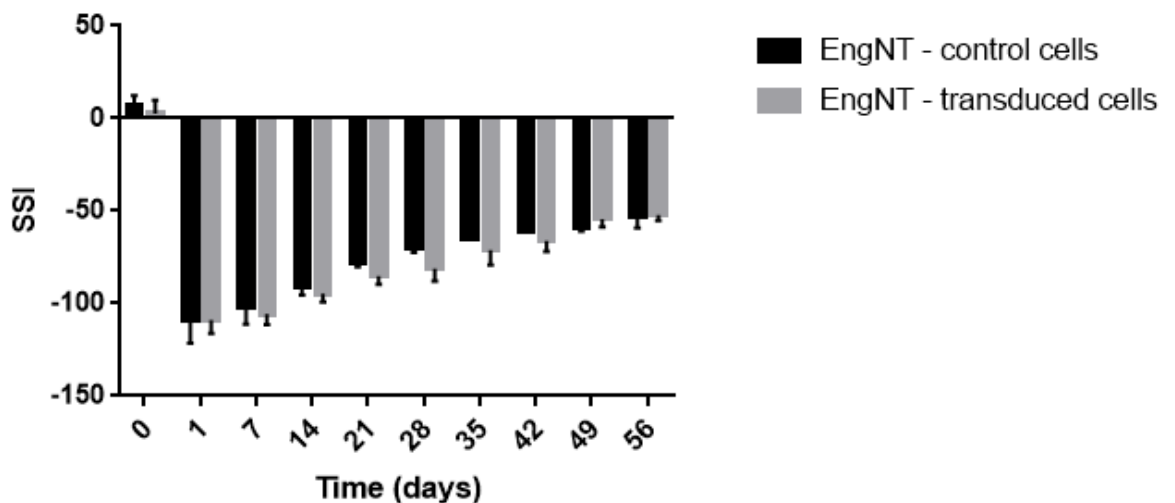
The SSI is a simple and non-invasive method for the evaluation of functional recovery of the sciatic nerve in rats (Bervar, 2000). It involves acquiring an image of the plantar aspect of the hind feet while the rat is in a static position and measuring the distance from the first to the fifth toe (the toe spread) and the distance from the second to the fourth toe (the intermediary toe spread) on both the injury and contralateral sides (figure 95). The toe spread factor and the intermediary toe spread factor are then calculated and incorporated into the formula described in section 3.17.5.2. The SSI fluctuates around 0 for normal nerve function while a value of around -100 represents total loss of function (Amniattalab and Mohammadi, 2017).

Figure 95. Calculating the SSI. Representative images for a) the animals treated with EngNT made from SCL4.1/F7 cells and b) the animals treated with EngNT made from SCL4.1/F7 cells overexpressing VEGF-A₁₆₅. In each set, the image on the left shows the hind feet before the procedure and the image on the right shows the hind feet after 8 weeks.



The SSI demonstrated that, although there was a trend for recovery over the 8 week period, the values were lower than the pre-operative values for both groups at the end of the study (figure 94). Both groups had similar SSI scores at the end of the study, with means of -57.6 and -52.2 for the animals treated with control cells and the animals treated with cells overexpressing VEGF-A₁₆₅ respectively. Interestingly, the animals treated with EngNT made from the control cells displayed higher SSI values over days 7 to 49, indicating that the control animals may have recovered faster (figure 96).

Figure 96. SSI monitoring during the study period. Before the procedure, all animals had an SSI of around 0, indicating full function. The SSI improved throughout the 8 week period but was still lower than day 0 for both groups by the end of the experiment. Both groups had similar values on day 56. The animals treated with the control cells displayed higher SSI values than the animals treated with the transduced cells over days 7 to 49. Data shown as the mean \pm SD (n = 3 for each group).



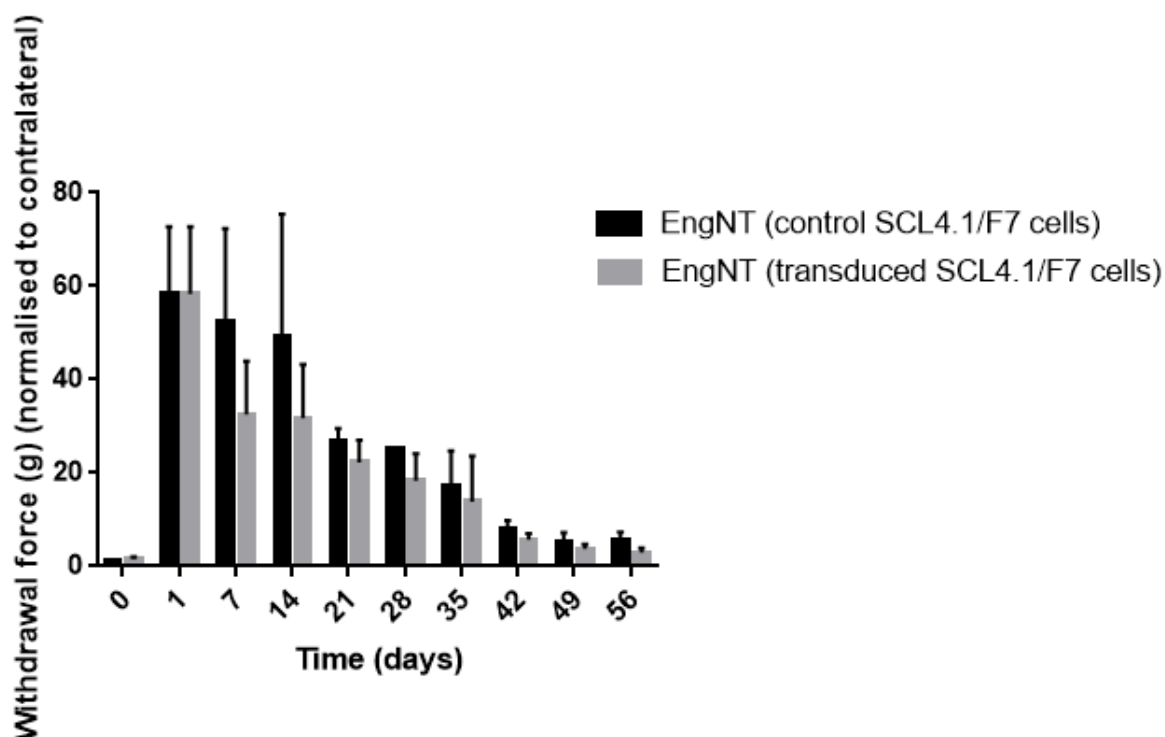
7.3.1.2 Von Frey

The sciatic nerve is a mixed nerve, consisting of both sensory and motor axons (Schmalbruch, 1986). For this reason, the rat sciatic nerve transection model permits the evaluation of both motor and sensory recovery. The SSI described in the previous section is a useful indicator of motor recovery (Korte *et al.*, 2011). In order to complement this, von Frey filaments were used to evaluate the return of sensory function following injury as described in section 3.17.5.1.

The withdrawal force of the injury side was divided by that of the contralateral side to produce a normalised value. Unlike the SSI, the normalised withdrawal force had

returned to the pre-operative values for both groups by the end of the 8 week period. Both groups had similar normalised withdrawal forces at the end of the study, with means of 5.4 and 3.0 for the animals treated with control cells and the animals treated with cells overexpressing VEGF-A₁₆₅ respectively. Interestingly, the animals treated with EngNT made from the transduced cells consistently showed lower withdrawal forces, indicating that these animals may have recovered faster (figure 97).

Figure 97. Von Frey testing. The force required to cause paw withdrawal in response to von Frey filaments was measured over the 8 week period. The withdrawal force of the injury side was normalised by dividing over the contralateral side. The withdrawal force at the end of the study was similar to the pre-operative values for both. Both groups displayed similar withdrawal forces at the end of the study. The animals treated with the transduced cells displayed consistently lower withdrawal forces than the animals treated with the cells throughout the study. Data shown as the mean \pm SD (n = 3 for each group).

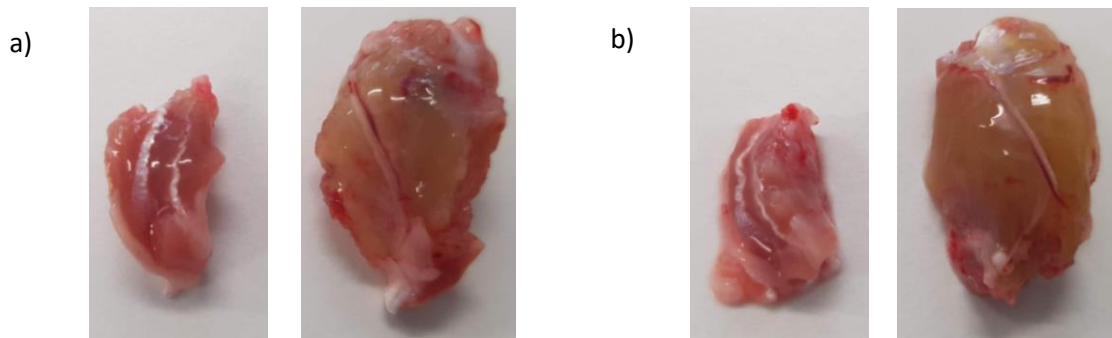


7.3.1.3 Gastrocnemius muscle mass

The atrophy of the gastrocnemius muscle, innervated by the sciatic nerve, provides an indication of the extent of nerve regeneration. Percentage muscle recovery was defined as (gastrocnemius muscle mass from the injury side/ gastrocnemius muscle mass from

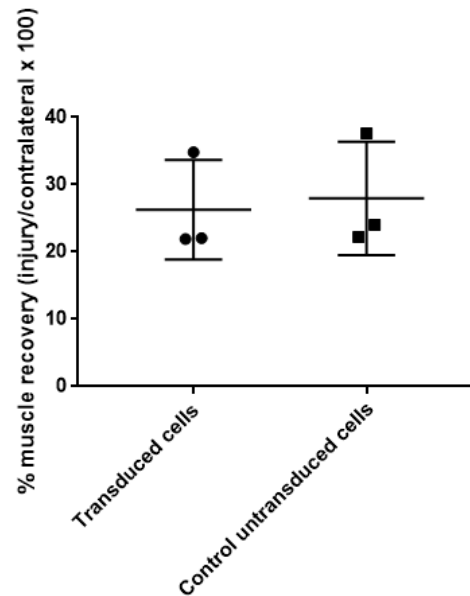
the contralateral control side) x 100, and was used to estimate the regeneration of the motor neuron component in sciatic nerve (figure 98).

Figure 98. Gastrocnemius muscles harvest at 8 weeks. Representative images to show the gastrocnemius muscle after 8 weeks in a) the animals treated with EngNT made from SCL4.1/F7 cells and b) the animals treated with EngNT made from SCL4.1/F7 cells overexpressing VEGF-A₁₆₅. In each set, the image on the left shows the gastrocnemius muscle harvested from the injury side and the image on the right shows the gastrocnemius muscle harvested from the contralateral side.



The gastrocnemius muscle mass was lower on the injury side compared to the contralateral side in all animals. The percentage recovery was similar in both groups, with means of 26.6% recovery for animals treated with the transduced cells and 28.0% recovery for animals treated with the control cells (figure 99).

Figure 99. Gastrocnemius muscle mass following sciatic nerve repair. The mass of the gastrocnemius muscle on the injury side was expressed as a percentage of the contralateral muscle to calculate the muscle recovery. A similar percentage recovery was obtained in both groups. Each data point represent the percentage muscle recovery from one animal (n = 3 for each group).



7.3.2 Electrophysiological outcomes

After 8 weeks animals were anaesthetised and nerve function was assessed electrophysiologically by comparing the repaired nerve to the contralateral nerve in each animal. Functional recovery was assessed through stimulation of the sciatic nerve proximal to the repair site and recording of the compound muscle action potential (CMAP) in the gastrocnemius muscle as described in section 3.17.6. In one of the animals treated with EngNT made with SCL4.1/F7 cells and in two of the animals treated with EngNT made with SCL4.1/F7 cells overexpressing VEGF-A₁₆₅, CMAP amplitude was below the threshold of detection. The latency of the evoked action potentials was greater in the repaired nerves compared with contralateral controls in all cases. The values recorded are shown in table 18. When expressed as a percentage of the contralateral, the amplitude of animal 2 was 23.4%. When expressed as a percentage of the contralateral, the amplitudes of animals 4 and 5 were 45 and 81.6% respectively.

Table 18. Electrophysiological evaluation of sciatic nerve 8 weeks postoperatively. CMAP amplitude values for repaired and contralateral nerves and the latency associated with evoked CMAP responses are shown.

Animals treated with EngNT made with SCL4.1/F7 cells overexpressing VEGF-A₁₆₅				
	<i>Contralateral</i>		<i>Injury</i>	
	Latency (ms)	Amplitude (μV)	Latency (ms)	Amplitude (μV)
Animal 1	1.51	8163	-	-
Animal 2	1.51	8540	8.91	2000
Animal 3	10.73	99279	-	-
Animals treated with EngNT made with control SCL4.1/F7 cells				
	<i>Contralateral</i>		<i>Injury</i>	
	Latency (ms)	Amplitude (μV)	Latency (ms)	Amplitude (μV)
Animal 4	2.03	1087	2.34	2415
Animal 5	3.49	99824	8.7	81429
Animal 6	1.61	15250	-	-

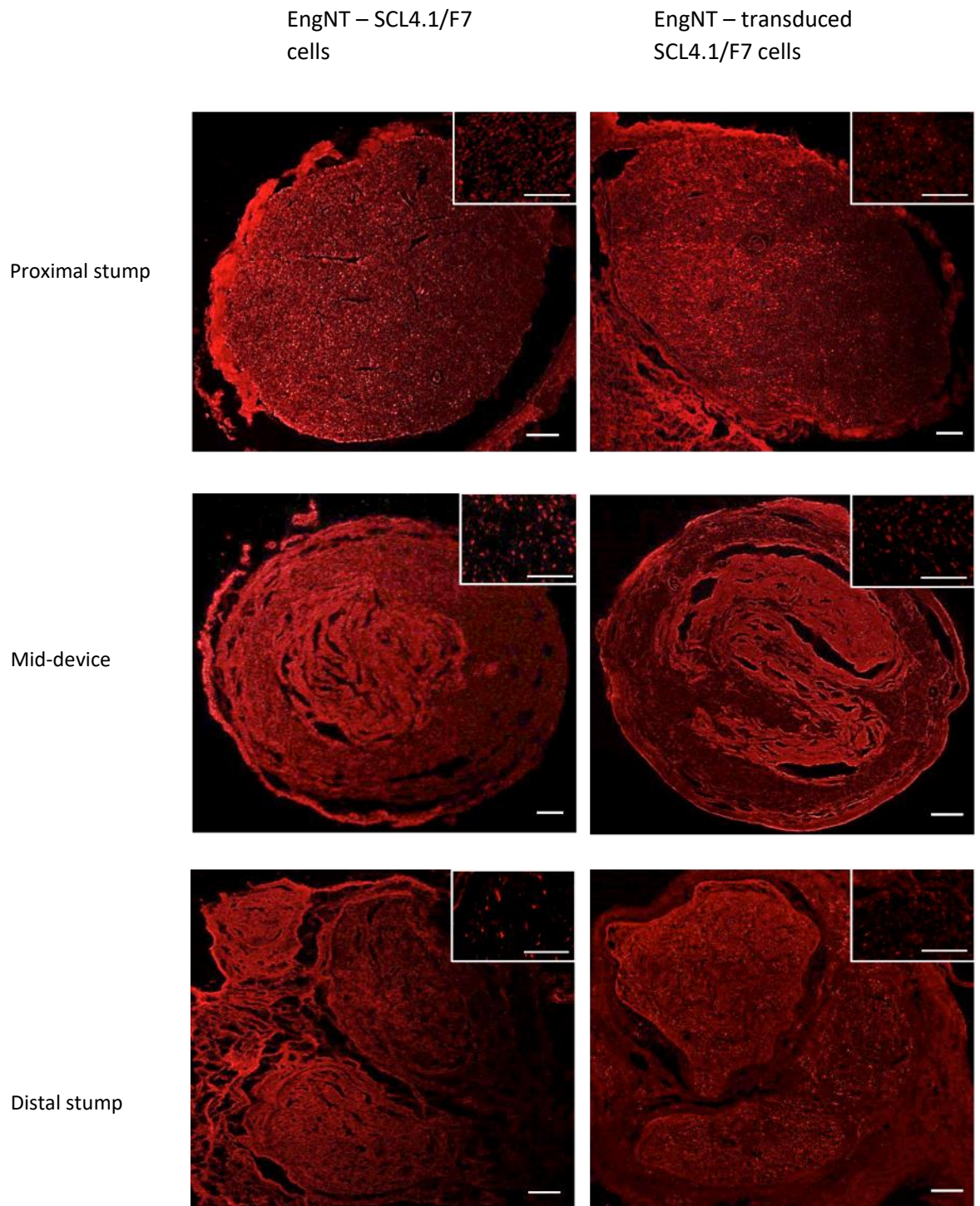
7.3.3 Histological outcomes

In addition to functional and electrophysiological assessment, nerve regeneration was also studied histologically. Transverse cryostat sections (10 μm thick) were prepared from the middle of the device and the proximal and distal parts of the nerve stumps at a constant temperature of -20 °C. The transverse sections that were used for analysis were from positions 1 mm into the proximal and distal stumps, measured from the end of the nerve stump in each case, and from the middle of the device.

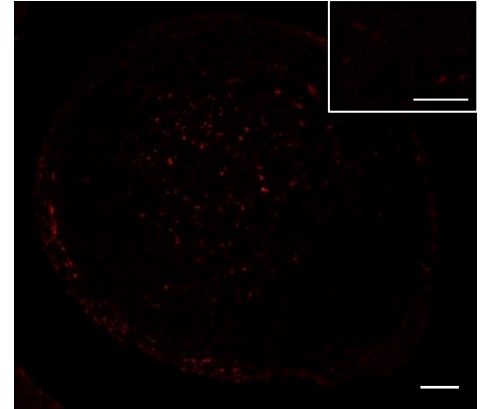
7.3.3.1 Axonal counts

Transverse sections through the regions described were used to determine the number of neurofilament-positive neurites present in the proximal and distal stumps as well as in the middle of the device (figure 100).

Figure 100. Axonal staining. Representative micrographs from transverse sections showing neurofilament positive axons at various positions in the repaired nerves. Scale bar: 100 μm , insert scale bar: 240 μm .

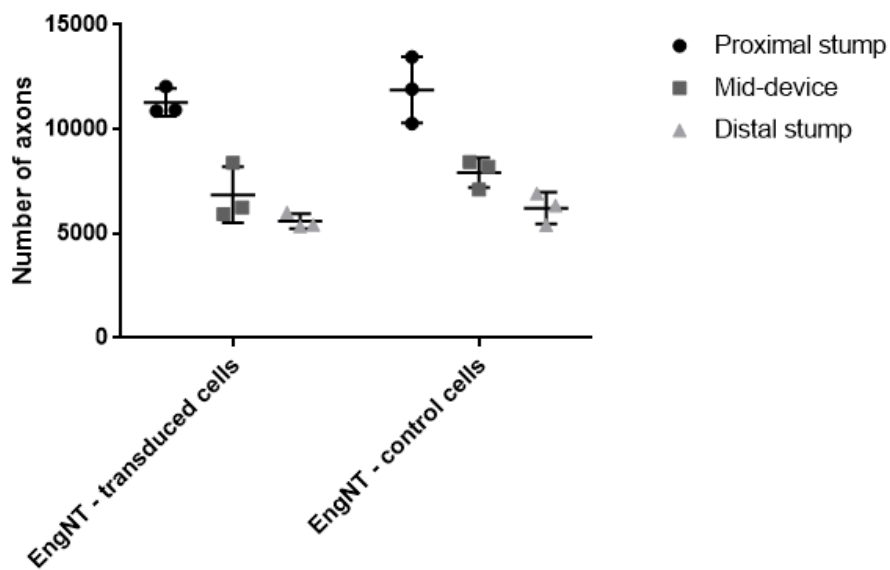


Immunostaining control (no secondary antibody)



To assess axonal growth, all of the neurofilament positive axons present in each transverse section were counted using automated image analysis protocols in Velocity (figure 101). Similar numbers of axons were counted in both groups at the 3 different positions. Both groups showed similar numbers of axons in the proximal and distal stumps as well as in the middle of the device. In both groups, the number of axons counted in the distal stump was lower than in the proximal stump, with means of around 11 000 and 6000 axons respectively. The mean number of axons in the mid-device for both groups was approximately 7000.

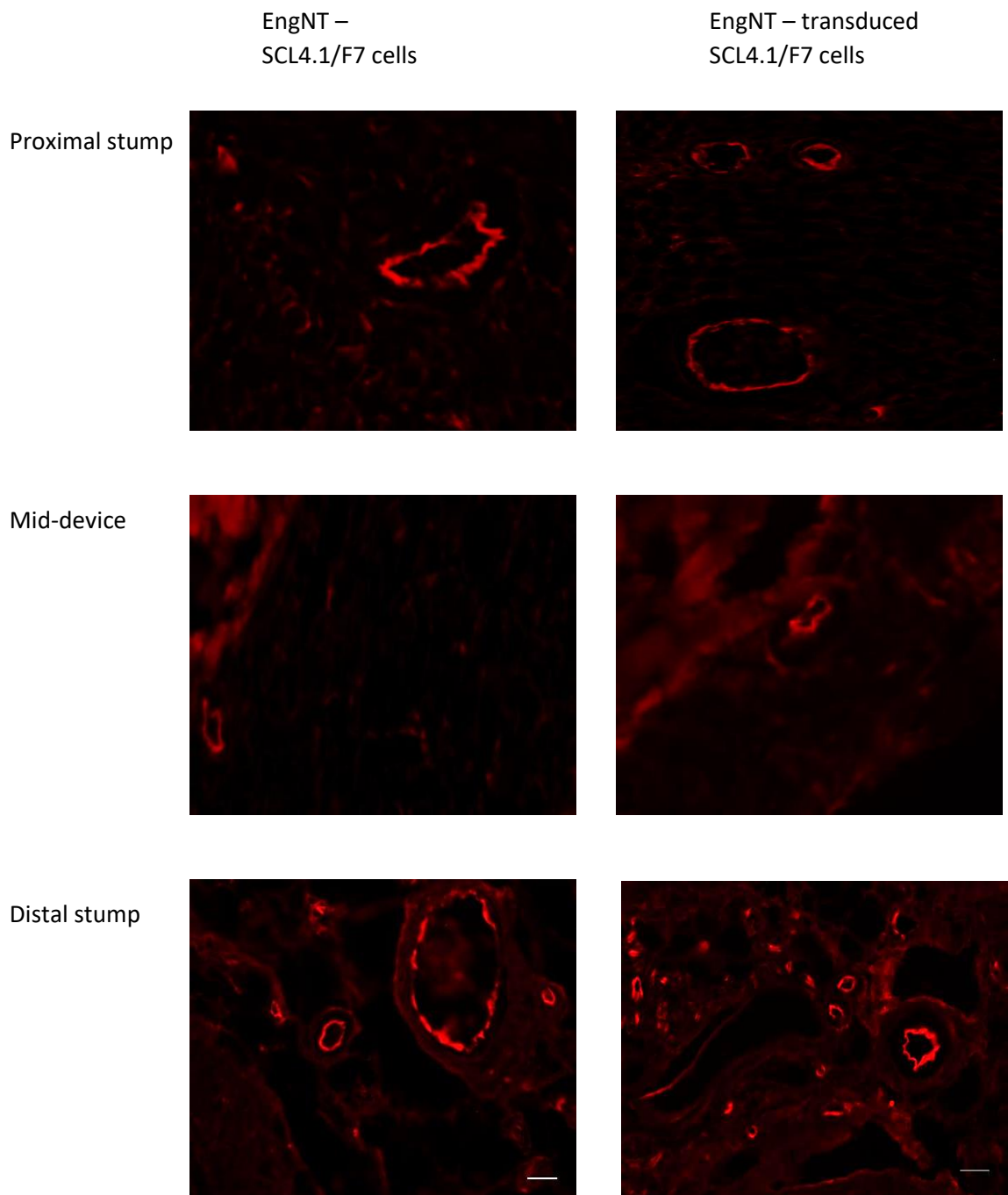
Figure 101. Quantification of neurites at different positions through repaired nerves. Each data point represents the number of neurofilament positive axons at each position (n = 3 for each group).



7.3.3.2 Vascularisation

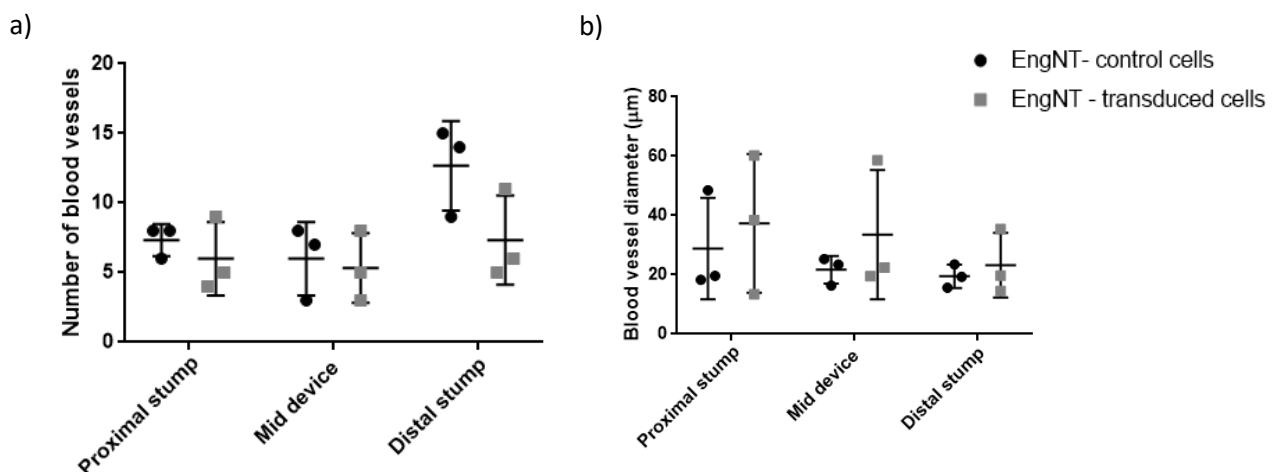
The vascularisation of proximal and distal stumps and of the middle of the device was examined via immunofluorescence staining of transverse sections using RECA-1 (figure 102).

Figure 102. Blood vessel analysis. Representative micrographs from transverse sections showing blood vessels at various positions in the repaired nerves. Scale bar: 50 μ m.



Analysis revealed the presence of blood vessels in all three regions examined. A mean of 7 and 6 blood vessels was counted in the proximal stump of the animals treated with the control and transduced cells respectively. A mean of 6 and 5 blood vessels was counted in the middle of the device in the animals treated with the control and transduced cells respectively. A lower number of blood vessels was counted in the distal stump of the animals treated with the transduced cells compared to the animals treated with the control cells, means of 7 and 12 respectively (figure 103). The blood vessel diameter in each region was also measured. Higher blood vessel diameter was observed at all three points in the animals treated with the transduced cells (figure 103). In both groups, the diameter of the blood vessels decreased distally. Blood vessels with a mean diameter of 37.3, 33.5 and 23.2 μm were measured in the proximal stump, mid-device and distal stump respectively in the animals treated with the transduced cells. In the animals treated with control cells, blood vessels with a mean diameter of 28.8, 21.7 and 19.5 μm were measured in the proximal stump, mid-device and distal stump respectively. Vasculature in contralateral nerves was examined, revealing an average of 17 blood vessels per nerve with a mean diameter of 18.35 μm .

Figure 103. Examination of vasculature within repair site. Quantitative analysis of a) the number and b) the diameter of blood vessels in transverse sections through the proximal and distal stumps and the middle of the repair device.



7.5 Discussion

Extensive research has been directed towards the development of tissue engineered constructs that can be used to replace the nerve autograft in repairing injured peripheral nerves. However, one of the current limitations of such constructs is insufficient vascularisation following implantation, leading to cell death. Further, vascularisation of tissue engineered constructs was found to increase peripheral nerve regeneration (Iijima *et al.*, 2016). According to D'Arpa *et al.* (2015), vascularised tissue engineered constructs are more functional for the reasons that they can reduce intraneural fibrosis and increase clearance of debris, hence reducing obstruction to axonal growth as well as promoting faster Wallerian degeneration.

This pilot study tested whether EngNT made from SCL4.1/F7 cells overexpressing VEGF-A₁₆₅ increased nerve regeneration through a 15mm gap in a rat sciatic nerve compared to EngNT made from control SCL4.1/F7 cells. These experiments, which used low numbers of animals, were performed to establish the safety and efficacy of VEGF-A₁₆₅ overexpression using the current experimental paradigm. Regeneration was assessed using motor and sensory outcomes, gastrocnemius muscle mass and nerve histology. As each group consisted of only 3 animals, the sample size was considered to be too low for reliable statistical analysis. It was thought that this study could be used for initial experiments to inform a power analysis to determine the group size for a future experiment.

The rat sciatic nerve is the most commonly used model for the study of nerve regeneration using nerve repair devices (Angius *et al.*, 2012). However, it is often difficult to compare results from different studies studying nerve regeneration, as researchers often use different gap lengths, rat strains and time points (Angius *et al.*, 2012). The 15 mm gap used in the current study created a challenging environment for testing regeneration as it represents a critical sized defect (Angius *et al.*, 2012), in which no recovery will occur without the presence of grafting or bridging. An 8 week recovery period was chosen as Georgiou *et al.* (2013) had previously shown, using histological analysis, that EngNT made from SCL4.1/F7 cells had supported robust neuronal regeneration across the gap by this time point.

Functional tests revealed that full motor and sensory recovery was not obtained by the end of the 8 week period in both groups. This observation is in general agreement with other studies, where full recovery during the study period was not achieved after repairing a complete transection with different nerve-gap bridging materials (Sinis *et al.*, 2009). Electrophysiological testing indicated that sufficient nerve regeneration to re-establish functional connections with the gastrocnemius muscle had not occurred in two out of the three animals treated with EngNT made using SCL4.1/F7 cells overexpressing VEGF-A₁₆₅ and one out of the three animals treated with EngNT made using control SCL4.1/F7 cells. It was revealed that these animals also had the lowest percentage of axons reaching the distal stump (section 7.3.3.1) and the highest gastrocnemius muscle atrophy (section 7.3.1.3). When expressed as a percentage of the contralateral, the amplitude of animal 2 was 23.4%. When expressed as a percentage of the contralateral, the amplitudes of the animals treated with the control untransduced SCL4.1/F7 cells were similar to values reported by O'Rourke *et al.* (2018), who implanted EngNT made from CTX0E03 cells into a rat model of sciatic nerve injury (gap length = 12 mm). However, it should be noted that the electrophysiological analysis in the current study yielded highly variable results (table 17), as can be seen from the latency and amplitude obtained for the contralateral nerves which should be all approximately equal.

Functional reinnervation was also confirmed indirectly by examining the gastrocnemius muscle mass. The percentage muscle recovery in the current study ranged between 20-33%, which was lower than expected since previous reports using autografts have shown muscle recovery of around 60% (Jin *et al.*, 2013; Reid *et al.*, 2013). However, these studies tended to use a longer time point, 12 weeks or 18 weeks (Reid *et al.*, 2013) and a shorter (10 mm) gap (Jin *et al.*, 2013; Reid *et al.*, 2013). The values obtained in the current study were comparable to those obtained by O'Rourke *et al.* (2018), who reported a mean recovery of 24% for animals treated with EngNT made from CTX0E03 cells into a rat model of sciatic nerve injury. This was significantly lower than the animals treated with an autograft, but higher than the animals treated with an empty nerve conduit only.

Quantification of neuronal growth revealed the presence of a similar number of neurites in the distal stump in both groups. Histological analysis of cross sections through the proximal and distal parts of the repaired nerves showed that approximately 50% of the number of the neurites in the proximal stump reached the distal stump. This was comparable to previous studies using EngNT constructs made using SCL4.1/F7 cells (Georgiou *et al.*, 2013), ADSCs (Georgiou *et al.*, 2015) and CTX0E03 cells (O'Rourke *et al.*, 2018). However, the rat strain, gap length and conduit material may preclude direct comparison.

The distribution of neuronal growth within the constructs is similar to that observed in earlier studies, with neurites located predominantly on or near the surface of the EngNT (Georgiou *et al.*, 2013; Georgiou *et al.*, 2015; O'Rourke *et al.*, 2018). Little neurite growth was observed in the middle of the EngNT itself, which was similar to observations made by O'Rourke *et al.* (2018) but differed from the original findings of Georgiou *et al.* (2013). However, this could be explained in terms of the implantable device design. In the current study, similar to the study by O'Rourke *et al.* (2018), one EngNT sheet was rolled up and inserted into the conduit. In contrast, Georgiou *et al.* (2013) had used two rolled EngNT rods per conduit. This suggests the number of cells used, as well as the configuration of the EngNT within the conduit, could further increase regeneration.

Unexpectedly, EngNT made of SCL4.1/F7 cells overexpressing VEGF-A₁₆₅ did not increase the number of blood vessels *in vivo* despite promising *in vitro* data. However, it was noted that the blood vessels in the animals treated with EngNT made from SCL4.1/F7 cells overexpressing VEGF-A₁₆₅ had wider diameters than the control group. *in vitro* assays analyse distinct processes of angiogenesis, such as endothelial cell proliferation, migration and tube formation and do not faithfully recapitulate the complex process of angiogenesis as a whole. The results obtained from this study highlight the complexity of angiogenesis, in which *in vitro* results were not representative of *in vivo* data. Immunofluorescence staining for RECA-1 showed the presence of blood vessel structures in the proximal and distal stumps as well as in the middle of the device in both groups. While the presence of VEGF-A₁₆₅ caused an increase in the blood vessel

diameter in the VEGF-A₁₆₅ treated group, it is not known whether this effect was due to the small sample size.

Early studies reported beneficial effects of VEGF on vascularisation, accompanied by increased regeneration in acellular or laminin-gel grafts (Sondell *et al.*, 1999; Hobson *et al.*, 2000; Rovak *et al.*, 2004). Pereira-Lopes *et al.* (2011) showed a positive relationship between increased vascularisation and enhanced nerve regeneration, indicating that VEGF-A₁₆₅ administration can support and enhance the growth of regenerating nerve fibres, probably through a combination of angiogenic and neurotrophic. Hoyng *et al.* (2014) implanted nerve autografts genetically modified to overexpress VEGF-A₁₆₅ in a 10mm gap in a rat sciatic nerve model. They reported that the overexpression of VEGF-A₁₆₅ in autografts induced the formation of blood vessels as early as 2 weeks and hypervascularisation was reported at 20 weeks. However, although enhanced angiogenesis was observed, no significant improvement in regeneration was seen. Conversely, Mohammadi *et al.* (2013) reported increased axonal regeneration at 12 weeks when silicone graft filled VEGF-A₁₆₅ was used to repair 10 mm in a rat sciatic nerve model. However, they did not investigate the effect of VEGF-A₁₆₅ on angiogenesis.

Nikolaev *et al.* (2013) implanted a poly(ϵ -caprolactone) conduit filled with fibrin hydrogel matrix into a 5 mm gap in a rat model of sciatic nerve injury. Immediately after implantation, a double-cassette plasmid delivering the *VEGF* and *FGF2* genes was injected proximally and distally of the reconstructed nerve. Compared to control animals which received the conduit without the therapeutic genes, animals which received the conduit in combination with the therapeutic genes showed an increased number of myelinated fibres in the proximal stump and S100 positive cells in the distal stump after 30 days. Improved motor and sensory recovery of the nerve function, as demonstrated by the sciatic functional index and pinch test, were also shown. An interesting observation made by Nikolaev *et al.* (2013) was that a poly(ϵ -caprolactone) conduit supported regeneration to a greater extent than a silicone conduit. Both conduits were used in combination with the therapeutic genes, but the porous and permeable nature of poly(ϵ -caprolactone) was thought to allow the entry of biomolecules required for regeneration, leading to better outcomes. This is particularly noteworthy as a silicone tube was used in the current study and regeneration was not improved in the animals

treated with EngNT made with SCL4.1/F7 cells overexpressing VEGF-A₁₆₅ compared to EngNT made with control SCL4.1/F7 cells.

Hoben *et al.* (2015) investigated whether the addition of VEGF improved axonal regeneration in acellular nerve allografts in a 20 mm gap in a rat model of sciatic nerve injury. 60 ng of human recombinant VEGF-A₁₆₅ was delivered in a fibrin matrix in the acellular nerve allograft. However, the acellular nerve allografts in combination with VEGF-A₁₆₅ did not increase axonal regeneration to the same extent as an isograft at 10 weeks. A reduced number of total myelinated axons and nerve fibre density was seen in the distal stump of the animals treated with the acellular nerve allografts in combination with VEGF-A₁₆₅. They suggested that this is due to inadequate dosing and delivery of VEGF-A₁₆₅. According to Hoben *et al.* (2015), vascularisation is a key difference between acellular nerve allografts and autografts. Autografts become vascularised through inosculation within 72 hours of implantation via the existing endothelial cell-lined vasculature, while acellular nerve allografts depend on the more extended process of angiogenesis.

Lee *et al.* (2016) repaired a 10-mm sciatic nerve defect in a rat model with an autologous nerve graft and implanted an osmotic pump delivering rat recombinant VEGF-A₁₆₄ adjacent to the graft. The pump delivered a sustained release of 70 ng VEGF/hour for 3 days. While the administration of VEGF-A₁₆₄ increased blood vessel formation, no significant improvement in nerve fibre density or functional recovery at 16 weeks was noted. The authors hypothesised that in autologous nerve grafts, vascularisation may occur rapidly due to intact cells and blood vessels. Thus, the effect of the administered VEGF was minimal. Similar to Hoben *et al.* (2015), they postulate that the effect of VEGF on nerve regeneration may be dose dependent and suggest that the dose and route of administration of VEGF administered was insufficient to enhance axonal elongation across the entire length of the nerve graft.

Man *et al.* (2016) transduced mesenchymal stem cells with a lentiviral vector delivering VEGF-A₁₆₅. *In vitro* assays revealed that the transduced cells significantly increased the proliferation of endothelial cells compared to control untransduced cells. However, when these cells were embedded within a 3D fibrin matrix and transplanted into a 4 mm

gap in a mouse sciatic nerve model, no significant effects on axon regeneration and angiogenesis compared to control cells were reported. The authors attributed this to the fact that while the transduced cells secreted higher levels of VEGF-A₁₆₅ than control cells, the levels may have not been sufficient for increasing angiogenesis *in vivo*. They reported that *in vitro* cultures of 100 000 transduced cells in a 3D matrix secreted a peak 3-day VEGF-A₁₆₅ concentration of approximately 16 ng/ml. This is a significant observation as the transduced SCL4.1/F7 cells in EngNT in silicone tubes in the current study secreted just under 2 ng/ml of VEGF-A₁₆₅ following one day of *in vitro* culture. A kinetic assessment of VEGF-A₁₆₅ release from transduced SCL4.1/F7 cells in EngNT in silicone tubes was not carried out and therefore the peak concentration of the secreted VEGF-A₁₆₅ is unknown.

Therapeutic benefits of cell therapy have been shown in several experimental models of peripheral nerve injury (Fairbairn *et al.*, 2015, Bhangra *et al.*, 2016). Nonetheless, the identification and selection of the most suitable cell source to enhance regeneration remains a significant challenge. The current study investigated the use of SCL4.1/F7 cells overexpressing VEGF-A₁₆₅ to enhance peripheral nerve regeneration. However, this did not result in improved regeneration compared to control SCL4.1/F7 cells. While this cell line has been previously shown to enhance peripheral nerve regeneration (Georgiou *et al.*, 2013), other cell types may result in improved regeneration when used in combination with gene delivery. When ADSCs and CTX0E03 cells were transduced with the lentiviral vector delivering the *VEGF-A₁₆₅* gene, they produced significantly more protein than SCL4.1/F7 cells (section 7.4). This is a significant result because as described in this section, the effects of VEGF-A₁₆₅ may be dose dependent. The higher amount of VEGF-A₁₆₅ produced by these two cell types may significantly increase regeneration compared to untransduced controls. Further, studies using rat ADSCs have shown that these cells can differentiate to a Schwann cell-like phenotype, making them ideal for use in peripheral nerve repair (Kingham *et al.*, 2007; Jiang *et al.*, 2008; Georgiou *et al.*, 2015) and CTX0E03 cells are a clinically relevant stem cell source which can also be differentiated down a glial lineage (Sinden *et al.*, 2017)

7.6 Conclusion

The results obtained from this chapter revealed that clinically relevant sources of stem cells, namely CTX0E03 cells and ADSCs, were amenable to lentiviral transduction and produced high levels of VEGF-A₁₆₅ *in vitro*. When implanted into a rat model of sciatic nerve injury, EngNT made with SCL4.1/F7 cells overexpressing VEGF-A₁₆₅ did not improve regeneration compared to EngNT made from untransduced SCL4.1/F7 cells. Similar numbers of blood vessels were counted in both groups. It was noted that the blood vessels in the animals treated with EngNT made from transduced SCL4.1/F7 cells had a wider diameter. However, this did not result in an improvement in the number of regenerating axons reaching the distal stump. Similar results in terms of functional recovery, electrophysiology and histology were obtained in both groups. The overexpression of VEGF-A₁₆₅ was not associated with any adverse effect *in vivo*.

Chapter 8: Discussion

8.1 Overview

Despite a substantially increased understanding of neuropathophysiology, insufficient functional recovery after peripheral nerve injury remains a significant clinical challenge. The autologous nerve graft is the current clinical gold standard treatment for nerve damage over a few centimetres in length (Pfister *et al.*, 2011). The autologous nerve graft bridges the nerve gap and supplies Schwann cells necessary for regeneration, but it is also associated with several disadvantages, including the sacrifice of a healthy nerve.

Tissue engineered nerve repair devices are emerging as a potential alternative to autologous nerve grafts (Bellamkonda, 2006). Successful tissue engineering strategies require the formation of a stable and mature vascular network following implantation of the tissue engineered construct. In the absence of such a network, the viability of the cells in the constructs is compromised due to mass transport limitations (Xia *et al.*, 2018). In the context of peripheral nerve injury, angiogenesis is also important for nerve regeneration. Studies have shown that vasculature can precede the outgrowth of axons from the proximal stump following injury, suggesting a close relationship between blood vessels and nerves (Hobson *et al.*, 1997). Further, the formation of new blood vessels can support the increased metabolic demands of regenerating nerves (Lovett *et al.*, 2009). Therefore, while nerve repair devices may assist in guiding regenerating nerves, satisfactory functional restoration may also require exogenous angiogenic factors.

VEGF-A₁₆₅ is a potent angiogenic factor that stimulates proliferation and migration of endothelial cells, formation of new blood vessels and enhances vascular permeability (Brockington *et al.*, 2004). Additionally, it has also been shown to increase axonal outgrowth and Schwann cell proliferation (Haninec *et al.*, 2012). Given the importance of VEGF-A₁₆₅ in peripheral nerve tissue engineering, there has been an interest in the development of strategies for delivering it to the implant site. A promising approach is the use of genetically modified cells overexpressing VEGF-A₁₆₅ which can be

incorporated into nerve repair devices to provide a localised and sustained release of VEGF-A₁₆₅.

The goal of this study was to develop an *ex vivo* gene delivery approach as one component of a comprehensive tissue engineering strategy to enhance peripheral nerve repair. Firstly, it was envisaged that labelling cells with luciferase would allow real-time and sustained imaging of the cells in EngNT following implantation *in vivo*. Secondly, it was thought that combined gene delivery and tissue engineering would exert dual beneficial effects on peripheral nerve regeneration: the cellular EngNT would guide and support the regenerating axons while the overexpression of VEGF-A₁₆₅ would exert angiogenic and neurotrophic effects.

8.2 Summary of results

An *in vitro* proof-of-concept study was carried out to deliver marker genes (luciferase and eGFP) to a rat Schwann cell line (SCL4.1/F7) using a lentiviral vector. After establishing that SCL4.1/F7 cells were transduced by monitoring eGFP expression using fluorescence microscopy, flow cytometry revealed a transduction efficiency of over 80%. Transduction did not affect cell morphology, viability or proliferation and long term transgene expression was observed in the transduced cells.

The genetically modified cells were used to construct EngNT and a Z-stack confirmed that cell distribution was uniform throughout. Further, bioluminescence imaging confirmed that the cells were still viable in the EngNT. It was initially thought the presence of the luciferase gene in the expression cassette would allow real-time and sustained imaging of the cells in the EngNT. Bioluminescence imaging provided a reliable method of monitoring the viability of cells in the EngNT *in vitro* but proved to be ineffective for *in vivo* imaging and yielded highly inconsistent data for *ex vivo* imaging.

Having established that SCL4.1/F7 cells were amenable to lentiviral transduction, a lentiviral vector delivering the VEGF-A₁₆₅ gene was designed and produced. Flow cytometry once again confirmed a transduction efficiency of over 80%. The VEGF-A₁₆₅ produced by the transduced SCL4.1/F7 cells increased endothelial cell viability,

migration and tube formation *in vitro*. VEGF-A₁₆₅ also increased SCL4.1/F7 cell proliferation and migration. SCL4.1/F7 cells overexpressing VEGF-A₁₆₅ were found to increase the number of junctions and meshes as well as the total mesh area formed by endothelial cells in a 3D co-culture model. A co-culture consisting of EngNT made from SCL4.1/F7 cells overexpressing VEGF-A₁₆₅ was found to increase PC12 neurite length. Taken together, these results demonstrated that the VEGF-A₁₆₅ produced had positive effects on endothelial cells, Schwann cells and neuron like cells. It was therefore postulated that implanting EngNT made from SCL4.1/F7 cells overexpressing VEGF-A₁₆₅ into a 15 mm gap rat model of sciatic nerve injury would enhance regeneration. Unexpectedly, this did not improve functional recovery, axon counts or overall angiogenesis compared to EngNT made from control SCL4.1/F7 cells. CTX0E03 cells and ADSCs were also successfully transduced with the lentiviral vector delivering VEGF-A₁₆₅, and produced significantly more VEGF-A₁₆₅ than SCL4.1/F7 cells.

8.3 Study limitations

The current study reported a transduction efficiency of over 80% following transduction with the lentiviral vector delivering VEGF-A₁₆₅, resulting in a mixed population of transduced and untransduced cells. Further, different cells in the transduced population potentially express different VEGF-A₁₆₅ levels depending on the vector copy number and on the transcriptional activity resulting from the chromatin organisation around the random integration site (Emery, 2011). Ozawa *et al.* (2004) suggest selecting clones which produce homogenous amounts of VEGF-A₁₆₅ to reduce the risk of aberrant angiogenesis. They showed that VEGF-A₁₆₅ induced angiogenesis depends on the micro environmental amount of VEGF-A₁₆₅ secreted rather than the total number of VEGF-A₁₆₅ expressing cells.

The SCL4.1/F7 Schwann cell line used in the present study was an ideal tool to develop a gene delivery protocol. However, it is a clonally derived diploid immortal rat cell line (Haynes *et al.*, 1994) and is not useful beyond the scope of testing the hypothesis of this study. A key factor limiting the translation of cellular tissue-engineered constructs towards clinical application is the source of therapeutic cells. The current study established that two types of clinically relevant cell types, namely CTX0E03 cells and

ADSCs, are amenable to lentiviral transduction and produced significantly more VEGF-A₁₆₅ than SCL4.1/F7 cells. Given the importance of the concentration of VEGF-A₁₆₅, these cell types could potentially increase regeneration to a greater extent than what was observed in the current study. However, due to time constraints the effect of CTX0E03 cells and ADSCs *in vivo* was not investigated.

Silicone tubes have been traditionally used to investigate peripheral nerve regeneration following injury (Lundborg *et al.*, 1982). While silicone tubes are generally well-tolerated, (Dahlin *et al.*, 2001; Gu *et al.*, 2011), the main problem associated with their use is that they are non-biodegradable and a second surgery is required for their removal (Merle *et al.*, 1989). Further, the impermeability of silicone may limit the diffusion and transport of growth factors through the wall (Stang *et al.*, 2009). The results obtained from the bioluminescence imaging carried out in the current study suggest that the silicone tube acts as a barrier between the cellular EngNT and the surrounding microenvironment. This could have potentially limited the utility of the overexpression of VEGF-A₁₆₅ by limiting its paracrine activity. This highlights the need for more epineurium like material to surround and support the EngNT.

8.4 Future work

Several suggestions for future work have already been made throughout this chapter, including the use of a pure cell population in tissue engineered constructs, genetically modifying clinically relevant cell types and replacing the silicone tube with a biomimetic material. However, further considerations which can improve the results presented in this thesis are discussed here. The tight control of regeneration and repair is one of the ultimate goals in tissue engineering research. Gene delivery offers the potential for both precise and adjustable regeneration enhancement, and is becoming a popular tool in tissue engineering strategies (Balmayor and van Griensven, 2015; Cucchiaroni *et al.*, 2016; Betz *et al.*, 2018). However, research has revealed that continuous overexpression of genes used to enhance regeneration can have deleterious consequences if expressed long-term (Hoyng *et al.*, 2014). There are several ongoing areas of research aimed at further improving gene delivery with the development of novel viral vector designs.

An area of interest is the use of non-integrating lentiviral vectors which have been developed to overcome the risk of insertional mutagenesis (Shaw and Cornetta, 2014). These vectors are deficient in the viral integrase protein and rather than integrating into the host genome DNA, the viral genome remains episomal (Philippe *et al.*, 2006). While gene expression may be expected to be short-lived in dividing cells, this may be useful when high long-term gene expression is not required (Milone and O'Doherty, 2018). According to Blesch and Tuszynski (2007), high levels of angiogenic and neurotrophic factors are only necessary to induce growth and low levels are sufficient to sustain axons that have extended into a cellular graft. Thus, the use of a non-integrating virus can mitigate the prolonged expression of such factors.

In a clinical setting, the SFFV promoter used in the current study is not favourable as it is derived from a gamma retrovirus and may cause safety concerns due to its potential for activating nearby genes leading to malignancy (Modlich *et al.*, 2009). Cellular promoters derived from human housekeeping genes, such as elongation factor-1 α or phosphoglycerate kinase, can reduce this risk (Everson *et al.*, 2018). The human phosphoglycerate kinase promoter has been successfully used in a clinical trial for metachromatic leukodystrophy with promising results (Biffi *et al.*, 2013). In light of this, viral vectors used in future studies aiming to improve peripheral nerve regeneration should incorporate a clinically relevant promoter.

Another means of regulating the expression of angiogenic and neurotrophic factors is the use of duration-controlled inducible gene expression. Ma *et al.* (2016) have described the use of genetically modified mesenchymal stem cells lines comprising two independent inducible gene expression modules, expressing the anti-apoptotic *bcl-2* gene and the chondrogenic master regulatory gene *sox9* for cartilage tissue engineering. Two non-toxic small molecules for specific induction were assembled in controlled-release modules with the gelatin sponge scaffold to permit controlled-duration gene expression. They showed that the anti-apoptotic effect of Bcl-2 could be restrictively activated within the first week upon implantation, while relatively long-term expression of Sox9 to facilitate chondrogenic commitment could persist for up to 4 weeks after implantation. This system was found to better mimic the *in vivo*

expression of these genes and resulted in improved cell cellularity and chondrogenic matrix secretion and prevented potential oncogenic and toxic effects associated with persistent expression of these genes. Time-course gene delivery may also be beneficial in peripheral nerve regeneration and warrants further investigation. In fact, promising results have been reported in a recent study by Mozafari *et al.* (2018). Human embryonic stem cells genetically modified to inducibly overexpress FGF-2 in a fibrin matrix were implanted in a mouse model of sciatic nerve injury. This treatment strategy was successful in the regeneration of sensory and motor fibres, as shown by von Frey testing and immunohistochemistry analysis. Similar results have also been previously reported by Shakhbazau *et al.* (2013) and Wu-Fienberg *et al.* (2014).

While VEGF-A₁₆₅ plays a significant role in angiogenesis, it is unclear whether VEGF-A₁₆₅ is sufficient to promote the formation of mature vessels that can provide adequate blood flow to tissue engineered constructs. Further, it has been shown that excessive administration of VEGF-A₁₆₅ induced the formation of immature and leaky vessels (Springer *et al.*, 1998). It has therefore been suggested that the co-delivery of angiogenic factors may have a synergistic effect on therapeutic angiogenesis. Previous studies have reported the use of VEGF-A₁₆₅ in combination with placental growth factor (Cheng and Sefton, 2009), platelet-derived growth factor (Chen *et al.*, 2007), transforming growth factor- β 1 (Freeman and Cohen, 2009) and basic fibroblast growth factor (Jiang *et al.*, 2016) in a number of animal models. In the context of peripheral nerve tissue engineering, it would be worth investigating whether the delivery of VEGF-A₁₆₅ in combination with another angiogenic factor increases angiogenesis and regeneration compared with the delivery of a single factor.

8.5 Conclusion

While there is a large body of preclinical evidence showing the benefits of gene delivery and tissue engineering to enhance peripheral nerve regeneration, the results in each study were contingent on the animal model used as well as the concentration and duration of the expression of the growth factors used. While the combination of gene delivery and tissue engineering did not improve regeneration in the current study, it emphasised several areas of research which are yet to be fully elucidated. These

include the identification of the best suited therapeutic gene(s), viral vector, cell type and biomaterials. It also highlights that attention needs to be paid to the dose and duration of expression of VEGF-A₁₆₅ to optimise both its angiogenic and neurotrophic effects.

The nerve injury site represents a complex environment with several growth factors and different cell types and a central requirement for successful peripheral nerve repair is the fast and adequate directing of regenerating axons to the correct target organ. An effective therapy may require a combinatorial approach that provides optimised guiding structures, ECM substrates, stimulatory factors and supporting cells. This study represents an important building block in designing a nerve repair device which incorporates all these factors.

9. References

Abbott NJ. Blood-brain barrier structure and function and the challenges for CNS drug delivery. *J Inher Metab Dis*. 2013 May;36(3):437-49.

Aiuti A, Biasco L, Scaramuzza S, Ferrua F, Cicalese MP, Baricordi C, Dionisio F, Calabria A, Giannelli S, Castiello MC, Bosticardo M, Evangelio C, Assanelli A, Casiraghi M, Di Nunzio S, Callegaro L, Benati C, Rizzardi P, Pellin D, Di Serio C, Schmidt M, Von Kalle C, Gardner J, Mehta N, Neduva V, Dow DJ, Galy A, Miniero R, Finocchi A, Metin A, Banerjee PP, Orange JS, Galimberti S, Valsecchi MG, Biffi A, Montini E, Villa A, Ciceri F, Roncarolo MG, Naldini L. Lentiviral hematopoietic stem cell gene therapy in patients with Wiskott-Aldrich syndrome. *Science*. 2013 Aug 23;341(6148):1233151.

Allen AB, Zulma Gazit, Susan Su, Hazel Y. Stevens, and Guldberg RE. In Vivo Bioluminescent Tracking of Mesenchymal Stem Cells Within Large Hydrogel Constructs. *Tissue Eng Part C Methods*. 2014 Oct 1; 20(10): 806–816.

Allodi I, Udina E, Navarro X. Specificity of peripheral nerve regeneration: interactions at the axon level. *Prog Neurobiol*. 2012 Jul;98(1):16-37.

Allodi I, Mecollari V, González-Pérez F, Eggers R, Hoyng S, Verhaagen J, Navarro X, Udina E. Schwann cells transduced with a lentiviral vector encoding Fgf-2 promote motor neuron regeneration following sciatic nerve injury. *Glia*. 2014 Oct;62(10):1736-46.

Amado RG, Chen IS. Lentiviral vectors--the promise of gene therapy within reach? *Science*. 1999 Jul 30;285(5428):674-6.

Angius D, Wang H, Spinner RJ, Gutierrez-Cotto Y, Yaszemski MJ, Windebank AJ. A systematic review of animal models used to study nerve regeneration in tissue-engineered scaffolds. *Biomaterials*. 2012 Nov; 33(32): 8034–8039.

Arthur-Farraj PJ, Latouche M, Wilton DK, Quintes S, Chabrol E, Banerjee A, Woodhoo A, Jenkins B, Rahman M, Turmaine M, Wicher GK, Mitter R, Greensmith L, Behrens A, Raivich G, Mirsky R, Jessen KR. c-Jun reprograms Schwann cells of injured nerves to generate a repair cell essential for regeneration. *Neuron*. 2012 Aug 23;75(4):633-47.

Alvites R, Caseiro AR, Santos Pedrosa S, Vieira Branquinho M, Ronchi G, Geuna S, Varejão ASP, Maurício AC, Spurkland A. Peripheral nerve injury and axonotmesis: state of the art and recent advances. *Cogent Med*. 2018; 5:1.

Amniattalab A, Mohammadi R. Functional, Histopathological and Immunohistochemical Assessments of Cyclosporine A on Sciatic Nerve Regeneration Using Allografts: A Rat Sciatic Nerve Model. *Bull Emerg Trauma*. 2017 Jul; 5(3): 152–159.

Antoine JC, Camdessanché JP. Peripheral nervous system involvement in patients with cancer. *Lancet Neurol*. 2007 Jan; 6(1):75-86.

Atanasoski S, Scherer SS, Sirkowski E, Leone D, Garratt AN, Birchmeier C, Suter U. ErbB2 signaling in Schwann cells is mostly dispensable for maintenance of myelinated peripheral nerves and proliferation of adult Schwann cells after injury. *J Neurosci*. 2006 Feb 15;26(7):2124-31.

Avolio E, Alvino VV, Ghorbel MT, Campagnolo P. Perivascular cells and tissue engineering: Current applications and untapped potential. *Pharmacol Ther*. 2017 Mar;171:83-92.

Aydin H, Azimi FC, Cook JD, Lee JE. A Convenient and General Expression Platform for the Production of Secreted Proteins from Human Cells. *J Vis Exp*. 2012; (65): 4041.

Baba S, Cho SY, Ye Z, Cheng L, Engles JM, Wahl RL. How reproducible is bioluminescent imaging of tumor cell growth? Single time point versus the dynamic measurement approach. *Mol Imaging*. 2007 Sep-Oct;6(5):315-22.

Badr CE. Bioluminescence imaging: basics and practical limitations. *Methods Mol Biol*. 2014;1098:1-18.

Bagó JR, Aguilar E, Alieva M, Soler-Botija C, Vila OF, Claros S, Andrades JA, Becerra J, Rubio N, Blanco J. In vivo bioluminescence imaging of cell differentiation in biomaterials: a platform for scaffold development. *Tissue Eng Part A*. 2013 Mar; 19(5-6): 593–603.

Bainbridge JW, Mehat MS, Sundaram V, Robbie SJ, Barker SE, Ripamonti C, Georgiadis A, Mowat FM, Beattie SG, Gardner PJ, Feathers KL, Luong VA, Yzer S, Balaggan K, Viswanathan A, de Ravel TJ, Casteels I, Holder GE, Tyler N, Fitzke FW, Weleber RG, Nardini M, Moore AT, Thompson DA, Petersen-Jones SM, Michaelides M, van den Born LI, Stockman A, Smith AJ, Rubin G, Ali RR. Long-term effect of gene therapy on Leber's congenital amaurosis. *N Engl J Med*. 2015 May 14;372(20):1887-97.

Balmayor ER, van Griensven M. Gene Therapy for Bone Engineering. *Front Bioeng Biotechnol*. 2015; 3: 9.

Battiston B, Titolo P, Ciclamini D, Panero B. Peripheral Nerve Defects: Overviews of Practice in Europe. *Hand Clin*. 2017 Aug;33(3):545-550.

Becquart P, Cambon-Binder A, Monfoulet LE, Bourguignon M, Vandamme K, Bensidhoum M, Petite H, Logeart-Avramoglou D. Ischemia is the prime but not the only cause of human multipotent stromal cell death in tissue-engineered constructs in vivo. *Tissue Eng Part A*. 2012 Oct;18(19-20):2084-94.

Belanger K, Dinis TM, Taourirt S, Vidal G, Kaplan DL, Egles C. Recent strategies in tissue engineering for guided peripheral nerve regeneration. *Macromol Biosci*. 2016 Apr;16(4):472-81.

Bellamkonda RV. Peripheral nerve regeneration: an opinion on channels, scaffolds and anisotropy. *Biomaterials*. 2006 Jul;27(19):3515-8.

Bellows CG, Melcher AH, Aubin JE. Contraction and organization of collagen gels by cells cultured from periodontal ligament, gingiva and bone suggest functional differences between cell types. *J Cell Sci*. 1981 Aug;50:299-314.

Benito C, Davis CM, Gomez-Sanchez JA, Turmaine M, Meijer D, Poli V, Mirsky R, Jessen KR. STAT3 controls the long-term survival and phenotype of repair Schwann cells during nerve regeneration. *J Neurosci*. 2017 Apr 19;37(16):4255-4269.

Berger F, Paulmurugan R, Bhaumik S, Gambhir SS. Uptake kinetics and biodistribution of 14C-D-luciferin--a radiolabeled substrate for the firefly luciferase catalyzed bioluminescence reaction: impact on bioluminescence based reporter gene imaging. *Eur J Nucl Med Mol Imaging*. 2008 Dec;35(12):2275-85.

Bervar M. Video analysis of standing--an alternative footprint analysis to assess functional loss following injury to the rat sciatic nerve. *J Neurosci Methods*. 2000 Oct 30;102(2):109-16.

Betz VM, Kochanek S, Rammelt S, Müller PE, Betz OB, Messmer C. Recent advances in gene-enhanced bone tissue engineering. *J Gene Med*. 2018 Jun;20(6):e3018.

Bhangra KS, Busuttill F, Phillips JB, Rahim AA. Using stem cells to grow artificial tissue for peripheral nerve repair. *Stem Cells Int.* 2016; 2016: 7502178.

Biffi A, Montini E, Lorioli L, Cesani M, Fumagalli F, Plati T, Baldoli C, Martino S, Calabria A, Canale S, Benedicenti F, Vallanti G, Biasco L, Leo S, Kabbara N, Zanetti G, Rizzo WB, Mehta NA, Cicalese MP, Casiraghi M, Boelens JJ, Del Carro U, Dow DJ, Schmidt M, Assanelli A, Neduva V, Di Serio C, Stupka E, Gardner J, von Kalle C, Bordignon C, Ciceri F, Rovelli A, Roncarolo MG, Aiuti A, Sessa M, Naldini L. Lentiviral hematopoietic stem cell gene therapy benefits metachromatic leukodystrophy. *Science.* 2013 Aug 23;341(6148):1233158.

Blesch A, Tuszynski MH. Transient growth factor delivery sustains regenerated axons after spinal cord injury. *J Neurosci.* 2007 Sep 26;27(39):10535-45.

Bonin RP, Bories C, De Koninck Y. A simplified up-down method (SUDO) for measuring mechanical nociception in rodents using von Frey filaments, *Mol Pain.* 2014; 10: 26.

Boyd JG, Gordon T. Glial cell line-derived neurotrophic factor and brain-derived neurotrophic factor sustain the axonal regeneration of chronically axotomized motoneurons in vivo. *Exp Neurol.* 2003 Oct;183(2):610-9.

Braga-Silva J. The use of silicone tubing in the late repair of the median and ulnar nerves in the forearm. *J Hand Surg Br.* 1999 Dec;24(6):703-6.

Brenneis C, Westhof A, Holschbach J, Michaelis M, Guehring H, Kleinschmidt-Doerr K. Automated Tracking of Motion and Body Weight for Objective Monitoring of Rats in Colony Housing. *J Am Assoc Lab Anim Sci.* 2017 Jan; 56(1): 18–31.

Brockington A, Lewis C, Wharton S, Shaw PJ. Vascular endothelial growth factor and the nervous system. *Neuropathol Appl Neurobiol.* 2004 Oct;30(5):427-46.

Brooks DN, Weber RV, Chao JD, Rinker BD, Zoldos J, Robichaux MR, Ruggeri SB, Anderson KA, Bonatz EE, Wisotsky SM, Cho MS, Wilson C, Cooper EO, Ingari JV, Safa B, Parrett BM, Buncke GM. Processed nerve allografts for peripheral nerve reconstruction: a multicenter study of utilization and outcomes in sensory, mixed, and motor nerve reconstructions. *Microsurgery.* 2012 Jan;32(1):1-14.

Brown RA, Wiseman M, Chuo CB, Cheema U, Nazhat SN. Ultrarapid Engineering of Biomimetic Materials and Tissues: Fabrication of Nano- and Microstructures by Plastic Compression. *Adv Funct Mater.* 2005;15(11):1762-1770.

Brown RA, Phillips JB. Cell responses to biomimetic protein scaffolds used in tissue repair and engineering. *Int Rev Cytol.* 2007;262:75-150.

Burnett MG, Zager EL. Pathophysiology of peripheral nerve injury: a brief review. *Neurosurg Focus.* 2004 May 15;16(5):E1.

Busuttill F, Rahim AA, Phillips JB. Combining gene and stem cell therapy for peripheral nerve tissue engineering. *Stem Cells Dev.* 2017 Feb 15;26(4):231-238.

Callaghan BC, Cheng HT, Stables CL, Smith AL, Feldman EL. Diabetic neuropathy: Clinical manifestations and current treatments. *Lancet Neurol.* 2012 Jun; 11(6): 521–534.

Campana WM. Schwann cells: activated peripheral glia and their role in neuropathic pain. *Brain Behav Immun.* 2007 Jul;21(5):522-7.

Campbell WW. Evaluation and management of peripheral nerve injury. *Clin Neurophysiol.* 2008 Sep;119(9):1951-65.

Carballo-Molina OA, Velasco I. Hydrogels as scaffolds and delivery systems to enhance axonal regeneration after injuries. *Front Cell Neurosci.* 2015; 9: 13.

Carletti E, Motta A, Migliaresi C. Scaffolds for tissue engineering and 3D cell culture. *Methods Mol Biol.* 2011;695:17-39.

Carpentier G. Angiogenesis Analyzer for ImageJ. 2012. Available from: <http://imagej.nih.gov/ij/macros/toolsets/Angiogenesis%20Analyzer.txt>. Accessed 05 Jul 2018.

Cartier N, Hacein-Bey-Abina S, Bartholomae CC, Veres G, Schmidt M, Kutschera I, Vidaud M, Abel U, Dal-Cortivo L, Caccavelli L, Mahlaoui N, Kiermer V, Mittelstaedt D, Bellesme C, Lahlou N, Lefrère F, Blanche S, Audit M, Payen E, Leboulch P, l'Homme B, Bougnères P, Von Kalle C, Fischer A, Cavazzana-Calvo M, Aubourg P. Hematopoietic stem cell gene therapy with a lentiviral vector in X-linked adrenoleukodystrophy. *Science.* 2009 Nov 6;326(5954):818-23.

Castellani S, Di Gioia S, Trotta T, Maffione AB, Conese M. Impact of lentiviral vector-mediated transduction on the tightness of a polarized model of airway epithelium and effect of cationic polymer polyethylenimine. *J Biomed Biotechnol.* 2010;2010:103976.

Castiello MC, Scaramuzza S, Pala F, Ferrua F, Uva P, Brigida I, Sereni L, van der Burg M, Ottaviano G, Albert MH, Grazia Roncarolo M, Naldini L, Aiuti A, Villa A, Bosticardo M. B-cell reconstitution after lentiviral vector-mediated gene therapy in patients with Wiskott-Aldrich syndrome. *J Allergy Clin Immunol.* 2015 Sep;136(3):692-702.e2.

Cattin AL, Burden JJ, Van Emmenis L, Mackenzie FE, Hoving JJ, Garcia Calavia N, Guo Y, McLaughlin M, Rosenberg LH, Quereda V, Jamecna D, Napoli I, Parrinello S, Enver T, Ruhrberg C, Lloyd AC. Macrophage-induced blood vessels guide Schwann cell-mediated regeneration of peripheral nerves. *Cell.* 2015 Aug 27;162(5):1127-39.

Chamcheu, Jean Christopher & M. Adhami, Vaqar & Siddiqui, Imtiaz & Mukhtar, Hasan. (2015). Cutaneous Cell- and Gene-Based Therapies for Inherited and Acquired Skin Disorders. 1091-1122. 10.1201/b18002-52.

Chang WG, Niklason LE. A short discourse on vascular tissue engineering. *NPJ Regen Med.* 2017;2. pii: 7.

Chaplan SR, Bach FW, Pogrel JW, Chung JM, Yaksh TL. Quantitative assessment of tactile allodynia in the rat paw. *J Neurosci Methods.* 1994 Jul;53(1):55-63.

Chen Z, Htay A, Dos Santos W, Gillies GT, Fillmore HL, Sholley MM, Broaddus WC. In vitro angiogenesis by human umbilical vein endothelial cells (HUVEC) induced by three-dimensional co-culture with glioblastoma cells. *J Neurooncol.* 2009 Apr;92(2):121-8.

Chen RR, Silva EA, Yuen WW, Mooney DJ. Spatio-temporal VEGF and PDGF delivery patterns blood vessel formation and maturation. *Pharm Res.* 2007 Feb;24(2):258-64.

Chen TT, Luque A, Lee S, Anderson SM, Segura T, Iruela-Arispe ML. Anchorage of VEGF to the extracellular matrix conveys differential signaling responses to endothelial cells. *J Cell Biol.* 2010 Feb 22;188(4):595-609.

Chen H, Thorne SH. Practical Methods for Molecular In Vivo Optical Imaging. *Curr Protoc Cytom.* 2012; 59(1224): 24.

Cheng D, Sefton MV. Dual delivery of placental growth factor and vascular endothelial growth factor from poly(hydroxyethyl methacrylate-co-methyl methacrylate) microcapsules containing doubly transfected luciferase-expressing L929 cells. *Tissue Eng Part A.* 2009 Aug;15(8):1929-39.

Cheng L, Liu Y, Zhao H, Zhang W, Guo YJ, Nie L. Lentiviral-mediated transfer of CDNF promotes nerve regeneration and functional recovery after sciatic nerve injury in adult rats. *Biochem Biophys Res Commun.* 2013 Oct 18;440(2):330-5.

Chiriac S, Facca S, Diaconu M, Gouzou S, Liverneaux P. Experience of using the bioresorbable copolyester poly(DL-lactide- ϵ -caprolactone) nerve conduit guide Neurolac™ for nerve repair in peripheral nerve defects: report on a series of 28 lesions. *J Hand Surg Eur Vol*. 2012 May;37(4):342-9.

Close DM, Xu T, Sayler GS, Ripp S. In vivo bioluminescent imaging (BLI): noninvasive visualization and interrogation of biological processes in living animals. *Sensors (Basel)*. 2011; 11(1): 180–206.

Cronin J, Zhang XY, Reiser J. Altering the tropism of lentiviral vectors through pseudotyping. *Curr Gene Ther*. 2005 Aug;5(4):387-98.

Cucchiari M, McNulty AL, Mauck RL, Setton LA, Guilak F, Madry H. Advances in combining gene therapy with cell and tissue engineering-based approaches to enhance healing of the meniscus. *Osteoarthritis Cartilage*. 2016 Aug;24(8):1330-9.

Cui L, Jiang J, Wei L, Zhou X, Fraser JL, Snider BJ, Yu SP. Transplantation of embryonic stem cells improves nerve repair and functional recovery after severe sciatic nerve axotomy in rats. *Stem Cells*. 2008 May;26(5):1356-65.

D'Arpa S, Claes KEY, Stillaert F, Colebunders B, Monstrey S, Blondeel P. Vascularised nerve “grafts”: just a graft or a worthwhile procedure? *Plast Aesthet Res*. 2015;2(4):183-94.

Dahlin LB, Lundborg G. Use of tubes in peripheral nerve repair. *Neurosurg Clin N Am*. 2001 Apr;12(2):341-52.

Daly W, Yao L, Zeugolis D, Windebank A, Pandit A. A biomaterials approach to peripheral nerve regeneration: bridging the peripheral nerve gap and enhancing functional recovery. *J R Soc Interface*. 2012 Feb 7;9(67):202-21.

Dégano IR, Vilalta M, Bagó JR, Matthies AM, Hubbell JA, Dimitriou H, Bianco P, Rubio N, Blanco J. Bioluminescence imaging of calvarial bone repair using bone marrow and adipose tissue-derived mesenchymal stem cells. *Biomaterials*. 2008 Feb;29(4):427-37.

DeLisa JA, Gans BM, Walsh NE. *Physical Medicine and Rehabilitation: Principles and Practice*. 2005; 4th ed., Lippincott Williams and Wilkins: Philadelphia, USA.

de Luca AC, Faroni A, Reid AJ. Dorsal root ganglia neurons and differentiated adipose-derived stem cells: an in vitro co-culture model to study peripheral nerve regeneration. *J Vis Exp*. 2015 Feb 26;(96).

de Ruitter GC, Malessy MJ, Yaszemski MJ, Windebank AJ, Spinner RJ. Designing ideal conduits for peripheral nerve repair. *Neurosurg Focus*. 2009 Feb;26(2):E5.

de Winter F, Hoyng S, Tannemaat M, Eggers R, Mason M, Malessy M, Verhaagen J. Gene therapy approaches to enhance regeneration of the injured peripheral nerve. *Eur J Pharmacol*. 2013 Nov 5;719(1-3):145-52.

Deumens R, Bozkurt A, Meek MF, Marcus MA, Joosten EA, Weis J, Brook GA. Repairing injured peripheral nerves: bridging the gap. *Prog Neurobiol*. 2010 Nov;92(3):245-76.

di Summa PG, Kingham PJ, Raffoul W, Wiberg M, Terenghi G, Kalbermatten DF. Adipose-derived stem cells enhance peripheral nerve regeneration. *J Plast Reconstr Aesthet Surg*. 2010 Sep;63(9):1544-52.

Ding F, Wu J, Yang Y, Hu W, Zhu Q, Tang X, Liu J, Gu X. Use of tissue-engineered nerve grafts consisting of a chitosan/poly(lactic-co-glycolic acid)-based scaffold included with bone marrow mesenchymal cells for bridging 50-mm dog sciatic nerve gaps. *Tissue Eng Part A*. 2010 Dec;16(12):3779-90.

- Dixon W. The up-and-down method for small samples. *J Am Stat Assoc.* 1965;60:967–978.
- Dixon AR, Jariwala SH, Bilis Z, Loverde JR, Pasquina PF, Alvarez LM Bridging the gap in peripheral nerve repair with 3D printed and bioprinted conduits. *Biomaterials.* 2018 Sep 12;186:44-63.
- Doddrell RD, Dun XP, Moate RM, Jessen KR, Mirsky R, Parkinson DB. Regulation of Schwann cell differentiation and proliferation by the Pax-3 transcription factor. *Glia.* 2012 Sep;60(9):1269-78.
- Domigan CK, Warren CM, Antanesian V, Happel K, Ziyad S, Lee S, Krall A, Duan L, Torres-Collado AX, Castellani LW, Elashoff D, Christofk HR, van der Blik AM, Potente M, Iruela-Arispe ML. Autocrine VEGF maintains endothelial survival through regulation of metabolism and autophagy. *J Cell Sci.* 2015 Jun 15; 128(12): 2236–2248.
- Donnelly ML, Luke G, Mehrotra A, Li X, Hughes LE, Gani D, Ryan MD. Analysis of the aphthovirus 2A/2B polyprotein 'cleavage' mechanism indicates not a proteolytic reaction, but a novel translational effect: a putative ribosomal 'skip'. *J Gen Virol.* 2001 May;82(Pt 5):1013-25.
- Du J, Liu J, Yao S, Mao H, Peng J, Sun X, Cao Z, Yang Y, Xiao B, Wang Y, Tang P, Wang X. Prompt peripheral nerve regeneration induced by a hierarchically aligned fibrin nanofiber hydrogel. *Acta Biomater.* 2017 Jun;55:296-309.
- Dull T, Zufferey R, Kelly MI, Mandel RJ, Nguyen M, Trono D, Naldini L. A third-generation lentivirus vector with a conditional packaging system. *J Virol.* 1998 Nov; 72(11): 8463–8471.
- Dun XP, Parkinson DB. Visualizing Peripheral Nerve Regeneration by Whole Mount Staining. *PLoS One.* 2015; 10(3): e0119168.
- East E, Blum de Oliveira D, Golding JP, Phillips JB. Alignment of Astrocytes Increases Neuronal Growth in Three-Dimensional Collagen Gels and Is Maintained Following Plastic Compression to Form a Spinal Cord Repair Conduit. *Tissue Eng Part A.* 2010 Oct; 16(10): 3173–3184.
- Eccleston PA, Mirsky R, Jessen KR. Spontaneous immortalisation of Schwann cells in culture: short-term cultured Schwann cells secrete growth inhibitory activity. *Development.* 1991 May;112(1):33-42.
- Edmondson R, Jenkins Broglie J, Adcock AF, Yang L. Three-Dimensional Cell Culture Systems and Their Applications in Drug Discovery and Cell-Based Biosensors. *Assay Drug Dev Technol.* 2014 May 1; 12(4): 207–218.
- Ee X, Yan Y, Hunter DA, Schellhardt L, Sakiyama-Elbert SE, Mackinnon SE, Wood MD. Transgenic SCs expressing GDNF-IRES-DsRed impair nerve regeneration within acellular nerve allografts. *Biotechnol Bioeng.* 2017 Sep;114(9):2121-2130.
- Ellison SM, Trabalza A, Tisato V, Pazarentzos E, Lee S, Papadaki V, Goniotaki D, Morgan S, Mirzaei N, Mazarakis ND. Dose-dependent Neuroprotection of VEGF₁₆₅ in Huntington's Disease Striatum. *Mol Ther.* 2013 Oct; 21(10): 1862–1875.
- Emery DW. The Use of Chromatin Insulators to Improve the Expression and Safety of Integrating Gene Transfer Vectors. *Hum Gene Ther.* 2011 Jun; 22(6): 761–774.
- Erba P, Mantovani C, Kalbermatten DF, Pierer G, Terenghi G, Kingham PJ. Regeneration potential and survival of transplanted undifferentiated adipose tissue-derived stem cells in peripheral nerve conduits. *J Plast Reconstr Aesthet Surg.* 2010 Dec;63(12):e811-7.

- Ernst A, Alkass K, Bernard S, Salehpour M, Perl S, Tisdale J, Possnert G, Druid H, Frisén J. Neurogenesis in the striatum of the adult human brain. *Cell*. 2014 Feb 27;156(5):1072-83.
- Eser F, Aktekin LA, Bodur H, Atan C. Etiological factors of traumatic peripheral nerve injuries. *Neurol India*. 2009 Jul-Aug;57(4):434-7.
- Everson EM, Hocum JD, Trobridge GD. Efficacy and safety of a clinically relevant foamy vector design in human hematopoietic repopulating cells. *J Gene Med*. 2018 Jul;20(7-8):e3028.
- Ezra M, Bushman J, Shreiber D, Schachner M, Kohn J. Porous and nonporous nerve conduits: the effects of a hydrogel luminal filler with and without a neurite-promoting moiety. *Tissue Eng Part A*. 2016 May 1; 22(9-10): 818–826.
- Fairbairn NG, Meppelink AM, Ng-Glazier J, Randolph MA, Winograd JM. Augmenting peripheral nerve regeneration using stem cells: A review of current opinion. *World J Stem Cells*. 2015 Jan 26; 7(1): 11–26.
- Fan X, Ren P, Dhal S, Bejerano G, Goodman SB, Druzin ML, Gambhir SS, Nayak NR. Noninvasive monitoring of placenta-specific transgene expression by bioluminescence imaging. *PLoS One*. 2011; 6(1): e16348.
- Faroni A, Rothwell SW, Grolla AA, Terenghi G, Magnaghi V, Verkhatsky A. Differentiation of adipose-derived stem cells into Schwann cell phenotype induces expression of P2X receptors that control cell death. *Cell Death Dis*. 2013 Jul 25;4:e743.
- Faroni A, Mobasser SA, Kingham PJ, Reid AJ. Peripheral nerve regeneration: experimental strategies and future perspectives. *Adv Drug Deliv Rev*. 2015 Mar;82-83:160-7.
- Ferrara N, Davis-Smyth T. The biology of vascular endothelial growth factor. *Endocr Rev*. 1997 Feb;18(1):4-25.
- Ferrara N, Gerber HP, LeCouter J. The biology of VEGF and its receptors. *Nat Med*. 2003 Jun;9(6):669-76.
- Ferrara N. Vascular endothelial growth factor: basic science and clinical progress. *Endocr Rev*. 2004 Aug;25(4):581-611.
- Ferrier J, Marchand F, Balayssac D. Assessment of Mechanical Allodynia in Rats Using the Electronic Von Frey Test. *Bio-protocol*. 2016; 6(18): e1933.
- Feuer WJ, Schiffman JC, Davis JL, Porciatti V, Gonzalez P, Koilkonda RD, Yuan H, Lalwani A, Lam BL, Guy J. Gene therapy for Leber hereditary optic neuropathy: initial results. *Ophthalmology*. 2016 Mar;123(3):558-70.
- Freeman I, Cohen S. The influence of the sequential delivery of angiogenic factors from affinity-binding alginate scaffolds on vascularisation. *Biomaterials*. 2009 Apr;30(11):2122-31.
- Fu KY, Dai LG, Chiu IM, Chen JR, Hsu SH. Sciatic nerve regeneration by microporous nerve conduits seeded with glial cell line-derived neurotrophic factor or brain-derived neurotrophic factor gene transfected neural stem cells. *Artif Organs*. 2011 Apr;35(4):363-72.
- Gao Y, Weng C, Wang X. Changes in nerve microcirculation following peripheral nerve compression. *Neural Regen Res*. 2013a Apr 15; 8(11): 1041–1047.
- Gao X, Wang Y, Chen J, Peng J. The role of peripheral nerve ECM components in the tissue engineering nerve construction. *Rev Neurosci*. 2013b; 24(4):443-53.
- Gallardo HF, Tan C, Ory D, Sadelain M. Recombinant retroviruses pseudotyped with the vesicular stomatitis virus G glycoprotein mediate both stable gene transfer and pseudotransduction in human peripheral blood lymphocytes. *Blood*. 1997 Aug 1;90(3):952-7.

Gaspar HB, Parsley KL, Howe S, King D, Gilmour KC, Sinclair J, Brouns G, Schmidt M, Von Kalle C, Barington T, Jakobsen MA, Christensen HO, Al Ghonaium A, White HN, Smith JL, Levinsky RJ, Ali RR, Kinnon C, Thrasher AJ. Gene therapy of X-linked severe combined immunodeficiency by use of a pseudotyped gammaretroviral vector. *Lancet*. 2004 Dec 18-31;364(9452):2181-7.

Gaudin R, Knipfer C, Henningsen A, Smeets R, Heiland M, Hadlock T. Approaches to peripheral nerve repair: generations of biomaterial conduits yielding to replacing autologous nerve grafts in craniomaxillofacial surgery. *Biomed Res Int*. 2016;2016:3856262.

Gautam P, Recino A, Foale RD, Zhao J, Gan SU, Wallberg M, Calne R, Lever AM. Promoter optimisation of lentiviral vectors for efficient insulin gene expression in canine mesenchymal stromal cells: potential surrogate beta cells. *J Gene Med*. 2016 Oct;18(10):312-321.

Geering B, Schmidt-Mende J, Federzoni E, Stoeckle C, Simon HU. Protein overexpression following lentiviral infection of primary mature neutrophils is due to pseudotransduction. *J Immunol Methods*. 2011 Oct 28;373(1-2):209-18.

Genetos DC, Cheung WK, Decaris ML, Leach JK. Oxygen tension modulates neurite outgrowth in PC12 cells through a mechanism involving HIF and VEGF. *J Mol Neurosci*. 2010 Mar;40(3):360-6.

Georgiou M, Bunting SC, Davies HA, Loughlin AJ, Golding JP, Phillips JB. Engineered neural tissue for peripheral nerve repair. *Biomaterials*. 2013 Oct;34(30):7335-43.

Georgiou M, Golding JP, Loughlin AJ, Kingham PJ, Phillips JB. Engineered neural tissue with aligned, differentiated adipose-derived stem cells promotes peripheral nerve regeneration across a critical sized defect in rat sciatic nerve. *Biomaterials*. 2015 Jan;37:242-51.

Geraghty RJ, Capes-Davis A, Davis JM, Downward J, Freshney RI, Knezevic I, Lovell-Badge R, Masters JR, Meredith J, Stacey GN, Thraves P, Vias M, Cancer Research UK. Guidelines for the use of cell lines in biomedical research. *Br J Cancer*. 2014 Sep 9;111(6):1021-46.

Gersey ZC, Burks SS, Anderson KD, Dididze M, Khan A, Dietrich WD, Levi AD. First human experience with autologous Schwann cells to supplement sciatic nerve repair: report of 2 cases with long-term follow-up. *Neurosurg Focus*. 2017 Mar;42(3):E2.

Gessmann J, Seybold D, Peter E, Schildhauer TA, MD, Köller M. Alignment of the Fibrin Network Within an Autologous Plasma Clot. *Tissue Eng Part C Methods*. 2016 Jan 1; 22(1): 30–37.

Geuna S, Raimondo S, Ronchi G, Di Scipio F, Tos P, Czaja K, Fornaro M. Chapter 3: Histology of the peripheral nerve and changes occurring during nerve regeneration. *Int Rev Neurobiol*. 2009;87:27-46.

Geuze RE, Prins HJ, Öner FC, van der Helm YJ, Schuijff LS, Martens AC, Kruyt MC, Alblas J, Dhert WJ. Luciferase labeling for multipotent stromal cell tracking in spinal fusion versus ectopic bone tissue engineering in mice and rats. *Tissue Eng Part A*. 2010 Nov;16(11):3343-51.

Gholipourmalekabadi M, Zhao S, Harrison BS, Mozafari M, Seifalian AM. Oxygen-Generating Biomaterials: A New, Viable Paradigm for Tissue Engineering? *Trends Biotechnol*. 2016 Dec;34(12):1010-1021.

Gholobova D, Decroix L, Van Muylder V, Desender L, Gerard M, Carpentier G, Vandenburg H, Thorrez L. Endothelial Network Formation Within Human Tissue-Engineered Skeletal Muscle. *Tissue Eng Part A*. 2015 Oct 1; 21(19-20): 2548–2558.

Giubellino A, Woldemichael GM, Sourbier C, Lizak MJ, Powers JF, Tischler AS, Pacak K. Characterization of two mouse models of metastatic pheochromocytoma using bioluminescence imaging. *Cancer Lett.* 2012 Mar; 316(1): 46–52.

Gnavi S, di Blasio L, Tonda-Turo C, Mancardi A, Primo L, Ciardelli G, Gambarotta G, Geuna S, Perroteau I. Gelatin-based hydrogel for vascular endothelial growth factor release in peripheral nerve tissue engineering. *J Tissue Eng Regen Med.* 2017 Feb;11(2):459-470.

Godinho MJ, Teh L, Pollett MA, Goodman D, Hodgetts SI, Sweetman I, Walters M, Verhaagen J, Plant GW, Harvey AR. Immunohistochemical, Ultrastructural and Functional Analysis of Axonal Regeneration through Peripheral Nerve Grafts Containing Schwann Cells Expressing BDNF, CNTF or NT3. *PLoS One.* 2013; 8(8): e69987.

Goliwas KF, Richter JR, Pruitt HC, Araysi LM, Anderson NR, Samant RS, Lobo-Ruppert SM, Berry JL, Frost AR. Methods to Evaluate Cell Growth, Viability, and Response to Treatment in a Tissue Engineered Breast Cancer Model. *Sci Rep.* 2017; 7: 14167.

Gomez-Sanchez JA, Carty L, Iruarrizaga-Lejarreta M, Palomo-Irigoyen M, Varela-Rey M, Griffith M, Hantke J, Macias-Camara N, Azkargorta M, Aurrekoetxea I, Gutiérrez De Juan V, Jefferies HBJ, Aspichueta P, Elortza F, Aransay A, Martínez-Chantar ML, Baas F, Mato JM, Mirsky R, Woodhoo A, Jessen KR. Schwann cell autophagy, myelinophagy, initiates myelin clearance from injured nerves. *J Cell Biol.* 2015 Jul 6; 210(1): 153–168.

Gordon T, English AW. Strategies to promote peripheral nerve regeneration: electrical stimulation and/or exercise. *Eur J Neurosci.* 2016 Feb; 43(3): 336–350.

Greenwood HL, Singer PA, Downey GP, Martin DK, Thorsteinsdóttir H, Daar AS. Regenerative medicine and the developing world. *PLoS Med.* 2006 Sep;3(9):e381.

Grinsell D, Keating CP, Grinsell D, Keating CP. Peripheral nerve reconstruction after injury: a review of clinical and experimental therapies. *BioMed Res Int.* 2014;2014:1–13.

Grochmal J, Dhaliwal S, Stys PK, van Minnen J, Midha R. Skin-derived precursor Schwann cell myelination capacity in focal tibial demyelination. *Muscle Nerve.* 2014 Aug;50(2):262-72.

Grounds MD. Obstacles and challenges for tissue engineering and regenerative medicine: Australian nuances. *Clin Exp Pharmacol Physiol.* 2018 Apr;45(4):390-400.

Gu X, Ding F, Williams DF. Neural tissue engineering options for peripheral nerve regeneration. *Biomaterials.* 2014 Aug;35(24):6143-56.

Haas DL, Case SS, Crooks GM, Kohn DB. Critical factors influencing stable transduction of human CD34(+) cells with HIV-1-derived lentiviral vectors. *Mol Ther.* 2000 Jul;2(1):71-80.

Haastert K, Lipokatic E, Fischer M, Timmer M, Grothe C. Differentially promoted peripheral nerve regeneration by grafted Schwann cells over-expressing different FGF-2 isoforms. *Neurobiol Dis.* 2006 Jan;21(1):138-53.

Hacein-Bey-Abina S, Hauer J, Lim A, Picard C, Wang GP, Berry CC, Martinache C, Rieux-Laucat F, Latour S, Belohradsky BH, Leiva L, Sorensen R, Debré M, Casanova JL, Blanche S, Durandy A, Bushman FD, Fischer A, Cavazzana-Calvo M. Efficacy of gene therapy for X-linked severe combined immunodeficiency. *N Engl J Med.* 2010 Jul 22;363(4):355-64.

Hall S. The response to injury in the peripheral nervous system. *J Bone Joint Surg Br.* 2005 Oct;87(10):1309-19.

Hamaguchi I, Woods NB, Panagopoulos I, Andersson E, Mikkola H, Fahlman C, Zufferey R, Carlsson L, Trono D, Karlsson S. Lentivirus vector gene expression during ES cell-derived hematopoietic development in vitro. *J Virol*. 2000 Nov;74(22):10778-84.

Han IS, Seo TB, Kim KH, Yoon JH, Yoon SJ, Namgung U. Cdc2-mediated Schwann cell migration during peripheral nerve regeneration. *J Cell Sci*. 2007 Jan 15;120(Pt 2):246-55.

Haninec P, Kaiser R, Bobek V, Dubový P. Enhancement of musculocutaneous nerve reinnervation after vascular endothelial growth factor (VEGF) gene therapy. *BMC Neurosci*. 2012 Jun 6;13:57. Hanjaya-Putra D, Yee J, Ceci D, Truitt R, Yee D, Gerecht S. Vascular endothelial growth factor and substrate mechanics regulate in vitro tubulogenesis of endothelial progenitor cells. *J Cell Mol Med*. 2010 Oct; 14(10): 2436–2447.

Harrisingh MS, Perez-Nadales E, Parkinson DB, Malcolm DS, Mudge AW, Lloyd AC. The Ras/Raf/ERK signalling pathway drives Schwann cell dedifferentiation. *EMBO J*. 2004 Aug 4; 23(15): 3061–3071.

Hart ML, Lauer JC, Selig M, Hanak M, Walters B, Rolauffs B. Shaping the Cell and the Future: Recent Advancements in Biophysical Aspects Relevant to Regenerative Medicine. *J Funct Morphol Kinesiol*. 2018; 3(1):2.

Hastie E, Cataldi M, Marriott I, Grdzlishvili VZ. Understanding and altering cell tropism of vesicular stomatitis virus. *Virus Res*. 2013 Sep;176(1-2):16-32.

Hayashi A, Koob JW, Liu DZ, Tong AY, Hunter DA, Parsadonian A, Mackinnon SE, Myckatyn TM. A double-transgenic mouse used to track migrating Schwann cells and regenerating axons following engraftment of injured nerves. *Exp Neurol*. 2007 Sep;207(1):128-38.

Haynes LW, Rushton JA, Perrins MF, Dyer JK, Jones R, Howell R. Diploid and hyperdiploid rat Schwann cell strains displaying negative autoregulation of growth in vitro and myelin sheath-formation in vivo. *J Neurosci Methods*. 1994 Jun;52(2):119-27.

He Q, Yao CL, Li L, Xin Z, Jing ZK, Li LX. Targeted gene therapy and in vivo bioluminescent imaging for monitoring postsurgical recurrence and metastasis in mouse models of liver cancer. *Genet Mol Res*. 2016 Aug 12;15(3).

Hirata K, Kawabuchi M. Myelin phagocytosis by macrophages and nonmacrophages during Wallerian degeneration. *Microsc Res Tech*. 2002;57:541–547.

Hoben G, Yan Y, Iyer N, Newton P, Hunter DA, Moore AM, Sakiyama-Elbert SE, Wood MD, Mackinnon SE. Comparison of acellular nerve allograft modification with Schwann cells or VEGF. *Hand (N Y)*. 2015 Sep; 10(3): 396–402.

Hobson MI, Green CJ, Terenghi G. VEGF enhances intraneural angiogenesis and improves nerve regeneration after axotomy. *J Anat*. 2000 Nov;197 Pt 4:591-605.

Hoeben A, Landuyt B, Highley MS, Wildiers H, Van Oosterom AT, De Bruijn EA. Vascular endothelial growth factor and angiogenesis. *Pharmacol Rev*. 2004 Dec;56(4):549-80.

Hoffman-Kim D, Mitchel JA, Bellamkonda RV. Topography, cell response, and nerve regeneration. *Annu Rev Biomed Eng*. 2010 Aug 15;12:203-31.

Holmes DIR, Zachary I. The vascular endothelial growth factor (VEGF) family: angiogenic factors in health and disease. *Genome Biol*. 2005; 6(2): 209.

Horch RE, Boos AM, Quan Y, Bleiziffer O, Detsch R, Boccaccini AR, Alexiou C, Sun J, Beier JP, Arkudas A. Cancer research by means of tissue engineering-is there a rationale? *J Cell Mol Med*. 2013 Oct;17(10):1197-206.

Houck KA, Leung DW, Rowland AM, Winer J, Ferrara N. Dual regulation of vascular endothelial growth factor bioavailability by genetic and proteolytic mechanisms. *J Biol Chem*. 1992 Dec 25;267(36):26031-7.

Hoyng SA, Gnavi S, de Winter F, Eggers R, Ozawa T, Zaldumbide A, Hoeben RC, Malessy MJ, Verhaagen J. Developing a potentially immunologically inert tetracycline-regulatable viral vector for gene therapy in the peripheral nerve. *Gene Ther*. 2014 Jun;21(6):549-57.

Hoyng SA, de Winter F, Tannemaat MR, Blits B, Malessy MJA, Verhaagen J. Gene therapy and peripheral nerve repair: a perspective. *Front Mol Neurosci*. 2015a; 8: 32.

Hoyng SA, De Winter F, Gnavi S, van Egmond L, Attwell CL, Tannemaat MR, Verhaagen J, Malessy MJ. Gene delivery to rat and human Schwann cells and nerve segments: a comparison of AAV 1-9 and lentiviral vectors. *Gene Ther*. 2015b Oct;22(10):767-80.

Hsu MN, Liao HT, Li KC, Chen HH, Yen TC, Makarevich P, Parfyonova Y, Hu YC. Adipose-derived stem cell sheets functionalized by hybrid baculovirus for prolonged GDNF expression and improved nerve regeneration. *Biomaterials*. 2017 Sep;140:189-200.

Hu X, Cai J, Yang J, Smith GM. Sensory axon targeting is increased by NGF gene therapy within the lesioned adult femoral nerve, *Exp Neurol*. 2010 May; 223(1): 153–165.

Huebner EA, Strittmatter SM. Axon regeneration in the peripheral and central nervous systems. *Results Probl Cell Differ*. 2009;48:339-51.

Hulkower KI, Herber RL. Cell migration and invasion assays as tools for drug discovery. *Pharmaceutics*. 2011 Mar 11;3(1):107-24.

Hung HA, Sun G, Keles S, Svaren J. Dynamic regulation of Schwann cell enhancers after peripheral nerve injury. *J Biol Chem*. 2015 Mar 13;290(11):6937-50.

Hwang DW, Jin Y, Lee DH, Kim HY, Cho HN, Chung HJ, Park Y, Youn H, Lee SJ, Lee HJ, Kim SU, Wang KC, Lee DS. In vivo bioluminescence imaging for prolonged survival of transplanted human neural stem cells using 3D biocompatible scaffold in corticectomized rat model. *PLoS One*. 2014a;9(9):e105129.

Hwang DW, Park KM, Shim HK, Jin Y, Oh H, Oh SW, Lee S, Youn H, Joung YK, Lee HJ, Kim SU, Park KD, Lee DS. In vivo bioluminescence imaging for viable human neural stem cells incorporated within in situ gelatin hydrogels. *EJNMMI Res*. 2014b; 4: 61.

Iijima Y, Ajiki T, Murayama A, Takeshita K. Effect of Artificial Nerve Conduit Vascularisation on Peripheral Nerve in a Necrotic Bed. *Plast Reconstr Surg Glob Open*. 2016 Mar 22;4(3):e665.

Inoue Y, Kiryu S, Izawa K, Watanabe M, Tojo A, Ohtomo K. Comparison of subcutaneous and intraperitoneal injection of D-luciferin for in vivo bioluminescence imaging. *Eur J Nucl Med Mol Imaging*. 2009 May;36(5):771-9.

Irvin MW, Zijlstra A, Wikswo JP, Pozzi A. Techniques and assays for the study of angiogenesis. *Exp Biol Med (Maywood)*. 2014 Nov; 239(11): 1476–1488.

Iwaguro H, Yamaguchi J, Kalka C, Murasawa S, Masuda H, Hayashi S, Silver M, Li T, Isner JM, Asahara T. Endothelial progenitor cell vascular endothelial growth factor gene transfer for vascular regeneration. *Circulation*. 2002 Feb 12;105(6):732-8.

Iwano S, Sugiyama M, Hama H, Watakabe A, Hasegawa N, Kuchimaru T, Tanaka KZ, Takahashi M, Ishida Y, Hata J, Shimozono S, Namiki K, Fukano T, Kiyama M, Okano H, Kizaka-Kondoh S, McHugh TJ, Yamamori T, Hioki H, Maki S, Miyawaki A. Single-cell bioluminescence imaging of deep tissue in freely moving animals. *Science*. 2018 Feb 23;359(6378):935-939.

Jabbarzadeh E, Starnes T, Khan YM, Jiang T, Wirtel AJ, Deng M, Lv Q, Nair LS, Doty SB, Laurencin CT. Induction of angiogenesis in tissue-engineered scaffolds designed for bone repair: a combined gene therapy-cell transplantation approach. *Proc Natl Acad Sci U S A*. 2008 Aug 12;105(32):11099-104.

Jessen KR, Mirsky R, Lloyd AC. Schwann cells: development and role in nerve repair. *Cold Spring Harb Perspect Biol*. 2015;7(7):a020487.

Jessen KR, Mirsky R. The repair Schwann cell and its function in regenerating nerves. *J Physiol*. 2016 Jul 1; 594(13): 3521–3531.

Jeyaraj R, G N, Kirby G, Rajadas J, Mosahebi A, Seifalian AM, Tan A. Vascularisation in regenerative therapeutics and surgery. *Mater Sci Eng C Mater Biol Appl*. 2015 Sep;54:225-38.

Jiang L, Zhu JK, Liu XL, Xiang P, Hu J, Yu WH. Differentiation of rat adipose tissue-derived stem cells into Schwann-like cells in vitro. *Neuroreport*. 2008 Jul 2;19(10):1015-9.

Jiang H, Qu W, Han F, Liu D, Zhang W. Establishment of immortalized Schwann cells derived from rat embryo dorsal root ganglia. *Int J Mol Med*. 2012 Sep; 30(3): 480–486.

Jiang X, Lin H, Jiang D, Xu G, Fang X, He L, Xu M, Tang B, Wang Z, Cui D, Chen F, Geng H. Co-delivery of VEGF and bFGF via a PLGA nanoparticle-modified BAM for effective contracture inhibition of regenerated bladder tissue in rabbits. *Sci Rep*. 2016; 6: 20784.

Jin J, Limburg S, Joshi SK, Landman R, Park M, Zhang Q, Kim HT, Kuo AC. Peripheral Nerve Repair in Rats Using Composite Hydrogel-Filled Aligned Nanofiber Conduits with Incorporated Nerve Growth Factor. *Tissue Eng Part A*. 2013 Oct; 19(19-20): 2138–2146.

Joglekar AV, Sandoval S. Pseudotyped Lentiviral Vectors: One Vector, Many Guises. *Hum Gene Ther Methods*. 2017 Dec;28(6):291-301.

Johnson PJ, Wood MD, Moore AM, Mackinnon SE. Tissue engineered constructs for peripheral nerve surgery. *Eur Surg*. 2013 Jun; 45(3):10.

Jundziłł A, Pokrywczyńska M, Adamowicz J, Kowalczyk T, Nowacki M, Bodnar M, Marszałek A, Frontczak-Baniewicz M, Mikułowski G, Kloskowski T, Gatherwright J, Drewa T. Vascularisation potential of electrospun poly(L-lactide-co-caprolactone) scaffold: the impact for tissue engineering. *Med Sci Monit*. 2017; 23: 1540–1551.

Jurecka W, Ammerer HP, Lassmann H. Regeneration of a transected peripheral nerve. An autoradiographic and electron microscopic study. *Acta Neuropathol*. 1975 Oct 1;32(4):299-312.

Kabiri M, Oraee-Yazdani S, Shafiee A, Hanaee-Ahvaz H, Dodel M, Vaseei M, Soleimani M. Neuroregenerative effects of olfactory ensheathing cells transplanted in a multi-layered conductive nanofibrous conduit in peripheral nerve repair in rats. *J Biomed Sci*. 2015; 22(1): 35.

Kaplan HM, Mishra P, Kohn J. The overwhelming use of rat models in nerve regeneration research may compromise designs of nerve guidance conduits for humans. *J Mater Sci Mater Med*. 2015; 26(8): 226.

Kaya Y, Sarikcioglu L. Sir Herbert Seddon (1903-1977) and his classification scheme for peripheral nerve injury. *Childs Nerv Syst*. 2015 Feb;31(2):177-80.

Kehoe S, Zhang XF, Boyd D. FDA approved guidance conduits and wraps for peripheral nerve injury: a review of materials and efficacy. *Injury*. 2012 May;43(5):553-72.

Keir PJ, Rempel DM. Pathomechanics of peripheral nerve loading. Evidence in carpal tunnel syndrome. *J Hand Ther*. 2005 Apr-Jun;18(2):259-69.

Keyaerts M, Verschueren J, Bos TJ, Tchouate-Gainkam LO, Peleman C, Breckpot K, Vanhove C, Caveliers V, Bossuyt A, Lahoutte T. Dynamic bioluminescence imaging for quantitative tumour burden assessment using IV or IP administration of D: -Luciferin: effect on intensity, time kinetics and repeatability of photon emission. *Eur J Nucl Med Mol Imaging*. 2008 May;35(5):999-1007.

Khalil AA, Jameson MJ, Broaddus WC, Chung TD, Golding SE, Dever S, Rosenberg E, Valerie K. Subcutaneous administration of D-luciferin is an effective alternative to intraperitoneal injection in bioluminescence imaging of xenograft tumors in nude mice. *ISRN Mol Imaging*. 2013; 2013: 689279.

Kim VN, Mitrophanous K, Kingsman SM, Kingsman AJ. Minimal requirement for a lentivirus vector based on human immunodeficiency virus type 1. *J Virol*. 1998 Jan;72(1):811-6.

Kim JB, Urban K, Cochran E, Lee S, Ang A, Rice B, Bata A, Campbell K, Coffee R, Gorodinsky A, Lu Z, Zhou H, Kishimoto TK, Lassota P. Non-Invasive Detection of a Small Number of Bioluminescent Cancer Cells In Vivo. *PLoS One*. 2010; 5(2): e9364.

Kim SH, Jun HJ, Jang SI, You JC. The determination of importance of sequences neighboring the Psi sequence in lentiviral vector transduction and packaging efficiency. *PLoS One*. 2012; 7(11): e50148.

Kim HA, Mindos T, Parkinson DB. Plastic fantastic: Schwann cells and repair of the peripheral nervous system. *Stem Cells Transl Med*. 2013 Aug;2(8):553-7.

Kim JI, Hwang TI, Aguilar LE, Park CH, Kim CS. A Controlled Design of Aligned and Random Nanofibers for 3D Bi-functionalized Nerve Conduits Fabricated via a Novel Electrospinning Set-up. *Sci Rep*. 2016; 6: 23761.

Kimura H, Fischer WH, Schubert D. Structure, expression and function of a schwannoma-derived growth factor. *Nature*. 1990 Nov 15;348(6298):257-60.

Kingham PJ, Kalbermatten DF, Mahay D, Armstrong SJ, Wiberg M, Terenghi G. Adipose-derived stem cells differentiate into a Schwann cell phenotype and promote neurite outgrowth in vitro. *Exp Neurol*. 2007 Oct;207(2):267-74.

Kingham PJ, Kolar MK, Novikova LN, Novikov LN, Wiberg M. Stimulating the neurotrophic and angiogenic properties of human adipose-derived stem cells enhances nerve repair. *Stem Cells Dev*. 2014 Apr 1;23(7):741-54.

Klein S, Vykoukal J, Felthaus O, Dienstknecht T, Prantl L. Collagen Type I Conduits for the Regeneration of Nerve Defects. *Materials (Basel)*. 2016 Mar 23;9(4). pii: E219.

Ko KR, Frampton JP. Developments in 3D neural cell culture models: the future of neurotherapeutics testing? *Expert Rev Neurother*. 2016 Jul;16(7):739-41.

Kokai LE, Bourbeau D, Weber D, McAtee J, Marra KG. Sustained Growth Factor Delivery Promotes Axonal Regeneration in Long Gap Peripheral Nerve Repair. *Tissue Eng Part A*. 2011 May; 17(9-10): 1263–1275.

Kokkalis ST, Mavrogenis AF, Vottis C, Papatheodorou L, Papagelopoulos PJ, Soucacos PN, Sotereanos DG. Median nerve biodegradable wrapping: Clinical outcome of 10 patients. *Acta Orthop Belg*. 2016 Aug;82(2):351-357.

Kömürcü F, Zwolak P, Benditte-Klepetko H, Deutinger M. Management strategies for peripheral iatrogenic nerve lesions. *Ann Plast Surg*. 2005 Feb;54(2):135-9.

Korte N, Schenk HC, Grothe C, Tipold A, Haastert-Talini K. Evaluation of periodic electrodiagnostic measurements to monitor motor recovery after different peripheral nerve lesions in the rat. *Muscle Nerve*. 2011 Jul;44(1):63-73.

Kouyoumdjian JA. Peripheral nerve injuries: a retrospective survey of 456 cases. *Muscle Nerve*. 2006 Dec;34(6):785-8.

Knight E, Przyborski S. Advances in 3D cell culture technologies enabling tissue-like structures to be created in vitro. *J Anat*. 2015 Dec;227(6):746-56.

Kuroda H, Kutner RH, Bazan NG, Reiser J. Simplified lentivirus vector production in protein-free media using polyethylenimine-mediated transfection. *J Virol Methods*. 2009 May;157(2):113-21.

Kutschka I, Chen IY, Kofidis T, Arai T, von Degenfeld G, Sheikh AY, Hendry SL, Pearl J, Hoyt G, Sista R, Yang PC, Blau HM, Gambhir SS, Robbins RC. Collagen matrices enhance survival of transplanted cardiomyoblasts and contribute to functional improvement of ischemic rat hearts. *Circulation*. 2006 Jul 4;114(1 Suppl):1167-73.

Lackington WA, Ryan AJ, O'Brien FJ. Advances in Nerve Guidance Conduit-Based Therapeutics for Peripheral Nerve Repair. *ACS Biomater Sci Eng*. 2017;3(7):1221-1235.

Laschke MW, Menger MD. Vascularisation in tissue engineering: angiogenesis versus inosculation. *Eur Surg Res*. 2012;48(2):85-92.

Lee KH, Byun SS, Paik JY, Lee SY, Song SH, Choe YS, Kim BT. Cell uptake and tissue distribution of radioiodine labelled D-luciferin: implications for luciferase based gene imaging. *Nucl Med Commun*. 2003 Sep;24(9):1003-9.

Lee CI, Kohn DB, Ekert JE, Tarantal AF. Morphological analysis and lentiviral transduction of fetal monkey bone marrow-derived mesenchymal stem cells. *Mol Ther*. 2004 Jan;9(1):112-23.

Lee JY, Giusti G, Friedrich PF, Bishop AT, Shin AY. Effect of Vascular Endothelial Growth Factor Administration on Nerve Regeneration after Autologous Nerve Grafting. *J Reconstr Microsurg*. 2016 Mar;32(3):183-8.

Leferink AM, van Blitterswijk CA, Moroni L. Methods of monitoring cell fate and tissue growth in three-dimensional scaffold-based strategies for in vitro tissue engineering. *Tissue Eng Part B Rev*. 2016 Aug;22(4):265-83.

Lehmann HC, Höke A. Use of engineered Schwann cells in peripheral neuropathy: Hopes and hazards. *Brain Res*. 2016 May 1;1638(Pt A):97-104.

Levenberg S, Rouwkema J, Macdonald M, Garfein ES, Kohane DS, Darland DC, Marini R, van Blitterswijk CA, Mulligan RC, D'Amore PA, Langer R. Engineering vascularised skeletal muscle tissue. *Nat Biotechnol*. 2005 Jul;23(7):879-84.

Li R, Liu Z, Pan Y, Chen L, Zhang Z, Lu L. Peripheral nerve injuries treatment: a systematic review. *Cell Biochem Biophys*. 2014 Apr;68(3):449-54.

Li M, Wang Y, Liu M, Lan X. Multimodality reporter gene imaging: Construction strategies and application. *Theranostics*. 2018 Apr 18;8(11):2954-2973.

Liard O, Segura S, Sagui E, Nau A, Pascual A, Cambon M, Darlix JL, Fusai T, Moysé E. Adult-brain-derived neural stem cells grafting into a vein bridge increases postlesional recovery and regeneration in a peripheral nerve of adult pig. *Stem Cells Int*. 2012;2012:128732.

Lim E, Modi KD, Kim J. In vivo bioluminescent imaging of mammary tumors using IVIS spectrum. *J Vis Exp*. 2009 Apr 29;(26). pii: 1210.

Lin H, Liu F, Zhang C, Zhang Z, Kong Z, Zhang X, Hoffman RM. Characterization of nerve conduits seeded with neurons and Schwann cells derived from hair follicle neural crest stem cells. *Tissue Eng Part A*. 2011 Jul;17(13-14):1691-8.

Lin P, Lin Y, Lennon DP, Correa D, Schluchter M, Caplan AI. Efficient Lentiviral Transduction of Human Mesenchymal Stem Cells That Preserves Proliferation and Differentiation Capabilities. *Stem Cells Transl Med*. 2012 Dec; 1(12): 886–897.

Lin MY, Manzano G, Gupta R. Nerve allografts and conduits in peripheral nerve repair. *Hand Clin*. 2013 Aug;29(3):331-48.

Liu Q, Spusta SC, Mi R, Lassiter RN, Stark MR, Höke A, Rao MS, Zeng X. Human neural crest stem cells derived from human ESCs and induced pluripotent stem cells: induction, maintenance, and differentiation into functional Schwann cells. *Stem Cells Transl Med*. 2012 Apr;1(4):266-78.

Liu Y, Nie L, Zhao H, Zhang W, Zhang YQ, Wang SS, Cheng L. Conserved dopamine neurotrophic factor-transduced mesenchymal stem cells promote axon regeneration and functional recovery of injured sciatic nerve. *PLoS One*. 2014 Oct 24;9(10):e110993.

Liu Z, Chen O, Wall JBJ, Zheng M, Zhou Y, Wang L, Ruth Vaseghi H, Qian L, Liu J. Systematic comparison of 2A peptides for cloning multi-genes in a polycistronic vector. *Sci Rep*. 2017 May 19;7(1):2193.

Logeart-Avramoglou D, Oudina K, Bourguignon M, Delpierre L, Nicola MA, Bensidhoum M, Arnaud E, Petite H. In vitro and in vivo bioluminescent quantification of viable stem cells in engineered constructs. *Tissue Eng Part C Methods*. 2010 Jun;16(3):447-58.

Lomakina GY, Modestova YA, Ugarova NN. Bioluminescence assay for cell viability. *Biochemistry (Mosc)*. 2015 Jun;80(6):701-13.

Lovett M, Lee K, Edwards A, Kaplan DL. Vascularisation strategies for tissue engineering. *Tissue Eng Part B Rev*. 2009 Sep;15(3):353-70.

Lundborg G, Dahlin LB, Danielsen N, Gelberman RH, Longo FM, Powell HC, Varon S. Nerve regeneration in silicone chambers: influence of gap length and of distal stump components. *Exp Neurol*. 1982 May;76(2):361-75.

Luo M, Huan Huang, Hou L, Shao S, Huang S, Zhao X. Construction and expression of a lentivirus expression vector carrying the VEGF165-EGFP fusion gene in breast cancer MCF-7 cells. *Oncol Lett*. 2017 Mar; 13(3): 1745–1752.

Ma F, Xiao Z, Meng D, Hou X, Zhu J, Dai J, Xu R. Use of Natural Neural Scaffolds Consisting of Engineered Vascular Endothelial Growth Factor Immobilized on Ordered Collagen Fibers Filled in a Collagen Tube for Peripheral Nerve Regeneration in Rats. *Int J Mol Sci*. 2014 Oct; 15(10): 18593–18609.

Ma Y, Li J, Yao T, Wei D, Wang R, Qiong W. A controlled double-duration inducible gene expression system for cartilage tissue engineering. *Sci Rep*. 2016; 6: 26617.

Madduri S, di Summa P, Papaloizos M, Kalbermatten D, Gander B. Effect of controlled co-delivery of synergistic neurotrophic factors on early nerve regeneration in rats. *Biomaterials*. 2010 Nov;31(32):8402-9.

Madduri S, Gander B. Growth factor delivery systems and repair strategies for damaged peripheral nerves. *J Control Release*. 2012 Jul 20;161(2):274-82.

Makarevich P, Tsokolaeva Z, Shevelev A, Rybalkin I, Shevchenko E, Beloglazova I, Vlasik T, Tkachuk V, Parfyonova Y. Combined transfer of human VEGF165 and HGF genes renders potent angiogenic effect in ischemic skeletal muscle. *PLoS One*. 2012;7(6):e38776.

Man AJ, Kujawski G, Burns TS, Miller EN, Fierro FA, Leach JK, Bannerman P. Neurogenic potential of engineered mesenchymal stem cells overexpressing VEGF. *Cell Mol Bioeng*. 2016 Mar 1; 9(1): 96–106.

Manassero M, Paquet J, Deschepper M, Viateau V, Retortillo J, Bensidhoum M, Logeart-Avramoglou D, Petite H. Comparison of Survival and Osteogenic Ability of Human Mesenchymal Stem Cells in Orthotopic and Ectopic Sites in Mice. *Tissue Eng Part A*. 2016 Mar;22(5-6):534-44.

Marquardt LM, Ee X, Iyer N, Hunter D, Mackinnon SE, Wood MD, Sakiyama-Elbert SE. Finely Tuned Temporal and Spatial Delivery of GDNF Promotes Enhanced Nerve Regeneration in a Long Nerve Defect Model. *Tissue Eng Part A*. 2015 Dec;21(23-24):2852-64.

Masgutov R, Masgutova G, Mukhametova L, Garanina E, Arkhipova SS, Zakirova E, Mukhamedshina YO, Margarita Z, Gilazieva Z, Syromiatnikova V, Mullakhmetova A, Kadyrova G, Nigmatzyanova M, Mikhail S, Igor P, Yagudin R, Rizvanov A. Allogenic Adipose Derived Stem Cells Transplantation Improved Sciatic Nerve Regeneration in Rats: Autologous Nerve Graft Model. *Front Pharmacol*. 2018; 9: 86.

Mason MR, Tannemaat MR, Malessy MJ, Verhaagen J. Gene therapy for the peripheral nervous system: a strategy to repair the injured nerve? *Curr Gene Ther*. 2011 Apr;11(2):75-89.

Maunder HE, Wright J, Kolli BR, Vieira CR, Mkandawire TT, Tatoris S, Kennedy V, Iqbal S, Devarajan G, Ellis S, Lad Y, Clarkson NG, Mitrophanous KA, Farley DC. Enhancing titres of therapeutic viral vectors using the transgene repression in vector production (TRIP) system. *Nat Commun*. 2017 Mar 27;8:14834.

Matsuse D, Kitada M, Kohama M, Nishikawa K, Makinoshima H, Wakao S, Fujiyoshi Y, Heike T, Nakahata T, Akutsu H, Umezawa A, Harigae H, Kira J, Dezawa M. Human umbilical cord-derived mesenchymal stromal cells differentiate into functional Schwann cells that sustain peripheral nerve regeneration. *J Neuropathol Exp Neurol*. 2010 Sep;69(9):973-85.

Maturana LG, Pierucci A, Simões GF, Vidigal M, Duek EA, Vidal BC, Oliveira AL. Enhanced peripheral nerve regeneration by the combination of a polycaprolactone tubular prosthesis and a scaffold of collagen with supramolecular organization. *Brain Behav*. 2013 Jul;3(4):417-30.

May F, Buchner A, Matiasek K, Schlenker B, Stief C, Weidner N. Recovery of erectile function comparing autologous nerve grafts, unseeded conduits, Schwann-cell-seeded guidance tubes and GDNF-overexpressing Schwann cell grafts. *Dis Model Mech*. 2016 Dec 1; 9(12): 1507–1511.

McGrath AM, Brohlin M, Wiberg R, Kingham PJ, Novikov LN, Wiberg M, Novikova LN. Long-Term Effects of Fibrin Conduit with Human Mesenchymal Stem Cells and Immunosuppression after Peripheral Nerve Repair in a Xenogenic Model. *Cell Med*. 2018; 10: 1-13.

Medical Research Council (2017) Regenerative medicine and stem cells. Medical Research Council. <https://www.mrc.ac.uk/research/initiatives/regenerative-medicine-stem-cells/>. Accessed 08 Oct 2018.

Menorca RMG, Fussell TS, Elfar JCE. Peripheral nerve trauma: mechanisms of injury and recovery. *Hand Clin*. 2013 Aug; 29(3): 317–330.

Merle M, Dellon AL, Campbell JN, Chang PS. Complications from silicon-polymer intubulation of nerves. *Microsurgery*. 1989;10(2):130-3.

Merten OW, Hebben M, Bovolenta C. Production of lentiviral vectors. *Mol Ther Methods Clin Dev*. 2016 Apr 13;3:16017.

Meyer C, Wrobel S, Raimondo S, Rochkind S, Heimann C, Shahar A, Ziv-Polat O, Geuna S, Grothe C, Haastert-Talini K. Peripheral nerve regeneration through hydrogel-enriched chitosan conduits containing engineered Schwann cells for drug delivery. *Cell Transplant*. 2016;25(1):159-82.

Millington M, Arndt A, Boyd M, Applegate T, Shen S. Towards a clinically relevant lentiviral transduction protocol for primary human CD34 hematopoietic stem/progenitor cells. *PLoS One*. 2009 Jul 30;4(7):e6461.

Milone MC, O'Doherty U. Clinical use of lentiviral vectors. *Leukemia*. 2018 Jul;32(7):1529-1541.

Mimura T, Dezawa M, Kanno H, Sawada H, Yamamoto I. Peripheral nerve regeneration by transplantation of bone marrow stromal cell-derived Schwann cells in adult rats. *J Neurosurg*. 2004 Nov;101(5):806-12.

Mirsky R, Woodhoo A, Parkinson DB, Arthur-Farraj P, Bhaskaran A, Jessen KR. Novel signals controlling embryonic Schwann cell development, myelination and dedifferentiation. *J Peripher Nerv Syst*. 2008 Jun;13(2):122-35.

Mitchell JJ, Chen C, Liechti DJ, Heare A, Chahla J, Bravman JT. Axillary Nerve Palsy and Deltoid Muscle Atrophy. *JBJS Rev*. 2017 Jul;5(7):e1.

Mizisin AP, Weerasuriya A. Homeostatic regulation of the endoneurial microenvironment during development, aging and in response to trauma, disease and toxic insult. *Acta Neuropathol*. 2011; 121(3): 291–312.

Mizuno H, Tobita M, Uysal AC. Concise review: Adipose-derived stem cells as a novel tool for future regenerative medicine. *Stem Cells*. 2012 May;30(5):804-10.

Modlich U, Navarro S, Zychlinski D, Maetzig T, Knoess S, Brugman MH, Schambach A, Charrier S, Galy A, Thrasher AJ, Bueren J, Baum C. Insertional Transformation of Hematopoietic Cells by Self-inactivating Lentiviral and Gammaretroviral Vectors. *Mol Ther*. 2009 Nov; 17(11): 1919–1928.

Mofford DM, Miller SC. Luciferins behave like drugs. *ACS Chem Neurosci*. 2015 Aug 19;6(8):1273-5.

Mohammadi R, Ahsan S, Masoumi M, Amini K. Vascular endothelial growth factor promotes peripheral nerve regeneration after sciatic nerve transection in rat. *Chin J Traumatol*. 2013;16(6):323-9.

Mohan RR, Rodier JT, Sharma A. Corneal Gene Therapy: Basic Science and Translational Perspective. *Ocul Surf*. 2013 Jul; 11(3): 150–164.

Moon JJ, West JL. Vascularisation of Engineered Tissues: Approaches to Promote Angio-genesis in Biomaterials. *Curr Top Med Chem*. 2008; 8(4): 300–310.

Moore AM, MacEwan M, Santosa KB, Chenard KE, Ray WZ, Hunter DA, Mackinnon SE, Johnson PJ. Acellular nerve allografts in peripheral nerve regeneration: a comparative study. *Muscle Nerve*. 2011 Aug;44(2):221-34.

Mosahebi A, Fuller P, Wiberg M, Terenghi G. Effect of allogeneic Schwann cell transplantation on peripheral nerve regeneration. *Exp Neurol*. 2002 Feb;173(2):213-23.

Mostoslavsky G, Kotton DN, Fabian AJ, Gray JT, Lee JS, Mulligan RC. Efficiency of transduction of highly purified murine hematopoietic stem cells by lentiviral and oncoretroviral vectors under conditions of minimal in vitro manipulation. *Mol Ther*. 2005 Jun;11(6):932-40.

Mozafari R, Kyrylenko S, Castro MV, Ferreira RS Jr, Barraviera B, Oliveira ALR. Combination of heterologous fibrin sealant and bioengineered human embryonic stem cells to improve regeneration following autogenous sciatic nerve grafting repair. *J Venom Anim Toxins Incl Trop Dis*. 2018 Apr 12;24:11.

Mukhatyar V, Karumbaiah L, Yeh J, Bellamkonda R. Tissue Engineering Strategies Designed to Realize the Endogenous Regenerative Potential of Peripheral Nerves. *Adv Mater*. 2009; 21:4670–4679.

Muratori L, Gnani S, Fregnan F, Mancardi A, Raimondo S, Perroteau I, Geuna S. Evaluation of Vascular Endothelial Growth Factor (VEGF) and Its Family Member Expression After Peripheral Nerve Regeneration and Denervation. *Anat Rec (Hoboken)*. 2018 Oct;301(10):1646-1656.

Muschler GF, Nakamoto C, Griffith LG. Engineering principles of clinical cell-based tissue engineering. *J Bone Joint Surg Am*. 2004 Jul;86-A(7):1541-58.

Nakayama K, Takakuda K, Koyama Y, Itoh S, Wang W, Mukai T, Shirahama N. Enhancement of peripheral nerve regeneration using bioabsorbable polymer tubes packed with fibrin gel. *Artif Organs*. 2007 Jul;31(7):500-8.

Nakhjavan-Shahraki B, Yousefifard M, Rahimi-Movaghar V, Baikpour M, Nasirinezhad F, Safari S, Yaseri M, Moghadas Jafari A, Ghelichkhani P, Tafakhori A, Hosseini M. Transplantation of olfactory ensheathing cells on functional recovery and neuropathic pain after spinal cord injury; systematic review and meta-analysis. *Sci Rep*. 2018 Jan 10;8(1):325.

Nam SY, Ricles LM, Suggs LJ, Emelianov SY. Imaging strategies for tissue engineering applications. *Tissue Eng Part B Rev*. 2015 Feb;21(1):88-102.

Nash KL, Lever AM. Green fluorescent protein: green cells do not always indicate gene expression. *Gene Ther*. 2004 Jun;11(11):882-3.

Nathwani AC, Reiss UM, Tuddenham EG, Rosales C, Chowdhary P, McIntosh J, Della Peruta M, Lheriteau E, Patel N, Raj D, Riddell A, Pie J, Rangarajan S, Bevan D, Recht M, Shen YM, Halka KG, Basner-Tschakarjan E, Mingozzi F, High KA, Allay J, Kay MA, Ng CY, Zhou J, Cancio M, Morton CL, Gray JT, Srivastava D, Nienhuis AW, Davidoff AM. Long-term safety and efficacy of factor IX gene therapy in hemophilia B. *N Engl J Med*. 2014 Nov 20;371(21):1994-2004.

Navarro X, Vivó M, Valero-Cabré A. Neural plasticity after peripheral nerve injury and regeneration. *Prog Neurobiol*. 2007 Jul;82(4):163-201.

Nayerossadat N, Maedeh T, Ali PA. Viral and nonviral delivery systems for gene delivery. *Adv Biomed Res*. 2012; 1: 27.

Negre O, Eggimann AV, Beuzard Y, Ribeil JA, Bourget P, Borwornpinyo S, Hongeng S, Haccin-Bey S, Cavazzana M, Leboulch P, Payen E. Gene Therapy of the β -Hemoglobinopathies by Lentiviral Transfer of the β (A(T87Q))-Globin Gene. *Hum Gene Ther*. 2016 Feb;27(2):148-65.

Nichols CM, Myckatyn TM, Rickman SR, Fox IK, Hadlock T, Mackinnon SE. Choosing the correct functional assay: a comprehensive assessment of functional tests in the rat. *Behav Brain Res*. 2005 Sep 8;163(2):143-58.

- Nightingale SJ, Hollis RP, Pepper KA, Petersen D, Yu XJ, Yang C, Bahner I, Kohn DB. Transient gene expression by nonintegrating lentiviral vectors. *Mol Ther*. 2006 Jun;13(6):1121-32.
- Nijhuis THJ, de Boer SAS, Wahegaonkar AL, Bishop AT, Shin AY, Hovius SER, Selles RW. A New Approach to Assess the Gastrocnemius Muscle Volume in Rodents Using Ultrasound; Comparison with the Gastrocnemius Muscle Index. *PLoS One*. 2013; 8(1): e54041.
- Nikolaev SI, Gallyamov AR, Mamin GV, Chelyshev YA. Poly(ϵ -caprolactone) nerve conduit and local delivery of VEGF and FGF2 genes stimulate neuroregeneration. *Bull Exp Biol Med*. 2014 May;157(1):155-8.
- Nishida Y, Yamada Y, Kanemaru H, Ohazama A, Maeda T, Seo K. Vascularisation via activation of VEGF-VEGFR signaling is essential for peripheral nerve regeneration. *Biomed Res*. 2018;39(6):287-294.
- Nitzan E, Pfaltzgraff ER, Labosky PA, Kalcheim C. Neural crest and Schwann cell progenitor-derived melanocytes are two spatially segregated populations similarly regulated by Foxd3. *Proc Natl Acad Sci USA*. 2013; 110(31): 12709–12714.
- Nomi M, Atala A, Coppi PD, Soker S. Principles of neovascularisation for tissue engineering. *Mol Aspects Med*. 2002 Dec;23(6):463-83.
- Nomi M, Miyake H, Sugita Y, Fujisawa M, Soker S. Role of growth factors and endothelial cells in therapeutic angiogenesis and tissue engineering. *Curr Stem Cell Res Ther*. 2006 Sep;1(3):333-43.
- Novikova LN, Mosahebi A, Wiberg M, Terenghi G, Kellerth JO, Novikov LN. Alginate hydrogel and matrigel as potential cell carriers for neurotransplantation. *J Biomed Mater Res A*. 2006 May;77(2):242-52.
- Novosel EC, Kleinhans C, Kluger PJ. Vascularisation is the key challenge in tissue engineering. *Adv Drug Deliv Rev*. 2011 Apr 30;63(4-5):300-11.
- O'Rourke C, Drake RA, Cameron GW, Loughlin AJ, Phillips JB. Optimising contraction and alignment of cellular collagen hydrogels to achieve reliable and consistent engineered anisotropic tissue. *J Biomater Appl*. 2015 Nov;30(5):599-607.
- O'Rourke C, Day AGE, Murray-Dunning C, Thanabalasundaram L, Cowan J, Stevanato L, Grace N, Cameron G, Drake RAL, Sinden J, Phillips JB. An allogeneic 'off the shelf' therapeutic strategy for peripheral nerve tissue engineering using clinical grade human neural stem cells. *Sci Rep*. 2018 Feb 13;8(1):2951.
- Olivo C, Alblas J, Verweij V, Van Zonneveld AJ, Dhert WJ, Martens AC. In vivo bioluminescence imaging study to monitor ectopic bone formation by luciferase gene marked mesenchymal stem cells. *J Orthop Res*. 2008 Jul;26(7):901-9.
- Oudina K, Cambon-Binder A, Logeart-Avramoglou D. Noninvasive bioluminescent quantification of viable stem cells in engineered constructs. *Methods Mol Biol*. 2011;740:165-78.
- Ozawa CR, Banfi A, Glazer NL, Thurston G, Springer ML, Kraft PE, McDonald DM, Blau HM. Microenvironmental VEGF concentration, not total dose, determines a threshold between normal and aberrant angiogenesis. *J Clin Invest*. 2004 Feb 15; 113(4): 516–527.
- Palladino SP, Helton ES, Jain P, Dong C, Crowley MR, Crossman DK, Ubogu EE. The Human Blood-Nerve Barrier Transcriptome. *Sci Rep*. 2017 Dec 12;7(1):17477.

- Pan Z, Fukuoka S, Karagianni N, Guaiquil VH, Rosenblatt MI. Vascular endothelial growth factor promotes anatomical and functional recovery of injured peripheral nerves in the avascular cornea. *FASEB J*. 2013 Jul; 27(7): 2756–2767.
- Park JE, Keller GA, Ferrara N. The vascular endothelial growth factor (VEGF) isoforms: differential deposition into the subepithelial extracellular matrix and bioactivity of extracellular matrix-bound VEGF. *Mol Biol Cell*. 1993 Dec; 4(12): 1317–1326.
- Park BW, Kang DH, Kang EJ, Byun JH, Lee JS, Maeng GH, Rho GJ. Peripheral nerve regeneration using autologous porcine skin-derived mesenchymal stem cells. *J Tissue Eng Regen Med*. 2012 Feb;6(2):113-24.
- Patel NP, Lyon KA, Huang JH. An update-tissue engineered nerve grafts for the repair of peripheral nerve injuries. *Neural Regen Res*. 2018 May;13(5):764-774.
- Peeters M, van Rijn S, Vergroesen PPA, Paul CPL, Noske DP, Vandertop WP, Wurdinger T, Helder MN. Bioluminescence-mediated longitudinal monitoring of adipose-derived stem cells in a large mammal ex vivo organ culture. *Sci Rep*. 2015; 5: 13960.
- Peltonen S, Alanne M, Peltonen J. Barriers of the peripheral nerve. *Tissue Barriers*. 2013 1;1(3):e24956.
- Peng J, Wang Y, Zhang L, Zhao B, Zhao Z, Chen J, Guo Q, Liu S, Sui X, Xu W, Lu S. Human umbilical cord Wharton's jelly-derived mesenchymal stem cells differentiate into a Schwann-cell phenotype and promote neurite outgrowth in vitro. *Brain Res Bull*. 2011 Feb 28;84(3):235-43.
- Pereira Lopes FR, Lisboa BC, Frattini F, Almeida FM, Tomaz MA, Matsumoto PK, Langone F, Lora S, Melo PA, Borojevic R, Han SW, Martinez AM. Enhancement of sciatic nerve regeneration after vascular endothelial growth factor (VEGF) gene therapy. *Neuropathol Appl Neurobiol*. 2011 Oct;37(6):600-12.
- Pettersson J, Kalbermatten D, McGrath A, Novikova LN. Biodegradable fibrin conduit promotes long-term regeneration after peripheral nerve injury in adult rats. *J Plast Reconstr Aesthet Surg*. 2010 Nov;63(11):1893-9.
- Pfister LA, Papaloizos M, Merkle HP, Gander B. Nerve conduits and growth factor delivery in peripheral nerve repair. *J Peripher Nerv Syst*. 2007 Jun;12(2):65-82.
- Pfister BJ, Gordon T, Loverde JR, Kochar AS, Mackinnon SE, Cullen DK. Biomedical engineering strategies for peripheral nerve repair: surgical applications, state of the art, and future challenges. *Crit Rev Biomed Eng*. 2011;39(2):81-124.
- Philippe S, Sarkis C, Barkats M, Mammeri H, Ladroue C, Petit C, Mallet J, Serguera C. Lentiviral vectors with a defective integrase allow efficient and sustained transgene expression in vitro and in vivo. *Proc Natl Acad Sci U S A*. 2006 Nov 21;103(47):17684-9.
- Pincus Z, Theriot JA. Comparison of quantitative methods for cell-shape analysis. *J Microsc*. 2007 Aug;227(Pt 2):140-56.
- Pollock K, Stroemer P, Patel S, Stevanato L, Hope A, Miljan E, Dong Z, Hodges H, Price J, Sinden JD. A conditionally immortal clonal stem cell line from human cortical neuroepithelium for the treatment of ischemic stroke. *Exp Neurol*. 2006 May;199(1):143-55.
- Porter S, Glaser L, Bunge RP. Release of autocrine growth factor by primary and immortalized Schwann cells. *Proc Natl Acad Sci U S A*. 1987 Nov;84(21):7768-72.

Prendergast A, Raible DW. Neural crest cells and peripheral nervous system development. In: Neural crest cells: Evolution, development, and disease. 2014; Elsevier Press: Oxford, UK.

Prest TA, Yeager E, LoPresti ST, Zygelyte E, Martin MJ, Dong L, Gibson A, Olutoye OO, Brown BN, Cheetham J. Nerve-specific, xenogeneic extracellular matrix hydrogel promotes recovery following peripheral nerve injury. *J Biomed Mater Res A*. 2018 Feb;106(2):450-459.

Prins HJ, Fernandes H, Rozemuller H, van Blitterswijk C, de Boer J, Martens AC. Spatial distribution and survival of human and goat mesenchymal stromal cells on hydroxyapatite and β -tricalcium phosphate. *J Tissue Eng Regen Med*. 2016 Mar;10(3):233-44.

Qu D, Li J, Li Y, Gao Y, Zuo Y, Hsu Y, Hu J. Angiogenesis and osteogenesis enhanced by bFGF ex vivo gene therapy for bone tissue engineering in reconstruction of calvarial defects. *J Biomed Mater Res A*. 2011 Mar 1;96(3):543-51.

Raimondo S, Fornaro M, Tos P, Battiston B, Giacobini-Robecchi MG, Geuna S. Perspectives in regeneration and tissue engineering of peripheral nerves. *Ann Anat*. 2011;193(4):334-40.

Rampersad SN. Multiple applications of Alamar Blue as an indicator of metabolic function and cellular health in cell viability bioassays. *Sensors (Basel)*. 2012; 12(9): 12347–12360.

Rasband MN. Glial Contributions to Neural Function and Disease. *Mol Cell Proteomics*. 2016; 15(2): 355–361.

Ray WZ, Mackinnon SE. Management of nerve gaps: Autografts, allografts, nerve transfers, and end-to-side neurorrhaphy. *Exp Neurol*. 2010 May; 223(1): 77–85.

Rayner MLD, Laranjeira S, Evans RE, Shipley RJ, Healy J, Phillips JB. Developing an In Vitro Model to Screen Drugs for Nerve Regeneration. *Anat Rec (Hoboken)*. 2018 Oct;301(10):1628-1637.

Reid AJ, de Luca AC, Faroni A, Downes S, Sun M, Terenghi G, Kingham PJ. Long term peripheral nerve regeneration using a novel PCL nerve conduit. *Neurosci Lett*. 2013 Jun 7;544:125-30.

Ren X, Tapias LF, Jank BJ, Mathisen DJ, Lanuti M, Ott HC. Ex vivo non-invasive assessment of cell viability and proliferation in bio-engineered whole organ constructs. *Biomaterials*. 2015 Jun;52:103-12.

Ren T, Faust A, van der Merwe Y, Xiao B, Johnson S, Kandakatla A, Gorantla VS, Badylak SF, Washington KM, Steketee MB. Fetal extracellular matrix nerve wraps locally improve peripheral nerve remodeling after complete transection and direct repair in rat. *Sci Rep*. 2018 Mar 14;8(1):4474.

Ribeiro-Resende VT, Koenig B, Nichterwitz S, Oberhoffner S, Schlosshauer B. Strategies for inducing the formation of bands of Büngner in peripheral nerve regeneration. *Biomaterials*. 2009 Oct;30(29):5251-9.

Rice BW, Cable MD, Nelson MB. In vivo imaging of light-emitting probes. *J Biomed Opt*. 2001 Oct;6(4):432-40.

Richner M, Ulrichsen M, Elmegaard SL, Dieu R, Pallesen LT, Vaegter CB. Peripheral nerve injury modulates neurotrophin signalling in the peripheral and central nervous system. *Mol Neurobiol*. 2014;50(3):945-70.

Roberts SL, Dun XP, Doddrell RDS, Mindos T, Drake LK, Onaitis MW, Florio F, Quattrini A, Lloyd AC, D'Antonio M, Parkinson DB. Sox2 expression in Schwann cells inhibits myelination in vivo and induces influx of macrophages to the nerve. *Development*. 2017 Sep 1;144(17):3114-3125.

Rochkind S, Shapira , Nevo Z. The Potential Clinical Utility of Novel Methods for Peripheral Nerve Regeneration: Where Are We Now? *Future Neurology*. 2014a;9(2):105-7.

Rochkind S, Nevo Z. Recovery of peripheral nerve with massive loss defect by tissue engineered guiding regenerative gel. *Biomed Res Int*. 2014b;2014:327578.

Rodrigues MC, Rodrigues AA Jr, Glover LE, Voltarelli J, Borlongan CV. Peripheral nerve repair with cultured Schwann cells: getting closer to the clinics. *ScientificWorldJournal*. 2012;2012:413091.

Rodrigues GA, Shalaev E, Karami TK, Cunningham J, Slater NKH, Rivers HM. Pharmaceutical Development of AAV-Based Gene Therapy Products for the Eye. *Pharm Res*. 2018 Dec 27;36(2):29.

Romeo-Guitart D, Forés J, Navarro X, Casas C. Boosted regeneration and reduced denervated muscle atrophy by NeuroHeal in a pre-clinical model of lumbar root avulsion with delayed reimplantation. *Sci Rep*. 2017 Sep 20;7(1):12028.

Rouwkema J, Rivron NC, van Blitterswijk CA. Vascularisation in tissue engineering. *Trends Biotechnol*. 2008 Aug;26(8):434-41.

Rouwkema J, Khademhosseini A. Vascularisation and Angiogenesis in Tissue Engineering: Beyond Creating Static Networks. *Trends Biotechnol*. 2016 Sep;34(9):733-745.

Rovak JM, Mungara AK, Aydin MA, Cederna PS. Effects of vascular endothelial growth factor on nerve regeneration in acellular nerve grafts. *J Reconstr Microsurg*. 2004 Jan;20(1):53-8.

Rowe L, Dikici E, Daunert S. Engineering bioluminescent proteins: expanding their analytical potential. *Anal Chem*. 2009 Nov 1; 81(21): 8662–8668.

Rücker E, Grivel JC, Münch J, Kirchhoff F, Margolis L. Vpr and Vpu are important for efficient human immunodeficiency virus type 1 replication and CD4+ T-cell depletion in human lymphoid tissue ex vivo. *J Virol*. 2004 Nov;78(22):12689-93.

Sadikot RT, Blackwell TS. Bioluminescence imaging. *Proc Am Thorac Soc*. 2005;2(6):537-40, 511-2.

Saheb-Al-Zamani M, Yan Y, Farber SJ, Hunter DA, Newton P, Wood MD, Stewart SA, Johnson PJ, Mackinnon SE. Limited regeneration in long acellular nerve allografts is associated with increased Schwann cell senescence. *Exp Neurol*. 2013 Sep;247:165-77.

Sanen K, Martens W, Georgiou M, Ameloot M, Lambrichts I, Phillips J. Engineered neural tissue with Schwann cell differentiated human dental pulp stem cells: potential for peripheral nerve repair? *J Tissue Eng Regen Med*. 2017 Dec;11(12):3362-3372.

Santiago LY, Clavijo-Alvarez J, Brayfield C, Rubin JP, Marra KG. Delivery of adipose-derived precursor cells for peripheral nerve repair. *Cell Transplant*. 2009;18(2):145-58.

Santosa KB, Jesuraj NJ, Viader A, MacEwan M, Newton P, Hunter DA, Mackinnon SE, Johnson PJ. Nerve allografts supplemented with schwann cells overexpressing glial-cell-line-derived neurotrophic factor. *Muscle Nerve*. 2013 Feb;47(2):213-23.

Sarker M, Naghieh S, McInnes AD, Schreyer DJ, Chen X. Strategic Design and Fabrication of Nerve Guidance Conduits for Peripheral Nerve Regeneration. *Biotechnol J*. 2018 Jul;13(7):e1700635.

Scheib J, Höke A. Advances in peripheral nerve regeneration. *Nat Rev Neurol*. 2013 Dec;9(12):668-76.

Schlimgen R, Howard J, Wooley D, Thompson M, Baden LR, Yang OO, Christiani DC, Mostoslavsky G, Diamond DV, Duane EG, Byers K, Winters T, Gelfand JA, Fujimoto G, Hudson TW, Vyas JM. Risks Associated With Lentiviral Vector Exposures and Prevention Strategies. *J Occup Environ Med*. 2016 Dec;58(12):1159-1166.

Schmalbruch H. Fiber composition of the rat sciatic nerve. *Anat Rec*. 1986 May;215(1):71-81.

Schmitt T, Fox PM, Woon CY, Farnebo SJ, Bronstein JA, Behn A, Pham H, Chang J. Human flexor tendon tissue engineering: in vivo effects of stem cell reseeded. *Plast Reconstr Surg*. 2013 Oct;132(4):567e-576e.

Scholz T, Krichevsky A, Sumarto A, Jaffurs D, Wirth GA, Paydar K, Evans GR. Peripheral nerve injuries: an international survey of current treatments and future perspectives. *J Reconstr Microsurg*. 2009 Jul;25(6):339-44.

Sebben AD, Lichtenfels M, da Silva JL. Peripheral nerve regeneration: cell therapy and neurotrophic factors. *Rev Bras Ortop*. 2015 Nov 16;46(6):643-9.

Seddon HJ. Three types of nerve injuries. *Brain*. 1943 Dec ;66(4):237-288.

Sekine H, Shimizu T, Sakaguchi K, Dobashi I, Wada M, Yamato M, Kobayashi E, Umezu M, Okano T. In vitro fabrication of functional three-dimensional tissues with perfusable blood vessels. *Nat Commun*. 2013;4:1399.

Shakhbazou A, Mohanty C, Shcharbin D, Bryszewska M, Caminade AM, Majoral JP, Alant J, Midha R. Doxycycline-regulated GDNF expression promotes axonal regeneration and functional recovery in transected peripheral nerve. *J Control Release*. 2013 Dec 28;172(3):841-51.

Shaw A, Cornetta K. Design and Potential of Non-Integrating Lentiviral Vectors. *Biomedicines*. 2014 Mar; 2(1): 14–35.

Shellman YG, Park YL, Marr DG, Casper K, Xu Y, Fujita M, Swerlick R, Norris DA. Release of vascular endothelial growth factor from a human melanoma cell line, WM35, is induced by hypoxia but not ultraviolet radiation and is potentiated by activated Ras mutation. *J Invest Dermatol*. 2003 Oct;121(4):910-7.

Shen J, Wang Z. The level and influencing factors of quality of life in patients with brachial plexus injury. *IJNSS*. 2014;1:171-175.

Shi Y, Zhou L, Tian J, Wang Y. Transplantation of neural stem cells overexpressing glia-derived neurotrophic factor promotes facial nerve regeneration. *Acta Otolaryngol*. 2009 Aug;129(8):906-14.

Shinde R, Perkins J, Contag CH. Luciferin derivatives for enhanced in vitro and in vivo bioluminescence assays. *Biochemistry*. 2006 Sep 19;45(37):11103-12.

Silva EA, Mooney DJ. Effects of VEGF temporal and spatial presentation on angiogenesis. *Biomaterials*. 2010 Feb;31(6):1235-41.

Sinden JD, Caroline Hicks, Paul Stroemer, Indira Vishnubhatla, and Randolph Corteling. Human Neural Stem Cell Therapy for Chronic Ischemic Stroke: Charting Progress from Laboratory to Patients. *Stem Cells Dev.* 2017 Jul 1; 26(13): 933–947.

Sinis N, Kraus A, Tselis N, Haerle M, Werdin F, Schaller HE. Functional recovery after implantation of artificial nerve grafts in the rat- a systematic review. *J Brachial Plex Peripher Nerve Inj.* 2009; 4: 19.

Sondell M, Lundborg G, Kanje M. Vascular endothelial growth factor stimulates Schwann cell invasion and neovascularisation of acellular nerve grafts. *Brain Res.* 1999a Nov 6;846(2):219-28.

Sondell M, Lundborg G, Kanje M. Vascular endothelial growth factor has neurotrophic activity and stimulates axonal outgrowth, enhancing cell survival and Schwann cell proliferation in the peripheral nervous system. *J Neurosci.* 1999b 15;19(14):5731-40.

Sondell M, Sundler F, Kanje M. Vascular endothelial growth factor is a neurotrophic factor which stimulates axonal outgrowth through the flk-1 receptor. *Eur J Neurosci.* 2000 Dec;12(12):4243-54.

Sowa Y, Kishida T, Imura T, Numajiri T, Nishino K, Tabata Y, Mazda O. Adipose-derived stem cells promote peripheral nerve regeneration in vivo without differentiation into Schwann-like lineage. *Plast Reconstr Surg.* 2016 Feb;137(2):318e-330e.

Speidel AT, Stuckey DJ, Chow LW, Jackson LH, Noseda M, Abreu Paiva M, Schneider M, Stevens MM. Multimodal Hydrogel-Based Platform To Deliver and Monitor Cardiac Progenitor/Stem Cell Engraftment. *ACS Cent Sci.* 2017 Apr 26; 3(4): 338–348.

Springer ML, Chen AS, Kraft PE, Bednarski M, Blau HM. VEGF gene delivery to muscle: potential role for vasculogenesis in adults. *Mol Cell.* 1998 Nov;2(5):549-58.

Sridharan R, Reilly RB, Buckley CT. Decellularized grafts with axially aligned channels for peripheral nerve regeneration. *J Mech Behav Biomed Mater.* 2015 Jan;41:124-35.

Stang F, Keilhoff G, Fansa H. Biocompatibility of Different Nerve Tubes. *Materials (Basel).* 2009 Dec; 2(4): 1480–1507.

Strohschein K, Radojewski P, Winkler T, Duda GN, Perka C, von Roth P. In vivo bioluminescence imaging – a suitable method to track mesenchymal stromal cells in a skeletal muscle trauma. *Open Orthop J.* 2015; 9: 262–269.

Subramanian A, Krishnan UM, Sethuraman S. Development of biomaterial scaffold for nerve tissue engineering: Biomaterial mediated neural regeneration. *J Biomed Sci.* 2009 Nov 25;16:108.

Sugimoto Y, Aksentijevich I, Murray GJ, Brady RO, Pastan I, Gottesman MM. Retroviral coexpression of a multidrug resistance gene (MDR1) and human alpha-galactosidase A for gene therapy of Fabry disease. *Hum Gene Ther.* 1995 Jul;6(7):905-15.

Sulaiman W, Gordon T. Neurobiology of peripheral nerve injury, regeneration, and functional recovery: from bench top research to bedside application. *Ochsner J.* 2013 Spring; 13(1): 100–108.

Sunderland S. A classification of peripheral nerve injuries producing loss of function. *Brain.* 1951 Dec;74(4):491-516.

Swanson AM, Rossi CA, Ofir K, Mehta V, Boyd M, Barker H, Ledwozyw A, Vaughan O, Martin J, Zachary I, Sebire N, Peebles DM, David AL. Maternal therapy with Ad.VEGF-A₁₆₅

increases fetal weight at term in a guinea-pig model of fetal growth restriction. *Hum Gene Ther.* 2016 Dec;27(12):997-1007.

Szymczak AL, Workman CJ, Wang Y, Vignali KM, Dilioglou S, Vanin EF, Vignali DA. Correction of multi-gene deficiency in vivo using a single 'self-cleaving' 2A peptide-based retroviral vector. *Nat Biotechnol.* 2004 May;22(5):589-94.

Takaku Y, Murai K, Ukai T, Ito S, Kokubo M, Satoh M, Kobayashi E, Yamato M, Okano T, Takeuchi M¹, Mochida J², Sato M⁵. In vivo cell tracking by bioluminescence imaging after transplantation of bioengineered cell sheets to the knee joint. *Biomaterials.* 2014 Feb;35(7):2199-206.

Tang Y, Garson K, Li L, Vanderhyden BC. Optimization of lentiviral vector production using polyethylenimine-mediated transfection. *Oncol Lett.* 2015 Jan;9(1):55-62.

Tannemaat MR, Eggers R, Hendriks WT, de Rooter GC, van Heerikhuizen JJ, Pool CW, Malessy MJ, Boer GJ, Verhaagen J. Differential effects of lentiviral vector-mediated overexpression of nerve growth factor and glial cell line-derived neurotrophic factor on regenerating sensory and motor axons in the transected peripheral nerve. *Eur J Neurosci.* 2008 Oct;28(8):1467-79.

Taylor CA, Braza D, Rice JB, Dillingham T. The incidence of peripheral nerve injury in extremity trauma. *Am J Phys Med Rehabil.* 2008 May;87(5):381-5.

Thomas CE, Ehrhardt A, Kay MA. Progress and problems with the use of viral vectors for gene therapy. *Nat Rev Genet.* 2003 May;4(5):346-58.

Thompson MJ, Patel G, Isaacs J, McMurtry J, Richards N, Daner W. Introduction of neurosupportive cells into processed acellular nerve allografts results in greater number and more even distribution when injected compared to soaking techniques. *Neurol Res.* 2017 Mar;39(3):189-197.

Tiffen JC, Bailey CG, Ng C, Rasko JEJ, Holst J. Luciferase expression and bioluminescence does not affect tumor cell growth in vitro or in vivo. *Mol Cancer.* 2010; 9: 299.

Toda K, Small JA, Goda S, Quarles RH. Biochemical and cellular properties of three immortalized Schwann cell lines expressing different levels of the myelin-associated glycoprotein. *J Neurochem.* 1994 Nov;63(5):1646-57.

Tögel F, Yang Y, Zhang P, Hu Z, Westenfelder C. Bioluminescence imaging to monitor the in vivo distribution of administered mesenchymal stem cells in acute kidney injury. *Am J Physiol Renal Physiol.* 2008 Jul;295(1):F315-21.

Tsai MJ, Pan HA, Liou DY, Weng CF, Hoffer BJ, Cheng H. Adenoviral gene transfer of bone morphogenetic protein-7 enhances functional recovery after sciatic nerve injury in rats. *Gene Ther.* 2010 Oct;17(10):1214-24.

Tseng TC, Hsu SH. Substrate-mediated nanoparticle/gene delivery to MSC spheroids and their applications in peripheral nerve regeneration. *Biomaterials.* 2014 Mar;35(9):2630-41.

Ubogu EE. The molecular and biophysical characterization of the human blood-nerve barrier: Current concepts. *J Vasc Res.* 2013; 50(4): 289–303.

van den Berg B, Walgaard C, Drenthen J, Fokke C, Jacobs BC, van Doorn PA. Guillain-Barré syndrome: pathogenesis, diagnosis, treatment and prognosis. *Nat Rev Neurol.* 2014 Aug;10(8):469-82.

Varejão AS, Melo-Pinto P, Meek MF, Filipe VM, Bulas-Cruz J. Methods for the experimental functional assessment of rat sciatic nerve regeneration. *Neurol Res.* 2004 Mar;26(2):186-94.

Vega-Avila E, Pugsley MK. An overview of colorimetric assay methods used to assess survival or proliferation of mammalian cells. *Proc West Pharmacol Soc.* 2011;54:10-4.

Verrier JD, Semple-Rowland S, Madorsky I, Papin JE, Notterpek L. Reduction of Dicer Impairs Schwann Cell Differentiation and Myelination. *J Neurosci Res.* 2010 Sep; 88(12): 2558–2568.

Vigna E, Naldini L. Lentiviral vectors: excellent tools for experimental gene transfer and promising candidates for gene therapy. *J Gene Med.* 2000 Sep-Oct;2(5):308-16.

Vila OF, Garrido C, Cano I, Guerra-Rebollo M, Navarro M, Meca-Cortés O, Ma SP, Engel E, Rubio N, Blanco J. Real-Time Bioluminescence Imaging of Cell Distribution, Growth, and Differentiation in a Three-Dimensional Scaffold Under Interstitial Perfusion for Tissue Engineering. *Tissue Eng Part C Methods.* 2016 Sep;22(9):864-72.

Virostko J, Chen Z, Fowler M, Poffenberger G, Powers AC, Jansen ED. Factors influencing quantification of in vivo bioluminescence imaging: application to assessment of pancreatic islet transplants. *Mol Imaging.* 2004 Oct;3(4):333-42.

Walsh S, Midha R. Practical considerations concerning the use of stem cells for peripheral nerve repair. *Neurosurg Focus.* 2009 Feb;26(2):E2.

Wang Y, Zang QS, Liu Z, Wu Q, Maass D, Dulan G, Shaul PW, Melito L, Frantz DE, Kilgore JA, Williams NS, Terada LS, Nwariaku FE. Regulation of VEGF-induced endothelial cell migration by mitochondrial reactive oxygen species. *Am J Physiol Cell Physiol.* 2011 Sep; 301(3): C695–C704. Wang C, Jia Y, Yang W, Zhang C, Zhang K, Chai Y. Silk fibroin enhances peripheral nerve regeneration by improving vascularisation within nerve conduits. *J Biomed Mater Res A.* 2018 Jul;106(7):2070-2077.

Wangenstein KJ, Kalliainen LK. Collagen Tube Conduits in Peripheral Nerve Repair: A Retrospective Analysis. *Hand (N Y).* 2010 Sep; 5(3): 273–277.

Warawa JM, Lawrenz MB. Bioluminescent imaging of bacteria during mouse infection. *Methods Mol Biol.* 2014;1098:169-81.

Watson NV, Breedlove SM. *The Mind's Machine.* 2015; 2nd ed., Sinaur Associates.

Weber RA, Breidenbach WC, Brown RE, Jabaley ME, Mass DP. A randomized prospective study of polyglycolic acid conduits for digital nerve reconstruction in humans. *Plast Reconstr Surg.* 2000 Oct;106(5):1036-45.

Wei GJ, Yao M, Wang YS, Zhou CW, Wan DY, Lei PZ, Wen J, Lei HW, Dong DM. Promotion of peripheral nerve regeneration of a peptide compound hydrogel scaffold. *Int J Nanomedicine.* 2013;8:3217-25.

Wigley C. Blood supply of peripheral nerves. In: *Gray's Anatomy: The anatomical basis of clinical practice.* 2008; 40th ed, Churchill Livingstone Elsevier: London, UK.

Williams LR, Danielsen N, Müller H, Varon S. Exogenous matrix precursors promote functional nerve regeneration across a 15-mm gap within a silicone chamber in the rat. *J Comp Neurol.* 1987 Oct 8;264(2):284-90.

Winiarska M, Nowis D, Firczuk M, Zagozdzon A, Gabrysiak M, Sadowski R, Barankiewicz J, Dwojak M, Golab J. Selection of an optimal promoter for gene transfer in normal B cells. *Mol Med Rep.* 2017 Sep;16(3):3041-3048.

- Woods NB, Muessig A, Schmidt M, Flygare J, Olsson K, Salmon P, Trono D, von Kalle C, Karlsson S. Lentiviral vector transduction of NOD/SCID repopulating cells results in multiple vector integrations per transduced cell: risk of insertional mutagenesis. *Blood*. 2003 Feb 15;101(4):1284-9.
- Worgall S, Crystal RG. Gene therapy. In: *Principles of Tissue Engineering*. 2014; 4th ed., Academic Press.
- Wu-Fienberg Y, Moore AM, Marquardt LM, Newton P, Johnson PJ, Mackinnon SE, Sakiyama-Elbert SE, Wood MD. Viral transduction of primary Schwann cells using a Cre-lox system to regulate GDNF expression. *Biotechnol Bioeng*. 2014 Sep; 111(9): 1886–1894.
- Yang JJ, Liu ZQ, Zhang JM, Wang HB, Hu SY, Liu JF, Wang CY, Chen YD. Real-time tracking of adipose tissue-derived stem cells with injectable scaffolds in the infarcted heart. *Heart Vessels*. 2013 May;28(3):385-96.
- Yang DP, Kim J, Syed N, Tung YJ, Bhaskaran A, Mindos T, Mirsky R, Jessen KR, Maurel P, Parkinson DB, Kim HA. p38 MAPK activation promotes denervated Schwann cell phenotype and functions as a negative regulator of Schwann cell differentiation and myelination. *J Neurosci*. 2012 May 23;32(21):7158-68.
- Ye Z, Yu X, Cheng L. Lentiviral gene transduction of mouse and human stem cells. *Methods Mol Biol*. 2008;430:243-53.
- Yi C, Dahlin LB. Impaired nerve regeneration and Schwann cell activation after repair with tension. *Neuroreport*. 2010 Oct 6;21(14):958-62.
- Yin H, Kanasty RL, Eltoukhy AA, Vegas AJ, Dorkin JR, Anderson DG. Non-viral vectors for gene-based therapy. *Nat Rev Genet*. 2014 Aug;15(8):541-55.
- Ylä-Herttuala S. Endgame: Glybera finally recommended for approval as the first gene therapy drug in the European Union. *Mol Ther*. 2012 Oct;20(10):1831-2.
- Ylä-Herttuala S. ADA-SCID gene therapy endorsed by European Medicines Agency for marketing authorization. *Mol Ther*. 2016 Jun; 24(6): 1013–1014.
- Yu X, Zhan X, D'Costa J, Tanavde VM, Ye Z, Peng T, Malehorn MT, Yang X, Civin CI, Cheng L. Lentiviral vectors with two independent internal promoters transfer high-level expression of multiple transgenes to human hematopoietic stem-progenitor cells. *Mol Ther*. 2003 Jun;7(6):827-38.
- Zhai Q, Wang J, Kim A, Liu Q, Watts R, Hoopfer E, Mitchison T, Luo L, He Z. Involvement of the ubiquitin-proteasome system in the early stages of Wallerian degeneration. *Neuron*. 2003 Jul 17;39(2):217-25.
- Zhang B, Pat Metharom, Howard Jullie, Kay AO Ellem, Geoff Cleghorn, Malcolm J West, Ming Q Wei. The significance of controlled conditions in lentiviral vector titration and in the use of multiplicity of infection (MOI) for predicting gene transfer events. *Genet Vaccines Ther*. 2004; 2: 6.
- Zhang SJ, Wu WL, Yang KY, Chen YZ, Liu HC. Phenotypic changes of Schwann cells on the proximal stump of injured peripheral nerve during repair using small gap conduit tube. *Neural Regen Res*. 2017 Sep;12(9):1538-1543.
- Xu T, Close DM, Webb JD, Ripp SA, Saylor GS. Autonomously bioluminescent mammalian cells for continuous and real-time monitoring of cytotoxicity. *J Vis Exp*. 2013; (80): 50972.

Zecchin A, Kalucka J, Dubois C, Carmeliet P. How Endothelial Cells Adapt Their Metabolism to Form Vessels in Tumors. *Front Immunol.* 2017; 8: 1750.

Ziegler L, Grigoryan S, Yang IH, Thakor NV, Goldstein RS. Efficient generation of Schwann cells from human embryonic stem cell-derived neurospheres. *Stem Cell Rev.* 2011 Jun;7(2):394-403.

Zinn KR, Chaudhuri TR, Adams Szafran A, O'Quinn D, Weaver C, Dugger K, Lamar D, Kesterson RA, Wang X, Frank SJ. Noninvasive bioluminescence imaging in small animals. *ILAR J.* 2008; 49(1): 103–115.

Zufferey R, Nagy D, Mandel RJ, Naldini L, Trono D. Multiply attenuated lentiviral vector achieves efficient gene delivery in vivo. *Nat Biotechnol.* 1997 Sep;15(9):871-5.

Zufferey R, Dull T, Mandel RJ, Bukovsky A, Quiroz D, Naldini L, Trono D. Self-inactivating lentivirus vector for safe and efficient in vivo gene delivery. *J Virol.* 1998 Dec;72(12):9873-80.

Zufferey R, Donello JE, Trono D, Hope TJ. Woodchuck hepatitis virus posttranscriptional regulatory element enhances expression of transgenes delivered by retroviral vectors. *J Virol.* 1999 Apr;73(4):2886-92.

Zupanc HRH, Alexander PG, Tuan RS. Neurotrophic support by traumatized muscle-derived multipotent progenitor cells: Role of endothelial cells and Vascular Endothelial Growth Factor-A. *Stem Cell Res Ther.* 2017; 8: 226.